SPECTROSCOPY AND DYNAMICS OF SMALL MOLECULES WITH LARGE AMPLITUDE MOTION

A Dissertation

Presented to

The Graduate Faculty of The University of Akron

In Partial Fulfillment

of the Requirements for the Degree

Doctor of Philosophy

Mahesh B. Dawadi

August, 2014

SPECTROSCOPY AND DYNAMICS OF SMALL MOLECULES WITH LARGE AMPLITUDE MOTION

Mahesh B. Dawadi

Dissertation

Approved:

_____
Advisor
Dr. David S. Perry

_____
Committee Member
Dr. Mesfin Tsige

_____
Committee Member
Dr. David A. Modarelli

_____
Committee Member
Dr. Alper Buldum

_____
Committee Member
Dr. Christopher J. Ziegler

Accepted:

_____
Department Chair
Dr. Michael J. Taschner

_____
Dean of the College
Dr. Chand Midha

_____
Dean of the Graduate School
Dr. George R. Newkome

_____
Date

ABSTRACT

This dissertation addresses the effect of large amplitude vibrations (LAV or LAVs) on the other small amplitude vibrations (SAVs) for investigating the vibrational dynamics on the molecular systems ranging from G_6 to G_{12} symmetry, including methanol, methylamine, nitromethane, 2-methylmalonaldehyde (2-MMA) and 5-methyltropolone (5-MT).

The study of the high-resolution infrared spectrum of methylamine (CH_3NH_2) in the ν_{11} asymmetric CH stretch region (2965-3005 cm^{-1}) under sub-Doppler slit-jet conditions reveals that the torsion-inversion tunneling patterns are heavily impacted by perturbations and hence different both from the ground state and from the theoretical predictions.

Two torsion-inversion tunneling models are reported for studying the high-barrier tunneling behavior in the methyl CH stretch vibrationally excited states of the molecules with G_{12} symmetry. These models predict the inverted tunneling pattern of the four tunneling states (A, B, E_1 and E_2 symmetries) in the asymmetric CH stretch excited states relative to the ground state. The trends in the patterns relative to tunneling rates and coupling parameters are presented and comparisons are made to the available experimental data.

Additionally, a remarkable result that follows from the approximate adiabatic separation of the fast and slow vibrations in methanol is the existence of vibrational

conical intersections (CIs) where the surfaces representing the two asymmetric CH stretches meet like the points of two cones touching point-to-point. The CIs occur in the slow coordinates space consisting of the torsion and the COH bend.

Finally, the analysis of the high-resolution synchrotron based Fourier transform infrared (FTIR) spectrum for NO_2 in-plane rock, ν_7, band of nitromethane reveals that the rotational energy pattern in the lowest torsional state ($m' = 0$) of the upper vibrational state is similar relative to the vibrational ground state.

DEDICATION

This dissertation is dedicated to

My wife Sabitra Dawadi (Regmi)

Daughter Anjila Dawadi

Parents Ram Nath Dawadi and Bishnu Maya Dawadi

ACKNOWLEDGEMENTS

I would like to acknowledge those people who have supported me during my pursuit of a doctorate in chemistry. Each person has in his or her own way made a contribution to the completion of this work and many have sustained me in times of difficulty.

First, I would like to express my gratitude and appreciation to my advisor Dr. David S. Perry for his patience, encouragement and guidance throughout my PhD study. His insights, attention to detail and constant support have led to the success of my study and research.

Special thanks to Dr. Sylvestre Twagirayezu and Dr. Brant E. Billinghurst for providing me an opportunity to work on Canadian Light Source, Saskatoon, Canada.

I am grateful to the dissertation committee members, Dr. David A. Modarelli, Dr. Alper Buldum, Dr. Mesfin Tsige, and Dr. Christopher J. Ziegler for very nice comments and suggestions to improve the dissertation. My special thanks go to the faculty and staffs in the department of Chemistry for their direct or indirect help during my study.

I acknowledge the fellowship and financial support from the Department of Chemistry of the University of Akron and the U.S. Department of Energy.

Finally, I would like to express deep appreciation to my family specially my parents, my wife and daughter for their continuous love and endless support.

TABLE OF CONTENTS

Page

LIST OF TABLES

LIST OF FIGURES

LIST OF ABBREVIATIONS

SAV - large amplitude vibration

2-MMA - 2-methylmalonaldehyde

5-MT - 5-methyltropolone

RRKM - Rice-Ramsperger-Kessel-Marcus

LADF - large amplitude degree of freedom

SADF - small amplitude degree of freedom

LAM - large amplitude motion

CNPI - complete nuclear permutation-inversion

RT - Renner-Teller

JT - Jahn-Teller

CIs - conical intersections

ECIs - electronic conical intersections

VCIs - vibrational conical intersections

FTIR - Fourier transform infrared

CRDS - cavity ring-down spectroscopy

CW - continuous wave

OPO - optical parametric oscillator

PPLN - periodically-poled lithium niobate

AOM - acousto-optic modulator

BO - Born-Oppenheimer

ZPD - zero path difference

CLS - Canadian light source

B3LYP - Becke's 3-parameter, Lee-Yang-Parr

CCSD(T) - coupled cluster single, doubles, and perturbative triples

DFT - Density functional theory

PE - potential energy

IRC - intrinsic reaction coordinate

G09 - Gaussian 09

MP2 - second-order Moller-Plesset

MEP - minimum energy path

RMS - root-mean-square

XHL - Xu, Hougen,Lees

FTFIR - Fourier transform far-infrared

GSCD - ground state combination difference

USCD - upper state combination difference

CHAPTER I

INTRODUCTION

1.1 Large amplitude motion

The reaction coordinate is a key concept in the description of a chemical reaction. The motion involved along that coordinate, as the reactants are converted into products, is large–amplitude nuclear motion. The most successful theories of reaction dynamics, including transition state theory [1-3] and Rice-Ramsperger-Kessel-Marcus (RRKM) theory [4], identify a reaction coordinate and assume thermal equilibrium among the other nuclear coordinates. In reactions at high energies, just below the threshold for a new fragmentation channel, there may be roaming trajectories [5, 6] favoring the product channels that involve more than one "active" degrees of freedom or large-amplitude degree of freedom (LADF). An alternative to the transition state theory is the adiabatic channel model [7-9] in which the excitation in one of more of the orthogonal degrees of freedom are assumed to be conserved as the system moves along the reaction coordinate. Therefore, we might consider each adiabatic channel as a separate transition state problem and the optimum transition state hypersurface will vary considerably over the accessible range of channels. In these approximate theories of chemical reaction, the active degrees of freedom, which include the large-amplitude reaction coordinate(s) are separated in different ways from the other ("inactive") degrees of freedom or the small-amplitude degrees of freedom (SADF).

In principle, the exact quantum nuclear dynamics for reactive systems may be calculated, however such calculations are computationally intensive and therefore limited to systems with only a few degrees of freedom. For example, if there are N atoms in a molecular system, the nuclear dynamics depends on 3N-6 vibrational degrees of freedom, thus calculation of nuclear dynamics in 3N-6 dimensional vibrational space requires the calculation of many *ab initio* points on potential energy hypersurface [10]. Furthermore, computation of the quantum nuclear dynamics for a polyatomic system is even more computationally demanding requiring in principle, a basis set of dimension $\sim 10^{3N-6}$. Even with state-of-the-art methods, including Lanczos diagonalization and basis set contraction [11-13], this limits full dimensional computation of the quantum nuclear dynamics to reactive systems with at most 4 or 5 atoms. Thus for reactive systems larger than 4 or 5 atoms [14, 15], the dimensionality of the problem must be reduced by an approximate separation of active modes, which include the large-amplitude reaction coordinate, and the other inactive nuclear degrees of freedom. Thus, current theories of chemical reaction depend critically on the validity of such separations of nuclear degrees of freedom. This dissertation probes the validity of such separations by examining the coupling between large- and small-amplitude nuclear degrees of freedom.

In this dissertation, we use large amplitude motion (LAM) in bound molecular systems, including methanol, nitromethane, methylamine, 2-MMA, and 5-MT, as a model of reaction coordinates to investigate the coupling of active degrees of freedom to other inactive degrees of freedom. This allows us to use the precision and power of high-resolution molecular spectroscopy to probe specific coupling mechanisms to test the

limits of approximate means of separating the active degrees of freedom from other (inactive) degrees of freedom, such as the adiabatic approximation [16].

In presence of LAM in a molecular system (e.g., methanol, methylamine, ethyl radical, nitromethane etc.), the system does not stay close to well-defined reference geometry. This challenges the concepts of the traditional theory of molecular vibrations, including the harmonic approximation [17]. In this context, the vibrational Hamiltonian is no longer separable, and the vibrational "normal" modes are no longer independent [18]. Among the consequences are:

(i) Point group symmetry, which relies on the well-defined reference geometry, is no longer applicable. To treat the symmetry of the Hamiltonian under these circumstances, permutation-inversion group theory [19], becomes an appropriate choice. The concept of complete nuclear permutation-inversion (CNPI) group relies on the fact that during the symmetry operations, (i.e. the permutation-inversion operations) the symmetry of Hamiltonian remains unchanged through out the process.

(ii) The symmetries of the vibrational normal modes no longer have unique symmetry designations [20].

(iii) If the molecular system has more than one LADF, they will couple with each other or to the SADF [21] and the coupling terms in the Hamiltonian can be substantial.

(iv) Any anharmonic terms (arising from the potential energy) along the large-amplitude coordinate may become quite large and may easily be greater than the energy difference between different normal mode states, thereby

affecting the coupling strength between LAM and small amplitude vibrations (SAVs) [22, 23].

(v) Force and inertial constants, equilibrium bond lengths, angles, reduced masses of other SAVs may vary significantly as a function of the LADF.

Therefore, a clear understanding of the nuclear dynamics of large amplitude motions in energized molecules is critically important. The particular kinds of LAM, in which we are interested, are torsion (internal rotation, γ), inversion, τ, and COH-bending, ρ, motions as shown in Figure 1.1. The purpose of this dissertation is to probe and then to understand the dynamics that result from the coupling between SADF in molecular systems with two or more LADF.

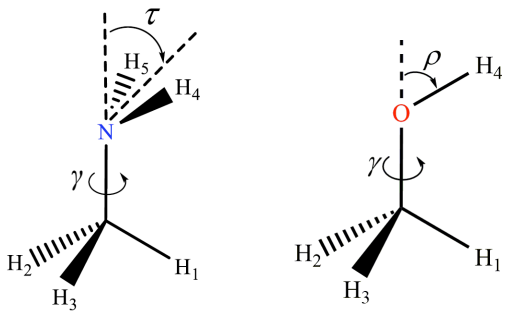

Figure 1.1 Molecular geometries of methylamine and methanol, showing large amplitude coordinates.

1.2 The local mode picture of molecular vibration

The normal mode theory [17], a traditional description of vibrational motions, is based on the classical harmonic approximation. At low vibrational energy, where the ratio of inter-bond coupling to bond-anharmonicity is relatively large, the harmonic

approximation is able to describe the molecular vibrations accurately. Early work by Siebrand and co-workers [24] and work by Henry [23] and by Child and co-workers [25] has shown, however, that the conventional normal mode description of molecular vibrations is not adequate for highly excited vibrational states. Thus, local mode treatment may be a suitable choice for treating the molecules in highly excited vibrational states.

The local mode approach is based on the vibrational modes localized to individual bonds, which are considered as a set of Morse oscillators [26]. The potential function for a vibration localized to a single bond might be approximated as the Morse Potential [27],

$$V = D_e\left[1-\exp(-\beta\delta r)\right] \qquad (1.1)$$

where β controls the width of the potential, δr is the displacement from the equilibrium length, and D_e is the bond dissociation energy. This bond-localized energy concept is different from the normal coordinate picture in which normal vibrational amplitude is non-localized and is distributed many of the other internal coordinates. Since the vibrational modes are coupled to each other in the local mode approach, the vibrational Hamiltonian in the local mode picture includes both the local oscillator energies in the local mode coordinate system and the off-diagonal local-local couplings.

Wang and Perry [28] successfully developed a local mode model to treat the torsion and the three C-H stretches of methanol in order to account for the observed torsional tunneling splittings. They found that this local mode model of the CH stretches which included only Jahn-Teller-like coupling terms in cosγ, (where, γ is torsional angle), gave the correct inverted torsional tunneling splittings of the ν_2 and ν_9 vibrations. The

successful implementation of the local mode approach on methanol, suggests that one might extend this approach to a higher dimensional vibrational problems. For example, torsion-inversion tunneling patterns for methylamine, 2- methylmalonaldahyde, (2-MMA), and 5-methyl tropolone, (5-MT) (see Chapter IV) were predicted successfully by the implementation of local mode approach in those molecular systems.

1.3 The adiabatic approximation

The adiabatic approach is one of the simplest and most extensively used methods for reducing the dimensionality of complex problems by separating the fast degrees of freedom from the slow degrees of freedom, thereby making approximate solutions tractable. The electronic adiabatic approximation-called the Born-Oppenheimer approximation (BO approximation) [29]-is a key concept in electronic spectroscopy and in the reaction dynamics involving multiple electronic states. The BO approximation is the approximate adiabatic separation of the fast electronic motion and the slower nuclear motions [30]. We refer this separation as the electronic adiabatic approximation. While BO-approximation involves the adiabatic separations of the fast electronic and slow nuclear motions, it is also possible in some cases to make an approximate adiabatic separation of fast high-frequency and slow low-frequency molecular vibrations in the electronic ground state [9, 16, 31]. In such a case, the high-frequency small-amplitude vibrations (e.g., hydride stretches) are solved quantum mechanically at fixed values of low frequency large amplitude (e.g., torsion or bending) coordinates and then the wavefunction for the low frequency coordinate(s) is(are) solved in the resulting effective potential. In the vibrational domain, such a separation is termed the vibrationally

adiabatic approximation. Thus the adiabatic separations of variables for the electronic and vibrational cases are mathematically analogous, and one might expect analogous phenomena in the two cases.

Fehrensen *et al*. [32] applied an adiabatic reaction path Hamiltonian to methanol to solve the 11 small amplitude vibrations at each torsion angle and then the torsional motion was solved in the effective potential of the other vibrations. They were able to account for both the decrease of the torsional tunneling splittings with OH stretch excitation, ν_1, and the inverted torsional tunneling splittings in the first excited states of the asymmetric CH stretches, ν_2, ν_9, and the rocks, ν_7, and ν_{11} vibrational modes of methanol. They found that for the vibrational modes with inverted torsional tunneling splittings, a geometric phase of -1 was accumulated when the torsional angle, γ, changes by 2π. Accordingly they solved the torsional wavefunctions with 4π boundary conditions. The internal coordinate model Hamiltonian of Wang and Perry [28] with torsion and 3 CH stretches has been successfully applied to account for the inverted torsional tunneling splittings of the ν_2 and ν_9 vibrations. Clasp and Perry [31] found that the vibrationally adiabatic approximation, when applied to this model, also gave qualitatively correct results for the tunneling splittings in the first excited CH stretch states. From these studies, one sees that the adiabatic treatment of torsional motion is useful for reducing the complexity of high-dimensional vibrational problems and for analyzing torsion-vibration spectra.

1.3.1 Renner-Teller effect

In a symmetrical nuclear configuration of high point group symmetry (a 3-fold axis or higher), there are degenerate electronic states [19] and also degenerate vibrational modes. For example, in linear molecules the Π, Δ, Φ,…. electronic states are degenerate. If the molecule is bent from the linearity, the energy states that are degenerate in the linear configuration split into a pair of non-degenerate potential energy curves. This splitting of a degenerate electronic state upon bending, and the subsequent coupling of the electronic, vibrational and rotational motions is called the Renner-Teller effect (RT) [19, 33]. In RT coupling, the splitting of degenerate electronic state has to be an even function of ρ, the deviation angle from linearity and therefore the coupling strength scales quadratically proportional to ρ^2 [34]. An example is the linear molecule hydrogen cyanide (HCN), for which the ground and first excited electronic states are $\sum^+$ and Π states respectively with the latter being doubly degenerate. However, when bent, the point group symmetry of HCN is reduced to C_s, and the Π state splits into A′ and A″ electronic states [35].

1.3.2 Jahn-Teller effect

The Jahn-Teller (JT) effect is the most well-known example of the vibronic coupling in non-linear polyatomic molecules. All non-linear polyatomic molecules, with C_{3V} or higher point group symmetry possess degenerate electronic states (*E*) and degenerate vibrational modes (*e*) [33]. For a non-linear molecular system in a degenerate electronic state, the C_{3V} nuclear configuration is unstable and undergoes a geometric distortion along a degenerate bending coordinate that reduces the point group symmetry

and the energy, thereby removing the degeneracy. This is termed the Jahn-Teller (JT) effect [19, 33]. The results are a pair of non-degenerate electronic potential energy surfaces that meet at the C_{3V} reference geometry in the form of two cones meeting end-to-end. Such a meeting point of two surfaces is called a conical intersection (CI) (Figure 1.2). The detail description of CI is given in the following sections. The JT theorem is based on the group theoretical analysis of the behavior of adiabatic potential energy surfaces of polyatomic systems near the CIs. In JT coupling, the splitting of the electronic states scales linearly with the deviation of ρ from the reference geometry [34]. As the JT effect is based on the coupling of degenerate electronic and vibrational states, the BO-approximation breaks down in the JT-active states.

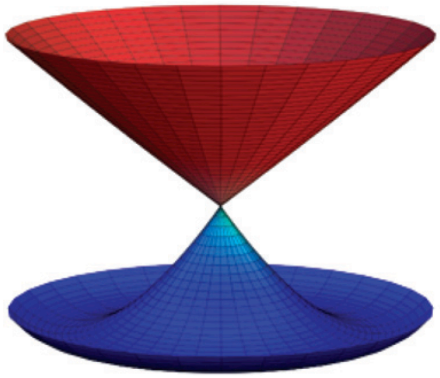

Figure 1. 2 Example of a linear JT conical intersection. This figure is taken from Ref. [36] with permission from the Elsevier publishers.

1.3.3 Breakdown of BO-adiabatic approximation

As mentioned in the previous section, the BO-adiabatic approximation assumes that electronic and nuclear motion are separable [37] , that is, non-interacting; however

this assumption is not always valid. When the potential energy surfaces approach each other with an energy spacing close to k_BT [38], the adiabatic approximation begins to break down and phenomena such as radiationless transitions occur [37, 39]. The rate of a radiationless transition depends on the energy difference between two electronic states, *I* and *J* and on the derivative coupling term, f_{IJ}, (measuring the variation the electronic wavefunction with nuclear coordinates) [38],

$$f_{IJ}(R) = \frac{\langle \psi_I | \nabla H | \psi_J \rangle}{E_J - E_I} \tag{1.2}$$

where, ∇ is the gradient operator over the nuclear coordinates R. The coupling is inversely proportional to the energy gap between the states. However, near resonance, when $\Delta E_{12} \leq 10^2$ cm^{-1} [37], the off diagonal derivative coupling (i.e., the nonadiabatic interactions) terms diverge. Where the electronic states become degenerate, they meet to form an electronic conical intersection (ECI). Under such conditions, the coupling between the nuclear and electronic degrees of freedom cannot be ignored and the BO-adiabatic approximation breaks down. The resulting non-adiabatic effects are usually important at the vicinity of the ECI or along a seam of ECI's in configuration space.

1.3.4 Electronic conical intersections

Electronic conical intersections (ECIs) are the crossing of two adiabatic potential energy surfaces of the two electronic states, forming a double cone in coordinate space (Figure 1.2) [33, 40]. ECIs are widespread throughout electronic spectroscopy and photochemistry and reaction dynamics of molecules and are responsible for ultrafast electronic relaxation in diverse circumstances [33, 40, 41]. A CI can act as a sort of

sinkhole that causes the nuclear motion to drop through and continue on a lower surface. The occurrence of degeneracy for the electronic surface of same symmetry at the intersection point is a result of non-crossing rule by Neumann and Wigner [42]. This rule states that "for a molecular system with N^{int} internal nuclear coordinates (N^{int} =3N-6), two electronic surfaces with same symmetry become degenerate when the dimension of the locus of the conical intersection is two less (N^{int}-2) than the number of total number of internal nuclear coordinates. Equivalently, two internal coordinates must be varied to find an intersection". Since the present dissertation focuses on the vibrational electronic conical intersections (VCIs) rather than ECIs, a review of the vast literature data emerge on ECIs during the past half-century is not our primary concern.

1.3.5 Vibrational conical intersections

Peter Hamm and Gerhard Stock introduced the first concept of vibrational conical intersections (VCIs) as a source of ultrafast vibrational relaxation, in the vibrational adiabatic states of the hydrogen-bonded system, malonaldehyde and water dimer [30, 43]. For example, in malonaldehyde, they found a VCI between the adiabatic surfaces formed by the OH stretch and COH bend vibrations when taken as functions of the two low-frequency coordinates, the length of the hydrogen bond and in–plane angle of the hydrogen bond.

Since the VCIs of a molecular system exist only in the context of an adiabatic separation of high- and low-frequency vibrations, the following are necessary components in the molecular system: (i) a set of large-amplitude, low-frequency coordinates, (ii) a group of high-frequency vibrations whose relative frequencies vary

significantly over the large amplitude space, and (iii) location(s) in the large-amplitude space where the splitting between a pair of zeroth-order vibrational frequencies and coupling between them both go to zero.

There are three kinds of CIs [38, 44] based on role of symmetry in meeting these criteria: (i) symmetric-required CIs, (ii) symmetric-allowed CIs, and (iii) accidental same-symmetry CIs. In a symmetry-required CI such as the Jahn-Teller CI at ρ =0, (Figure 1.2) both the zeroth-order frequency splitting and the coupling go to zero by symmetry. On the other hand, in symmetry-allowed CI, there is a sub-space of high-symmetry conformations in which the two high-frequency vibrations transform as different symmetry species and therefore are uncoupled. Examples of this are the staggered and eclipsed conformations of methanol, which have C_s symmetry. The CIs then occur at locations in this sub-space at which the zeroth-order splittings are zero. But for an accidental-same symmetry CI, symmetry plays no role. The discovery of VCIs between adiabatic surfaces in methanol is reported in Chapter V of this dissertation.

1.3.6 The role of geometry phase

Longuet-Higgins [45] and Herzberg [46] first pointed out that the real electronic wavefunction changes sign when transported around a closed loop in nuclear coordinate space that encloses a CI. This result was subsequently analyzed by Mead and Truhlar [47] and the theory generalized by Berry [48], the effect has known as geometric phase or Berry's phase. The Geometric phase is the signature property of a conical intersection. Such effects are now known to be widespread in chemistry and spectroscopy, including in reactive systems [33, 38, 40, 41, 49].

Zwanziger and Grant [34] showed that when both Jahn-Teller and Renner-Teller couplings are active, then a set of four related CIs is expected. Further, they showed that the geometric phase accumulated along a path that encloses a number (n) of CIs is $(-1)^n$ with $n = 0, 1, 2, \ldots$. It means that when an odd number of CIs is enclosed, one expects a phase change of -1. When an even number is enclosed, one expects a phase change of +1.

1.4 Contributions of this dissertation

In this dissertation, the patterns of torsion-inversion-rotation energy levels of the high-resolution spectrum in the ν_{11} asymmetric CH stretch of methylamine are explored. The ν_{11} asymmetric CH stretch band in CH_3NH_2 has tunneling patterns heavily impacted by perturbations and hence different both from the ground state and from the theoretical predictions. Two Model Hamiltonians are developed in order to predict the torsion-inversion tunneling splittings patterns in the CH-stretch vibrationally excited states of the molecules with G_{12} symmetry, including methylamine, 2-methylmalonadlehyde (2-MMA) and 5-methyltropolone (5-MT). The model predictions are compared to the available experimental data and other theoretical treatments. These model Hamiltonians will help spectroscopists to understand the dynamics that result from the interaction between the LAMs and between LAMs and SAVS. The presence of a set of seven CIs between the vibrationally adiabatic surfaces of methanol are investigated with the aid of high-level *ab intio* calculation. The preeminent consequence of CIs for molecular dynamics is the prediction of ultrafast energy transfer between the connected surfaces that is localized in low-frequency coordinate space near the CIs. Application areas potentially impacted include combustion and solar energy conversion. Finally, this

dissertation reports the rotational energy patterns for the NO_2-in-plane rock (ν_7) band of CH_3NO_2 in the lowest torsional state based on an analysis of the high-resolution synchrotron-based Fourier transform infrared spectrum.

1.5 Organization of this dissertation

This dissertation is organized as follows: Detailed description of slit-jet single-resonance and synchrotron based Fourier transform infrared (FTIR) experiments, are presented in Chapter II. Chapter III presents the analysis of the high-resolution infrared spectrum of ν_{11} asymmetric CH stretch of methylamine in the region 2965-3005 cm^{-1}. This work has been published in the Journal of Chemical Physics [50]. The development of two model torsion-inversion-vibration Hamiltonians and their application to molecules with G_{12} symmetry are described in Chapter IV. The contents of Chapter IV have been published in the Journal of Physical Chemistry A [51]. Chapter V describes the discovery of a set of seven conical intersections between the vibrationally adiabatic surfaces in methanol. The results of this Chapter have been published as a Communication featured on the cover of the Journal of Chemical Physics [52]. Chapter VI addresses the analysis of synchrotron based FTIR spectrum of NO_2-in-plane rock band of nitromethane in the region of 440-510 cm^{-1}. Chapter VII gives the summary of the work. Finally, the supplementary materials, which support each Chapter, are given in the appendices.

CHAPTER II

EXPERIMENTAL METHODS

Most of the data presented in this dissertation were obtained using two different experimental techniques: (i) slit-jet single-resonance spectroscopy at the University of Akron and (ii) synchrotron-based Fourier transform infrared (FTIR) spectroscopy in collaboration with Canadian Light Source Inc. in Saskatoon, Canada. An overview of the slit-jet experiment is described in section (2.1) including by a brief description of cavity ring-down spectroscopy (2.1.2). A brief description of synchrotron-based Fourier transform infrared spectroscopy is presented in section (2.2).

2.1 Slit-jet single-resonance experiment

The slit-jet single resonance experiment is well established and has been used in our laboratory in past years to study various molecules [53, 54]. It has a slit-jet nozzle that produces a planar jet of gas into the vacuum chamber and also increases the effective optical path length. The resultant spectra of the jet-cooled molecules have a narrower sub-Doppler linewidth and an enhanced signal/noise ratio. The data presented in Chapter III was obtained using this technique.

2.1.1 Direct-absorption slit-jet spectroscopy

Direct absorption spectroscopy is a simple laser-based absorption technique for obtaining the absorption spectrum of the gaseous sample. A schematic diagram for the direct-absorption technique is shown in Figure 2.1. A detailed description of the experimental set-up has been reported previously, [55, 56] therefore, only a brief summary will be given here. An F-center laser (Burleigh FCL-10), optically pumped by a Coherent Krypton Ion Laser, provides single mode, continuous wave, continuously tunable infrared light from 2.3 to 3.3 μm. A pulsed 2 × 0.01 cm slit nozzle and a multi-reflection cell [57] were used to increase the infrared absorption optical path length and the resolution. The infrared spectrum is obtained by recording the intensity of transmitted light with an InSb detector as the laser frequency is scanned. A mixture of 10% by volume methylamine in argon was expanded through the slit nozzle at a backing pressure of 100 kPa. A Viton-tipped piezoelectrically-driver plunger controls the flow of gas mixture from the reservoir to the channel. Two matched InSb detectors, one before and the other after the slit jet, were used to reduce the noise by baseline subtraction.

The residual Doppler width in the slit-jet is 0.0025 cm^{-1}. Relative wavenumber calibration of the recorded lines is achieved with a temperature-controlled sealed 150 MHz marker etalon with a precision of ~0.00025 cm^{-1} as judged by the standard deviation of combination loops involving a set of more intense infrared lines. Absolute wavenumber calibration is established by a fit of the marker etalon fringe positions to ethylene gas cell absorption lines [56] (standard deviation 0.0005 cm^{-1}). The important advantages of direct absorption spectroscopy are that a low power (~1 μ W) laser can be used and eigenstate-resolved spectra of jet-cooled molecules can be obtained [58].

A prominent drawback of direct absorption spectroscopy is that the signal relies on the relative attenuation of the laser power, results a sensitivity still limited by the intensity fluctuations of the laser source. Therefore, this technique is not applicable for measuring spectra of the weakest combination and overtone bands and of weakly perturbing levels.

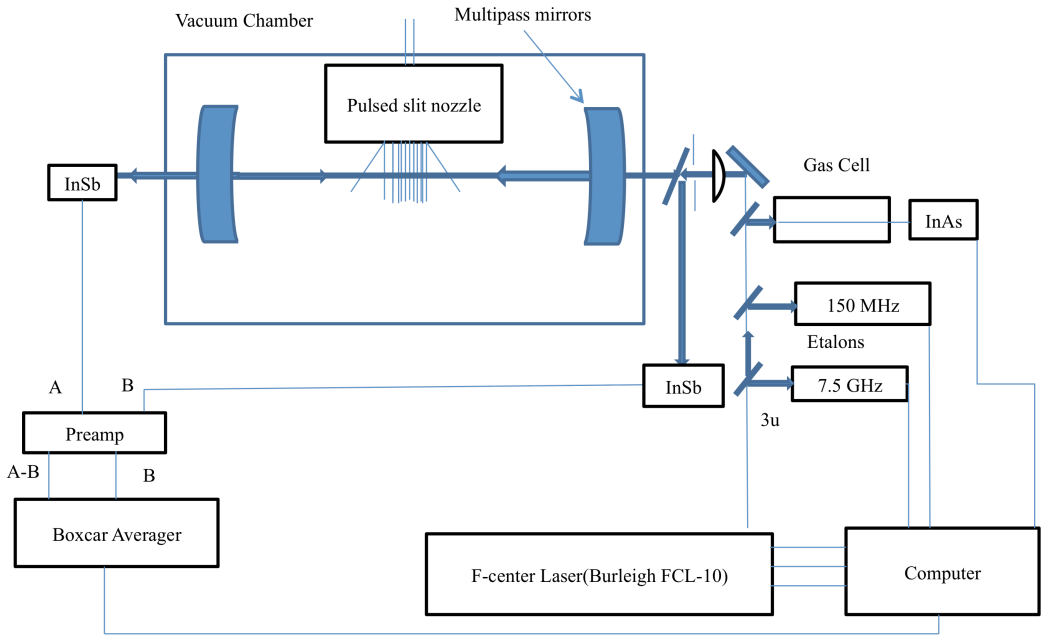

Figure 2.1 A schematic diagram for single resonance absorption apparatus extracted from Refs. [55, 56] and modified.

The direct absorption detection under sub-Doppler slit-jet conditions high-resolution infrared (IR) spectrum of methylamine in the ν_{11} CH-stretch region (2965–3005 cm^{-1}) is presented in Chapter III.

2.1.2 Cavity ring-down spectroscopy

Cavity ring-down spectroscopy (CRDS) is a more sophisticated, highly sensitive, laser-based technique for the measurement of absorption spectra [59]. This technique measures the rate of absorption of a light confined in a stable optical cavity formed by two highly reflective mirrors. The inserted laser beam is reflected back and forth and, each time the light is reflected, a small fraction leaks out leading to an exponential decay of the beam in the cavity. The decay time, τ, (ring-down time) of the cavity is determined by measuring the time dependence of the intensity of light leaking out the cavity. Since the laser used to fill the cavity with light is shut off before the decay measurements are made, the ringdown technique is completely insensitive to the intensity fluctuations of the light source. Light absorbed by the sample between the mirrors will increase the decay of light and hence reduce the ring-down time, τ. The molecular absorption coefficient, α, is directly linked to the ring-down time, τ, and thus, an absorption spectrum is obtained by plotting the cavity loss, 1/cτ, as a function of frequency, ν. The relationship between the time constant decay, τ, and absorption coefficient, α is given by the following expression [59] ,

$$\tau = \frac{d}{c(L - \alpha l)} \qquad (2.1)$$

where d is the cavity length, $L = (1 - R)$ represents the reflection loss for a cavity mirror of reflectivity R, and αl is the absorbance of the sample α times the sample length l. Such technology is highly delicate and applicable to making highly sensitive quantitative measurements of trace molecular gaseous samples [60] and to perform the kinetics studies on transient gaseous species. In CRDS technique, the ring-down time depends on

the mirror reflectivities. If the sample coats the surface of the mirror, this decreases the reflectivity and results a shorter ring-down time.

Pulsed lasers have been used as a light source in most of the CRDS techniques. Generally, these pulsed lasers have a substantial laser linewidth, which results in low spectral brightness (defined as power per unit frequency interval) and a very small fraction of the light entering the cavity. Further, the substantial linewidth of pulsed lasers results in multimode excitation and mode beating that prevents an accurate determination of the ring-down time, τ [60]. In order to overcome these drawbacks of CRDS, one can use a narrow-band tunable continuous wave (CW) laser source [59, 61], which ensures the excitation of one single axial and transverse mode (TEM_{00}) of the ring-down cavity thereby avoiding mode beating and the consequent uncertainties in the ring-down time, τ. A CW laser source also enables higher repetition rate and a better spectral resolution.

2.1.3 Continuous wave laser source PPLN-OPO

The present experimental setup (Figure 2.2) comprised of (i) a narrow bandwidth optical parametric oscillator (OPO) laser (Linous OS 4500, ~50 KHz bandwidth) which has a periodically-poled lithium niobate (PPLN) crystal equipped with 18 gratings, Nd: YAG pump laser (Innolight Mephisto 1200, 1064 nm, 1 Watt), and intra-cavity etalon, (ii) an acousto-optic modulator to switch the laser beam away from the cavity, (iii) a slit-jet vacuum chamber containing a ringdown cavity, (iv) two spectrum analyzers for laser diagnostics, and (v) beam-handling optics and data collection electronics.

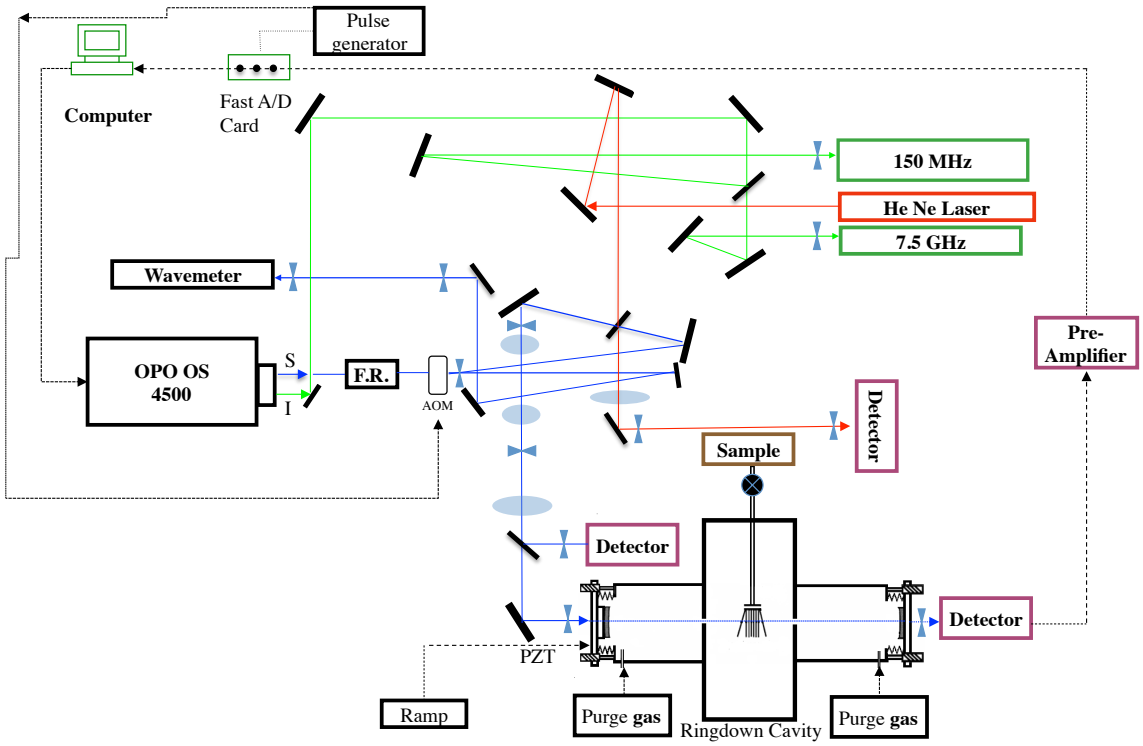

Figure 2. 2 Continuous-wave cavity ring-down experiment set up.

The OPO infrared laser produces two new beams, the signal (1.38-2.00 μm, ~ 50 mW) and idler beam(2.28-4.67 μm, ~ 100 mW). The idler beam (green line) is aligned through a Faraday rotor and splits into two fractions using the beam splitter. One fraction of the beam is directed into a 150 MHz marker etalon (Burleigh CFT100P) and another fraction is directed to a 7.5 GHz spectrum analyzer (Burleigh FCL975), which are the diagnostic tools for relative frequency calibration. The signal beam (blue line) is aligned through a second Faraday rotor (optics for research IO-05-1650/1770-VLP) and is directed through infrared acousto-optic modulator (AOM, IntraAction crop, model ACM-1002AA23). The first-order diffracted beam (~78%) from the AOM is mode-matched to TEM_{00} of the near-confocal ring-down cavity (98.98 cm) with the aid of first two lenses together with a third lens and a pinhole. The transmitted signal (leak out) from the ring-

down cavity is registered on an InSb detector. A very small fraction (~5%) of the first order-diffracted beam is aligned into the second InSb detector before the ring-down cavity to monitor the laser power. The zeroth-order undiffracted beam form the AOM is aligned into a wavemeter in which the reference frequency of the experiment is measured. The experiment is equipped with CW-slit jet nozzle, which changes the dimensionality of the expansion, and ensures higher repetition rate.

The PPLN OPO has (i) broader tunability (1.4 to 4.6 microns), (ii) narrower bandwidth (50 kHz), and (iii) produce more output power as comparable to the external cavity diode laser. The practical tuning of the PPLN OPO however is difficult. Coarse tuning is achieved by selecting one of the 18 gratings and temperature tuning the PPLN crystal. Then tuning of mode hop steps of OPO cavity can be controlled by a combination angle-tuning of the intra-cavity etalon (via a galvanometer) while synchronously scanning the temperature of the PPLN crystal. The finest tuning is accomplished by piezo-scanning the OPO cavity length.

To achieve rapid extended scans, CW-PPLN-OPO is the most convenient technique in which the scanning involves interlaced mode-hop scans. Each cavity ring-down is an independent measure of the absorption strength, which means that interlaced scans can be assembled into a high-resolution spectrum. In this technique, the laser wavenumber can be measured precisely at every mode-hop and repositioned precisely for successive mode-hop scans, which help to get high-sensitivity high-resolution spectra of jet-cooled molecules in a short period of time. These capabilities of successive mode of scanning are advantageous for extended frequency ranges, signal averaging, multiple sample conditions and multiple species.

However, this CW-PPLN-OPO laser has the following drawbacks:

(i) Signal wavelength increases rapidly as the amplification bandwidth of the parametric process increases, which causes the sudden frequency jumps relative to the free spectral range of the etalon.

(ii). It is not easily scanable over an extended range because both the signal wave and the pump wave are resonating in the OPO cavity. For example, if we tune OPO mode-hops (450 MHz) by scanning intra-cavity etalon (0.5 mm coated with 50% of YAG), we found that there are holes (~ 2.9 cm^{-1}) in the scan over a free spectral range (FSR) of an etalon, (Figure 2.3).

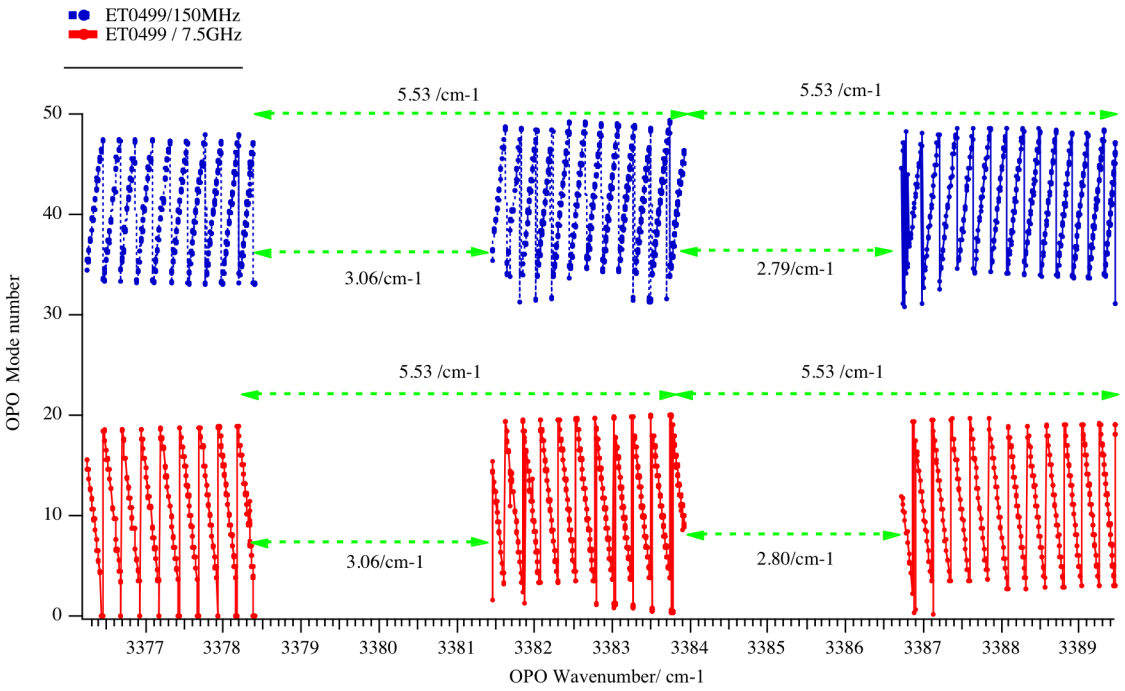

Figure 2. 3 OPO mode hops (450 MHz and 7.5 GHz) as a function of OPO frequency. The OPO frequency is tuned by scanning the intra-cavity etalon. The holes and free spectral range of the etalon is shown by double headed green arrows.

2.1.4 Data acquisition and ring-down time

Once the transmitted signal from the ring-down cavity is registered in InSb detector, it is sent through a voltage pre-amplifier (Standard Research System, Model SR 560). One of the amplified signal output is digitized using a 16 bit analog/digital (A/D) (Gaze, CompuScope 1012) with a sampling rate of 10 Ms/s. The other amplified signal output is used to trigger a pulse delay generator (AvTech Model AV-1020-C) that in turn triggers the ring down signal via AOM driver. When the detector signal reaches a suitable trigger level, it triggers a ring-down transient by simultaneously switching off the AOM and triggering the digitization of a ring-down signal (Figure 2.4) with the aid of the LABVIEW 8 program. A flow chat of all subroutines is shown in Appendix A and the detailed LABVIEW block diagram and front panel are given in Appendices B, and C.

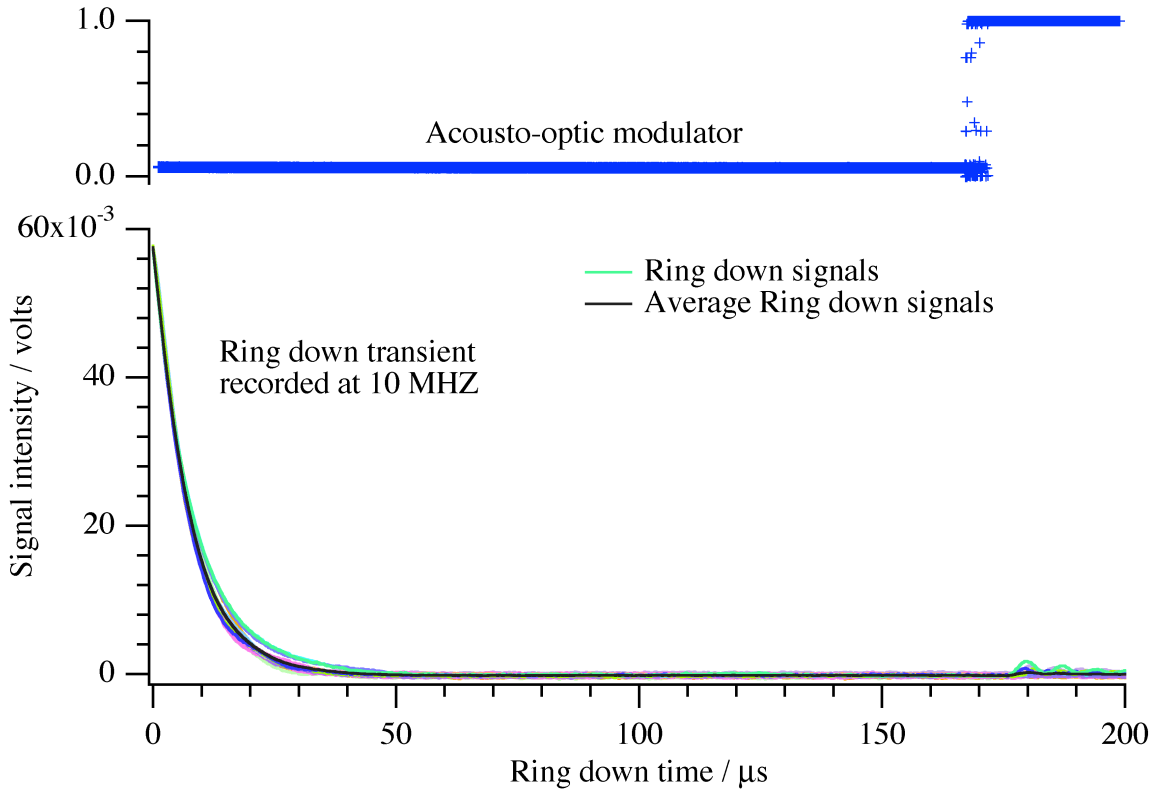

Figure 2. 4 The triggering of the ring-down signals by acousto-optic modulator.

About 114 shots of ring-down signals (Figue 2.5) were collected using the LABVIEW 8 program. The least square-fitting algorithm is used to fit 96 ring-down data points. The remaining 18 data points are not included in the fit because they are more scattered and hence named as outliers (Figure 2.5). The observed fitted ring-down time (τ) is 7.299 ± 0.015 µs, at 1.55 µm wavelength of laser, which is far below the expected values. Some of the possible reasons for getting a very short ring-down time might be either (i) some of the dust particles or oil strain coated on the cavity mirrors, since the sampling rate and data collection time are directly related on the reflectivity of the cavity ring-down mirrors, or (ii) laser beam in the cavity could not be well aligned and mode-matched to the cavity.

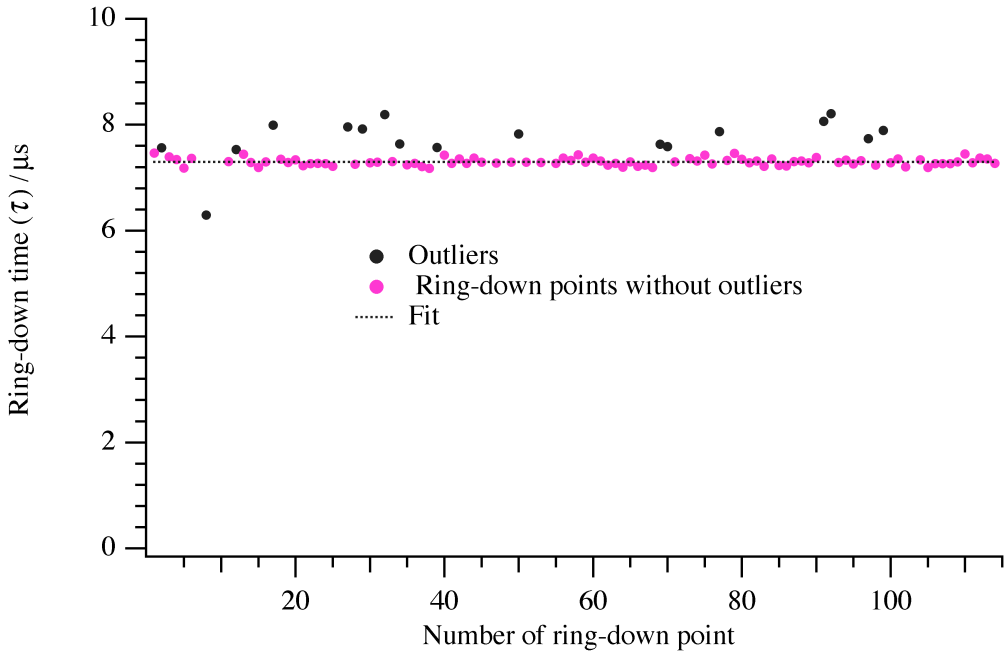

Figure 2. 5 The ring-down time (τ) is plotted for each sequential ring-down data point.

2.2 Synchrotron based Fourier transform infrared (FTIR) spectroscopy

Synchrotron based FTIR is advantageous in the far-infrared region for detecting the weak absorptions of the trace sample with very low concentration or weak combination and overtone bands. When synchrotron radiation is used as a source, it offers the following advantages over conventional infrared sources [62-64]:

1. Synchrotron sources produce much brighter beam than conventional sources. The brightness of the source is directly related to the signal to noise ratio (S/N) of the individual scans under experimental conditions. It means that the S/N of the recorded spectra can be increased with the source brightness (brilliance), which is defined as,

$$Brilliance = \frac{photons/\sec ond}{(mrad)^2 (mm^2 sourcearea)(band\ width)} \quad ,$$

The brightness of the synchrotron radiation is an order of magnitude higher than conventional sources.

2. Synchrotron sources do not require any external calibration with respect to a radiometric standard, hence referred to as absolute sources because of their direct dependence on the storage ring beam current, which can be measured accurately.
3. Synchrotron radiations can be used as a radiation sources over a broad spectral region (12-1000 cm^{-1}), hence referred as broad-band sources (i.e. have wide spectral bandwidth).
4. Synchrotron radiation is highly polarized in the plane of the storage ring and has well-defined incidence angles that ensure a suitable source for polarizing FTIR spectrometers.

In spite of these advantages over the conventional source, synchrotron based FTIR spectroscopy suffers from the following difficulties [65-67]:

1. The recorded spectra become more complicated for analysis and interpretation because of the presence of some of the channel spectra in it. The channel spectra are the result of extra interferences between the light beams inside the FTIR spectrometer. These extra interferences produce additional interference patterns called “spikes” that have a different zero path difference (ZPD) than the main spectrometer ZPD. These spikes in the interferogram space will produce a sinusoidal wave in the spectrum space. Upon Fourier transformation, these spikes transform into periodic intensity changes in the baseline of the observed spectrum.

2. Since synchrotron also produces very high-energy photon beams (e.g. X-rays), it is very hard to handle this power using optical elements.
3. A number of steering mirrors need to be aligned in order to guide the beam properly from the source into the spectrometer that increases chance of losing some amount of power and also increases the number of possible sources for getting the channeling spectra. Thus, it may be complicated to trace and analyze the sources of channeling. The optical layout at the Canadian Light Source (CLS) far-infrared beamline has been previously reported in Figure 1 of Ref. [68].
4. Since synchrotron facilities operate in decay mode, the new current injection is made when the initial storage current decays to near half of its value [69]. The time interval between the current injections is generally 8 to 12 hours. During this long period between injections, the decaying current and radiation intensity can produce thermal instabilities in the beamline optics, which could be a responsible source to give rise in the spikes in the interferogram.

2.2.1. Experimental setup

The experimental set-up for the far-infrared beam line at the CLS is shown in Figure 2.6. A detailed description of the Far-Infrared (Far-IR) and its capability has been previously given elsewhere [70-76], therefore, only a brief summary will be given here.

The synchrotron infrared radiation (beam) is alligned to the sample compartment of the Bruker IFS 125HR spectrometer, (nominal resolution of 0.00096cm^{-1} and a sampling rate of 80kHz), using a 1.15mm aperture, a wedged KBr window and a series of flat and ellipsoidal mirrors. The synchrotron radiation, which is modulated by the

spectrometer, is then passed through a 72 m multi-pass cell containing the gas sample. The gas pressure is monitored using 0-1000 torr Baratron MKS gauge. A T-type thermocouple, which is mounted inside the cell monitors the cell temperature. Finally, the radiation is recorded by a cooled Ge:Cu detector mounted with an optical filter.

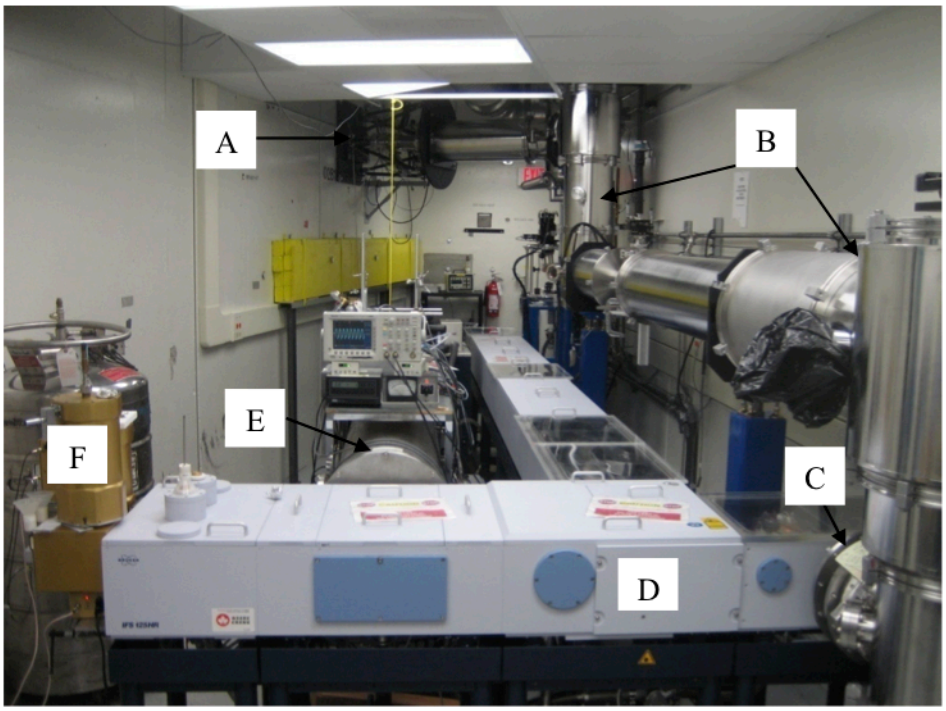

Figure 2. 6 Far infrared beamline experimental set-up at CLS showing the synchrotron port (A), transfer optics (B), spectrometer port (C), Bruker optics IFS125 HR spectrometer (D), the multi-pass cell (E), and detector (F) [77].

The recorded synchrotron based FTIR spectra for the four different bands of nitromethane, namely: NO_2 in-plane rock (475.2 cm^{-1}), NO_2 out-of-plane rock (604.9 cm^{-1}), NO_2 symmetric bend (657.1 cm^{-1}), and CN stretch (917.2 cm^{-1}), are shown in Figure 2.7, the detailed analysis and interpretation of the NO_2 in-plane rock (475.2 cm^{-1}) band are presented in Chapter V.

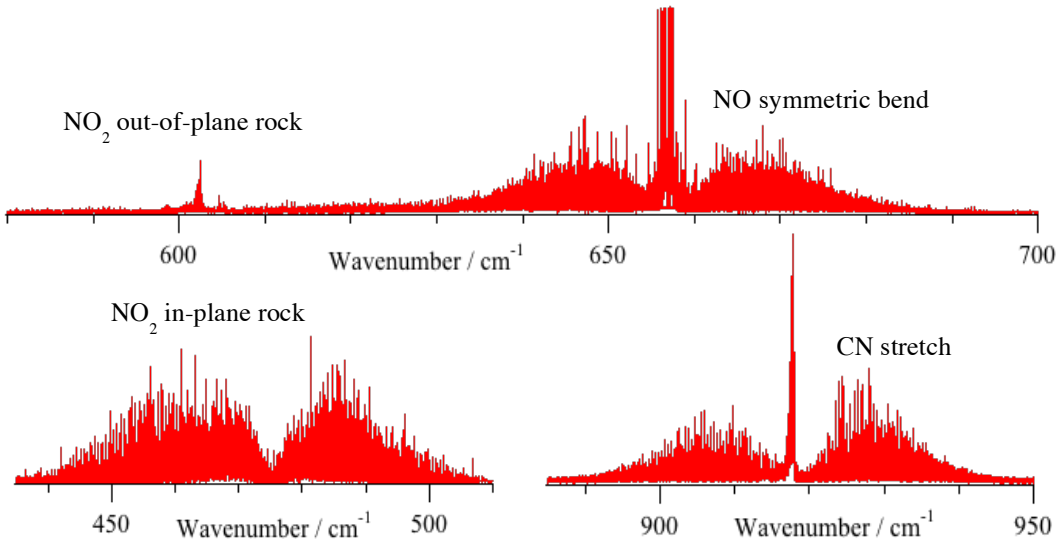

Figure 2.7 High-resolution synchrotron based FTIR spectra of nitromethane recorded at CLS.

2.2.2. Synchrotron radiation safety

Radiation safety of synchrotron radiation beamline is critical important. The following are the summary of safety instructions must be compiled to avoid any hazard due to synchrotron radiation [77]:

1. Any contact of skin with radiation should be avoided.
2. Safety glasses should be worn.
3. Radioactive materials shall be stored in a safe and secured place.
4. The radiation dosimeter should be worn all the times to estimate the radiation dose deposited in an individual wearing the device.

CHAPTER III

NOVEL PATTERNS OF TORSION-INVERSION-ROTATION ENERGY LEVELS IN THE ν_{11} ASYMMETRIC CH-STRETCH SPECTRUM OF METHYLAMINE

The content of this chapter has been published as "Novel Patterns of Torsion- Inversion-Rotation Energy Levels in the ν_{11} Asymmetric CH-Stretch Spectrum of Methylamine" by Mahesh B Dawadi, C. Michael Lindsay, Andrei Chirokolava, David S. Perry and Li-Hong Xu; [*M.B.Dawadi, C.M. Lindsay, A. Chirokolava, D.S. Perry, L.-H Xu, J.Chem. Phys.* ***138*** *(10), 104305 (2013)*]. *It is reproduced here with only the minimal editing necessary to confirm to the format and style of this dissertation.*

The high-resolution infrared spectrum of methylamine (CH_3NH_2) has been recorded using slit-jet direct absorption spectroscopy in the ν_{11} CH-stretch region (2965–3005 cm^{-1}) with a resolution of 0.0025 cm^{-1}. The 621 lines assigned by ground state combination differences represent 27 substates with $|K'| \leq 2$ for the A, B, E_1 and E_2 symmetries. The spectrum of CH_3NH_2 is complicated by torsion and inversion tunneling connecting six equivalent minima. The upper states $K' = 0, \pm 1$ for E_1 and E_2 are substantially perturbed by "dark" states. The result in the spectrum is multiplets of two or three states with mixed bright/dark character.

The analysis of the spectrum reveals two qualitative differences in the energy level pattern relative to the vibrational ground state and relative to available data on the lower frequency vibrations (NH_2 wag and CN stretch). First at $J' = 0$, there is a different ordering of the levels connected by torsion-inversion tunneling. Second, the low-J splittings indicative of torsion-rotation coupling are greatly reduced in the ν_{11} excited state relative to the vibrational ground state for both the E_1 and E_2 species, suggesting the partial suppression of torsional tunneling in the ν_{11} CH-stretch excited state.

3.1 Introduction

CH_3NH_2 is a prototypical molecule with two large amplitude degrees of freedom: the internal rotation of the methyl (CH_3) group (ν_{15} torsional motion) and the inversion motion of the hydrogen atoms of the amine (NH_2) group (ν_9 wagging motion) [78-81]. The two large amplitude vibrations (LAV) are coupled to each other and to the small amplitude vibrations (SAV) [80-83]. These couplings are reflected in the energy level structure and impact the patterns of transitions observed in microwave and infrared spectra.

The potential energy surface for the ground electronic state of methylamine has six equivalent minima connected by torsional and inversion tunneling. The tunneling dynamics can be understood in terms of the torsional and inversion tunneling parameters, $h_{3v} = -0.083$ cm^{-1} and $h_{2v} = -0.052$ cm^{-1} respectively [80, 84-86]. The order of the energy levels in the ground state tunneling multiplet (at $K''=0$, $J''=0$) is $A_1 < B_1 < E_1 < E_2$ [87]. Since the C_s point group designations are not adequate for labeling the resolved tunneling states, these vibrational symmetry species refer to irreducible representations in the G_{12}

molecular symmetry group [19]. For $K'' > 0$, the term values show a sinusoidal variation when plotted as K''-reduced energies (Figure 3 of Ref. [88]).

In vibrationally excited states where one of the LAV is excited, a change in the ordering of the levels in the tunneling multiplet is possible. For example in the ν_9 wagging excited vibration of methylamine, the inversion tunneling parameter increases in magnitude by about 40× to $h_{2v} = -1.93$ cm^{-1} [89] while the torsional tunneling parameter increases more modestly to $h_{3v} = -0.152$ cm^{-1}. The result [89, 90] is the tunneling ordering for the wagging excited state: $A_1 < E_1 < E_2 < B_1$. Other examples of LAV excitation producing changes in the ordering of tunneling doublets are the torsionally excited states of S_1 acetaldehyde [91] and the excited wagging state of NH_2D [92].

In vibrationally excited states where one of the SAV is excited, three kinds of changes in the patterns of the torsion-inversion-rotation energy level structure might be observed. First, quantitative changes in the tunneling spacings and accompanying changes in the periodic torsion-rotation structure variation with K' might be observed while maintaining the "normal" ordering of the torsion-inversion tunneling multiplets. An example of such a case is the CN stretch fundamental band of methylamine [88, 93] where both the ordering of the tunneling levels and the pattern of variation with K' is qualitatively the same as in the ground state. The K'-dependent amplitude associated with the inversion splitting is very close to the ground state value, but the amplitude associated with torsional tunneling is increased by 50% indicating a lower effective torsional barrier in the CN stretch excited state [88]. This case can be understood in terms of an approximate adiabatic separation of the LAV from the SAV, in which the motion in the (slow) LAV is considered to occur in an effective potential determined by

the (fast) SAV. Thus, the effective torsional or inversion barrier can be different in the SAV vibrationally excited state, resulting in a quantitative change in the tunneling splittings. For example, such an adiabatic treatment of the torsional barrier has been applied to the ν_1 OH and ν_3 symmetric CH stretch vibrationally excited states of methanol [31, 32, 94]. Typically, the same form of the spectroscopic Hamiltonian can be used in this case to fit both ground state and excited state spectra.

The second kind of change that might occur when a SAV is excited is a qualitatively different ordering of the tunneling levels. Until the present work, such a case has not been observed in methylamine. However, in methanol, the asymmetric CH stretches, ν_2 and ν_9, [28, 55, 95, 96] and a number of other fundamental bands [28, 97] have been found to have inverted torsional tunneling splittings relative to the ground state. Fehrensen *et al*.[32] provided a systematic explanation for the inverted torsional tunneling splittings in methanol by including the concept of geometric phase in their adiabatic treatment and solving for torsional wavefunctions with 4π boundary conditions. This invokes the application of geometric phase in the adiabatic separation of the LAV and SAV. A number of other theoretical approaches have also been applied to the inverted tunneling in methanol [20, 28, 97, 98].

The third kind of change results from "accidental" perturbations by nearly resonant overtone or combination vibrations. Perturbations may shift some of the levels in a tunneling multiplet by larger amounts or in different directions than others. Such "contamination" [99] of the tunneling pattern results in splittings that are not characteristic of an effective barrier in the large amplitude coordinate. In fact, as has been shown for three bands in the fingerprint region (900-1050 cm^{-1}) of propene, the

relative perturbation shift may be large enough to change the sign of the tunneling splitting [99]. In general, one finds that perturbations occur in the same spectra as the systematic effects discussed above [88, 89, 93].

This chapter reports the high-resolution infrared spectrum of the ν_{11} asymmetric CH-stretch band (2965-3005 cm^{-1}) of jet-cooled methylamine, including assignments, a perturbation analysis, and plots of K'-reduced term values. The impact of the asymmetric CH stretch excitation on the torsion-inversion-rotational energy level structure is explored.

3.2 Results and discussion

An overview of the assigned and unassigned spectrum of the ν_{11} asymmetric CH-stretch band, along with the data analysis and interpretation are presented in the following sections.

3.2.1 Overview of the spectrum

The high resolution infrared spectrum in the ν_{11} asymmetric CH-stretch band is shown in Figure 3.1 and the transition wavenumbers along with the relative intensities are tabulated in Appendix D. The observed spectrum has 1543 lines, and most above 2985 cm^{-1} are assigned. The lower wavenumber part of the spectrum has many unassigned lines, which may belong to the ν_2 asymmetric CH-stretch band and also to perturbing bands [95]. The equally spaced Q-branches clearly evident in Figure 3.1 are the signature of $\Delta K = \pm 1$ selection rules in a near-prolate asymmetric rotor. On close inspection, each of these Q-branches is a stack of sub-Q-branches corresponding to the various symmetry species in the G_{12} molecular symmetry group.

3.2.2 Symmetry, selection rules and spectroscopic background

This paper follows the notation of Ohashi and Hougen [79]. The symmetry species in the G_{12} molecular symmetry group are {A_1, A_2, B_1, B_2, E_1, and E_2} [79] and are respectively equivalent to {A_1', A_2', A_2'', A_1'', E'', and E'} [19]. The traditional notation {A_s, A_a, E_s, and E_a} corresponds to {A, B, E_1, and E_2},[88, 100] where the 1-2 distinction in the non-degenerate species has been suppressed. The A, B, E_1, and E_2 torsion-wagging-rotation species combine with different nuclear spin combinations that have their respective nuclear spin statistical weights [79, 81, 88, 100].

In the vibrational ground state, the species of the torsion-wagging-rotation states are ${}^{twr}\Gamma'' = A_1+B_1+ E_1+ E_2$ for $K'' = 0$, and $A_1+A_2+B_1+B_2+2E_1+2E_2$ for $K''\neq 0$ [79]. Note that the symmetries of basis functions for the individual degrees of freedom may not be unique in permutation-inversion group theory; however, the species of the observable quantum states, which represent the combined torsion-wagging-rotation motion, are unique. For example, different authors [19, 79] employ different species in G_{12} for the rigid rotor basis functions.

Likewise, the symmetries of the vibrational normal modes are not uniquely determined in the presence of large-amplitude motion [19, 101]. In the usual spectroscopic convention, the normal modes of methylamine are categorized and numbered in the C_S point group as it applies to the global minimum-energy conformation. The two asymmetric CH stretches are ν_2 and ν_{11}, which are A′ and A″ respectively in C_S. Of these, the fundamental ν_{11} is higher in frequency [102, 103] and is the subject of this work. In the presence of large-amplitude motion, there are multiple choices for the symmetry species of the normal modes in the G_{12} molecular symmetry group [19, 101].

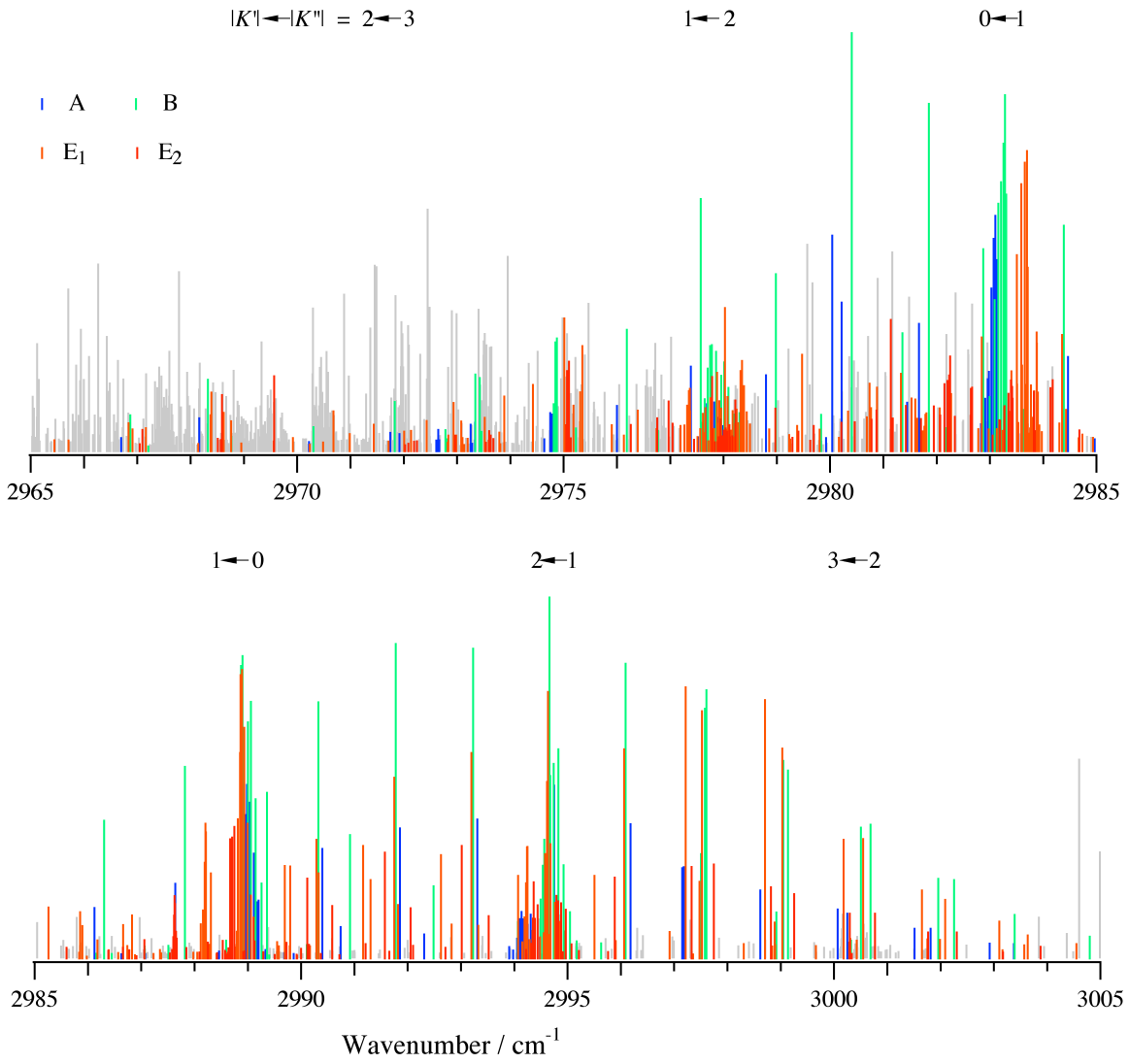

Figure 3. 1 A stick representation of the slit-jet infrared spectrum of CH_3NH_2 in the ν_{11} CH-stretch region (2965-3005 cm-1), with $|K'| \leftarrow |K''|$ transitions labeled. The assigned transitions for A, B, E_1 & E_2 species are colored with blue, green, orange and red respectively. The grey lines indicate all unassigned transitions in the observed spectrum.

The choices for the pair of asymmetric CH stretches ν_2 and ν_{11} are A_1+A_2, B_1+B_2, E_1, or E_2 (Table 15-4 of Ref. [19]). Following Bunker and Jensen's analysis for nitromethane (Eq. 15-65 of Ref. [19]), we identify the second choice, B_1 for ν_2 and B_2 for

ν_{11}, as the "best" choice for methylamine. Accordingly, the species of the torsion-wagging tunneling multiplet at $J' = 0$ of the ν_{11} vibrationally excited state are ${}^{twrv}\Gamma' = B_2 \otimes [A_1 + B_1 + E_1 + E_2] = [B_2 + A_2 + E_1 + E_2]$.

CH_3NH_2 is a slightly asymmetric prolate top with an asymmetry parameter $\kappa = -0.97$). When symmetric top notation is used, we identify $|K| \equiv K_a$. The transition dipole moment of the ν_{11} band is in the direction of the *b*-rotational axis, that is, parallel to a line connecting the two-amine hydrogens. The rigid near-prolate asymmetric rotor rotational selection rules for *b*-type transitions are $\Delta J = 0, \pm 1$ (except $J = 0 \nleftrightarrow J = 0$); $\Delta K_a = \pm 1$ and $\Delta K_c = \pm 1, \pm 3$. In the G_{12} group, allowed transitions in methylamine[19, 104] obey ${}^{twrv}\Gamma' \otimes {}^{twrv}\Gamma'' \otimes A_2' \supset A_1$; where ${}^{twrv}\Gamma'$ and ${}^{twrv}\Gamma''$ are the torsion-wagging-rotation-vibration species of methylamine in the excited and ground states, respectively. Thus, $A_1 \leftrightarrow A_2$; $B_1 \leftrightarrow B_2$; $E_1 \leftrightarrow E_1$; $E_2 \leftrightarrow E_2$ [79].

The non-rigidity of methylamine gives rise to further complications in the rotational selection rules [105]. For the ${}^{twrv}\Gamma = A$ and B species, the rotational wavefunctions are well described as rigid asymmetric rotor functions, and these species obey *b*-type rotational selection rules as above. As usual, the asymmetric rotor Hamiltonian has four blocks according to the Viergruppe symmetries of the Wang functions [104]

$$\left|JK\gamma\right\rangle = \frac{1}{\sqrt{2}}\left(\left|JK\right\rangle + (-1)^{\gamma}\left|J,-K\right\rangle\right) \qquad (3.1)$$

where $\gamma = 0$ or 1 for $K > 0$ and $\left|JK\gamma\right\rangle = \left|JK\right\rangle$ for $K = 0$. The symmetric rotor functions are notated as $\left|JK\right\rangle$ and $\left|J,-K\right\rangle$ where the quantum number M has been suppressed. In the present near-prolate asymmetric rotor limit, each rotational wavefunction for the A and B species is well-approximated by one of the Wang functions. For the E_1 and E_2 species,

the rotational wavefunctions are linear combinations of the $\gamma = 0$ and 1 Wang functions for a given K, with the result that "extra" rotational transitions appear in the spectrum [105]. In the context of the Wang basis, these "extra" transitions appear to have *c*-type selection rules, but can alternatively be interpreted as *b*-type transitions between states of mixed rotational symmetry. A symmetric rotor-like notation with a signed value of K has been used in the literature for the E species, [78, 106] and the levels are labeled E_{1+1} and E_{2+1} for $K \geq 0$, and E_{1-1} and E_{2-1} for $K < 0$. In this symmetric rotor basis, there are "extra" symmetric rotor-forbidden ($\Delta K = \pm 3$) transitions that arise from the mixed rotational character (e.g., $E_{1+1} \leftrightarrow E_{1-1}$) of the $|K|=1$ levels. Such transitions have been reported in the NH_2 wagging band of methylamine [89].

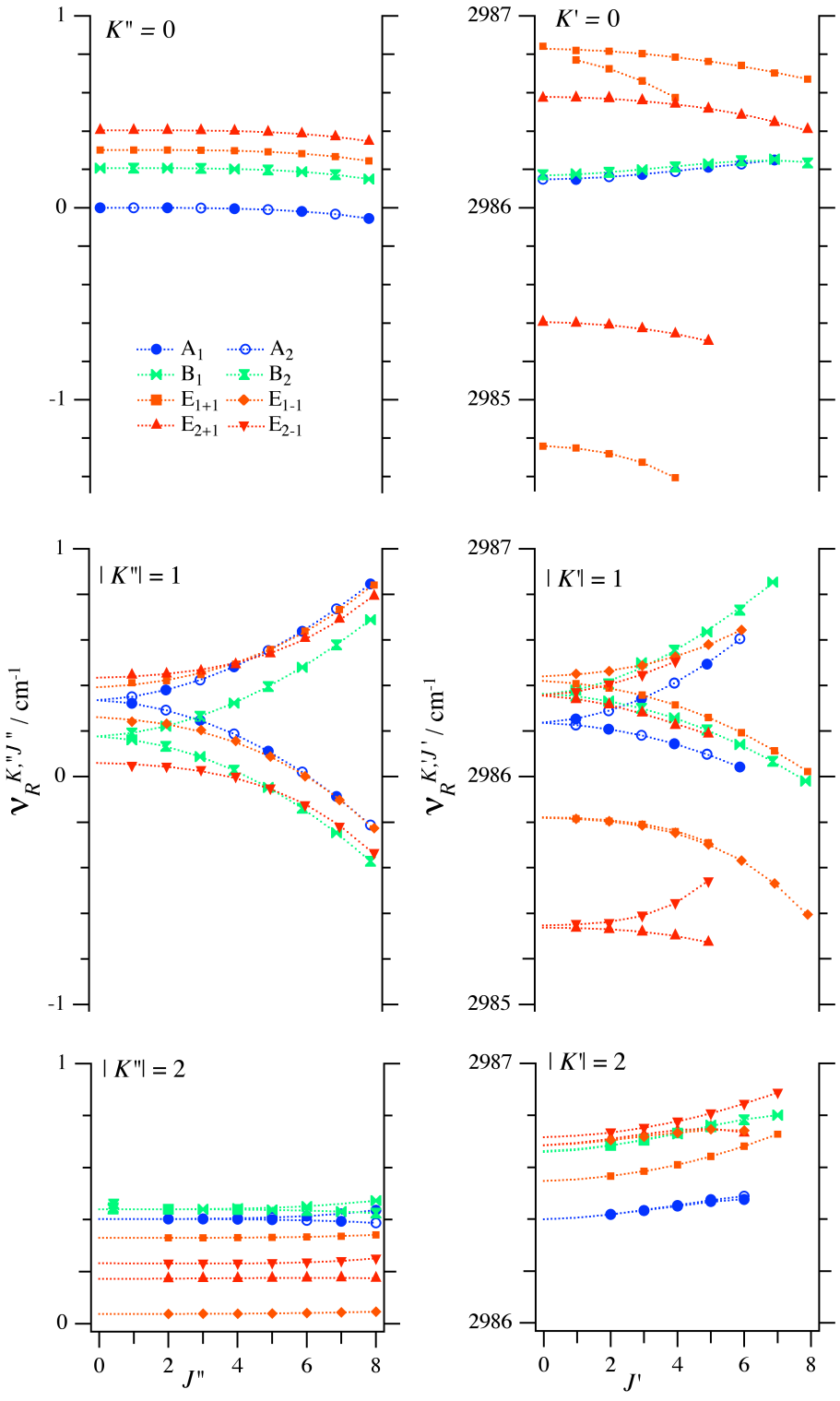

Figure 3.2 Reduced term values of the ground (a) and excited (b) vibrational states plotted as a function of angular momentum quantum number (J). The plotted term values

are $\nu_R^{K,J} = \nu^{K,J} - \frac{1}{2}(B''+C'')J(J+1) - [A''-\frac{1}{2}(B''+C'')]\,K^2$, where the ground state rotational constants are from Ref. ([80, 103]). Perturbations in the E_1 and E_2 species result in two or three upper state levels with the same J', K', Γ' assignment, and their relative intensities are indicated approximately by the area of the markers.

For the vibrational ground state of methylamine, the splitting patterns of the rotational levels are shown in Figure 3.2(a). For the A and B species, the asymmetry splittings behave as expected [107] for a rigid near-prolate asymmetric rotor, approaching 0 as $J''\rightarrow 0$. For the E_1 and E_2 species, the $K'' = 1$ splittings approach the rigid asymmetric rotor limit for large J'' (≈7-8), but do not approach 0 as $J''\rightarrow 0$. The limiting splitting at $J''=0$ is a measure of the symmetric rotor torsion-rotation coupling. Thus, these J-dependent splittings might be termed torsion-rotation-asymmetry splittings. These splittings reflect a transition of the $K''=1$ rotational wavefunctions from the symmetric rotor limit at low J'' to the asymmetric rotor limit at high J''. At $K''=2$, asymmetry in this near-prolate top contributes less to the splittings, and all of the plotted J'' values are close to the symmetric rotor limit.

3.2.3 Assignments

The pattern of the torsion-wagging-rotation levels in the vibrational upper state of the ν_{11} CH-stretch fundamental band is not known a priori. Coupling of the large amplitude motions to the asymmetric CH-stretch may affect the K-dependent torsion-inversion splittings and also the J-dependent torsion-rotation-asymmetry splittings. Further, accidental perturbations expected for a vibrationally excited state will cause

frequency shifts and result in additional observable transitions. Accordingly, in the present work, assignments are based on ground state combination differences [78, 106] using the known ground state term values supplied by N. Ohashi [103]. With the selection rules, $\Delta J = 0, \pm1$, $\Delta K = \pm1, \pm3$, there are up to twelve possible transitions reaching particular J', K', $^{twrv}\Gamma'$ upper states, of which a maximum of eight have been assigned in this work. The only $\Delta K = \pm3$ transitions observed are those "extra" transitions that are expected from the mixed rotational character of the $|K|=1$ levels. The precision of ~0.00025 cm^{-1} in these combination loops provides considerable confidence in the assignments. In total, 621 lines out of 1543-recorded lines were assigned and are tabulated in Appendices E, F, G, and H.

Table 3.1 The numbers of symmetric-rotor allowed ($\Delta K = \pm1$) and forbidden ($\Delta K = \pm3$) transitions assigned for E_1 and E_2 species in the methylamine ν_{11} band.

$\|K'\| \leftarrow \|K''\|$	$1 \leftarrow 0, 2$		$0, 2 \leftarrow 1$		$2 \leftarrow 3$
$^{twrv}\Gamma'$	$\Delta K = \pm1$	$\Delta K = \pm 3$	$\Delta K = \pm1$	$\Delta K = \pm 3$ [a]	$\Delta K = \pm1$
$E_{1\,-1}$	39	8	19	9	6
E_{1+1}	69	10	81	10	6
E_{2-1}	26	8	14	2	6
E_{2+1}	34	10	69	3	2

[a] "Extra" symmetric rotor-forbidden transitions that arise from the mixed ($E_{1+1} \leftrightarrow E_{1-1}$ or $E_{2+1} \leftrightarrow E_{2-1}$) rotational character of the $|K|=1$ levels [105].

Table 3.1 summarizes the number of symmetric-rotor allowed and forbidden transitions assigned for the degenerate species. The transitions of the E_1 and E_2 species

for K′ = 0, +1, -1 are perturbed (Table 3.2). Because of the challenges posed by numerous perturbations and because of the lack of a torsion-inversion-rotation Hamiltonian suitable for the CH-stretch excited state, a detailed global fit of the observed transitions has not been attempted.

3.2.4 Reduced term values

For the purpose of visualizing the trends of the state energies, it is convenient to represent them as reduced term values from which the rigid symmetric rotor part of the energy has been subtracted. The individual rotational levels of the upper and lower vibrational states are thus represented as reduced term values in Figure 3.2. Vibrational substates are specified by the combination of the *K* rotational quantum number and the symmetry species. The computation of reduced substate term values is explained in the next paragraph.

The upper state term values ($\nu^{K',J'}$) of the ν_{11} CH-stretch are obtained by adding the relevant ground state term values to the wavenumber of each observed transition. Then, the upper state term values were fit to the expression,

$$\nu^{K',J'} = \nu_0^{K'} + B_{eff}^{K'} J'(J'+1) - D_{eff}^{K'} J'(J'+1)^2, \qquad (3.2)$$

where B_{eff} and D_{eff} are effective rotational and effective centrifugal distortion constants respectively. The resulting substate origins $\nu_O^{K'}$ are converted to reduced substate term values $\nu_R^{K'}$ by subtracting the remaining symmetric-rigid-rotor energy,

$$\nu_R^{K'} = \nu_0^{K'} - [A'' - \frac{(B''+C'')}{2}]K'^2. \qquad (3.3)$$

The excited substate origins ($\nu_o^{K'}$) and reduced term values ($\nu_R^{K'}$) are listed in Table 3.2.

Table 3.2 Substate origins, reduced substate term values, and effective rotational constants [a].

Substate identifiers[b]	$\|K'\|$	${}^{twrv}\Gamma'$	$\nu_0^{K'}$ cm^{-1}	B_{eff} cm^{-1}	D_{eff} 10^{-6} cm^{-1}	$\nu_R^{K'}$ cm^{-1}	$\sum I^{K'}$
100	0	A	2986.146(1)	0.7418(2)	10(3)	2986.147	168
200	0	B	2986.168(2)	0.7424(3)	27(4)	2986.168	368
[c]300	0	E_{1+1}	2986.791(2)	0.7282(4)	-18(2)	2986.792	64
[c]301	0	E_{1+1}	2986.827(4)	0.7374(3)	0.89(41)	2986.828	259
[c]302	0	E_{1+1}	2984.758(2)	0.7339(6)	13(2)	2984.758	46
[c]500	0	E_{2+1}	2985.405(1)	0.7368(1)	24(1)	2985.405	97
[c]501	0	E_{2+1}	2986.578(1)	0.7377(3)	96(12)	2986.579	96
110	1	A	2988.928(1)	0.7484(4)	-31(10)	2986.227	89
110	1	A	2988.926(1)	0.7347(1)	2.3(10)	2986.225	123
210	1	B	2989.060(1)	0.7339(1)	0.4(4)	2986.359	320
210	1	B	2989.055(2)	0.7501(20)	25(35)	2986.354	185
[c]310	1	E_{1+1}	2989.121(1)	0.7343(1)	5.4(10)	2986.419	244
[c]311	1	E_{1+1}	2988.521(1)	0.7371(1)	49(1)	2985.819	171
[c]410	1	E_{1-1}	2989.141(2)	0.7433(3)	-24(6)	2986.439	224
[c]411	1	E_{1-1}	2988.523(3)	0.7378(4)	66(11)	2985.821	25
[c]510	1	E_{2+1}	2989.056(5)	0.7324(8)	-46(26)	2986.269	104
[c]511	1	E_{2+1}	2988.038(1)	0.7384(2)	38(4)	2985.337	69
[c]610	1	E_{2-1}	2989.058(3)	0.7472(6)	19(26)	2986.357	57
[c]611	1	E_{2-1}	2988.049(6)	0.7409(10)	-17(1)	2985.347	22
120	2	A	2997.204(2)	0.7427(3)	33(5)	2986.399	70
120	2	A	2997.204(3)	0.7428(4)	28(7)	2986.399	37
220	2	B	2997.464(2)	0.7438(2)	20(3)	2986.658	134
220	2	B	2997.468(1)	0.7432(1)	32(4)	2986.663	137
320	2	E_{1+1}	2997.352(1)	0.7425(1)	-0.27(7)	2986.547	146
420	2	E_{1-1}	2997.489(3)	0.7429(3)	49(5)	2986.684	146
520	2	E_{2+1}	2997.490(9)	0.7440(9)	80(21)	2986.685	53
620	2	E_{2-1}	2997.521(1)	0.7425(1)	-0.94(14)	2986.716	63

[a] Substate origins ($\nu_0^{K'}$) and reduced substate term values ($\nu_R^{K'}$) are related by Eq. (3.3). For $\nu_0^{K'}$, B_{eff} and D_{eff} the uncertainties are given as two standard deviations of the fit (in parentheses) in units of last digit. $\sum I^{K'}$ is the sum of the intensities for each substate.

[b] The substate identifiers are used in the detailed line lists in the Appendix E. The first digit of substate identifier encodes the symmetry, ${}^{twrv}\Gamma'$; the second digit is K', and the last digit distinguishes the levels in an interaction doublet or triplet. The deperturbation results for these multiplets are summarized in Table 3.3.

3.2.5 Perturbation analysis

The ν_{11} fundamental of CH_3NH_2 exhibits multiple perturbations affecting most of the E_1 and E_2 upper state rotational levels. Each perturbation reflects the mixing of a "bright" rotational level [108] of the ν_{11} vibrationally excited state with rotational levels of one or more nearly resonant "dark" vibrational states. In the deperturbation analysis below, it is assumed that the rotational levels of the dark vibrational states carry no oscillator strength from the ground state. When a perturbation mixing occurs, the "dark" rotational levels appear as observable transitions in the spectrum with intensities proportional to their "borrowed" bright state character. The extent of mixing depends on the size of the coupling matrix elements relative to the zeroth-order energy spacings.

The signature of these perturbations is the fragmentation of expected single lines into a multiplets of two or three transitions with the same J', K', Γ' assignment (Figure 3.2(b) and Table 3.2). Such perturbations were not found for the A and B species. It is likely that there are additional perturbations in the present spectrum - for the A and B species as well as for the E_1 and E_2 species – for which the relevant "dark" levels did not borrow sufficient intensity to be detected at the present sensitivity and resolution. Such additional undetected perturbations may still cause frequency shifts of the observed transitions. The evident propensity for more perturbations in the degenerate E_1 and E_2 species could be attributable in part to the expected larger numbers of the degenerate vibrational states among the nearly resonant "dark" combination and overtone vibrations [109].

To determine the hypothetical unperturbed torsion-wagging-rotation tunneling patterns in the vibrationally excited state, it is necessary to deperturb the substates where

perturbations occur. In most cases, only a pair of levels is observed, the bright level and one dark level that borrows intensity, and the standard 2-level deperturbation formulae [55, 56] may be used. For each interacting pair, the relative intensities as well as the observed transition wavenumbers are needed to determine the hypothetical unperturbed upper state term values $\nu^{K', J'}$ and the effective coupling matrix element, $W_{ij}^{J', K'}$. For one substate, $K' = 0$ E_1, three interacting levels are observed, one bright level and two dark levels, which can be deperturbed using the Lawrance and Knight (LK) deconvolution method [110, 111]. For the case of three interacting levels, there are three possible coupling matrix elements, one connecting each pair. The LK deconvolution yields two matrix elements, the two that connect the bright level to the interacting pair of dark levels. It also yields the deperturbed bright level term value and the term values of the two interacting dark levels. The LK deconvolution method does not directly give any information about the matrix element coupling the two dark levels to each other, nor does it deperturb the interacting dark levels.

Examples of the derived coupling matrix elements W_{ij} are shown in Figure 3.3. For the three interacting levels of the $K' = 0$ E_1 species, two matrix elements are derived at each J', one larger ~0.8 cm^{-1} and one smaller <0.2 cm^{-1} (Figure 3.3 (a)). The larger matrix element shows some scatter, but is approximately independent of J', which is the behavior expected for either anharmonic coupling or for *a*-axis Coriolis coupling. Since *a*-axis Coriolis coupling is null for $K' = 0$, it is likely that this matrix element represents anharmonic coupling with the rotational levels of a dark vibrational state. The smaller matrix element increases approximately linearly with $[J'(J'+1)]^{1/2}$, which is the behavior expected for a *b*- or *c*–type Coriolis interaction [112]. As noted above, we do not know

the matrix element and coupling type connecting the two dark states. Given that the two computed matrix elements scale differently with J', one explanation is that the bright level couples to the two dark levels by the indicated mechanisms and the coupling between the dark levels is negligible. Other coupling schemes may also be consistent with the data.

For the $K' = 0$ E_2 species (Figure 3.3(b)), there are two interacting levels, one bright and one dark. The deperturbed coupling matrix element is independent of J' at ~0.6 cm^{-1}, indicating anharmonic coupling. The transitions in the E_{1+1}, E_{1-1}, E_{2+1}, and E_{2-1} substates are also perturbed by apparent anharmonic interactions as shown in Appendix I.

The scatter in Figure 3.3 arises primarily from uncertainties in the intensity measurements, the wavenumber measurements being much more precise. In addition, these uncertainties result in significant uncertainties in the deperturbed term values. The effect of intensity uncertainties is most readily seen in sets of transitions reaching the same upper state J', K' level via different selection rules, e.g., P, Q, R transitions. Such P, Q, R transitions were deperturbed separately and are represented by separate points in Figure 3.3. Since there are multiple determinations of each coupling matrix element, more precise matrix elements can be obtained as the average $\overline{W_{ij}}$ of all independent determinations. In addition to the separate analysis of the P, Q, and R transitions, the J'-dependence (Figure 3.3.) provides more determinations.

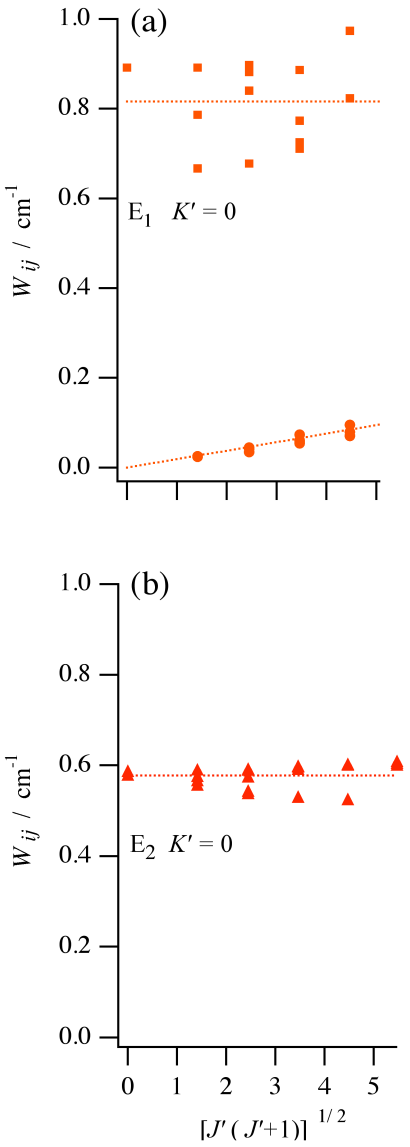

Figure 3.3 (a) Coupling matrix elements (W_{ij}) for the $K' = 0$ E_1 species in the excited state as a function of $[J'(J'+1)]^{1/2}$ [112]. Matrix elements attributed to a *b*/*c*-type Coriolis interaction are denoted with circular markers and those attributable to an anharmonic interaction of the same CH-stretch bright states are represented with square markers. (b) Coupling matrix elements W_{ij} attributed to an anharmonic interaction for the $K' = 0$ E_2 species. The lines are fits to the data given the deduced mechanisms: constant with J' for anharmonic and proportional to $[J'(J'+1)]^{1/2}$ for *b*/*c*-type Coriolis coupling.

Of course, use of the J'-dependent data for this purpose, assumes the validity of the above explanations of the perturbations as one-case of *b/c*-Coriolis coupling and several cases of anharmonic coupling. Then with the more precise $\overline{W_{ij}}$, more precise deperturbed substate origins can also be calculated. The results of the deperturbation analysis are summarized in Table 3.3. The uncertainties given in Table 3.3 and Figure 3.4 for the deperturbed term values include only the statistical uncertainties of this analysis. Additional systematic errors likely result from the existence of additional - as yet undetected - perturbing vibrations.

3.2.6 The torsion-inversion-rotation structure

As noted in Section III.B. above and shown in Figure 3.2(a), the J''-dependent splittings for the K''=1 E_1 and E_2 species are predominantly asymmetry splittings at high J'' but become torsion-rotation splittings at low J''. The low-J'' limits of these torsion-rotation splittings are 0.13 and 0.38 cm^{-1} for E_1 and E_2, respectively. Figure 3.2(b) shows that the pattern is qualitatively different in the vibrationally excited state In the $|K'|$ = 1 E_2 the upper state, a perturbation results in two mixed substates with comparable amounts of bright/dark character, one near 2985.3 cm^{-1} in Figure 3.2(b) and the other near 2986.3 cm^{-1}. For each of these substates, one can see in Figure 3.2(b) that the torsion-rotation-asymmetry splittings separating the E_{2+1} and E_{2-1} levels approach 0 as $J' \rightarrow 0$. The $|K'|$ = 1 E_1 upper state behaves similarly, except that the E_1 substate centered near 2986.43 cm^{-1} has a small residual splitting (0.02 cm^{-1}) at J' = 0. Thus the $|K'|$=1 E_1 and E_2 species show little or no torsion-rotation coupling and revert to the rigid asymmetric rotor pattern such as is seen (Figure 3.2) for the A and B species in both the ground and excited vibrational

states. At $|K| = 2$, the torsion-inversion-rotation splitting patterns for the ground and excited states are more similar. The E_1 and E_2 splittings for $|K'| = 2$ in the upper state are approximately constant showing little variation with J, but the magnitude of the splittings is less than in the ground state.

Table 3.3 Average coupling matrix elements, deperturbed reduced term values and types of interactions.[a]

${}^{twrv}\Gamma'$	K'	$\nu_{dep,R}^{K'}$ cm^{-1}	$\overline{W}_{ij}$ cm^{-1}	Coupling type
E_{1+1}	0	2986.437(76)	0.82(7)	Anharmonic
E_{1+1}	0		0.018(3) [b]	*b/c*-Coriolis
E_{2+1}	0	2986.086(20)	0.58(2)	Anharmonic
E_{1+1}	1	2986.256(21)	0.28(2)	Anharmonic
E_{1-1}	1	2986.322(50)	0.32(5)	Anharmonic
E_{2+1}	1	2986.030(39)	0.42(4)	Anharmonic
E_{2-1}	1	2986.094(50)	0.47(5)	Anharmonic

[a] For average coupling matrix elements $\overline{W_{ij}}$ and upper state deperturbed reduced term values ($\nu_{dep,R}^{K'}$), the statistical uncertainties are given as two standard deviations (in parentheses) in units of the last digit. Deperturbed upper state term values $\nu_{dep}^{K',J',\Gamma'}$ were calculated from the average matrix elements, fitted to Eq. (3.2), and reduced according to Eq.(3.3) using the ground state rotational constants, $A''-(B''+C'')/2 = 2.701$ cm^{-1} from Ref. ([80, 103]).

[b] For the *b/c*-Coriolis interactions (bottom of Figure 3.3(a)), the J'-dependent matrix elements were fit to the expression, $W_{ij}^{J'} = \overline{W_{ij}} \left[J'(J'+1)\right]^{1/2}$.

Reduced, deperturbed term values, $\nu_{dep,R}^{K'}$, for the upper state are compared in Figure 3.4 to the corresponding reduced term values, $\nu_R^{K'}$, for the ground state. The

ground state torsion-inversion tunneling splittings for methylamine follow the well-established pattern, [80, 87, 88, 106] with the A and B species for $K''=0$ at lower energy than the E_1 and E_2 species (Figure 3.4(a)). For $|K''|>0$, the energies of the E_1 and E_2 species split by the torsion-rotation interaction according to the relative signs of the torsional and rotational angular momentum. For example at $|K''|=1$, the E_{1+1} states are above the E_{1-1} states and the E_{2+1} states are above the E_{2-1} states (Figure 3.4(a)). The K''-dependence of the ground state term values follows a sinusoidal variation (Figure 3 of Ref. [88]) that is most readily appreciated when plotted in terms of Dennison's torsional symmetry index, τ [88, 113]. Similar, but simpler, oscillatory patterns are well known in torsional molecules like methanol [55, 114, 115]. The presence of inversion tunneling in additional to torsional tunneling in methylamine serves to increase the number of symmetry species and to make a more complicated pattern.

The pattern of the torsion-inversion tunneling splittings in the ν_{11} CH-stretch excited state (Figure 3.4(b)) is qualitatively different from the ground state. For $K'=0$, the origin for the E_2 tunneling state is at the bottom of the multiplet, below E_1, A and B, rather than at the top as in the ground state. As noted in the introduction, the inversion of the ordering of the torsional tunneling states in methanol [20, 28, 55, 95-98] was found to reflect the systematic coupling of the large-amplitude torsional motion to the other SAV, including the asymmetric CH stretches. Since methylamine has analogous torsional tunneling it is not surprising to see the same kind of effect here.

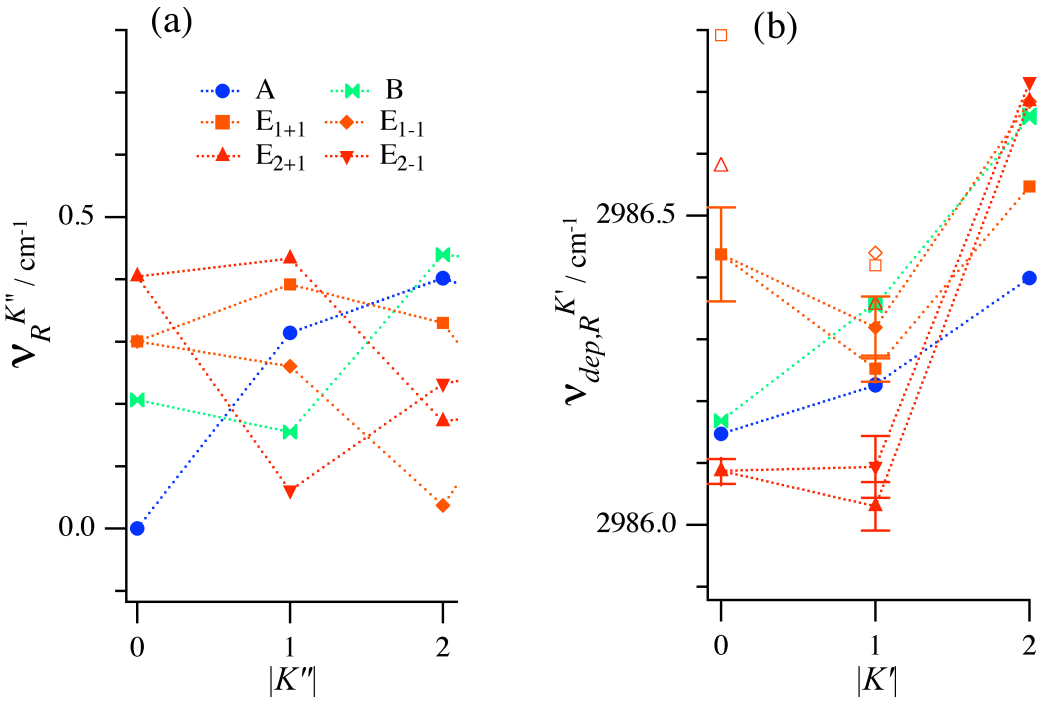

Figure 3. 4 (a) Reduced substate term values ($\nu_R^{K'}$) for the ground state as a function of rotational quantum number K'' and (b) deperturbed reduced term values ($\nu_{dep,R}^{K'}$) as a function of K' for the ν_{11} vibrationally excited state. For the excited state, hollow markers indicates split upper state reduced term values (Table 3.2) while the solid filled markers indicate deperturbed reduced term values for the E_1 and E_2 species (Table 3.3). The error bars, given as two standard deviations, represent the precision of the deperturbation analysis.

The group theoretical formalism of Hougen and Ohashi [79] allows for a range of tunneling patterns expected in G_{12} molecules. The relative energies of the symmetry species at J=0, K=0 are given [79, 116] in terms of the tunneling parameters h_{2v} and h_{3v}:

$$
\begin{aligned}
E\left({}^{tw}\mathrm{A}_1\right) &= +2h_{2\mathrm{v}} + 2h_{3\mathrm{v}} \\
E\left({}^{tw}\mathrm{E}_1\right) &= +h_{2\mathrm{v}} - h_{3\mathrm{v}} \\
E\left({}^{tw}\mathrm{E}_2\right) &= -h_{2\mathrm{v}} - h_{3\mathrm{v}} \\
E\left({}^{tw}\mathrm{B}_1\right) &= -2h_{2\mathrm{v}} + 2h_{3\mathrm{v}}
\end{aligned}
\tag{3.4}
$$

For the ground state of methylamine, the tunneling parameters are both negative, $h_{2\mathrm{v}}$ = -0.052 and $h_{3\mathrm{v}}$ = -0.083 cm^{-1} [80, 84, 86]. In vibrationally excited states, the effective tunneling parameters might have the same signs as for CN stretch [93] or a different sign combination might apply. For example in the first torsionally excited state of methylamine, which has the "inverted" energy ordering $\mathrm{E}_2 < \mathrm{E}_1 < \mathrm{B}_1 < \mathrm{A}_1$, both effective tunneling parameters are positive, $h_{2\mathrm{v}}$ = +0.172 and $h_{3\mathrm{v}}$ = +2.006 cm^{-1} [103]. Equation (3.4), taken in the limit $h_{2\mathrm{v}} \rightarrow 0$, can also be used to model the vibrationally excited states of methanol. For example, the "normal" symmetric CH stretch ν_3 [115] can be modeled with $h_{3\mathrm{v}}$ = -3.03 cm^{-1}, and the "inverted" asymmetric CH stretches, ν_2 and ν_9, [55], [28] can be modeled with $h_{3\mathrm{v}}$ = +1.09 and +1.83 cm^{-1} respectively. Accordingly, one might expect to find a combination of tunneling parameters that accounts for the experimental K' = 0 pattern in Figure 3.4(b) for the methylamine ν_{11} vibrationally excited state. Unfortunately, the experimental energy ordering, $\mathrm{E}_2 < \mathrm{A} < \mathrm{B} < \mathrm{E}_1$, is not consistent with Eq. (3.4) for any combination of parameters. As noted above, Eq. (3.4) does allow E_2 to be at the bottom of the tunneling multiplet for a suitable sign combination of $h_{2\mathrm{v}}$ and $h_{3\mathrm{v}}$, but not at the same time as E_1 is at the top.

The most likely explanation for the inconsistency of the deperturbed K' = 0 term values with Eq. (3.4) is the presence of additional undetected perturbations that have shifted one or more of the substates enough to change the energy ordering. Whereas in

methanol the tunneling splittings are rather large (≤ 9.1 cm^{-1}), in methylamine the splittings are much smaller (≤ 0.4 cm^{-1}) and are comparable to the shifts expected from perturbations.

At $|K'|=1$, the splittings (Figure 3.4) between the pair E_{1+1} and E_{1-1}, and between E_{2+1} and E_{2-1} are greatly reduced in magnitude (by 2× and by 6× respectively) in the excited state relative to the ground state. The $|K'|=1$ splittings obtained from the deperturbation are actually inverted relative to the corresponding ground states (Figure 3.4), but the error bars overlap, meaning that the splittings are small enough that they could be zero within the uncertainties of the deperturbations. For $|K'|=2$, the splitting between E_{1+1} and E_{1-1} and between the E_{2+1} and E_{2-1} is reduced by about a factor of two relative to the ground state. At $|K'|=2$, the sign of the E_1 splitting is inverted relative to the ground state while the sign of the E_2 splitting remains the same as in the ground state.

The observation of reduced E_1 and E_2 splittings for $|K'|>0$ indicates that the torsion-rotation coupling is partially quenched in the ν_{11} CH-stretch excited state of methylamine, which, in turn, suggests a partial suppression of the torsional tunneling in the excited state. Such a suppression of the torsional tunneling splittings has been reported in methanol in the CH stretch overtone region [97]. As noted in the introduction, the tunneling splittings in the $\nu_{CH}=1$ vibrations of methanol can be treated with an adiabatic model in which the (fast) CH stretch motion is solved at each torsional angle and then the (slow) torsional motion is solved in the effective potential that results from the CH stretch excited states. In such an adiabatic model, the character of the fast wavefunctions changes qualitatively along the slow coordinate. For example, in the asymmetric stretch $\nu_{CH}=1$ vibrations, the CH amplitude moves between methanol's three

CH bonds as the torsional angle changes (Figure 8 of Ref. [16]). At v_{CH}=4 and higher, the spectroscopically accessible CH stretch vibrations in methanol become largely localized in single CH bonds, which means that, in the adiabatic model, four or more quanta of CH stretch need to move from one CH bond to the next as the torsional angle changes. Thus in the higher CH stretch overtones, the coupling between localized diabatic states becomes successively higher in order, and therefore, weaker until the adiabatic approximation breaks down and the torsional tunneling is quenched (Figure 7(a) of Ref. [16]). In methylamine, the torsional tunneling rate in the ground state is 36 times slower than in methanol, which means at the v_{CH}=1 level, the coupling between diabatic states is correspondingly weaker than in methanol. The torsional tunneling in methylamine appears to be already somewhat suppressed at the v_{CH}=1 level.

3.3 Summary

The high resolution infrared spectrum of the methylamine ν_{11} CH stretch fundamental band reveals different spectral patterns from those in the vibrational ground state, including (i) an altered ordering of the torsion-inversion tunneling levels and (ii) substantially reduced torsion-rotation couplings suggestive of a partial suppression of torsional tunneling in the vibrationally excited state. It is likely that these changes result in part from the systematic coupling of the LAV to the CH stretches and in part from accidental perturbations that have not been fully deperturbed.

CHAPTER IV

TORSION-INVERSION TUNNELING PATTERNS IN THE CH-STRETCH VIBRATIONALLY EXCITED STATES OF THE G_{12} FAMILY OF MOLECULES INCLUDING METHYLAMINE

*The content of this chapter has been published as "Torsion-Inversion Tunneling Patterns in the CH-Stretch Vibrationally Excited States of the G_{12} Family of Molecules Including Methylamine" by Mahesh B Dawadi, Ram S Bhatta, and David S. Perry; [M.B Dawadi, R.S Bhatta, D.S. Perry, J. Phys.Chem. A, **117** (50), 13356-13367 (2013)]. It is reproduced here with only the minimal editing necessary to confirm to the format and style of this dissertation.*

Two torsion-inversion tunneling models (Models I and II) are reported for the CH-stretch vibrationally excited states in the G_{12} family of molecules. The torsion and inversion tunneling parameters, h_{2v} and h_{3v} respectively, are combined with low-order coupling terms involving the CH-stretch vibrations. Model I is a group theoretical treatment starting from the symmetric rotor methyl CH stretch vibrations; Model II is an internal coordinate model including the local-local CH stretch coupling. Each model yields predicted torsion-inversion tunneling patterns of the four symmetry species, A, B, E_1 and E_2, in the CH-stretch excited states.

Although the predicted tunneling patterns for the symmetric CH stretch excited state are the same as for the ground state, inverted tunneling patterns are predicted for the asymmetric CH stretches. The qualitative tunneling patterns predicted are independent of the model type and of the particular coupling terms considered. In Model I, the magnitudes of the tunneling splittings in the two asymmetric CH stretch excited states are equal at half of that in the ground state, but in Model II, they differ when the tunneling rate is fast. The model predictions are compared across the series of molecules: methanol, methylamine, 2-methylmalonaldehyde and 5-methyltropolone and to the available experimental data.

4.1 Introduction

The presence of large-amplitude vibrations (LAV) in stable molecules impacts the spectroscopy of the other small-amplitude vibrations (SAV). In methanol, an important example with one large amplitude degree of freedom, inverted torsional tunneling patterns have been found in a number of vibrationally excited states [16, 55, 96, 117-119] including the two asymmetric CH stretch bands, ν_2 and ν_9 [16, 55, 96]. The vibrational ground state of methanol has the "normal" tunneling pattern for a 3-fold barrier with the *A*-symmetry level below the *E*-symmetry level, but in the inverted case one finds *E* below *A*. A number of theoretical models [20, 28, 31, 120] and more detailed simulations [6, 32, 98, 121-124] have also been applied to the treatment of these inverted tunneling patterns. All of these approaches make use of permutation-inversion group theory and the G_6 molecular symmetry group [19]. Different approaches make use of normal mode [20, 122] or local mode [28, 31, 124] representations and some invoke geometric phase [32]

and analogies with the Jahn-Teller and Renner-Teller [20, 125] couplings in electronic spectroscopy.

A class of molecules with two large-amplitude tunneling degrees of freedom includes methylamine, 2-methylmalonadlehyde (2-MMA) and 5-methyltropolone (5-MT) [79, 82, 85, 87, 116]. In these molecules, one LAV is a 3-fold methyl internal rotor and the other has a 2-fold symmetric barrier. In methylamine, the coordinate with the 2-fold barrier is the NH_2 wag, which becomes umbrella-type inversion at large amplitude (Figure 4.1(a)) [81, 82, 126]. In 2-MMA [87, 116] and 5-MT, [127] the 2-fold coordinate is proton transfer accompanied by a change in the alternation of the single and double bonds (Figures 4.1(b) and (c)). In both cases, tunneling through the two-fold barrier involves a 60° rotation of the methyl rotor. The 2-dimensional torsion-inversion tunneling surface for methylamine shown in Figure 4.2 has six equivalent minima. The torsion-proton-transfer surfaces of 2-MMA and 5-MT are quantitatively similar. The two-dimensional tunneling dynamics connecting the six minima have been modeled [79, 87, 116] in terms of torsional and inversion tunneling parameters, h_{3v} and h_{2v}, respectively. The range of possible tunneling patterns in the vibrational ground state [87, 127] for the four different sign combinations of h_{3v} and h_{3v} are shown in Figure 4.3.

The symmetry properties of these tunneling motions are treated in the context of permutation-inversion group theory using the G_{12} molecular symmetry group [19, 79] (Figure 4.1(d)). The tunneling state with no nodes in either the torsional or inversion coordinate (A_1 symmetry in G_{12}) is the lowest in energy in the vibrational ground state. Therefore, the energy level patterns in Figure 4.3(a) with both h_{3v} and h_{2v} less than zero are appropriate for vibrational ground state molecules [80]. The actual values of the

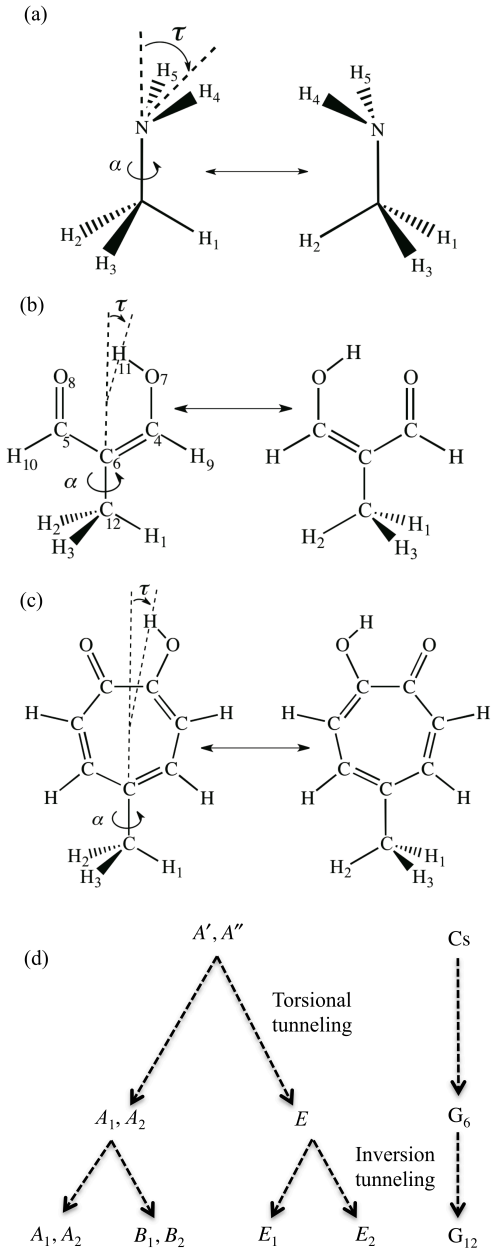

Figure 4.1 The molecular structures and large-amplitude tunneling coordinates, α and τ, are depicted for (a) methylamine (b) 2-methylmalonadlehyde (2-MMA) and (c) 5-methyltropolone (5-MT). In (d), symmetry correlations are given going from the rigid molecules (C_s) to torsional tunneling only (G_6) to both torsional and inversion tunneling (G_{12}).

tunneling parameters depend upon the reduced mass for motion along the tunneling coordinates and on the height and width of the potential barriers. The patterns of the tunneling splittings vary as the relative values of h_{3v} and h_{2v} are changed. When the torsional tunneling is faster $\left(\left|h_{3v}\right| > \left|h_{2v}\right|\right)$ as in methylamine, the energy ordering of the tunneling states is $A < B < E_1 < E_2$.[87] Conversely, when the 2-fold tunneling dominates as in 2-MMA, the ordering is $A < E_1 < E_2 < B$ [87]. The tunneling pattern for 5-MT is intermediate between these two cases.

When one or both of the LAV are excited, the tunneling patterns may be different from the ground state. If the torsion is excited with an odd number of quanta, the energy ordering of the tunneling multiplet becomes inverted relative to the ground state as shown in Figure 4.3(b), implying that effective tunneling parameters should be used in this case with both h_{3v} and h_{2v} positive. Otherwise, excitation of the large-amplitude torsional and inversion degrees of freedom yields patterns represented in Figure 4.3(a) [126, 128-130]. Torsional excitation increases the torsional tunneling rate and hence the magnitude of the effective tunneling parameter h_{3v}, moving such states further to the left within the relevant panel of Figure 4.3 [103, 106, 128, 130]. Conversely, wagging excited states are displaced to the right in Figure 4.3 [128, 129]. Up to the present, the patterns resulting from the other sign combinations of h_{3v} and h_{2v} (Figures 4.3(c) and (d)) have not been found in any known cases.

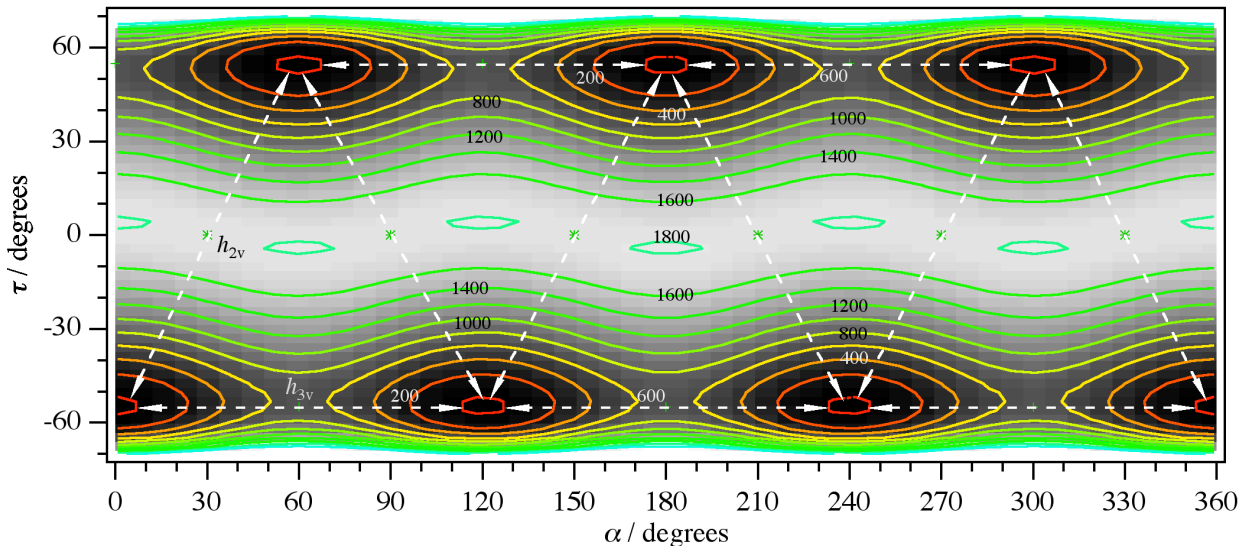

Figure 4.2 An *ab initio* two-dimensional potential energy surface for CH_3NH_2 as a function of the torsional (α) and inversion (τ) angles, computed at the level CCSD(T)/6-311++G(3df,2p)// MP2/6-311++G(3df,2p) [126]. Contours are separated by 200 cm-1. The tunneling pathways connecting the six equivalent minima are indicated by the white dashed arrows. The potential energy surfaces for the two large-amplitude tunneling coordinates in 2-MMA and 5-MT are qualitatively similar.

The motivation for this study is to explore the ways in which the torsion-inversion tunneling patterns change in G_{12} molecules when small-amplitude vibrations (SAV), particularly the CH stretches are excited. Experimentally, altered torsion-inversion tunneling patterns have also been observed in the ν_{11} asymmetric CH stretch of methylamine,[50] but these are attributable in part to perturbations as well as to systematic torsion-inversion-vibration couplings. In this work, two simple models of the interaction of the CH stretch vibrations with the torsion-inversion tunneling dynamics are developed. Both models rely on reduction of the tunneling dynamics to the two ground state tunneling parameters, h_{2v} and h_{3v} [79, 80, 116] but they differ in the way the CH

stretch vibrations are handled. Systematic trends in the patterns of the tunneling multiplets are derived and comparison is made to the available experimental data.

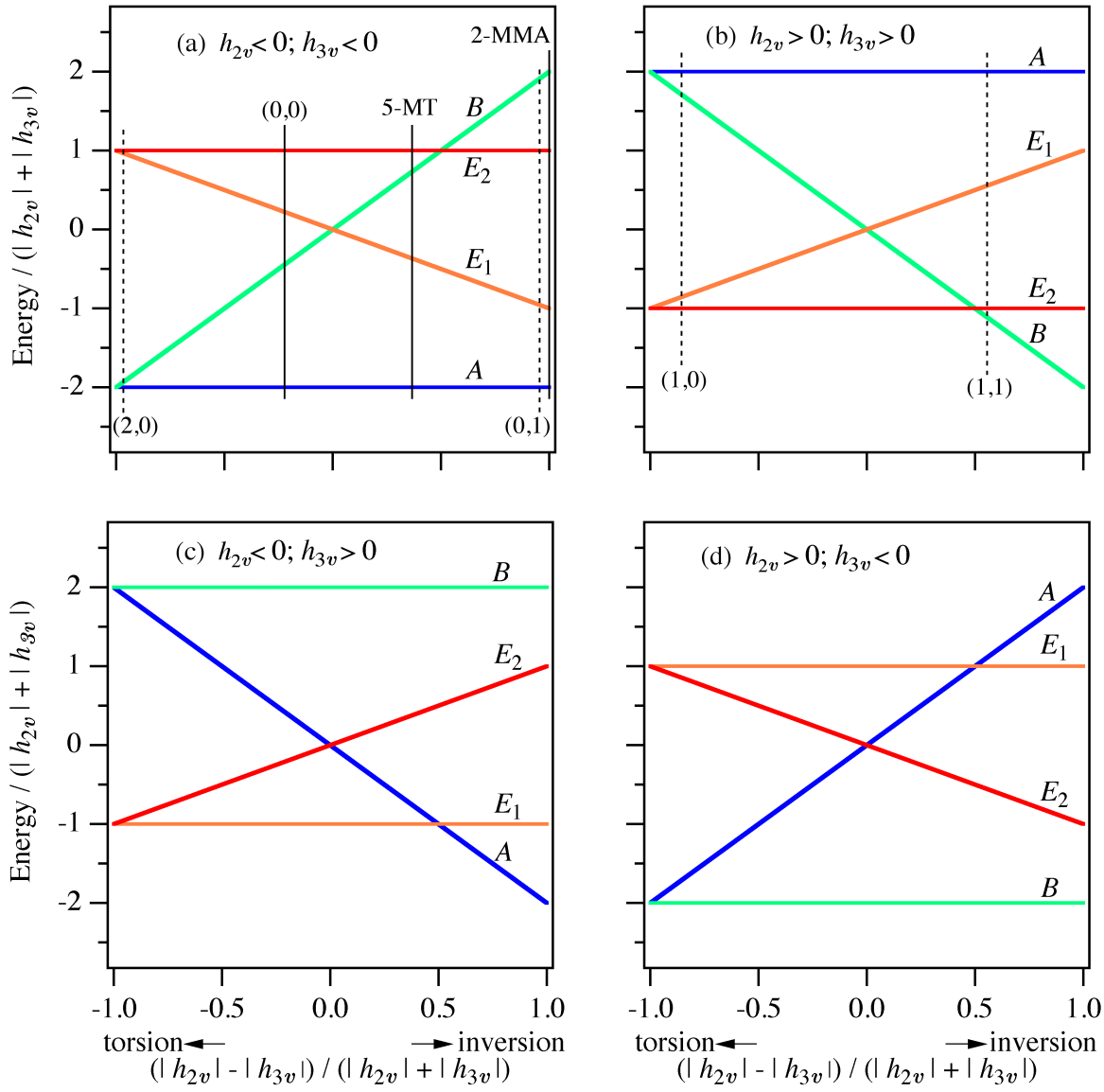

Figure 4. 3 The range of torsion-inversion tunneling patterns in the ground vibratonal state are given for the four different sign combinations of the torsion-inversion tunneling parameters, h_{2v} and h_{3v}. The abscissa specifies the relative values of h_{2v} and h_{3v} and the ordinate gives the normalized energy levels. These figures are plotted according to Eqs. (5) of Ref. [116], repeated here as Eq. (4.3). For methylamine, in addition to the ground

vibrational states (0,0) [80], the effective tunneling parameters for some torsion-inversion excited states (ν_{15}, ν_9) [103, 106, 128-130] are indicated by dashed lines. The tunneling patterns for 2-MMA [87, 116] and 5-MT [127] are also indicated. For the ground state level, $J''=0$, $K''=0$, the four levels in the tunneling multiplet are A_1, B_1, E_1, and E_2. The symmetries indicated are species in G_{12} with the subscripts 1 and 2 on the non-degenerate (A and B) species suppressed.

4.2 Theoretical approach

The following sections provide a detail description of a theoretical approach employed in the development of two models Hamiltonian.

4.2.1 Overview

The central assumption of the two models developed in this work is that torsion-inversion tunneling in the SAV excited states can be modeled in the same way as it is in the vibrational ground state (i. e., with the ground state values of h_{2v} and h_{3v}), but with the added provision of appropriate couplings between the LAV and the SAV.

In the established spectroscopic model of torsion-inversion tunneling that has been applied to the vibrational ground states, [79, 87, 116, 127, 131, 132] the torsion-inversion wavefunctions are linear combinations of basis functions, one basis function centered on each of the six equivalent potential wells. As illustrated in Figure 4.1, α is the torsional angle, and τ is the other large-amplitude coordinate. The torsion-inversion basis functions are written as

$$\left|\phi_k\right\rangle = \psi\left(\alpha - \alpha_k\right)\chi\left(-\tau + \tau_k\right). \qquad (4.1)$$

where the equivalent minima, enumerated as k = 1, 2, …6, are located at $\alpha_k = (k-1)\frac{\pi}{3}$ and $\tau_k = -\tau_{eq}\cos 3\alpha_k$ (Figure 4.2). The tunneling is then modeled in terms of the two tunneling parameters, h_{2v} and h_{3v}, that link adjacent wells by inversion or torsional tunneling respectively (Figure 4.2). The tunneling matrix elements are

$$\left\langle \phi_{k\pm(j-1)} \middle| \hat{h}_{jv} \middle| \phi_k \right\rangle = h_{jv} \tag{4.2}$$

with j = 1, 2, and 3. The diagonal elements h_{1v}, which give an energy offset, are either set to zero or replaced with an offset value as appropriate in each of the sections below.

This work addresses high barrier situations where the torsion-inversion amplitudes are substantially contained in small regions close to the global minima. Therefore, direct tunneling between non-adjacent minima (e.g., between wells 1 and 4) is neglected. For the evaluation of certain coupling matrix elements in the sections below, the torsion and inversion basis functions, ψ and χ, will be approximated as delta functions [20].

For the vibrational ground state, the torsion-wagging tunneling Hamiltonian is represented in this basis as the 6×6 matrix shown in Figure 4.4. The torsion-wagging eigenvalues that result from the diagonalization of this matrix are [50, 79, 116]

$$\begin{aligned} E\left({}^{tw}A_1\right) &= +2h_{2v} + 2h_{3v} \\ E\left({}^{tw}E_1\right) &= +h_{2v} - h_{3v} \\ E\left({}^{tw}E_2\right) &= -h_{2v} - h_{3v} \\ E\left({}^{tw}B_1\right) &= -2h_{2v} + 2h_{3v}\,. \end{aligned} \tag{4.3}$$

These are the eigenvalues plotted in Figure 4.3 for the four different sign combinations and for different relative magnitudes of h_{2v} and h_{3v}.

In the present approach, the CH stretches are treated in the two different ways that have been applied to the torsion-vibration problem in methanol. Model I follows the development of Hougen cases (1) and (2) [20]. Hougen's case (2) treats the two asymmetric CH stretches (ν_2 and ν_9 in methanol) and represents them in the vibrational angular momentum basis. Hougen's case (1) is the "trivial" case of the symmetric CH stretch (ν_3 in methanol), which by symmetry leaves the ground state tunneling pattern unchanged [20]. In Model II, following the approach of Wang and Perry [28] and Hougen's case (3),[20] the three methyl CH stretches are represented in the local mode basis. In both models, the lowest-order symmetry-allowed terms coupling the CH stretches to the large-amplitude tunneling motions are included in the Hamiltonian.

$$
{}^{tw}H = \begin{array}{c} \begin{array}{cccccc} k=1 & 2 & 3 & 4 & 5 & 6 \end{array} \\ \begin{bmatrix} h_{1v} & h_{2v} & h_{3v} & 0 & h_{3v} & h_{2v} \\ h_{2v} & h_{1v} & h_{2v} & h_{3v} & 0 & h_{3v} \\ h_{3v} & h_{2v} & h_{1v} & h_{2v} & h_{3v} & 0 \\ 0 & h_{3v} & h_{2v} & h_{1v} & h_{2v} & h_{3v} \\ h_{3v} & 0 & h_{3v} & h_{2v} & h_{1v} & h_{2v} \\ h_{2v} & h_{3v} & 0 & h_{3v} & h_{2v} & h_{1v} \end{bmatrix} \end{array}
$$

Figure 4.4 The ground state torsion-wagging Hamiltonian (${}^{tw}H$) matrix in the localized basis $|\phi_k\rangle$ with k = 1…6. The torsional (h_{3v}) and inversion (h_{2v}) tunneling parameters connect the adjacent wells in Figure 4.2. The diagonal parameter h_{1v} represents the energy of the zeroth-order non-tunneling states.

The result is a 12×12 Hamiltonian matrix for the asymmetric CH stretches in Model I and an 18×18 Hamiltonian matrix for Model II. The ground state tunneling parameters are used to make model predictions for the tunneling splittings in the excited vibrational states.

4.2.2 Symmetry classification

This paper follows the group theoretical notation of Ohashi and Hougen [79]. The molecular symmetry group, G_{12}, for methylamine is generated by two permutation-inversion group operators, $\boldsymbol{a}$ and $\boldsymbol{b}$:

$$\boldsymbol{a} = (123)\,(45)$$

$$\boldsymbol{b} = (23)\,(45)^* \qquad (4.4)$$

where, the hydrogen atoms are numbered 1, 2, 3 and 4, 5 for methyl and amino groups, respectively as indicated in Figure 4.1(a). The transformation properties of the torsion and inversion angles [79, 93] are summarized in appendix J. For a molecule initially at one of the six equivalent minima (Figure 4.2), the group generator, $\boldsymbol{a}$, serves to transform the molecule to the next minimum with the torsional angle α changed by 60˚ and the inversion angle τ changing sign. Successive applications of $\boldsymbol{a}$ serve to move the system in a zig-zag pattern across Figure 4.2 from one minimum to the next until $\boldsymbol{a}^6 = \boldsymbol{e}$ brings it back to the starting point.

The group G_{12} is also appropriate for the treatment of the internal rotation and proton transfer degrees of freedom in 2-MMA (Figure 4.1(b)) with the group generators,

$\boldsymbol{a}$ = (123) (45) (78) (9,10) (4.5)

$\boldsymbol{b}$ = (23)* ,

similar group generators can be designated for 5-MT. With these group generators, the 2-dimensional large-amplitude motion of all three molecules can be treated with the same formalism [116]. In the present work, the formalism is extended to include the methyl CH stretches, and the same development is equally applicable to methylamine, 2-MMA, and 5-MT. Further details relevant to group theoretical treatment of G_{12} molecules can be found in published work [19, 79, 82, 83, 88, 93, 132-134].

The present formulation may also be applied to three-fold torsional molecules, such as methanol, in the limit that the inversion tunneling parameter goes to zero, $h_{2v} \to 0$. For methanol, the G_6 group has the generators, $\boldsymbol{a}$ = (123) and $\boldsymbol{b}$ = (23)*. This limit for the ground state of methanol corresponds to the left edge of Figure 4.3(a), and the species correlations are $A \oplus B \to A$ and $E_1 \oplus E_2 \to E$ (Figure 4.1(d)). In methanol, the tunneling splitting Δ is defined [122] as the energy difference between the E and A torsional levels, $\Delta \equiv E\left(E\right) - E\left(A\right)$. As pointed out above, Δ > 0 for ν_3 but Δ < 0 for ν_2 and ν_9. For convenient reference in the G_{12} systems, we define Δ in the same way in the limit, $h_{2v} \to 0$. The parameter Δ is a convenient single measure of the magnitude and sign of the tunneling splittings, but it does not specify the detailed level ordering reflected in the different panels of Figure 4.3.

4.3 Model I: Vibrational angular momentum basis

Hougen's case (2) treatment [20] of the torsional splittings in the CH-stretch excited states of methanol used a basis of the two vibrational angular momentum components for a degenerate *E*-type asymmetric CH stretch and coupled them with the lowest-order torsionally mediated terms. Model I is the extension of Hougen's cases (1) and (2) to include both tunneling degrees of freedom present in G_{12} molecules. In permutation-inversion group theory, the symmetries of the vibrational normal modes are not completely specified as they are in point group theory for rigid molecules (Ref. [101] and p 507 of Ref. [19]). In G_{12} molecules, one could in principle choose degenerate vibrational coordinates with either E_1 or E_2 symmetry for the CH stretches. The former transform as $e^{\pm i\alpha}$ and correspond to the pair of vibrational angular momentum states with $l = \pm 1$, whereas the latter transform as $e^{\pm 2i\alpha}$ and correspond to $l = \pm 2$. The vibrational coordinates $Q_{\pm}$ used in Hougen's case (2) treatment of methanol [20] correspond to the $l = \pm 1$, and transform like $e^{\pm i\alpha}$ so that in the present context they belong to the E_1 species. However, the three methyl CH stretch coordinates in G_{12} molecules transform as $A_1(l = 0) + E_2(l = \pm 2)$, (Table 15-5, p 509 of Ref. [19]) and they are the basis for Model I.

The CH stretch basis used in Model I is notated

$$\left\{ \left| {}^{v}E_{2\pm} \right\rangle \right\} = \left\{ \left| {}^{v}E_{2-} \right\rangle, \left| {}^{v}E_{2+} \right\rangle \right\}, \tag{4.6}$$

where the subscripts + and – indicate $l = +2$ and -2, respectively. This basis spans the asymmetric CH stretch fundamental vibrations, specifically, modes ν_2 and ν_x, where x = 11, 21, and 33 for CH_3NH_2, 2-MMA and 5-MT respectively. Combination of these with the torsion-inversion basis (Eq. (4.1)) yields the product basis

$$\left\{\left|\phi_k\right\rangle\left|{}^{v}E_{2\pm}\right\rangle\right\} = \left\{\left|k, l\right\rangle\right\} \tag{4.7}$$

with $k = 1, 2, \ldots 6$ and $l = \pm 2$. The torsion-wagging tunneling in each CH stretch basis state is treated with the same tunneling parameters, h_{2v} and h_{3v}, as the ground vibrational state (Eq. (4.2) and Figure 4.4).

Following the approach of Hougen,[20] the lowest-order torsion-vibration coupling term with A_1 symmetry in G_{12} is

$$H^{(1)} = \frac{g}{h}\left[\hat{Q}_{2+}^2 e^{2i\alpha} + \hat{Q}_{2-}^2 e^{-2i\alpha}\right] \tag{4.8}$$

where g and h are constants. Here, $\hat{Q}_{2\pm}$ are methyl CH stretch vibrational coordinates that transform as $e^{\pm 2i\alpha}$, which have the vibrational matrix elements,

$$\left\langle {}^{v}E_{2\pm}\left|\hat{Q}_{2\pm}^2\right|{}^{v}E_{2\mp}\right\rangle = h\,. \tag{4.9}$$

Combining Eqs. (4.1), (4.7) and (4.9), the matrix elements of the operator in the Eq. (4.8) are

$$\left\langle k, 2\left|H^{(1)}\right|j, -2\right\rangle = g\delta_{kj}\varepsilon^{2(k-1)} \tag{4.10}$$

where $\varepsilon = \exp\left(\pi i/3\right)$.

In the same way, the lowest-order coupling term that also includes inversion and has A_1 symmetry is

$$H^{(2)} = \frac{p}{h}\left[\hat{Q}_{2+}^2 \tau^2 e^{2i\alpha} + \hat{Q}_{2-}^2 \tau^2 e^{-2i\alpha}\right] \tag{4.11}$$

where p is a constant. The matrix elements are

$$\left\langle k, 2\left|H^{(2)}\right|j, -2\right\rangle = p\delta_{kj}\tau_{eq}^2\varepsilon^{2(k-1)}\,. \tag{4.12}$$

For suitable values of the constants, the matrix elements in Eqs. (4.10) and (4.12) are equivalent, so the above treatment yields only a single distinct coupling term for the Model I.

The form of the resulting 12×12 Hamiltonian matrix for the pair of asymmetric CH stretch excited states is given in Figure 4.5. Details of the derivation are given in the Appendix J. The structure of Model I is graphically depicted in Figure 4.6(a).

No interaction of the symmetric CH stretch with the asymmetric CH stretches is included in Model I. For each of the molecules considered here, the symmetric methyl CH stretch is ν_3. The Hamiltonian matrix for the ν_3 excited state is then the same as Figure 4.4. Figures 4.4 and 4.5, when taken together with appropriate values of the diagonal energies h_{1v} and then diagonalized, provide predictions of the tunneling splitting patterns in the three methyl CH stretch excited states in the target group of molecules.

Diagonalization of the 12×12 matrix in Figure 4.5 yields the following torsion-wagging-vibration eigenvalues,

$$\begin{aligned} E\left({}^{twv}A\right) &= \pm g - h_{2v} - h_{3v} \\ E\left({}^{twv}E_1\right) &= \pm g - \tfrac{1}{2}h_{2v} + \tfrac{1}{2}h_{3v} \\ E\left({}^{twv}E_2\right) &= \pm g + \tfrac{1}{2}h_{2v} + \tfrac{1}{2}h_{3v} \\ E\left({}^{twv}B\right) &= \pm g + h_{2v} - h_{3v} \end{aligned} \qquad (4.13)$$

The effect of the torsion-wagging-vibration interaction is to split the degenerate *E*-type asymmetric stretch basis states into two CH vibrations. For one of these vibrations containing the upper sign, the species of the tunneling multiplet are

${}^{twv}\Gamma = \{A_1,\ E_1,\ E_2,\ B_1\}$ and for the CH vibration with the lower sign, $\{A_2,\ E_1,\ E_2,\ B_2\}$. The species of these two CH stretch vibrations correlate to A' and A'', respectively in the C_s point group. The energy splitting between these two asymmetric CH stretch vibrations is $2g$. Since $|g| \gg |h_{2v}| + |h_{3v}|$ for the molecules studied here, the two sets of four tunneling levels associated are well separated (Figure 4.6(a)), which supports the use of the traditional A' and A'' labels for the two asymmetric CH stretch modes.

$$
{}^{twv}H = \begin{array}{c|cccccc|cccccc}
 & \multicolumn{6}{c|}{|{}^{v}E_{2+}\rangle} & \multicolumn{6}{c}{|{}^{v}E_{2-}\rangle} \\
k = & 1 & 2 & 3 & 4 & 5 & 6 & 1 & 2 & 3 & 4 & 5 & 6 \\
\hline
 & h_{1v} & h_{2v} & h_{3v} & 0 & h_{3v} & h_{2v} & g & 0 & 0 & 0 & 0 & 0 \\
 & h_{2v} & h_{1v} & h_{2v} & h_{3v} & 0 & h_{3v} & 0 & g\varepsilon^{2} & 0 & 0 & 0 & 0 \\
 & h_{3v} & h_{2v} & h_{1v} & h_{2v} & h_{3v} & 0 & 0 & 0 & g\varepsilon^{4} & 0 & 0 & 0 \\
 & 0 & h_{3v} & h_{2v} & h_{1v} & h_{2v} & h_{3v} & 0 & 0 & 0 & g\varepsilon^{6} & 0 & 0 \\
 & h_{3v} & 0 & h_{3v} & h_{2v} & h_{1v} & h_{2v} & 0 & 0 & 0 & 0 & g\varepsilon^{8} & 0 \\
 & h_{2v} & h_{3v} & 0 & h_{3v} & h_{2v} & h_{1v} & 0 & 0 & 0 & 0 & 0 & g\varepsilon^{10} \\
\hline
 & g & 0 & 0 & 0 & 0 & 0 & h_{1v} & h_{2v} & h_{3v} & 0 & h_{3v} & h_{2v} \\
 & 0 & g\varepsilon^{-2} & 0 & 0 & 0 & 0 & h_{2v} & h_{1v} & h_{2v} & h_{3v} & 0 & h_{3v} \\
 & 0 & 0 & g\varepsilon^{-4} & 0 & 0 & 0 & h_{3v} & h_{2v} & h_{1v} & h_{2v} & h_{3v} & 0 \\
 & 0 & 0 & 0 & g\varepsilon^{-6} & 0 & 0 & 0 & h_{3v} & h_{2v} & h_{1v} & h_{2v} & h_{3v} \\
 & 0 & 0 & 0 & 0 & g\varepsilon^{-8} & 0 & h_{3v} & 0 & h_{3v} & h_{2v} & h_{1v} & h_{2v} \\
 & 0 & 0 & 0 & 0 & 0 & g\varepsilon^{-10} & h_{2v} & h_{3v} & 0 & h_{3v} & h_{2v} & h_{1v}
\end{array}
$$

Figure 4.5 The 12 × 12 torsion-wagging-vibration Hamiltonian $({}^{twv}H)$ matrix as derived from Model I for the two asymmetric CH stretch excited states with $\varepsilon = \exp(\pi i/3)$.

The value of torsion-inversion-vibration coupling parameter g is determinable from the experimental frequencies [28, 50, 135] of the two asymmetric CH stretch modes ν_2 and ν_x where known (Table 4.1). Since these experimental frequencies have not been reported for 2-MMA and 5-MT, they have been estimated from *ab initio* calculations (Table 4.1).

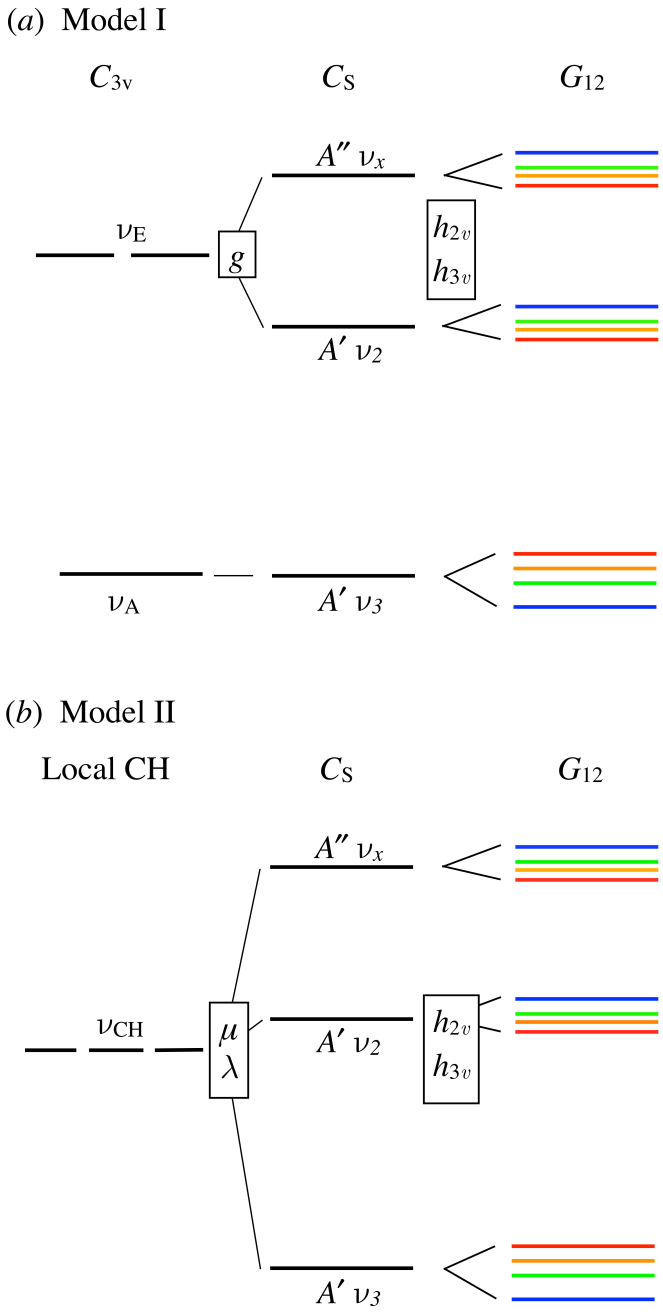

Figure 4.6 Schematic representations of the three sets of four tunneling levels for the three methyl CH stretch excited states for (a) Model I and (b) Model II. In this Figure, the coupling parameters in each model are turned on in steps from left to right as indicated. The vertical axis depicts relative energy but is not to scale with the smaller splittings being exaggerated.

Table 4. 1 Experimental and calculated vibrational frequencies, tunneling parameters, and torsion-inversion-vibration coupling parameters (in cm^{-1}) for G_{12} molecules.

Experimental	5-MT-d4	CH_3NH_2	2-MMA	CH_3OH
h_{2v}	-0.0218 [d]	-0.0516 [e]	-0.7008 [f]	0
h_{3v}	-0.0098 [d]	-0.0831 [e]	-0.0037 [f]	-3.035
$\nu_2(A')$ [a]	2993 [g], 3005 [h]	2961 [i]	2984 [g], 2992 [h]	2998.77 [k]
$\nu_3(A')$ [a]	2892 [g], 2919 [h]	2820 [i]	2893 [g], 2919 [h]	2844.69 [k]
$\nu_x(A'')$ [a]	2965 [g], 2962 [h]	2986.23 [j]	2965 [g], 2961 [h]	2956.91 [k]
g [b]	14 [g], 21.6 [h]	-12.6	9.5 [g], 15.5 [h]	20.8
ω [c]	2950 [g], 2962.2 [h]	2922.4	2947.8 [g], 2957.3 [h]	2933.5
λ [c]	-27.2 [g], -17.9 [h]	-49.9	-26.2 [g], -16.7 [h]	-42.2
μ [c]	12.1 [g], 16.5 [h]	-13.9	8.5 [g], 13.1 [h]	18.2
$\lvert\mu\rvert / (\lvert h_{2v}\rvert + \lvert h_{3v}\rvert)$	382 [g], 522 [h]	103	12.1 [g], 18.6 [h]	6.0

[a] CH stretch vibrational frequencies where $\nu_x = \nu_{33}$, ν_{11}, ν_{21}, and ν_9 for 5-MT-d4, CH_3NH_2, 2-MMA and CH_3OH respectively.

[b] Model I coupling parameter fit to ν_2 and ν_x.

[c] Model II parameters fit to ν_2, ν_3 and ν_x with λ' constrained to be 0.

[d] Ref. [127].

[e] Refs. [80, 84, 86, 103].

[f] Refs. [87, 116].

[g] MP2/ 6-311++G(3df,2p) vibrational frequencies [136] scaled by 0.943 [137] and the corresponding fit parameters ω, λ and μ.

[h] B3LYP/ 6-311++G(3df,2p) vibrational frequencies[136] scaled by 0.967[137] and the corresponding fit parameters ω, λ and μ.

[i] Ref. [135].

[j] Ref. [50] and [k] Ref. [28].

The frequency calculations were done on 5-MT-d4, in which the four ring hydrogens were deuterated, to avoid the complication of couplings of the methyl CH stretches to other CH stretch fundamentals. The sign of *g* is positive for 2-MMA and 5-MT-d4 but negative for CH_3NH_2, which reflects the ordering of the fundamental frequencies: $\nu_2 > \nu_x$ for 2-MMA and 5-MT-d4 but $\nu_2 < \nu_{11}$ for CH_3NH_2. Model I can also be applied to CH_3OH using the model in the limit that inversion tunneling is suppressed, $h_{2v} \to 0$. The computed magnitudes of *g* vary by about 45% in each of the four compounds depending on the level of the calculation and they agree with the experimental values within about 50% where the experimental data are known. Fortunately, the signs of *g* are consistent at all levels of calculations attempted and also agree with the available experimental data. Even the determination of *g* from the experimental fundamental frequencies is complicated by the CH 1:2 stretch-bend resonances. These resonances, which are well documented in methanol, [138] result in substantial intensity borrowing and frequency shifts of the fundamentals. Thus the values of *g* determined from the experimental "CH stretch" fundamentals are really effective values reflecting, in part, these stretch-bend interactions.

The Model I predictions of the torsion-inversion tunneling patterns in the three methyl CH stretch excited states are represented as the lines in Figure 4.7. As indicated by Eq. (4.13), the tunneling patterns do not depend on the sign or magnitude of the coupling parameter, *g*. The experimental values of the ground state tunneling parameters h_{2v} and h_{3v} for CH_3NH_2, [80, 84, 86] 5-MT,[127] and 2-MMA [87, 116] (Table 4.1) are used to calculate the specific tunneling patterns of each of the three molecules in their vibrationally excited states. The ν_3 symmetric CH stretch tunneling splittings (Figure

4.7(b)) are predicted to be the same as for the ground state (Figure 4.3(a)). However the computed asymmetric CH stretch tunneling splittings (Eq. 4.13 and Figure 4.7(a)) are only half as big as those in the ground state (Eq. (4.3) and Figure 4.3(a)) and the ordering of the tunneling levels is different depending on the relative values of h_{2v} and h_{3v}. As can be seen from Figure 4.7, the relative values of h_{2v} and h_{3v} are such that the level ordering is different for each of three molecules. For cases in which $|h_{2v}| >> |h_{3v}|$, such as 2-MMA, the ordering of the tunneling levels is $B < E_2 < E_1 < A$ for ν_2 and ν_x, and $A < E_1 < E_2 < B$ for ν_3. For $|h_{2v}| < |h_{3v}|$, which includes CH_3NH_2, the ordering is $E_2 < E_1 < B < A$ for ν_2 and ν_x, and $A < B < E_1 < E_2$ for ν_3. In the intermediate range $|h_{3v}| < |h_{2v}| < 3|h_{3v}|$, which includes 5-MT, the ordering is $E_2 < B < E_1 < A$ for ν_2 & ν_x, and $A < E_1 < B < E_2$ for ν_3. In all of these cases, the pattern of the tunneling splittings is predicted to be inverted in the ν_2 and ν_x excited states relative to the ground state and ν_3.

In Figures 4.3 and 4.7, the subscripts 1 and 2 on the *A* and *B* symmetry species have been suppressed. For $J = 0$ levels of vibrational states without torsional excitation, these subscripts are 1 for the A' vibrations, ν_2 and ν_3, and 2 for the A'' vibrations, ν_x. The 1's and 2's then alternate with rotational [50, 84, 86, 131] and torsional [83, 88, 89, 93, 101, 103, 106, 134, 139] excitation.

4.4 Model II: Local CH stretch basis

The Wang and Perry internal coordinate model of torsion-vibration coupling in methanol [28] employed a direct product basis of harmonic oscillators for the local CH-stretches and free internal rotor functions for the torsional motion. The lowest-order

symmetry-allowed torsion-vibration coupling was invoked. Model II is both a simplification and an extension of Wang and Perry's treatment of methanol [28]. The treatment of torsional tunneling is reduced to the single torsional tunneling parameter, h_{3v}. Model II is an extension of the Wang and Perry Model in that inversion tunneling is also treated by virtue of inclusion of the tunneling parameter h_{2v}.

Model II incorporates the same torsion-inversion basis (Eq. (4.1)) and tunneling matrix elements (Eq.(4.2)) as Model I. Three local CH-stretch harmonic oscillator coordinates q_1, q_2, and q_3 are used, one on each of the CH bonds. The corresponding basis states,

$$\left\{\left|100\right\rangle,\left|010\right\rangle,\left|001\right\rangle\right\} = \left\{\left|1\right\rangle,\left|2\right\rangle,\left|3\right\rangle\right\} \tag{4.14}$$

are used, each representing one quantum of excitation on one of the three CH bonds. The shorthand notation on the right side of Eq. (4.14) is used for convenience. This vibrational basis spans the three methyl CH stretch fundamental vibrations, ν_2 (A'), ν_3 (A') and ν_x (A''), in the subject molecules. The direct product basis set is then

$$\left\{\left|\phi_k\right\rangle\left|n\right\rangle\right\} = \left\{\left|k,\, n\right\rangle\right\} \tag{4.15}$$

with k = 1, 2, … 6 and n = 1, 2, 3.

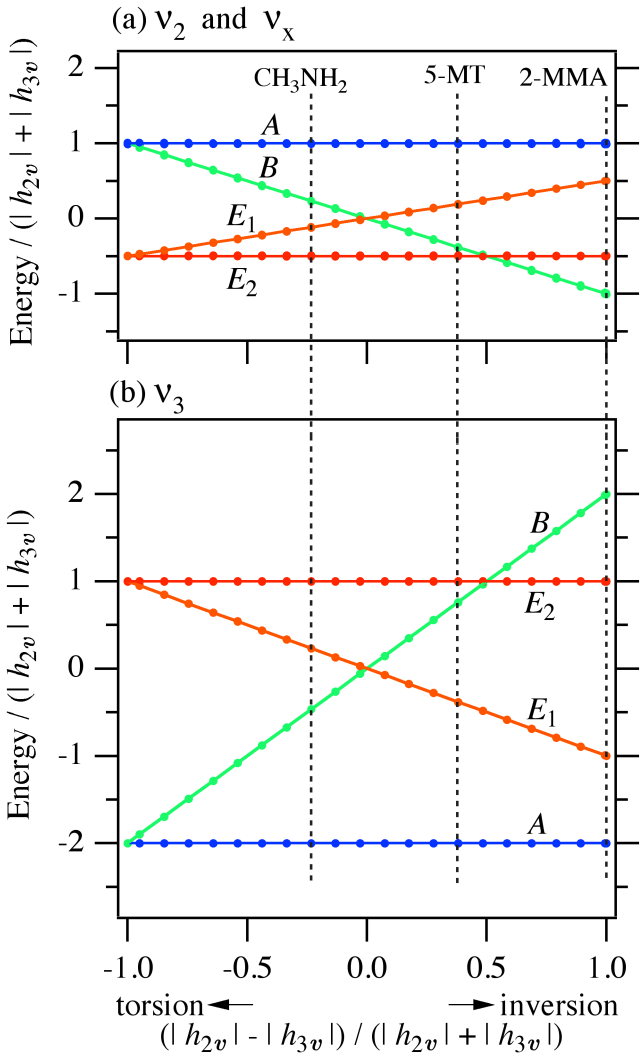

Figure 4.7 Computed torsion-inversion tunneling splitting patterns as a function of the relative magnitudes of tunneling parameters, h_{2v} and h_{3v}, for (a) the two asymmetric CH stretch excited states, ν_2 and ν_x, and (b) the symmetric CH-stretch, ν_3. The lines are the results for Model I as given by Eq. (4.13). The points are the results for Model II, computed by matrix diagonalization (Figure 4.8) in the slow tunneling limit, $|\mu| >> |h_{2v}| + |h_{3v}|$. The vertical dashed lines represent the abscissa values appropriate to the three indicated molecules.

The Model II Hamiltonian is formulated as the sum of three parts, (i) the torsion-wagging Hamiltonian ${}^{tw}H$ as given by Eq. (4.2), (ii) the Hamiltonian for each local CH stretch H_{str}, and (iii) the local-local coupling H_{l-l} connecting the local CH stretches,

$$\begin{aligned} {}^{twv}H &= {}^{tw}H + H_{str} + H_{l-l} \\ &\approx {}^{tw}H + H_{str}^{(0)} + H_{l-l}^{(0)} + H_{str}^{(1)} + H_{l-l}^{(1)} + H_{str}^{(2)} + H_{l-l}^{(2)} \end{aligned} \tag{4.16}$$

The torsion-wagging-vibration interaction is addressed by expanding both H_{str} and H_{l-l} as Fourier series in the torsional angle α and a power series in the inversion angle τ. The lowest-order Hamiltonian terms with A_1 symmetry in the G_{12} molecular symmetry group are represented in the second line of Eq. (4.16) and are elaborated below. The zeroth-order terms, $H_{str}^{(0)}$ and $H_{l-l}^{(0)}$, treat the CH stretches in the absence of any coupling to the large-amplitude motions. The coupling terms, $H_{str}^{(1)}$, $H_{l-l}^{(1)}$, $H_{str}^{(2)}$, and $H_{l-l}^{(2)}$, contain the torsion and inversion dependence of those quantities.

Of the zeroth-order terms, $H_{str}^{(0)}$, contain only the diagonal harmonic oscillator energies,

$$H_{str}^{(0)} = \omega(v_1 + \frac{1}{2} + v_2 + \frac{1}{2} + v_3 + \frac{1}{2}), \tag{4.17}$$

where v_1, v_2 and v_3 are each 0 or 1 according the left side of Eq. (4.14). The local mode frequency ω is taken initially to be the average of the three fundamental CH stretch frequencies. No anharmonicity is included in the present work, but it is possible to do so, [16, 97] given sufficient information about the higher CH stretch excited states. The symmetrized off-diagonal local-local coupling Hamiltonian, $H_{l-l}^{(0)}$, is

$$H_{l\text{-}l}^{(0)} = \lambda(a_1^+ a_2 + a_1 a_2^+ + a_2^+ a_3 + a_2 a_3^+ + a_3^+ a_1 + a_3 a_1^+) \qquad (4.18)$$

where λ is the local-local coupling parameter and a_n and a_n^+ are the harmonic oscillator ladder operators acting on each of the three local CH stretch vibrations.

The combination of Eqs. (4.17) and (4.18) constitute the implementation of a standard local mode CH stretch Hamiltonian [25, 140] for molecules with G_{12} symmetry. If the large-amplitude degrees of freedom are suppressed, this local mode Hamiltonian can be expressed in the harmonic CH stretch basis (Eq. (4.14)) as

$$H_{str}^{(0)} = \begin{bmatrix} \omega & \lambda & \lambda \\ \lambda & \omega & \lambda \\ \lambda & \lambda & \omega \end{bmatrix} . \qquad (4.19)$$

In Eq. (4.19), the energy of the zero-point level, $E_0 = \frac{3}{2}\omega$, has been subtracted from the diagonal terms. The zeroth-order vibration-only Hamiltonian represented in Eq. (4.19) splits the three CH-stretch vibrations into A_1 and E_2 vibrational modes with the eigenvalues, [20]

$$\begin{aligned} E(^v A_1) &= \omega + 2\lambda \\ E(^v E_{2\pm}) &= \omega - \lambda \end{aligned} \qquad (4.20)$$

In the present cases (Table 4.1), λ is negative displacing the degenerate *E*-type CH stretch to higher frequency from the symmetric CH stretch (ν_3, A_1 in G_{12} or A' in C_s). At the level of Eq. (4.19), the *E*-type CH stretch remains degenerate; the splitting between ν_2 and ν_x (A' and A'' respectively in C_s) occurs only on the application of the higher order terms in Eq. (4.16) (represented by the parameter μ in Figure 4.6(b)). The eigenfunctions obtained by diagonalizing Eq. (4.19) are

$$\left|{}^{v}A_1\right\rangle = \frac{1}{\sqrt{3}}\left[\left|1\right\rangle + \left|2\right\rangle + \left|3\right\rangle\right]$$
$$\left|{}^{v}E_{2+}\right\rangle = \frac{1}{\sqrt{3}}\left[\left|1\right\rangle + \varepsilon^{2}\left|2\right\rangle + \varepsilon^{4}\left|3\right\rangle\right] \qquad (4.21)$$
$$\left|{}^{v}E_{2-}\right\rangle = \frac{1}{\sqrt{3}}\left[\left|1\right\rangle + \varepsilon^{-2}\left|2\right\rangle + \varepsilon^{-4}\left|3\right\rangle\right]$$

where $\varepsilon = \exp\left(\pi i/3\right)$. These eigenfunctions are the basis states used in Model I.

Now, returning to the full torsion-inversion-vibration problem, we examine in turn each of the four lowest-order coupling terms in Eq. (4.16). The lowest-order coupling term in the expansion of H_{str} that involves only the torsional coordinate α is

$$H_{str}^{(1)} = \mu^{(1)}\left[\left(a_1^{+}a_1 + a_1a_1^{+}\right)\cos 2\alpha + \left(a_2^{+}a_2 + a_2a_2^{+}\right)\cos(2\alpha - \tfrac{2\pi}{3}) + \left(a_3^{+}a_3 + a_3a_3^{+}\right)\cos(2\alpha + \tfrac{2\pi}{3})\right] \qquad (4.22)$$

where $\mu^{(1)}$ is the torsion-vibration coupling parameter.

As with methanol, this coupling term produces the splitting between the two asymmetric CH-stretches, ν_2 and ν_x (Figure 4.6(b)). To evaluate the coupling matrix elements, the torsion and inversion basis functions in Eq. (4.1) are approximated as delta-functions [20]. The matrix elements of the operator $H_{str}^{(1)}$ in Eq. (4.22) are then

$$\left\langle j, m\left|H_{str}^{(1)}\right|k, n\right\rangle = 2\mu^{(1)}\delta_{jk}\cos\left(2\alpha_k - \theta_m - \theta_n\right) \qquad (4.23)$$

where the phase angles are θ_n = 0, -2π /3 and +2π /3 for n = 1, 2, 3, and $\alpha_k = (k-1)\frac{\pi}{3}$. The form of the resulting 18×18 Hamiltonian matrix is given in Figure 4.8.

$^{twv}H =$

	|1⟩						|2⟩						|3⟩					
$k=$	1	2	3	4	5	6	1	2	3	4	5	6	1	2	3	4	5	6
	d_1	h_{2v}	h_{3v}	0	h_{3v}	h_{2v}	d_3	0	0	0	0	0	d_3	0	0	0	0	0
	h_{2v}	d_2	h_{2v}	h_{3v}	0	h_{3v}	0	d_3	0	0	0	0	0	d_4	0	0	0	0
	h_{3v}	h_{2v}	d_2	h_{2v}	h_{3v}	0	0	0	d_4	0	0	0	0	0	d_3	0	0	0
	0	h_{3v}	h_{2v}	d_1	h_{2v}	h_{3v}	0	0	0	d_3	0	0	0	0	0	d_3	0	0
	h_{3v}	0	h_{3v}	h_{2v}	d_2	h_{2v}	0	0	0	0	d_3	0	0	0	0	0	d_4	0
	h_{2v}	h_{3v}	0	h_{3v}	h_{2v}	d_2	0	0	0	0	0	d_4	0	0	0	0	0	d_3
	d_3	0	0	0	0	0	d_2	h_{2v}	h_{3v}	0	h_{3v}	h_{2v}	d_4	0	0	0	0	0
	0	d_3	0	0	0	0	h_{2v}	d_1	h_{2v}	h_{3v}	0	h_{3v}	0	d_3	0	0	0	0
	0	0	d_4	0	0	0	h_{3v}	h_{2v}	d_2	h_{2v}	h_{3v}	0	0	0	d_3	0	0	0
	0	0	0	d_3	0	0	0	h_{3v}	h_{2v}	d_2	h_{2v}	h_{3v}	0	0	0	d_4	0	0
	0	0	0	0	d_3	0	h_{3v}	0	h_{3v}	h_{2v}	d_1	h_{2v}	0	0	0	0	d_3	0
	0	0	0	0	0	d_4	h_{2v}	h_{3v}	0	h_{3v}	h_{2v}	d_2	0	0	0	0	0	d_3
	d_3	0	0	0	0	0	d_4	0	0	0	0	0	d_2	h_{2v}	h_{3v}	0	h_{3v}	h_{2v}
	0	d_4	0	0	0	0	0	d_3	0	0	0	0	h_{2v}	d_2	h_{2v}	h_{3v}	0	h_{3v}
	0	0	d_3	0	0	0	0	0	d_3	0	0	0	h_{3v}	h_{2v}	d_1	h_{2v}	h_{3v}	0
	0	0	0	d_3	0	0	0	0	0	d_4	0	0	0	h_{3v}	h_{2v}	d_2	h_{2v}	h_{3v}
	0	0	0	0	d_4	0	0	0	0	0	d_3	0	h_{3v}	0	h_{3v}	h_{2v}	d_2	h_{2v}
	0	0	0	0	0	d_3	0	0	0	0	0	d_3	h_{2v}	h_{3v}	0	h_{3v}	h_{2v}	d_1

Figure 4.8 The 18 ×18 torsion-wagging-vibration Hamiltonian (^{twv}H) matrix according to Model II for the three CH-stretch excited states, where

$d_1 = 2\mu + \omega$, $d_2 = -\mu + \omega$, $d_3 = \lambda + \frac{1}{2}\lambda'$, and $d_4 = \lambda - \lambda'$.

The next lowest-order term in the expansion of H_{str} involves both of the large-amplitude coordinates, α and τ,

$$H_{str}^{(2)} = \mu^{(2)}\left[\left(a_1^+ a_1 + a_1 a_1^+\right)\tau\cos\alpha + \left(a_2^+ a_2 + a_2 a_2^+\right)\tau\cos(\alpha + \tfrac{2\pi}{3}) + \left(a_3^+ a_3 + a_3 a_3^+\right)\tau\cos(\alpha - \tfrac{2\pi}{3})\right] . \quad (4.24)$$

The Hamiltonian matrix elements of this term are given by,

$$\begin{aligned}\left\langle j,m\left|H_{str}^{(2)}\right|k,n\right\rangle &= -2\mu^{(2)}\delta_{jk}\tau_{eq}\cos 3\alpha_k\cos\left(\alpha_k-\theta_m-\theta_n\right)\\ &= -2\mu^{(2)}\delta_{jk}\tau_{eq}\cos\left(2\alpha_k-\theta_m-\theta_n\right)\end{aligned} \tag{4.25}$$

where θ_n and α_k have the same definitions as in Eq. (4.23). These matrix elements are the same as Eq. (4.23), except that $\mu^{(1)}$ is replaced by $-\mu^{(2)}\tau_{eq}$. In Figure 4.8, the coupling parameter, $\mu=\mu^{(1)}-\mu^{(2)}\tau_{eq}$, incorporates the combined contributions from these two coupling terms.

The lowest-order coupling terms that result from the expansion of H_{l-l} in terms of α and τ are

$$\begin{aligned}H_{l\text{-}l}^{(1)} = -\lambda^{(1)}\Big[&\left(a_2^+a_3+a_2a_3^+\right)\cos 2\alpha+\left(a_1^+a_3+a_1a_3^+\right)\cos(2\alpha-\tfrac{2\pi}{3})\\ &+\left(a_1^+a_2+a_1a_2^+\right)\cos(2\alpha+\tfrac{2\pi}{3})\Big]\end{aligned} \tag{4.26}$$

and

$$\begin{aligned}H_{l\text{-}l}^{(2)} = -\lambda^{(2)}\Big[&\left(a_2^+a_3+a_2a_3^+\right)\tau\cos\alpha+\left(a_1^+a_3+a_1a_3^+\right)\tau\cos(\alpha+\tfrac{2\pi}{3})\\ &+\left(a_1^+a_2+a_1a_2^+\right)\tau\cos(\alpha-\tfrac{2\pi}{3})\Big]\end{aligned} \tag{4.27}$$

The Hamiltonian matrix elements resulting from Eq. (4.26) and (4.27) are given by

$$\left\langle j,m\left|H_{l-l}^{(1)}\right|k,n\right\rangle = -\lambda^{(1)}\delta_{jk}\cos\left(2\alpha_k-\theta_m-\theta_n\right)\left(1-\delta_{mn}\right) \tag{4.28}$$

and

$$\begin{aligned}\left\langle j,m\left|H_{l-l}^{(2)}\right|k,n\right\rangle &= \lambda^{(2)}\delta_{jk}\tau_{eq}\cos 3\alpha_k\cos\left(\alpha_k-\theta_m-\theta_n\right)\left(1-\delta_{mn}\right)\\ &= \lambda^{(2)}\delta_{jk}\tau_{eq}\cos\left(2\alpha_k-\theta_m-\theta_n\right)\left(1-\delta_{mn}\right)\end{aligned} \tag{4.29}$$

Eq. (4.28) and (4.29) are the same except that $\lambda^{(1)}$ is replaced by $-\lambda^{(2)}\tau_{eq}$. In Figure 4.8, the coupling parameter, $\lambda'=\lambda^{(1)}-\lambda^{(2)}\tau_{eq}$, incorporates the combined contributions from

these two terms. That is, at the present level of development, the derived coupling terms yield two coupling terms, with parameters μ and λ' respectively, in the torsion-wagging-vibration Hamiltonian, ${}^{twv}H$ (Eq. (4.16) and Figure 4.8). Although μ appears on the diagonal of ${}^{twv}H$ and λ' is off-diagonal, these two coupling terms have equivalent impacts on the energy eigenvalues. That is, μ and λ' are not independently determinable from torsion-wagging-vibration eigenvalue spectra, yielding effectively a single distinct coupling term. For convenience, we will set $\lambda' = 0$ and vary μ along with ω and λ to fit available spectral data. An alternative set of Model II parameters with μ constrained to zero is given in Appendix K.

Although the same eigenvalues can be obtained with many different combinations of the four parameters, $\mu^{(1)}$, $\mu^{(2)}$, $\lambda^{(1)}$ and $\lambda^{(2)}$, the implications for the nuclear motion are not the same. The present model, relying on the simple parameterized treatment of torsion and inversion tunneling, does not include interactions with states one or more quanta of torsion or inversion excitation. To obtain a more realistic model of the nuclear motion, one would need to combine the four coupling terms with a more complete torsion-inversion basis set [28, 128]. Then, when modeling torsion and inversion excited states built on the CH stretch excited states, one might also find that each of these four terms has a different impact on the energy eigenvalues. However at the level of the present model, where we deal only with the energies of the lowest torsion-inversion tunneling states in each CH stretch excited state, the four coupling terms are equivalent leaving us only with a single distinct coupling term.

The implementation of Model II employs the ground state values of the tunneling parameters, h_{2v} and h_{3v}, as determined from microwave spectra (Table 4.1). The other three parameters, ω, λ, and μ, can be determined from the three CH stretch fundamental frequencies. As indicated above, these frequencies are known from infrared spectroscopy for CH_3NH_2 and CH_3OH but are estimated from *ab intio* molecular structure calculations using Gaussian 09 [136] for 2-MMA and 5-MT-d4 (Table 4.1). The same *ab initio* levels used for 2-MMA and 5-MT-d4 were tested on CH_3NH_2 and CH_3OH and compared to the experimental frequencies, with MP2/6-311G++(3df, 2p) giving overall a little better agreement for the coupling parameters λ and μ than B3LYP/6-311G++(3df, 2p). The computed values of λ were larger than the experimental values (by 30% – 35% for MP2), and the computed values of μ are smaller (by ~50% for MP2). The agreement between the two computational methods (up to 16% variation of λ and μ) is relatively improved. As noted above in the context of the parameter *g* in Model I, the values of ω, λ, and μ determined from experimental frequencies are effective values affected by CH stretch-bend interactions within the methyl group [138]. In methanol, the six CH bending combination bands fall between the asymmetric CH stretches, ν_2 and ν_9, on the high side and ν_3 on the low side. Therefore, the perturbation shifts from the 1:2 stretch:bend resonance increase the separation of the CH fundamentals, resulting in a larger effective value of λ. Since the relative methyl group vibrational frequencies are similar in the other subject molecules, similar effects can be anticipated. With allowance for these uncertainties, the following picture emerges: (i) The parameter μ is positive in each case, except for CH_3NH_2, reflecting $\nu_2 > \nu_x$ for 2-MMA, 5-MT-d4, and CH_3OH but $\nu_2 < \nu_{11}$ for

CH_3NH_2. (ii) The magnitudes of λ and μ are similar across the four molecules, with a much greater variation (up to 800×) in the tunneling parameters, h_{2v} and h_{3v}.

The torsion-inversion tunneling patterns predicted by Model II for three CH-stretch excited states (ν_2, ν_3 and ν_x) are represented as the markers in Figure 4.7. The most striking result evident from Figure 4.7 is that, in the slow tunneling limit (i.e., when $|\mu| >> |h_{2v}| + |h_{3v}|$), Model II predicts the same tunneling patterns as Model I. In this limit, we have the correspondence between the parameters of Models I and II,

$$g \approx \mu\left(1 - \frac{17\mu}{48\lambda}\right). \qquad (4.30)$$

Derivation of Eq. (4.30) involves expansion of an expression for the eigenvalues as a Taylor series in μ/λ. Eq. (4.30) is equivalent to Eq. (21a) of Ref. ([20]) except for the correction to Ref. ([28]) noted in Ref. (9) and with the addition of the first-order term in μ/λ. It should be noted however that even in this slow tunneling limit, the two models are not exactly equivalent. In Model I, because the modes ν_2 and ν_3 (both A′ in C_s) do not interact, ν_3 has equal amplitudes on each of the three methyl hydrogens. However in Model II, the A' modes do interact and the relative amplitudes on the three methyl hydrogens depend on the values of μ and λ. The slow tunneling limits of the two models become exactly equivalent in the limit $|\lambda| >> |\mu|$.

In Model II, when the ratio $|\mu| / \left(|h_{2v}| + |h_{3v}|\right)$ is varied over the range of the subject molecules, the ordering of the tunneling levels and the qualitative pattern of the spacings remain unchanged; however, the absolute spacings do vary noticeably (Figure 4.9). Most

of the range of the abscissa $|\mu|/(|h_{2v}|+|h_{3v}|)$ in Figure 4.9 results from the variation of the tunneling parameters, h_{2v} and h_{3v}. At high tunneling rates (right side of Figure 4.9), the magnitudes of the tunneling splittings |Δ| for the two asymmetric CH stretch vibrations are no longer equal. The splittings for the vibration with higher frequency of the pair decrease relative to the other. In most cases, ν_2 is higher frequency vibration except for CH_3NH_2 where μ is negative and ν_{11} is the higher. The values of Δ follow the sum rule,

$$\Delta(\nu_2)+\Delta(\nu_x)=-\Delta(\nu_3)=-\Delta(gs) \qquad (4.31)$$

where *gs* refers to the ground state. Model I also follows this sum rule but with the condition, $\Delta(\nu_2)=\Delta(\nu_x)$.

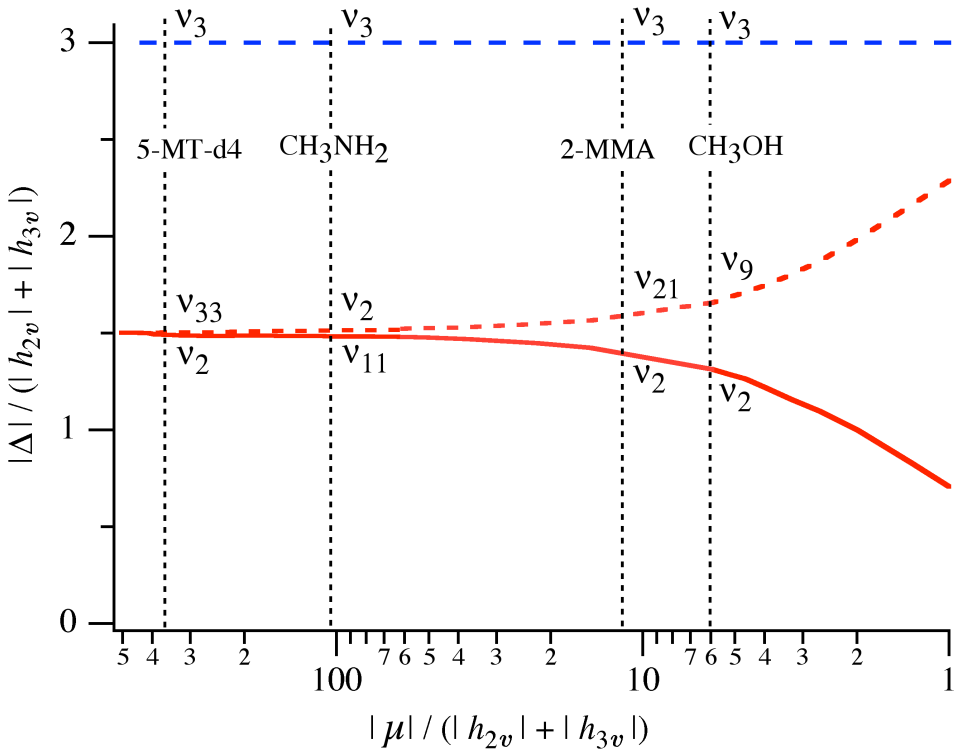

Figure 4.9 The magnitude, |Δ|, of the torsion-inversion-vibration tunneling spacings for the subject molecules as a function of ratio of the torsion-vibration coupling parameter to the tunneling parameters. The slow tunneling limit is at the left of the figure and fast tunneling at the right. Parameter values are tabulated in Table 4.2. The splitting Δ is the energy difference of the A and E_2 tunneling levels: $\Delta \equiv E\left({}^{tvv}E_2\right) - E\left({}^{tvv}A\right)$.

4.5 Discussion and conclusion

The qualitative agreement of the Models I and II across the range of possible tunneling parameters adds confidence to the predictions about the tunneling patterns in G_{12} molecules. The ground state tunneling pattern (Figure 4.3(a)) applies to the symmetric CH stretch (Figure 4.7(b)), but an inverted tunneling pattern (Figure 4.7(a)) applies to the asymmetric CH stretches. With the assumption that the tunneling

parameters h_{2v} and h_{3v} are the same in the CH stretch excited states as they are in the ground state, both models predict that the magnitude of the tunneling splittings for the symmetric CH stretch will be the same as in the ground state ($\Delta(\nu_3) = \Delta(gs)$), but for the two asymmetric CH stretches, only about half of that, $\Delta(\nu_x) \approx \Delta(\nu_2) \approx -\frac{1}{2}\Delta(gs)$ (Figure 4.7). Unlike Model I, Model II predicts unequal tunneling splittings ($\Delta(\nu_x) \neq \Delta(\nu_2)$) for the two asymmetric CH-stretches when the tunneling is fast (i.e., large $|h_{2v}| + |h_{3v}|$). The models predict a significant dependence of the magnitude and pattern of tunneling splittings on the values of the tunneling parameters h_{2v} and h_{3v}, but at most, a modest dependence on the other molecular parameters. The models also make predictions for G_6 systems with only methyl torsional tunneling by applying the limit, $h_{2v} \to 0$.

Happily, existing spectral fitting programs [82, 103] that have been applied to the ground state rotational spectra are also applicable to the model predictions for the CH vibrationally excited states provided that the "effective" tunneling parameters, h_{2v}^{eff} and h_{3v}^{eff}, used to fit the spectra are allowed to vary in both sign and magnitude relative to their ground state values. The tunneling patterns obtainable are shown in Figure 4.3. Specifically, for the symmetric CH stretch excited state, one expects $h_{2v}^{eff} \approx h_{2v}$ and $h_{3v}^{eff} \approx h_{3v}$, where both are negative and for the asymmetric CH stretches, $h_{2v}^{eff} \approx -\frac{1}{2}h_{2v}$ and $h_{3v}^{eff} \approx -\frac{1}{2}h_{3v}$.

At present, there is little available experimental data to compare with the model predictions. The high-resolution spectrum of the ν_{11} band of methylamine has been reported, [50] but unfortunately that band contains multiple perturbations, some causing level shifts larger than the expected tunneling splittings. The deperturbed experimental splitting pattern for the ν_{11} excited state as shown in Figure 4.10 is different from both the ground state and from the model predictions suggesting that the deperturbations are incomplete. A reasonable explanation of the experimental ν_{11} splitting pattern is the combined effects of such residual perturbations together with the systematic changes in the splitting pattern predicted by the present models for the ν_{11} excited state. The ethyl radical is another analogous 6-well system for which high resolution spectra of the CH fundamentals are available. However in the ethyl radical, the torsion-inversion barrier is very low (17 cm^{-1}) [141], rendering the present high-barrier models inapplicable.

Methanol is the only system with complete experimental data in the CH stretch region that can be compared to the model predictions. With the limit $h_{2v} \to 0$ and the $G_{12} \to G_6$ symmetry correlations in Figure 4.1(d), the predicted tunneling splittings for the three CH stretch excited states can be obtained. The predictions of Models I and II are compared to the experimental splittings [28, 142] and to two other theoretical treatments [28, 122] in Table 4.2. The sum rule from Model II, Eq. (4.31), is in agreement with the experimental data, but the ratio $\Delta(\nu_9)/\Delta(\nu_2)$ is larger in the experiment (1.7 vs 1.3). Clearly, Model I which sets $\Delta(\nu_9)=\Delta(\nu_2)$ is missing the interaction that causes these splittings to differ. Model II includes interactions among the three local CH stretches that affect the relative values of the splittings for ν_2 and ν_9 (Figure 4.9).

Models I and II are subject to the following limitations: (i) The assumption of a localized basis functions for the large-amplitude degrees of freedom is best for high-barrier situations where the probability amplitude is restricted to small regions around each of the six equivalent minima. (ii) The tunneling parameters have been assumed to be independent of vibrational excitation. An adiabatic vibrational dependence of torsional tunneling has been applied to model the decreased splittings in the OH stretch overtones of methanol [32, 94] and hydrogen peroxide [143, 144] and could be implemented here if it were found necessary to do so. While the available data are limited, the success of the sum rule in methanol is an indication that it may not be necessary for methyl CH stretches. (iii) Both models neglect entirely the other vibrational degrees of freedom that can cause level shifts from Fermi resonances and other perturbations.

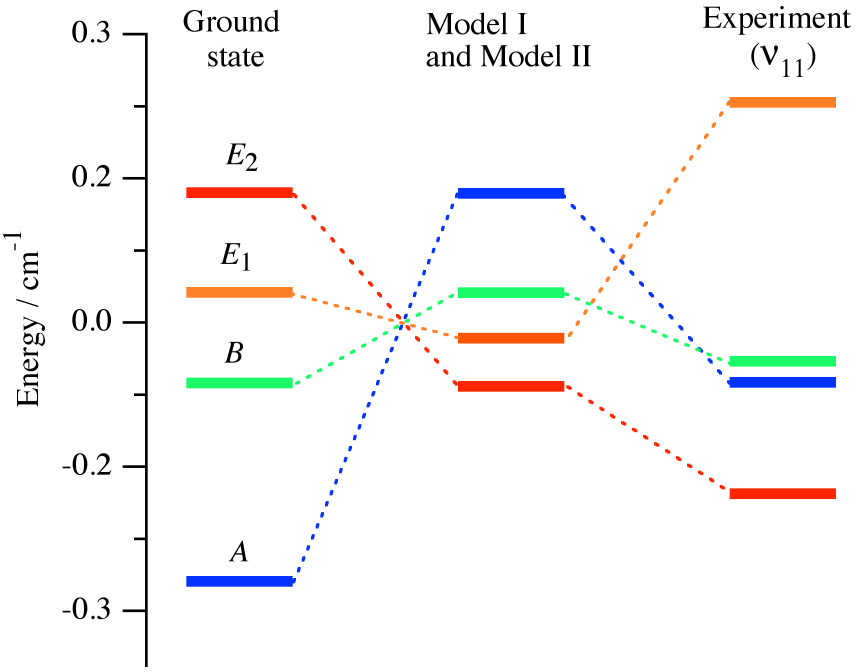

Figure 4.10 Comparison of the observed torsion-inversion tunneling pattern in the ν_{11} asymmetric CH-stretch vibrationally excited state of CH_3NH_2 with the ground state pattern and with the predictions of Models I and II. The plotted energy is relative to the weighted mean energy of the tunneling multiplet.

Table 4. 2 Methanol Tunneling Splittings, Δ, in cm-1

Vibrational State	Model I	Model II	Wang and Perry [b]	Sibert and Castillo-Chara [c]	Expt [b].
Ground [a]	9.1	9.1	9.1	8.8	9.1
ν_3	9.1	9.0	8.9	5.6	8.8
ν_2	-4.6	-3.9	-2.6	-2.8	-3.3
ν_9	-4.6	-5.1	-6.6	-4.0	-5.5

[a] Ground state splitting are from Ref. [142].
[b] Ref. [28].
[c] Ref. [122].

The Wang and Perry internal coordinate model [28] is similar in concept to Model II but it includes a free internal rotor torsional basis that allows calculation of the torsional dependence of the torsion-vibration wavefunctions. In terms of the level structure, it includes interactions of the ν_2 and ν_9 vibrations with torsionally excited states built on ν_3. A first principles full dimensional treatments of the methanol tunneling splittings by Sibert and Castillo-Chara [122] included all of the other nearly resonant vibrational states, including the six binary CH bend combination bands that have been shown to interact strongly with the CH fundamentals [95, 121, 122]. Each of these two treatments and Model II yield different discrepancies relative to experiment (Table 4.2), but overall, the agreement with experiment is comparable.

CHAPTER V

CONICAL INTERSECTIONS BETWEEN VIBRATIONALLY ADIABATIC SURFACES IN METHANOL

The content of this chapter has been published as "Conical Intersections between Vibrationally Adiabatic Surfaces in Methanol" by Mahesh B Dawadi, and David S. Perry; [M.B. Dawadi, D.S. Perry, J. Chem. Phys.-Communication, ***140*** *(16), 161101 (2014)]. It is reproduced here with only the minimal editing necessary to confirm to the format and style of this dissertation*

A set of seven conical intersections (CIs) in methanol between vibrationally adiabatic surfaces is reported. The intersecting surfaces represent the energies of the two asymmetric CH stretch vibrations regarded as adiabatic functions of the torsion and COH bend angles. The *ab initio* data are well described by an extended Zwanziger and Grant ($E\otimes e$) model (J. Chem. Phys. **87**, 2954 (1987)) that might also be regarded as an extension of the XHL model (J. Mol. Spectrosc. **293-294**, 38 (2013)). The CIs illuminate the role of geometric phase in methanol. More generally, they suggest the importance of energy transfer processes localized near the CIs.

5.1 Introduction

The existence of conical intersections between electronic potential energy surfaces is well established and has now been shown to be widespread throughout the electronic spectroscopy and responsible for ultrafast electronic relaxation in diverse circumstances [30, 43]. Whereas these electronic surfaces represent the adiabatic separation of electronic and nuclear motions under the Born-Oppenheimer approximation, it is also possible in some cases to make an (approximate) adiabatic separation of fast and slow vibrational motions. In such cases, the motion of the high frequency vibrations, which might include hydride stretches, can be solved quantum mechanically at each molecular geometry along the low frequency, large-amplitude torsional or bending coordinates. These slower motions are then solved in the effective potential that is the sum of the electronic potential plus the variation of the high-frequency vibrational energies in the large-amplitude space. Recently, Hamm and Stock [43] have pointed out that conical intersections between vibrationally adiabatic surfaces could lead to ultrafast vibrational relaxation.

Methanol is a molecular case to which the adiabatic approximation has been applied, the high frequency vibrations being the OH and CH stretches (3860, 2999, 2956, and 2844 cm^{-1}) and the low frequency coordinate being the torsional angle, γ. Fehrensen *et al.*[32] applied an adiabatic reaction path Hamiltonian to account for both the decrease of the torsional tunneling splittings with OH stretch excitation, ν_1, and also the inverted torsional tunneling splittings in the first excited states of the asymmetric CH stretches, ν_2 and ν_9. They found that a geometric phase of -1 was accumulated for the CH vibrations ν_2 and ν_9 on a torsional rotation of 2π. Accordingly they solved the torsional motion

with 4π boundary conditions. Wang and Perry [28] found that an internal coordinate model of the CH stretches with only Jahn-Teller-like coupling terms in cosγ gave the correct tunneling splittings. Renner-Teller-like coupling terms in cos2γ were also derived in that work, but were not implemented in the model because the cosγ terms were sufficient to obtain agreement with the available experimental data. Clasp and Perry [31] showed that an adiabatic approximation to this model also gave qualitatively correct results for the tunneling splittings in the first excited CH stretch states. Recently, Xu *et al*.[145] have preformed *ab initio* frequency calculations along the steepest descent internal rotation path. To describe these results, they developed a two-state model in which the E-type symmetric rotor CH stretch basis states are coupled by both Jahn-Teller like ($\exp(i\gamma)$) and Renner-Teller-like ($\exp(-2i\gamma)$) coupling terms to form the two asymmetric CH stretch states. Xu *et al*. [146] found that the vibrational amplitudes for both ν_2 and ν_9 returned to their original values (did not change sign) upon a 2π internal rotation along the minimum energy path (MEP); that is, the geometric phase accumulated is +1.

Zwanziger and Grant [34] studied $E\otimes e$ systems in which both Jahn-Teller and Renner-Teller couplings are present, the former scaling linearly with the deviation ρ from the C_{3v} reference geometry and the latter scaling quadratically. They showed that there are necessarily four CIs between the coupled electronic surfaces, one at the C_{3v} reference geometry and three more at distorted geometries of C_s symmetry at the values of ρ where the magnitudes of the linear and quadratic couplings become equal. Transport along a path in the 2-dimensional (γ, ρ) coordinate space that encloses one CI results in the

accumulation by the electronic wavefunctions of a geometric phase of -1 and that a path enclosing all four CIs results in a geometric phase of $(-1)^4 = +1$.

While their work was formulated in the context of a doubly degenerate (*E*) electronic state interacting with a degenerate (*e*) vibrational mode, the same formalism applies also to the case of methanol, where the adiabatic separation is not between degenerate Born-Oppenheimer electronic states and a degenerate vibrational mode, but now between a high frequency degenerate vibrational state in the electronic ground state, adiabatically separated from a pair of large-amplitude low-frequency modes. Specifically, we will consider the vibronic surfaces formed by considering the energies of the asymmetric CH stretch vibrations as a function of the torsional angle, γ, and the COH bend angle, ρ. The C_{3v} reference geometry occurs at $\rho = 0$ where the COH group is linear. In this reference geometry, the two asymmetric CH stretch vibrations (ν_2 and ν_9) become degenerate (*E*), and the large-amplitude coordinates ρ and γ together become a degenerate COH bending coordinate (*e*).

One significant difference encountered when applying the $E \otimes e$ formalism to the vibrationally adiabatic surfaces in methanol is that the equilibrium geometry is now far from the C_{3v} reference geometry ($\rho = 71^\circ$) rather than close to it as is typically the case for Jahn-Teller coupling between electronic surfaces. Whereas Zwanziger and Grant [34] neglected anharmonicity and kept only the coupling terms of the lowest order in ρ ($\rho\exp(i\gamma)$ and $\rho^2\exp(-2i\gamma)$, respectively), it will be necessary in the methanol case to include higher-order terms in ρ.

In this Chapter, *ab initio* calculations reveal a set of seven conical intersections between vibrationally adiabatic surfaces in methanol and the resulting surfaces are fitted

to an extended expression of the type presented by Zwanziger and Grant [34]. When the CO stretch is included along with ρ and γ as a low frequency mode, the conical intersections become seams of conical intersections that are mapped out in this three-dimensional space. The implications for spectroscopy and dynamics are explored.

5.2 Conical intersections revealed by *ab initio* data

The eclipsed (torsional saddle point: γ=0˚, ρ=70.95˚) and staggered (torsional global minimum: γ=180˚, ρ=71.42˚) geometries in the C_s symmetry of methanol were optimized with G09 package [136] at the same MP2 level of theory employed by Xu *et al*. [146] (MP2=Full/6-311+G(3df,2p), OPT=(Z-matrix,Vtight)). In addition, DFT calculations with a smaller basis set (B3LYP/6-31+G(2d,p), OPT=(Z-matrix, tight) were undertaken to illustrate the dependence of the results on the level of theory. For both the eclipsed (γ=0˚, 120˚, 240˚) and staggered (γ=60˚, 180˚, 300˚) conformers, additional partially optimized calculations were carried out with the COH bend angles ρ at a series of fixed values from 0 to 100˚. At each of these partially optimized C_s geometries, the vibrational frequencies of the two asymmetric CH stretch vibrations (ν_2 A′ and ν_9 A″) and harmonic force constants for the in-plane and out-of-plane CH bonds were calculated as a function of COH bend angle ρ (Figures 5.1 (a) and (b)). From Figure 5.1, it is clearly seen that for the eclipsed geometry, both the vibrational frequencies and the harmonic force constants cross when the COH angle is bent at ρ = 62˚ and 93˚ from linear.

There are a number of conceptual steps to identify the crossing of these frequencies and force constants with CIs. Within the harmonic approximation used in the normal mode analysis, the CH stretch frequencies provide approximations to the energies

of the quantum mechanical CH stretch excited states relative to the zero-point vibrational level. Since these vibrational energies are calculated for the high-frequency CH stretch modes as a function of the large-amplitude coordinates ρ and γ, they represent an adiabatic separation of the high- and low-frequency vibrational modes.

Strictly speaking, the normal mode calculation is only valid at the stationary points: the global minima, the torsional saddle points, and the C_{3v} geometry ($\rho = 0^{\circ}$). However, we argue that the CH stretches mix only negligibly with the low frequency modes and that the computed "normal mode" frequencies provide a credible description of how these frequencies vary as a function of the low-frequency coordinates. Evidence to support this assertion comes from a comparison of Figures 5.1((a) and (b)). Figure 5.1(b) shows that for the eclipsed conformations, the single CH bond force constants cross at close to the same locations as the crossings of the normal modes ν_2 and ν_9. In the C_s geometries, the two out-of-plane CH force constants are equal by symmetry, so that when these are both equal to the in-plane CH force constant then all three CH force constants are equal.

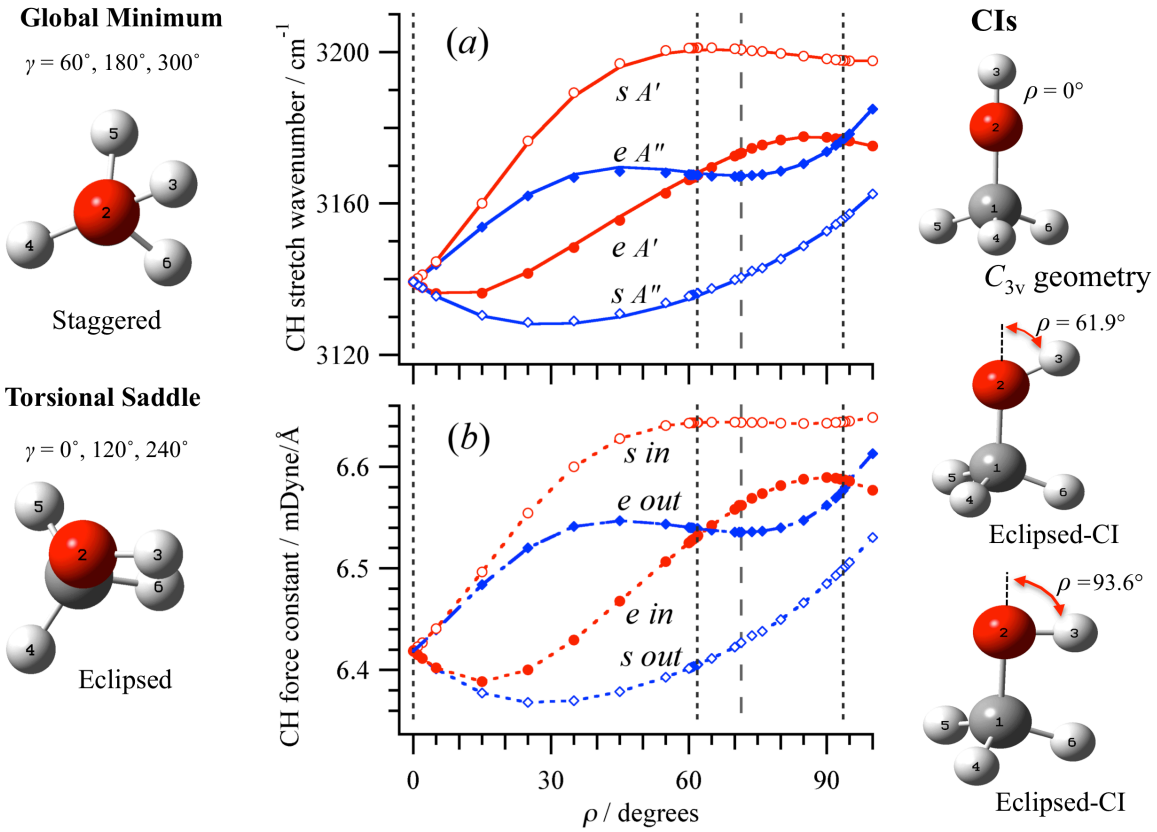

Figure 5. 1 (a) Vibrational frequencies for the two asymmetric CH stretch vibrations (ν_2 A′ and ν_9 A″) of methanol computed at the *ab initio* levels MP2/6-311+G(3df,2p) for conformations of C_s symmetry. The abscissa is the COH bend angle ρ, measured relative to linearity ($\rho = 0^\circ$). The staggered (s) and eclipsed conformations (e) are indicated. The model calculation is shown as solid lines. The vertical lines, extending through both parts of the figure, indicate the ρ angles at which the A′ and A″ frequencies cross (short dashes) and also the equilibrium geometry (long dashes). (b) The harmonic force constants for individual CH bonds in the C_s plane of symmetry (in) and out-of-plane (out) cross at nearly the same ρ angles. The molecular geometries are the optimized structure of global minimum, torsional saddle point and CIs points of C_s symmetry conformations of methanol.

In the case three equal CH stretch force constants, a coupled local mode treatment, in which the CH stretches are isolated form all other modes, would yield two asymmetric CH stretches of equal frequency and a symmetric CH stretch shifted in frequency as a result of the local-local coupling. In fact, the whole pattern of the variation of the ν_2 and ν_9 frequencies in Figure 5.1(a) is reflected in the pattern of the single-bond force constants in Figure 5.1(b). We conclude that the existence and locations of the frequency crossings is primarily attributable to the variation of the single-bond force constants. Additional evidence supporting the validity of the CH stretch normal mode frequencies computed at non-stationary points will be presented in the sections below.

The above discussion has been limited to the C_s geometries in which the two asymmetric CH stretch vibrations have different symmetries, A′ and A″. Accordingly, there is no coupling between them and there are true crossings of the eclipsed frequencies in Figure 5.1(a). Away from the C_s geometries, the coupling is not required to be zero by symmetry. Accordingly a number of partially optimized points (Figure 5.2) were calculated at non- C_s geometries in the vicinity of the crossings to document the shape of the conical intersections.

To this point, we have discussed only five of the twelve vibrational modes, the two asymmetric CH stretches, ρ and γ. The roles of the other seven vibrational modes will be discussed further below. Finally, the relative energies of the different conical intersections are given by the variation of the energies of the CH-stretch states added to the much larger variation of the electronic potential. For example at the present MP2 level, the torsional saddle points are 357 cm^{-1} above the global minima and the C_{3v} symmetry point at $\rho = 0^\circ$ is at 10,967 cm^{-1}. The overall appearance of the graphs in

Figures 5.1((a) and (b)) are very similar, suggesting that the existence and locations of the frequency crossings is primarily attributable to the variation of the single-bond force constants.

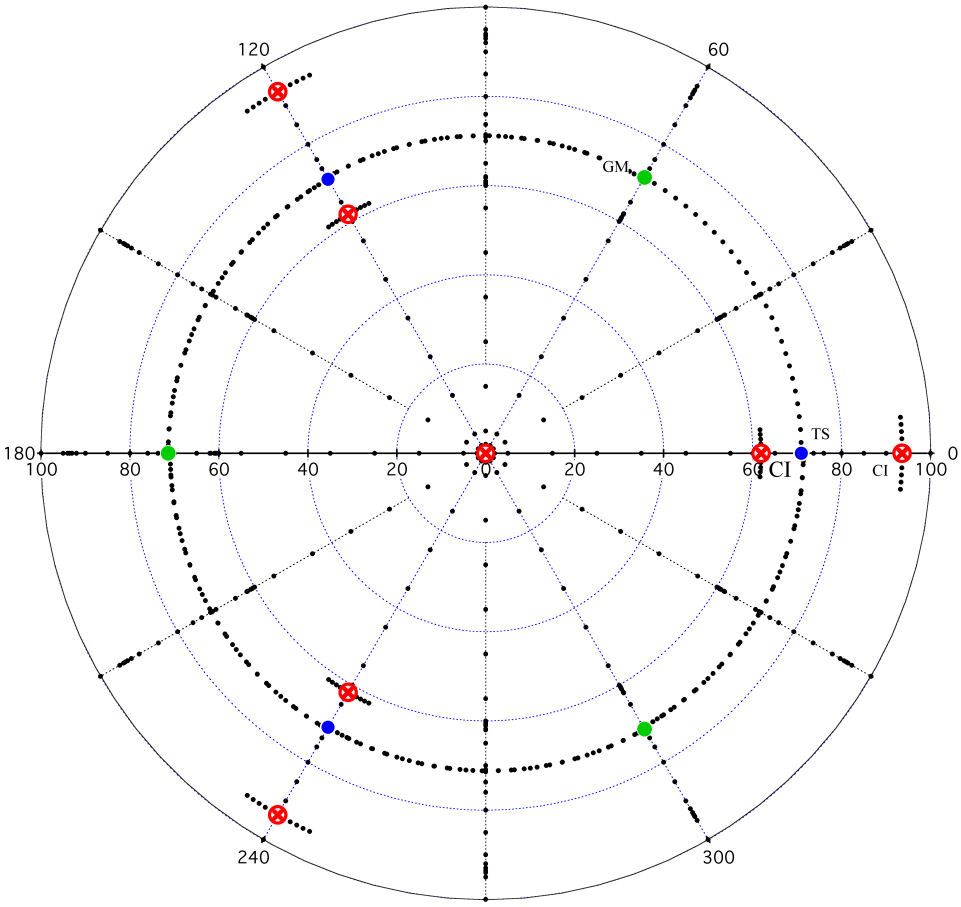

Figure 5. 2 A map in the two-dimensional coordinate space of the COH bend angle ρ and the torsional angle γ showing the locations of the computed points and the conical intersections. The red markers represent the conical intersections points with ρ = 0, 62˚ and 93˚. The blue markers represent the torsional saddle points, the green markers represent the global minima points and the black markers are the computed points along the MEP.

Calculations at the lower level, B3LYP//6-31+G(2d,p), yielded frequency crossings in the same locations (±0.5˚) and the resulting graphs (Appendix L) are essentially identical in appearance to Figure 5.1. In new report, [145] higher level calculations (CCSD(T)/aug-cc-pVTZ) confirm the MP2 results of *Xu et al*.,[146] regarding the behavior along the torsional MEP.

The consistency across different levels suggests that neither the existence nor the locations of the CIs are strongly dependent on the level of calculation. Along the minimum energy path (MEP) connecting the global minima and torsional saddle points, three different types of ab initio frequency calculations were carried out: (i) along the path of steepest descent from the torsional saddle point (intrinsic reaction coordinate,"IRC"), a series of points with an 11-dimensional normal mode analysis at each point, projecting out the reaction coordinate itself, (ii) along the same IRC path, ordinary 12-dimensional (non projected) normal mode analyses, and (iii) at partially optimized structures at a series of fixed torsional angles, ordinary 12-dimensional (non projected) normal mode analyses. Calculation (i) is the same as was done by Xu *et al*. [146] with the three-step G09 procedure: (a) MP2= Full/6-311+G(3df,2p), OPT=(Z-matrix, Vtight, TS, Nrscale,Noeigen) Nosymm, (b)MP2=Full/6-311+G(3df,2p), Geom=check Nosymm IRC=(Stepsize=6, Maxpoints=28,Forward,RCFC,Vtight), and (c) MP2=Full/6-311+G(3df,2p), Freq=HPModes, where in step (c) the input geometries along the MEP are from the IRC calculation outputs. The projected vibrational frequencies along the MEP are given in Table 5 of Ref. [147] in terms of Fourier expansion coefficients and values from those Fourier coefficients are depicted in Figure 5.3. In the partial optimization procedure (iii), we used the same convergence criterion,

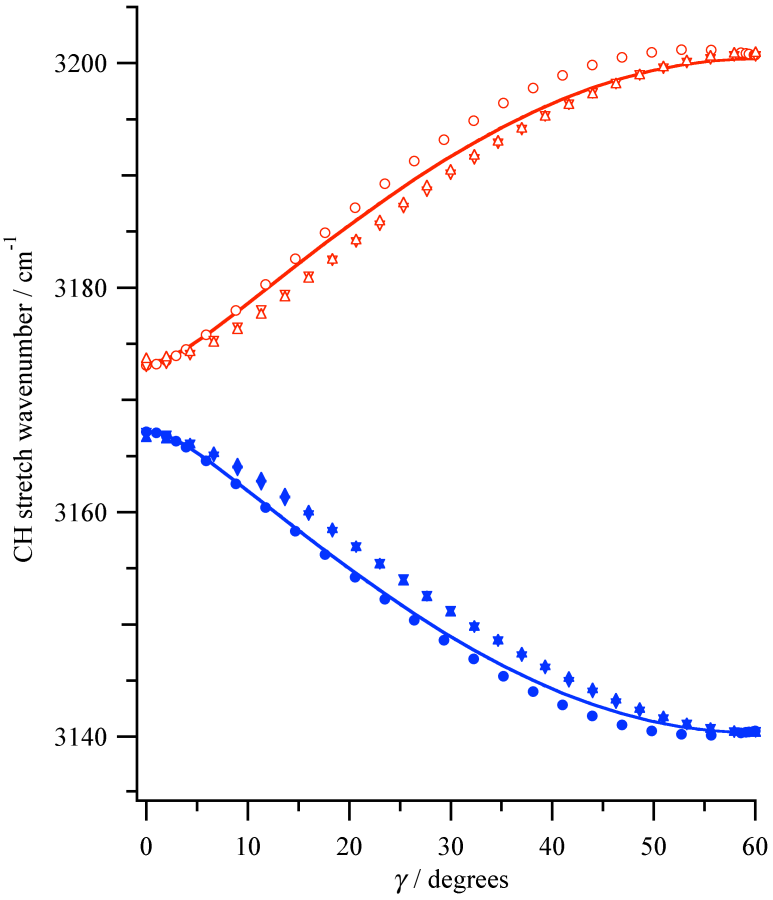

Figure 5. 3 Variation of the computed frequencies of two asymmetric CH stretch vibrations (A′ and A″) of methanol along paths connecting the global energy minimum (staggered). *Ab initio* points at the MP2/6-311+G(3df,2p) level are indicated by markers and the line is the model calculation. All unfilled (open) markers indicates the A′ vibrations while all filled markers are A″ vibrations. Three kinds of calculations are represented. (i) Triangles indicate the calculated projected frequencies along the IRC path (Table 5 of Ref.[147]). (ii) Diamonds represent values of unprojected frequencies along the IRC path from Gaussian 09 calculations. (iii) Circles represent computed frequencies of partially optimized geometries.

basis set and theory level. For each partially optimized geometry, the vibrational frequencies and average torsional angle γ [147] were calculated. For each of these three kinds of calculation, computed vibrational frequencies for the two asymmetric CH stretch vibrational modes of methanol are plotted in Figure 5.3 as a function of torsional angle γ. The 95 *ab initio* points in non-C_s geometries were computed in the vicinities of the crossings, along the torsional MEP, and at γ= 30˚ to make a total of 159 unique *ab initio* points (Appendices M and N).

5.3 Model calculations

For two electronic states coupled by both Jahn-Teller ($\rho\exp(i\gamma)$) and Renner-Teller ($\rho^2\exp(-2i\gamma)$) couplings, Zwanziger and Grant [34] derived the following 2x2 Hamiltonian for the adiabatic electronic energies:

$$H_{el}^{adiabatic} = \begin{bmatrix} \frac{1}{2}\rho^2 & k\rho e^{-i\gamma} + \frac{1}{2}g\rho^2 e^{2i\gamma} \\ k\rho e^{i\gamma} + \frac{1}{2}g\rho^2 e^{-2i\gamma} & \frac{1}{2}\rho^2 \end{bmatrix} \qquad (5.1)$$

for which the eigenvalues are

$$E_{\pm}^{adiabatic} = \frac{1}{2}\rho^2 \pm \left(k^2\rho^2 + kg\rho^3\cos 3\gamma + \frac{1}{4}g^2\rho^4\right)^{\frac{1}{2}} \quad . \qquad (5.2)$$

When viewed as a function of the distortion magnitude ρ and the distortion angle γ, these adiabatic energies form two surfaces that intersect at four conical intersections. When *k* and *g* have the same sign, one symmetry-required conical intersection at at ρ = 0 and three additional "accidental" symmetry-allowed conical intersections at ρ =2*k*/*g* with γ = π/3, π, and 5π/3. When *k* and *g* have opposite signs, they occur at ρ = 0 and at ρ =-2*k*/*g* with γ = 0, 2π/3 and 4π/3. The difference between these two situations is simply the

definition of where $\gamma = 0$. In this work, we use the latter convention in order to be consistent with notation of Xu *et al*. [146].

For the vibrationally adiabatic case in methanol, we note that the equilibrium geometry and the accidental conical intersections are all far from the undistorted C_{3v} geometry ($\rho = 0$). Therefore, we allow a more general ρ-dependence for both the diagonal and off-diagonal terms in Eq. (5.1),

$$\frac{H_{vib}^{adiabatic}}{hc} = \begin{bmatrix} \omega_0(\rho) & \frac{1}{2} f(\rho) e^{-i\gamma} + \frac{1}{2} g(\rho) e^{2i\gamma} \\ \frac{1}{2} f(\rho) e^{i\gamma} + \frac{1}{2} g(\rho) e^{-2i\gamma} & \omega_0(\rho) \end{bmatrix}. \quad (5.3)$$

The eigenvalues of the Hamiltonian in (5.3) in wavenumber units are

$$\omega_{\pm}^{adiabatic}(\gamma,\rho) = \omega_0(\rho) \pm \frac{1}{2}\left[f^2(\rho) + 2f(\rho)g(\rho)\cos 3\gamma + g^2(\rho)\right]^{\frac{1}{2}} \quad (5.4)$$

The functions of ρ are expressed as truncated polynomial expansions beginning at the lowest terms appearing in Eq. (5.1),

$$\begin{aligned} \omega_0(\rho) &= \omega_0^{(0)} + \sum_{i=2}^{7} \omega_0^{(i)} \rho^i \\ f(\rho) &= \sum_{i=1}^{7} f^{(i)} \rho^i \\ g(\rho) &= \sum_{i=2}^{7} g^{(i)} \rho^i \end{aligned} \quad . \quad (5.5)$$

Equation (5.4) was used to fit the *ab initio* frequencies of the asymmetric CH stretches for methanol in its C_s geometries, including both the staggered and eclipsed conformations. The ρ-dependent parameters, $\omega_0(\rho)$, $f(\rho)$ and $g(\rho)$, are plotted in Figure 5.4, and the resulting adiabatic surfaces are plotted in Figure 5.5. Although the fit

included only data from the C_s geometries, the resulting surfaces also provides a satisfactory fit to all of the data, including both the IRC and POPT points along the minimum energy path, the $\rho \neq 0$ points in the vicinities of the conical intersections, and the $\rho = 30^\circ$ points (Figure 5.2). The overall root-mean-square (RMS) deviation is 0.9 cm^{-1}. The lowest-order coefficients in Eq. (5.5) are reasonably well determined, but the higher-order coefficients are not. The functional forms in Eq. (5.5) simply provide the flexibility needed for a good overall fit to the ρ-dependence of the *ab initio* data.

To model their *ab initio* frequencies along the minimum energy torsional path, Xu *et al*. [146] developed a model (referred to here as the XHL Model) with two coupling parameters, k_1 and k_2,

$$\omega_{\pm}^2(\gamma) = \frac{1}{m}\left\{k_E \pm \left[k_1^2 + k_1^2 + 2k_1k_2\cos 3\gamma\right]^{\frac{1}{2}}\right\}. \qquad (5.6)$$

Here $\omega_{\pm}$ are the XHL Model frequencies for the asymmetric CH stretches; m is the reduced mass for the torsional motion, and k_E is the force constant for the hypothetical degenerate asymmetric CH stretch. Since the value of the COH bend angle ρ varies only slightly (by about 0.5˚) along the minimum energy path, Eq. (5.4) can be compared to Eq. (5.6) for fixed ρ. Within the approximation $\sqrt{1+x} \approx 1 + \frac{1}{2}x$ for small x, Eq. (5.4) is equivalent to Eq. (5.6) with $\omega_0^2 = k_E/m$, $f^2 = k_1^2/mk_E$, and $g^2 = k_2^2/mk_E$.

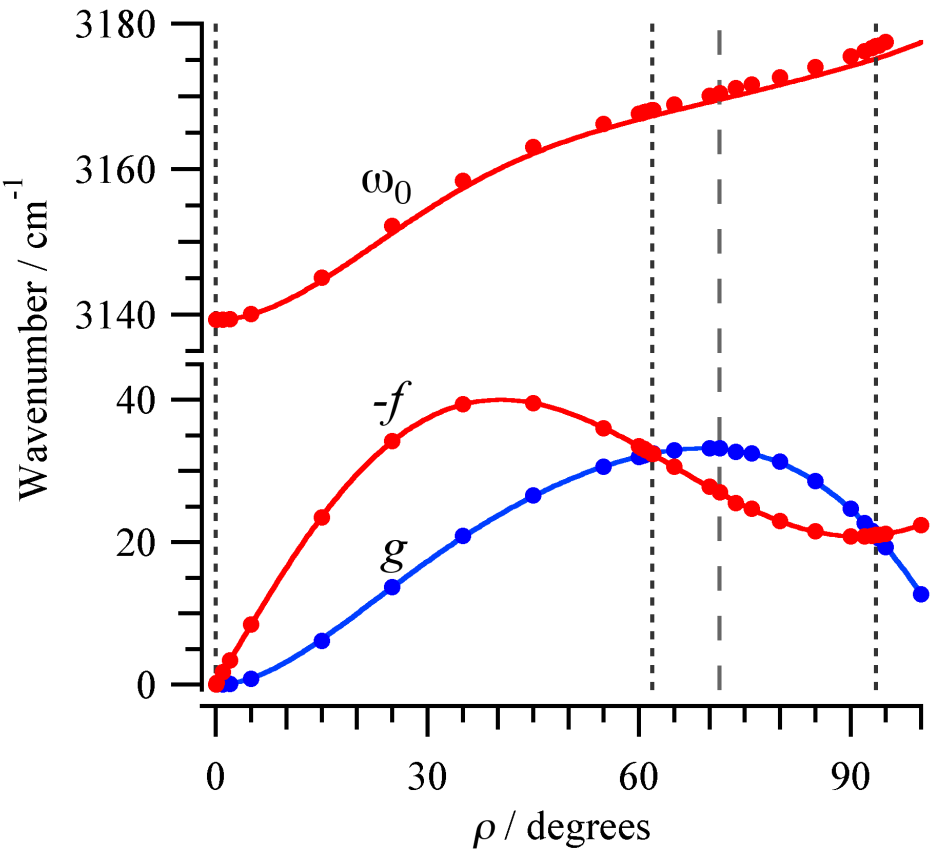

Figure 5. 4 The model parameters obtained from the overall fit (lines) and computed independently at each value of ρ (points). The vertical guide lines are the same as in Figure 5.1.

Indeed the present model calculation (Eq. (5.4) shown in Figure 5.3 is virtually identical to the model calculation (Eq. (5.6) presented in Figure 9 of Ref. [146]). Therefore, the present model can be thought of as an extension of the XHL Model to include the ρ-dependence of their parameters, k_E, k_1, k_2, and m.

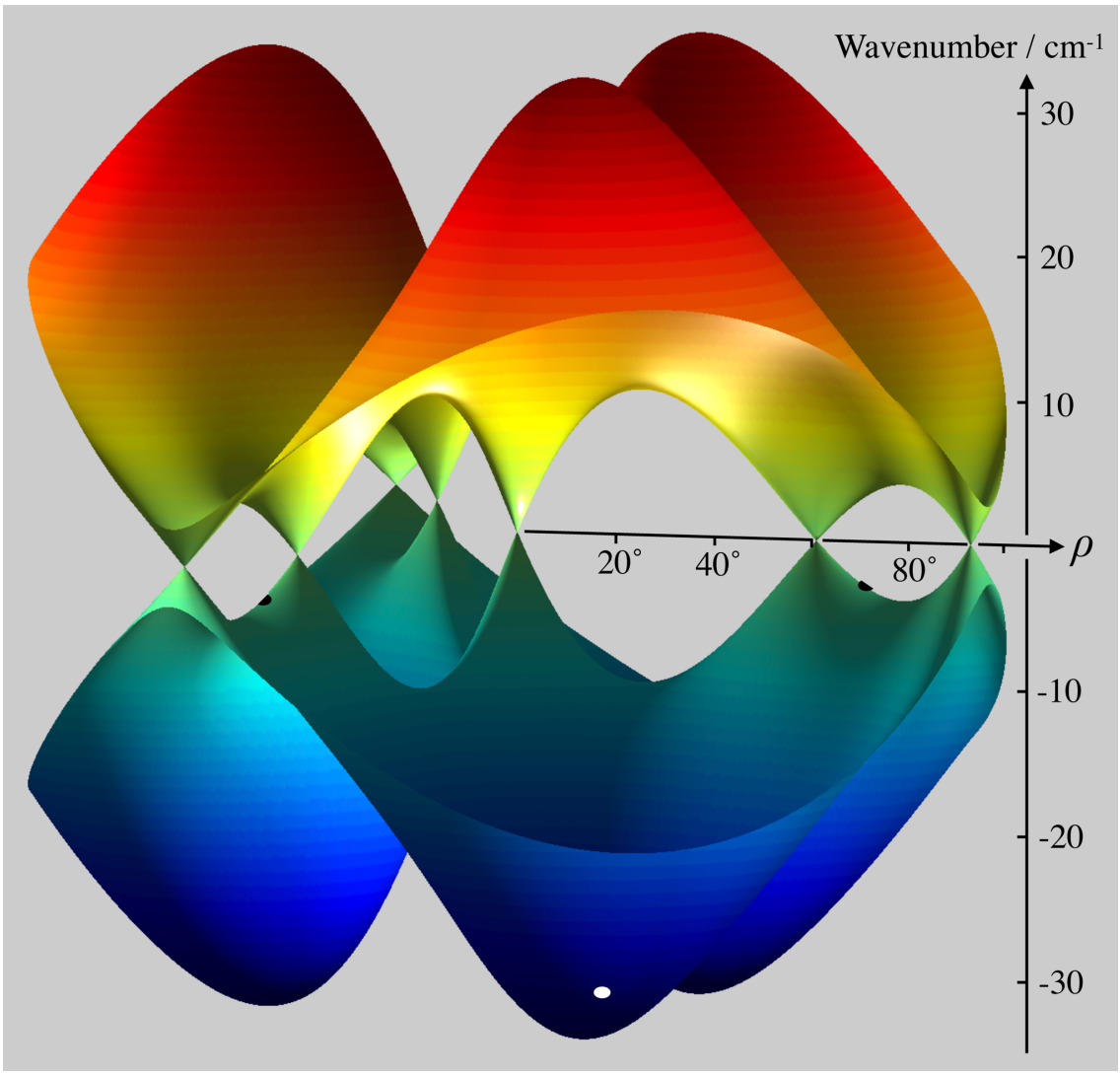

Figure 5. 5 Relative model frequencies of the two asymmetric CH stretch vibrations in methanol, represented as surfaces in the two-dimensional coordinate space of the COH bend angle ρ and the torsional angle γ. The figure shows seven conical intersections: one at $\rho = 0^{\circ}$, three at $\rho = 62^{\circ}$, and three at $\rho = 94^{\circ}$.

Most prominent in the present *ab initio* calculations (Figures 5.1, 5.2, and 5.3) and in the present model (Figures 5.1, 5.3, 5.4, and 5.5) is the presence of seven conical intersections, one occurring in the C_{3v} reference geometry ($\rho = 0^{\circ}$), and six more

occurring in eclipsed conformations with C_s symmetry at ρ = 61.9° and 93.6°. The former is a symmetry-required conical intersection of the type found in Jahn-Teller problems. The latter six are symmetry-allowed conical intersections that may occur because the two asymmetric CH stretch frequencies have different symmetries in the C_s geometries (A′ and A″), which allows a true crossing to occur when the two frequencies are equal. In the present case, we find two different values of ρ in the eclipsed conformation for which this occurs. In principle, the two asymmetric CH stretch frequencies could also become equal at certain angle ρ for in the staggered C_s conformations, leading to conical intersections for staggered conformations as well. However, in the present case, the two asymmetric CH stretch frequencies for staggered conformations remain well separated for all $\rho > 0$ and no crossings have been found.

5.4 Seams of conical intersections

As shown in Figure 5.5, conical intersections can occur when the adiabatic energies for two high-frequency modes are regarded as functions of two low-frequency, large-amplitude coordinates. When the dimensionality of the low-frequency coordinate space is 3 or more, then the CIs become seams or hyper seams of CIs. All eight of the low-frequency modes, including the methyl rocks and deformations, could arguably be included in the low-frequency coordinate space. At present, for purpose of exemplifying seams of CIs, we choose to include just one additional coordinate, the CO stretch $r_{CO,}$ to form a 3-dimensional low-frequency coordinate space. In CH_3OH, the CO stretch is the second lowest frequency mode, and in CH_3OD, it is the third lowest frequency mode after the torsion and the COD bend. Proceeding with the same methodology as above, we

varied ρ at several different fixed values of the CO bond length (r_{CO}) to find CIs. The locations of these CIs are shown in Figure 5.6. The resulting seam of CIs lies in the eclipsed plane at different combinations of ρ and r_{CO}.

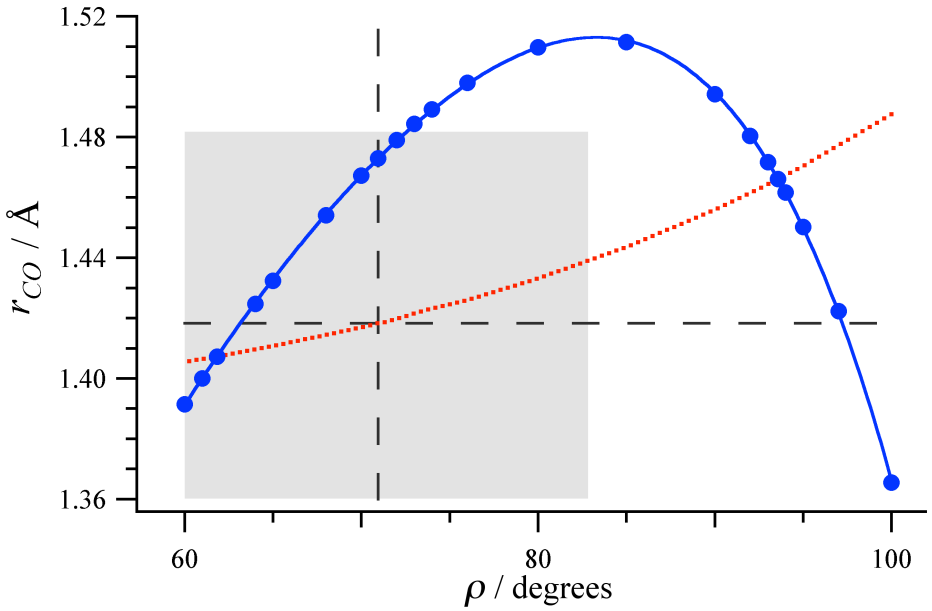

Figure 5.6 The location of the seam of conical intersections for eclipsed methanol (markers) and a polynomial fit (solid blue line) is plotted in terms of the CO bond length and the COH bending angle. The red dotted line represents the partially optimized calculations of Figure 5.1 and the CIs shown in Figures 5.1 and 5.5 are located at the intersections of the blue solid and red dotted lines. The dashed lines indicate the zero-point geometries of both coordinates, and the grey shaded area represents the approximate extent of the zero-point amplitudes.

It is clear from Figure 5.6 that the CIs at ρ = 61.9˚ and 93.6˚ belong to the same seam of CIs. Given that the conical intersections at 61.9˚ lie within the zero-point

bending amplitude of the torsional saddle point, it is evident that a significant length of the seam of CIs in Figure 5.6 also lies within the range of the zero-point motions of the COH bend and CO stretch. This reinforces our assertion that the CIs are accessible to the dynamics at relatively low energies. Altogether then in the 3-dimensional γ, ρ, r_{CO} space, there are four seams of CIs, one symmetry-required seam along the C_{3v} symmetry line $\rho = 0^\circ$, and three more symmetry-allowed seams like the one represented in Figure 5.6, one in each eclipsed plane, $\gamma = 0^\circ$, 120° and 240°.

5.5 Discussion and summary

These conical intersections illuminate the role of geometric phase in methanol. Since four CIs are enclosed by the MEP for a 2π torsional rotation, the Zwanziger and Grant theorem [34] predicts a geometric phase of +1 in agreement with the findings of Xu *et al*. [146]). However, from a semiclassical point of view, one might consider additional classical paths for a 2π torsional rotation. Since the COH zero-point bending amplitude is large ($\pm 11^\circ$) extending through the location of the CIs at 62°, there are other possible torsional paths that could enclose an odd number of CIs, say one or three. Thus, in a fully coupled treatment, the ν_2 and ν_9 wavefunctions may be linear combinations of basis states of differing geometric phase, with the +1 contribution being dominant. States with mixed geometric phase have been found previously in model calculations on methanol [16, 28, 31, 97].

Since these CIs exist only as an abstraction in the context of an approximate adiabatic separation of high- and low-frequency vibrations, it is relevant to ask, what, if any, impact do they have on the observable energy level structure of methanol? Xu *et al*.

[146] have already shown that physically different models [28, 32, 116] containing one or both of the Jahn-Teller- and Renner-Teller-like coupling terms are equally good at predicting the inverted torsional tunneling splittings in the CH-stretch fundamentals. However, the CIs will likely impact the energy level patterns of the higher torsional and COH bending levels built on the CH stretch fundamentals and overtones.

The CIs have direct implications for both the intramolecular and intermolecular dynamics of methanol. Xu *et al*. [146,147] have shown that the vibrational characters of ν_2 and ν_9 change sharply over a small range of the torsional angle near the eclipsed conformation. The presence of nearby CIs explains this behavior and will allow quantitative predictions of non-adiabatic processes (surface hopping) near the eclipsed geometry. In general, in the context of either intramolecular or collision-induced dynamics, the CIs provide a connection between the vibrationally adiabatic surfaces. Therefore, one should expect acceleration of energy transfer processes in localized regions around the CIs. Just as electronic conical intersections are now known to be ubiquitous throughout electronic spectroscopy, [41, 148, 149] vibrational conical intersections may also be widespread, consequently impacting the vibrational dynamics [30, 43] in diverse chemical systems.

CHAPTER VI

HIGH-RESOLUTION FOURIER TRANSFORM SYNCHROTRON SPECTROSCOPY OF NITROMETHANE IN THE NO_2-IN-PLANE ROCK BAND

The high-resolution rotationally resolved Fourier transform far-infrared (FTFIR) spectrum of the NO_2 in plane-rock band (440-510 cm^{-1}) of nitromethane (CH_3NO_2) has been recorded using the Far-Infrared Beamline at the Canadian Light Source, with a resolution of 0.00096 cm^{-1}. About 1773 transitions have been assigned for $m' = 0; Ka' \leq 7; J' \leq 50$ using an automated ground state combination difference program together with the traditional Loomis Wood approach [C.F.Neese, An Interactive Loomis-Wood Package, V2.0, 56th OSU International Symposium on Molecular Spectroscopy (2001)]. Transitions involving $m' = 0; Ka' \leq 7; J' \leq 22$ in the upper vibrational state are fit using the six-fold torsion-rotation program developed by Ilyushin *et.al.* [*J. Mol. Spectrosc*, **259**, 26-38 (2010)]. The analysis of the spectrum for the $m = 0$ torsional state reveals that the rotation energy level structure in the upper vibrational state is similar to that of the ground vibrational state, but the sign and magnitude of high order constants are significantly changed.

6.1 Introduction

Nitromethane (CH_3NO_2) is a slightly oblate asymmetric top ($\kappa = 0.25$) with a light methyl (CH_3) rotor and a heavy nitro (NO_2) group (Figure 6.1) [150-152]. The very low 6-fold barrier to internal rotation, 2.10 cm^{-1} [150-152] makes nitromethane a benchmark system for the studies of large amplitude torsional motion in a 6-fold potential and for the resulting vibrational dynamics [152, 153]. In many other methyl rotor systems, the torsional potential is dominated by 3-fold terms, which are much larger, typically several hundred cm^{-1}. Since the heavy atoms are co-planar in its equilibrium geometry, symmetry dictates that the 3-fold potential term in nitromethane is zero, leaving only the much smaller 6-fold term. However, distortion along a non-totally-symmetric vibrational coordinate relieves this restriction, opening the way for much higher 3-fold terms [126]. Spectroscopic work on CH overtones of nitromethane [153] indicates a large increase in the torsional barrier upon the vibrational excitation.

The microwave spectrum of nitromethane has been investigated by several groups [150, 151, 154-157]. Recently, Slingerland *et al*.[158] have reported low resolution spectra in the Terahertz region (9 to 40 cm^{-1}). In the infrared, low resolution [159, 160], high-resolution [161, 162], and overtone [152] spectra have been reported. The nitromethane fundamental vibrations and mode descriptions are listed in Table 1. All of the vibrational bands as listed in Table 1, except torsion, are infrared active. Infrared spectra of the CN-stretch at 917.5 cm^{-1} [161] and in the NO-asymmetric stretch at 1584 cm^{-1} [162] have been recorded at 0.005 cm^{-1} resolution with a BOMEM Fourier transform spectrometer, and the transitions of the lowest torsional state ($m = 0$) analyzed.

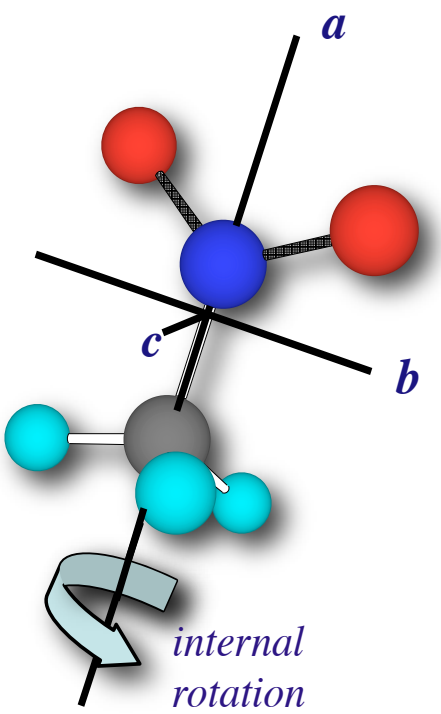

Figure 6.1 Representation of reference geometry of CH_3NO_2 indicating the molecular fixed axes a, b, and c along the z, x and y coordinates respectively where, a is the prolate axis, c is the oblate axis and dipole moment is along the b axis.

Most of the vibrational bands of CH_3NO_2 remain unexplored at high resolution. Four fundamental bands, the NO_2 in-plane rock, NO_2 out-of-plane rock, the NO-symmetric bend, and CN-stretch, all fall within the operating range (30-1000 cm^{-1}) of the Far-Infrared beamline at Canadian Light Source. This beamline is equipped with a high-resolution Bruker IFS125HR spectrometer (0.00096 cm^{-1}). The brightness and stability of this synchrotron radiation source provides a signal-to-noise advantage over conventional sources within its operating range [63, 64, 163]. This Chapter reports the first high-resolution synchrotron-based FTFIR spectrum of the NO_2 in-plane rock band

Table 6.1 Fundamental vibrational frequencies for nitromethane.

Normal Mode[a]	Normal Mode[b,c]	Symmetry G_{12} (D_{3h})	Description[d]	Frequency / cm^{-1}	Frequency[b] / cm^{-1}	Frequency[c] /cm^{-1}	Frequency[h] / cm^{-1}
ν_1	ν_1	A_1'	$\nu(CH)_s$	---	2973.9	2964.3	2972
ν_2	ν_4	A_1'	ν(C-N)	917.55[e]	917.9	917.1	918
ν_3	ν_2	A_1'	$\nu(NO)_s$	---	1397.4	1397	1397
ν_4	ν_5	A_1'	$\delta(NO)_s$	---	657.4	656	658
ν_5	ν_3	A_1'	$\delta(CH)_s$	---	1378.4	1378.8	1377
ν_6	ν_7	A_1''	$\nu(NO)_a$	1583.81[f]	1583.8	1583.3	1586
ν_7	ν_8	A_1''	$\rho(NO_2)_i$	475.3628(58)[g]	475.2	----	477
ν_9	ν_6	A_2''	$\rho(NO_2)_o$	---	602.5	----	605
ν_{10}	ν_9	E'	$\nu(CH)_a$	---	3080	3080.4	3065
ν_{11}	ν_{11}	E'	$\rho(CH_3)$	---	1119	1091	1100
ν_{12}	ν_{10}	E'	$\delta(CH)_a$	---	---	1438	1482

[a] The vibrational mode numbering from (Tables 15-5 and A-24) of Ref. [19] will be used in this paper.

[b] Vibrational mode numbering and frequencies from Ref.[164].

[c] Vibrational mode numbering and frequencies from Ref.[160].

[d] ν = stretch; δ = bend; ρ = rock; δ = bend; a = asymmetric; s = symmetric; i = in-plane; o = out-of-plane.

[e] From Ref. [161].

[f] From Ref.[162].

[g] Present work.

[h] From Ref.[165]

(440-510 cm^{-1}) of CH_3NO_2, together with detailed assignments and analysis of the transitions of the lowest torsional state (m = 0). The analysis of the torsionally excited states (m > 0) is underway and will be reported in the future.

6.2 Result and discussion

6.2.1 Symmetry and selection rules

The molecular symmetry group for $CH_3N^{16}O_2$ is G_{12}, which is isomorphic to D_{3h} point group symmetry and has the irreducible representations {A_1', A_1'', A_2', A_2'', E', E''}[19, 150, 151, 156]. The G_{12} group is also isomorphic to C_{6v} and that notation may also be used with the respective symmetry species {A_1, B_2, A_2, B_1, E_2, E_1} [166]. Levels with the total species A_1'', A_2'', and E'' are odd under the interchange of the two ^{16}O atoms and are therefore forbidden [19]. For the vibrational ground state, this means that only levels with $K_a + m$ = even exist [19, 150, 151, 156], but in the NO_2 in-plane-wag (ν_7, A_1'') vibrationally excited state, only the levels with odd $K_a + m$ exist. The b-type selection rules for the ν_7 band are: ΔJ =0, ±1 (except $J = 0 \neq J = 0$); ΔK_a = ±1, ±3, …; ΔK_c = ±1, ±3, …; and Δm =0 , where m is the internal rotation quantum number. Since nitromethane is more oblate than prolate (κ = 0.25), prolate-fobidden transitions with ΔK_a = ±3 will have significant intensity.

6.2.2 Assignments

The synchrotron based FTIR spectrum of nitromethane in the NO_2 in-plane rock is shown in Figure 6.2. As expected for a b-type band, the spectrum is dominated by strong R and P branches. However, the spectrum is very congested by transitions

originating in the internal rotor states up to about m = 9, which are populated at the sample temperature. Accordingly, the assignments required the combined use of the traditional Loomis-Wood approach together with an automated search for groups of transitions obeying the ground states combination differences known (GSCD). For this work, the ground state energies were obtained from Ilyushin [167] and are in agreement with the limited set of ground state energies previously obtained from Soerensen [151].

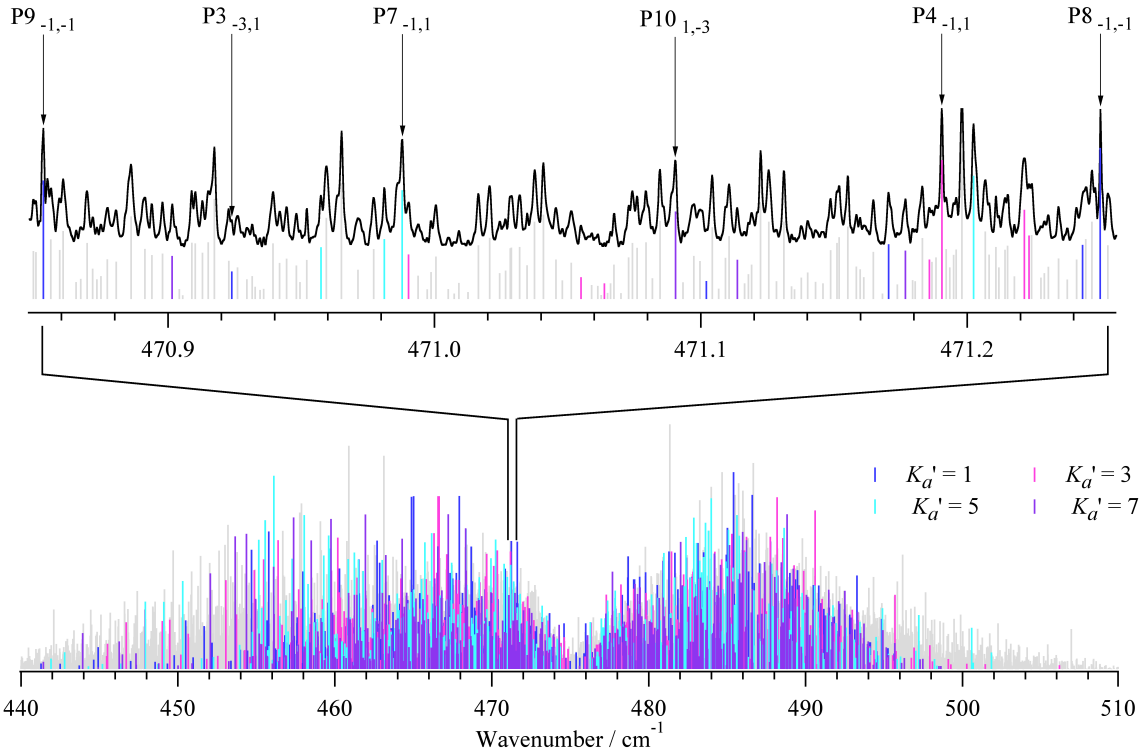

Figure 6.2 The high-resolution synchrotron-based FTIR spectrum in the ν_7 NO_2 in-plane rock region of CH_3NO_2. A small portion (~0.40 cm^{-1}) of the actual spectrum is as shown in black, accompanied by a stick representation of the observed peaks colorized according to their assigned upper state K_a' values and leaving the unassigned features in grey.

The assignment of m = 0 transitions was accomplished in three steps. First, the lines in a *P* or *R* branch were identified with a Loomis-Woods program [168] based on the anticipated spacing (2B= ~0.39 cm^{-1}). Second, the obtained *P* or *R* branch lines were then linked to *P, Q,* and *R* lines orginating from the same lower states rotational level using the automated GSCD algorithm [169]. This program searches through peak-find list and looks for multiple sets of transitions that match the known GSCD within the experimental resolution (0.0010 cm^{-1}). Figure 2(a) shows typical sets of different ground transitions that reach the same upper state. Instead of taking the difference between two ground state energies that reach the same upper state, all ground state levels that reach the same upper state were used. The program then searches in the spectrum for sets of lines consistent with this spacing. Third, the assignment is confirmed by examining ground state combination difference between transitions that reach the same upper state. The assignment of a particular GSCD set (Figure 2(a)) is considered accurate if (a) each GSCD is reproduced within experimental uncertainty (~ 0.0010 cm^{-1}); (b) the same upper state is reached at least from 4-6 different transitions; and (c) the transitions are not outliers in the fit of all GSCD to a torsion-rotation Hamiltonian. This fit and the handling of outliers are discussed in the sections below.

A total of 1773 transitions lines, for $m' = 0$; $Ka' \leq 7$; $J' \leq 50$, were assigned and are tabulated in Appendix O. Figure 6.4 provides a summary of the assigned m = 0 subbands. The unassigned transitions in Figure 6.2 are largely attributable to $m > 0$ lines and also to weaker unassigned m = 0 lines including perturbations.

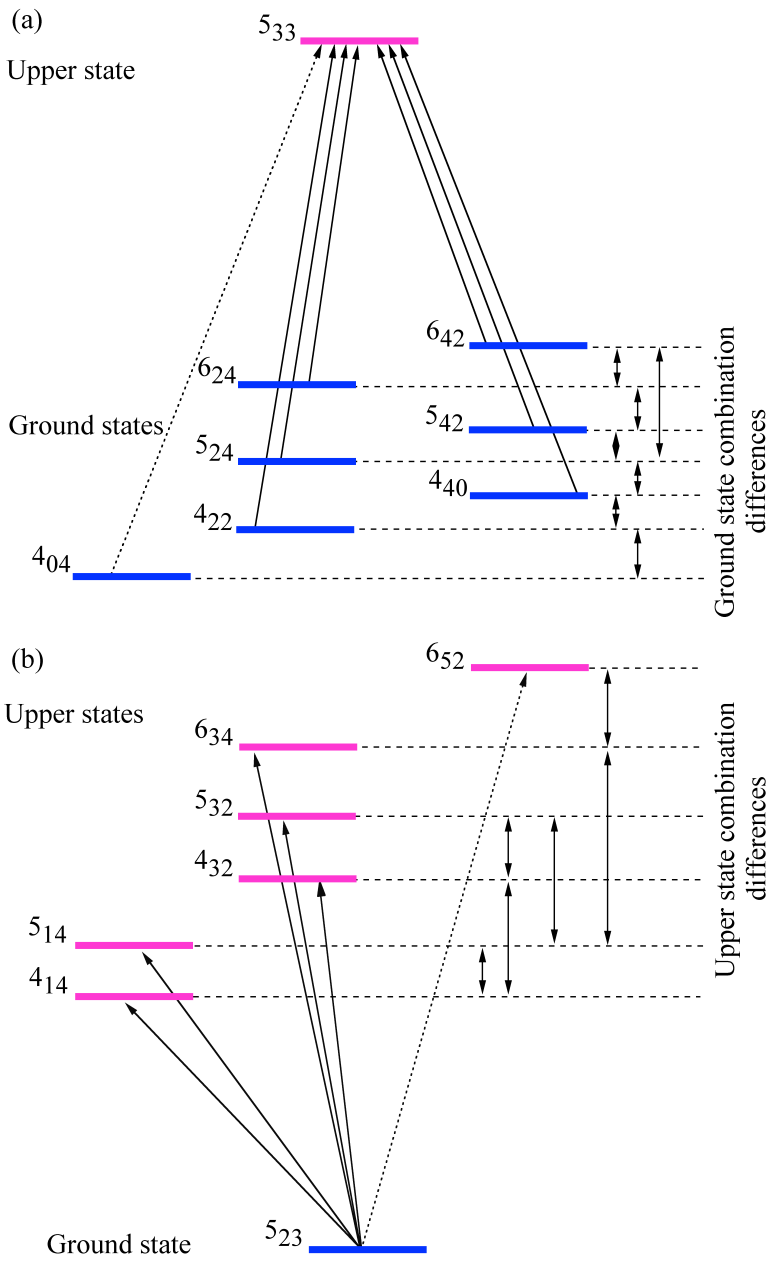

Figure 6.3 (a) An example of the set of ground state combination difference (GSCD) resulting form the seven transitions reaching a particular upper state rotational level. (b) An example of the set of upper state combination differences (USCD) resulting from the six transitions originating from a particular lower state rotational level.

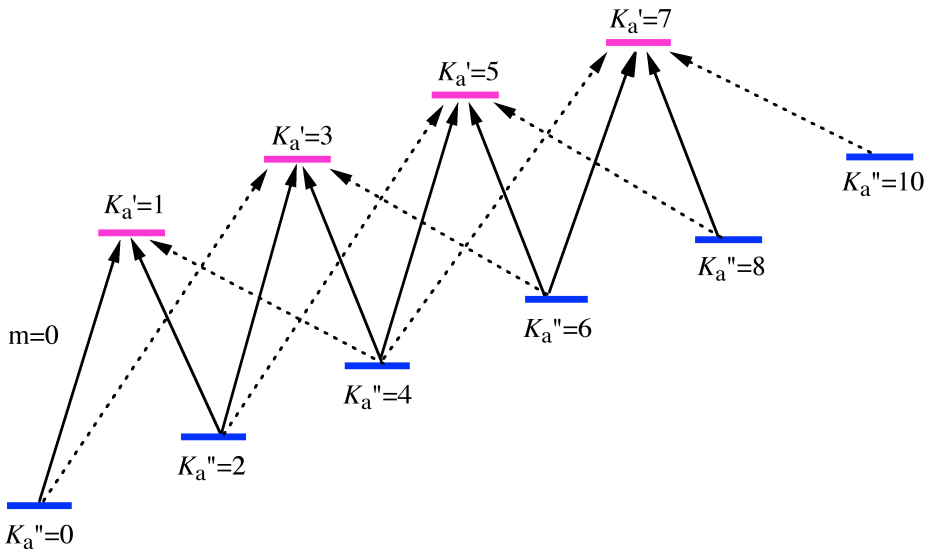

Figure 6.4 Graphical representation of the *b*-type selection rule employed in the present work for *m*=0 state of nitromethane.

6.2.3 Analysis and discussion

The upper state term values, $\nu^{J'Ka'}$, are calculated by adding the known ground state term values $\nu^{J''Ka''}$ [167] to the wavenumber, ν, of each observed transition,

$$\nu^{J'Ka'} = \nu + \nu^{J''Ka''} . \qquad (6.1)$$

To display the pattern of rotational energy levels for both lower and upper states, it is convenient to plot reduced term values. The reduced term values, $\nu_R^{J,Ka}$, are obtained by subtracting the *J*-dependent rigid symmetric rotor part of the energy,

$$\nu_R^{J''Ka''} = \nu^{J''Ka''} - \tfrac{1}{2}(B'' + C'')J''(J''+1) . \qquad (6.2)$$

The ground state rotational constants [167] were used to compute the reduced term values in both the upper and lower states. Since ground state term values are only available for

even K_a, the hypothetical ground state term values, $\nu_u^{J''Ka''}$, for odd K_a are calculated with the six-fold torsion-rotation program [166] using the same ground state constants [167].

The patterns of the reduced term values, for the upper and the lower states are compared in Figure 6.5. The $m = 0$ reduced term values of the lower state (Figure 6.5(b)) follow the usual asymmetric rotor pattern with asymmetry splittings that increases with J decrease with K_a , Since upper state pattern appears identical when plotted on the same scale as Figure 6.5(b), only the change of the upper state levels relative to the ground state is plotted in Figure 6.5(a).

The present data are fit to the six-fold torsion-rotation Hamiltonian of Ilyushin *et al*. [166] using their fitting program. In principle, the present $m = 0$ data could be fit to an ordinary asymmetric-rotor centrifugal-distortion Hamiltonian, but for consistency with the future analysis of the $m > 0$ transitions, we chose to use the full torsion-rotation Hamiltonian. Since the program [166] fits only a single vibrational state, it was applied in two steps. First, combination differences for the ground state (e.g., Figure 6.3(a)) were fit as a check on the quality of the spectra and the validity of the assignments. Second, combination differences for the upper state (e.g., Figure 6.3(b)) were fit to determine the upper state rotational constants.

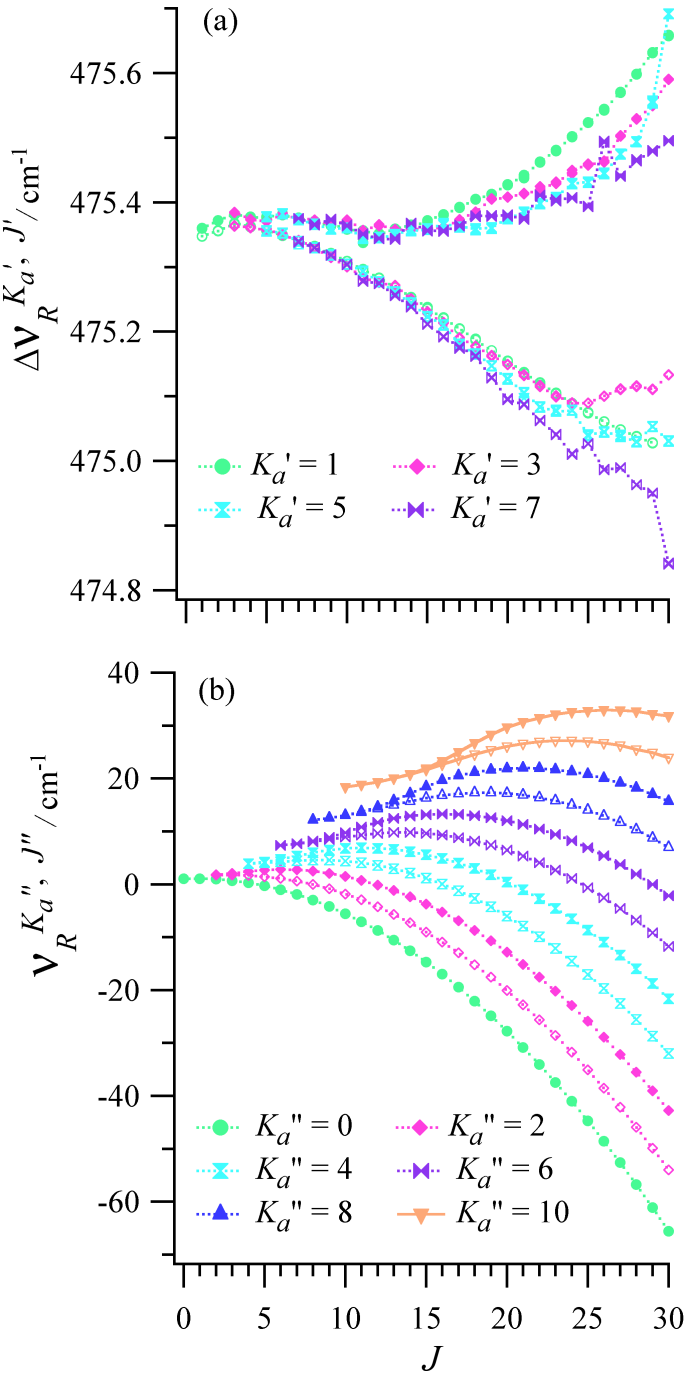

Figure 6.1 Reduced term values of the ground (b) and the excited (a) vibrational states plotted as a function of angular momentum quantum number (J) for m = 0 state. The plotted term values are derived from Eq. (6.2).

A total of 1670 ground state combination differences involving quantum numbers, m"=0, $J'' \leq 50$ and $K_a'' \leq 10$ (Appendix P) were fit with additional sextic and octic centrifugal distortion terms added as necessary to improve the quality of the fit (Table 6.2). During the fitting of the data, the pure torsional constants and torsion-rotation interaction constants of the program were held fixed to their ground state values (Appendix Q) [167]. Equal weights were used for all the transitions. The values of A_{eff}, B and C, and the lower order quartic and sextic centrifugal distortion constants as determined from the fit are in good agreement within the statistical error of our fit, with the more precise microwave values [151, 161, 162, 167]. However, the centrifugal distortion constants determined here are significantly different because higher rotational levels up to $J'' = 50$ and $K_a'' = 10$ and also higher-order constants were included in the present fit. Additional high order sextic and octic constants were determined, some with marginally significant values (Table 6.2), but they still contribute to the quality of the fit. The root-mean-square deviation ($\sigma = 0.00063$ cm^{-1}) is less than the linewidth (0.0010 cm^{-1}) and just a little larger than the expected instrumental accuracy. The residuals are apparently random function of J, K_a and K_c likely attributable in part to blended lines in the congested spectrum. To ensure the validity of the assignments, individual lines beyond 2σ were removed from the fit.

On the other hand, upper state combination differences are calculated from the assigned infrared transitions that arise from the same ground state reaching the different upper states (Figure 6.5(a)). The 497 transitions involving $m' = 0; Ka' \leq 7; J' \leq 22$ in the upper vibrational state (Appendix R) have been fit using the same six-fold torsion-rotation program. One subband, consisting of the levels $K_a' = 1$ and $K_c' = J'$, significantly

perturbed being shifted to lower wavenumber by as much as 0.6 cm^{-1} at $J' = 22$. Accordingly, those levels for $11 \leq J' \leq 22$ were removed from the fit. As for the ground state, the pure torsional constants and torsion-rotation interaction constants were held fixed with their ground state values [167] (Appendix Q) and only the rotational and centrifugal distortion constants were floated. The $m' = 0$ upper vibrational state molecular constants determined from the fit are given in Table 6.2. Even fitting a greatly reduced number of rotational levels ($0 \leq J' \leq 22$), the root-mean-square (RMS) deviation of the upper state fit (0.0058 cm-1) was nearly an order of magnitude larger than for the ground state fit. Although lines with J' up to 50 have been assigned, we were not able to achieve a meaningful fit for upper state combinations beyond $J' = 22$. The size and distribution of these residuals relative to those of the ground state, plus the substantial shift of levels in the $K_a' = 1$, $K_c' = J'$ subband, appear to indicate the presence of multiple perturbing levels. All combination differences included in the fit for the ground state and for the upper state, the common upper or lower state levels, and the residuals (observed-calculated) are listed in the Appendices P and R, respectively.

As expected, the rotational constants, A′, B′, and C′, of the vibrationally excited state (Table 6.2) are close to those in the ground state, but each is slightly larger. The centrifugal distortion constants are qualitatively different from the ground state (Table 6.2), with most constants much larger in magnitude and many even have the opposite sign. Such unphysical values of the centrifugal distortion constants are the result of trying to fit the level shifts due to perturbations with a centrifugal distortion Hamiltonian. The identity of the specific perturbing level(s) is not yet known. Since the in-plane rock

is the lowest frequency normal mode, the only possible source of perturbations is the excited torsional states built on the ground state of this molecule.

Although the ground state combinations were fit with good precision, the spectrum is very dense with many as yet unassigned lines. Thus, it is possible that there are still some errors in the detailed assignments. Up to now, we have not been able to assign any of the weaker "dark" perturbing lines.

Table 6. 2 The molecular fitted parameters for the NO_2 in-plane-rock band of nitromethane using the six-fold torsion-rotation program from Ref. [166].[a]

Operators	Parameters	Ground state cm^{-1}	Excited state cm^{-1}
P_a^2	$A_{eff}-(\frac{1}{2})(B+C)$	0.1711325(60)	0.17096(14)
P^2	$(\frac{1}{2})(B+C)$	0.2738760(27)	0.274592(98)
$P_b^2-P_c^2$	$(\frac{1}{2})(B-C)$	0.0778731(14)	0.078176(41)
$-P^4$	Δ_J	2.30(12) × 10^{-7}	-4.72(82) × 10^{-6}
$-P^2P_a^2$	Δ_{JK}	1.50(52) × 10^{-9}	6.2(26) × 10^{-6}
$-P_a^4$	Δ_K	1.48(82) × 10^{-7}	-1.34 (36) × 10^{-5}
$-P^2(P_b^2-P_c^2)$	δ_J	9.7(6) × 10^{-8}	1.77(27) × 10^{-6}
$-\{P_a^2,(P_b^2-P_c^2)\}$	δ_K	4.18(15) × 10^{-7}	2.5(05) × 10^{-6}
P^6	H_J	1.37(28) ×10^{-10}	7.8(27)× 10^{-9}
$P^4P_a^2$	H_{JK}	-6.2(12) × 10^{-10}	3.1(12) × 10^{-8}
P_a^6	H_K	2.19(30) × 10^{-9}	-6.1(40) × 10^{-8}
$\{P_a^4,(P_b^2-P_c^2)\}$	h_K	2.71(59) × 10^{-10}	8.45(75)× 10^{-8}
$\{P^4,(P_b^2-P_c^2)\}$	h_J	6.87(14) × 10^{-11}	5.1(10) × 10^{-11}
P^8	L_J	1.8(41) × 10^{-15}	------
P_a^8	L_K	-7.80(40) × 10^{-12}	1.7(12) × 10^{-10}
$P^6P_a^2$	L_{JJK}	8.4(32) × 10^{-15}	-6.78(99) × 10^{-11}
$P^4P_a^4$	L_{JK}	1.11(19) × 10^{-13}	------
No. of Transitions		1576	497
RMS deviation		0.00063 cm^{-1}	0.0058 cm^{-1}
J		$0 \le J'' \le 50$	$1 \le J' \le 22$
K_a		0,2,4,6,8,10	1,3,5,7

[a] The torsional parameters in the torsion-rotation Hamiltonian were held fixed at the ground state values listed in Appendix Q [167].

[b] The number in parentheses are standard deviations in units of the last digits.

[a] Ground state constants are obtained by fitting the ground state combination difference derived from the 1576 infrared transitions of the lowest torsional state (m = 0) (Appendix P).

[b] Excited state constants are obtained by fitting 497 upper state combination difference in the lowest torsional state (m = 0) of the upper vibration state (Appendix R).

6.3 Summary

The lowest internal rotor state (m' = 0) of the NO_2 in-plane rock band of nitromethane has been assigned and analyzed. The rotational constants and higher order centrifugal distortion constants are derived for the ground and upper state. The pattern of reduced term values indicates that the rotational energy level structure of the upper state is similar to that of the ground state. The unphysical values of the centrifugal distortion constants obtained, together with the magnitude and pattern of the residuals, indicate widespread perturbations in the in-plane wag vibrationally excited state. Some transitions involving excited internal rotor (m' = 3) states have already been assigned. The next stage of the work will be assignment of as many as possible of the m' > 0 transitions with the aim of probing the coupling of the in-plane wag vibration to internal rotation.

CHAPTER VIII

SUMMARY

In this dissertation, we have implemented both experimental and theoretical approaches to study large amplitude nuclear degrees of freedom(s) (LADF) and their effect on the small amplitude vibrations (SAVs) in bound model systems (eg. methanol, methylamine, 2-MMA, and 5-MT). Except for methanol, they represent a class of molecules with six equivalent minimum energy geometries connected by two LADF. One LAV is a 3-fold methyl internal rotor and other has a two-fold symmetric coordinate, which is either inversion or a proton transfer. The experimental approaches employed are both direct absorption and synchrotron based FTIR techniques. The theoretical approach implemented combines group theory and quantum mechanical (*ab-initio*) molecular structure calculations.

The analysis of high-resolution infrared spectrum of methylamine in the ν_{11} asymmetric CH-stretch region (2965-3005 cm^{-1}) showed that the pattern of the torsion-inversion tunneling splittings is qualitatively different from the ground state and torsion-rotation coupling are significantly reduced in the vibrationally excited state relative to ground state. In addition, the coupling of the torsional and inversion motions to the CH stretch vibrationally excited states of molecules with G_{12} symmetry was investigated with two model tunneling Hamiltonians for methylamine, 2-MMA, 5-MT, similar to those previously applied to methanol. These models predict the torsion-inversion tunneling

patterns in the CH stretch excited states of above mentioned molecules, which are compared with available experimental data.

The first discovery of a set of seven conical intersections (CIs) in methanol between vibrationally adiabatic surfaces has been reported. These CIs in methanol, which are related by symmetry and connected as seams of CIs in a higher dimensional space, provide a conceptual unity with electronic phenomena and provide a new way of thinking about ultrafast vibrational dynamics. Since the molecular system may go easily and smoothly from one surface to another at the places where the surfaces meet, one expects to find ultrafast vibrational relaxation processes that are localized at those places in the large amplitude coordinate space. Such vibrational CIs exist only in the context of an adiabatic separation of high-and low-frequency vibrations.

In general, a molecular system may have many different vibrations, with the surfaces representing each pair of vibrations touching in at different places in configuration space. Therefore, one can imagine a maze of CIs that controls the pathways by which the vibrational energy may be converted from one form to another.

Just as electronic CIs are now appreciated to be ubiquitous, controlling the rates of many photochemical processes, the present work, combined with that of P. Hamm and G. Stock [30, 43], suggests that vibrational CIs may also be widespread, possibly controlling the outcome of some high-energy processes where vibrationally excited species are present. While the present work addresses only the couplings within a bound molecule, the concept of vibrational CIs providing pathways for ultrafast relaxation also applies to weakly bound complexes, to molecular collisions, and to surface chemistry.

One prominent application of these results is in the area of combustion, currently the largest source of the nation's energy supply. One wants to convert fuel and air into a maximum amount of usable energy with a minimum amount of pollution. Combustion of even a simple fuel involves thousands of different elementary reactions, many bimolecular (involving the collision of two molecules), and others unimolecular (involving a single energized molecule). The progress of these reactions depends on the nature of the vibrational excitation of the reactive molecules, and thus is impacted, even controlled, by the energy transfer pathways such as those defined by the vibrational conical intersections noted above. Thus, the understanding of energy transfer processes that results from this discovery of vibrational conical intersections may contribute to the design of more efficient and environmentally friendly combustion systems.

Finally, we have reported the first spectroscopic assignment of synchrotron-based FTIR spectrum of NO_2 in-plane rock, ν_7 band of nitromethane.

Suggestions for future work:

(i) The concept of vibrational conical intersection in methanol can be applied to search such conical intersections in other torsional molecules.

(ii) The time-dependent vibrational dynamics for methanol can be computed in order to determine the extent of the localization of surface hoping near the conical intersections and the rates of such energy transfer event.

(iii) The phenomenology of geometric phase and its impact can be examined on the observable energy levels for a range of model systems in which the conical intersections occur in different locations relative to the torsional minimum energy path.

(iv) The interactions of of NO_2 in-plane rock (477 cm^{-1}), NO_2 out-of-plane rock (605 cm^{-1}), the NO_2 scissors (658 cm^{-1}), and the CN stretch (918 cm^{-1}) vibrations with highly excited internal rotation and overall rotation of nitromethane can be characterized.

REFERENCES

[1] Y. Georgievskii, S.J. Klippenstein, *J. Phys. Chem. A* 107 (2003) 9776-9781.

[2] Y. Georgievskii, S.J. Klippenstein, *J. Chem. Phys.* 122 (2005) 194103/1-194103/17.

[3] T. Bartsch, T. Uzer, J.M. Moix, R. Hernandez, *J. Phys. Chem. B* 112 (2008) 206-212.

[4] S.J. Klippenstein, W.D. Allen, *Ber. Bunsen-Ges.* 101 (1997) 423-437.

[5] D. Townsend, S.A. Lahankar, S.K. Lee, S.D. Chambreau, A.G. Suits, X. Zhang, J. Rheinecker, L.B. Harding, J.M. Bowman, *Science (Washington, DC, U. S.)* 306 (2004) 1158-1161.

[6] J.M. Bowman, X. Huang, N.C. Handy, S. Carter, *J. Phys. Chem. A* 111 (2007) 7317-7321.

[7] M. Quack, J. Troe, *Ber. Bunsenges. Phys. Chem.* 78 (1974) 240-52.

[8] M. Quack, J. Troe, Encyclopedia of Computational Chemistry, 1998, p 2708.

[9] B. Fehrensen, D. Luckhaus, M. Quack, *Chem. Phys. Lett.* 300 (1999) 312-320.

[10] W.H. Miller, *J. Phys. Chem.* 87 (1983) 3811-19.

[11] M.J. Bramley, T. Carrington, *J. Chem. Phys.* 101 (1994) 8494-507.

[12] X.-G. Wang, T. Carrington, Jr., *J. Chem. Phys.* 119 (2003) 101-117.

[13] X.-G. Wang, T. Carrington, Jr., *J. Chem. Phys.* 121 (2004) 2937-2954.

[14] A.W. Jasper, D.G. Truhlar, *J. Chem. Phys.* 122 (2005) 044101/1-044101/16.

[15] W. Hu, G.C. Schatz, *J. Chem. Phys.* 125 (2006) 132301/1-132301/15.

[16] D.S. Perry, *J. Mol. Spectrosc.* 257 (2009) 1-10.

[17] E.B. Wilson, Jr., J.C. Decius, P.C. Cross, Molecular Vibrations,. Dover Publications, Inc., New York, (1995).

[18] B.M. Wong, W.H. Green, Jr., *Mol. Phys.* 103 (2005) 1027-1034.

[19] P.R. Bunker, P. Jensen, Molecular Symmetry and Spectroscopy, Second Edition, NRC Research Press: Ottawa, (1998).

[20] J.T. Hougen, *J. Mol. Spectrosc.* 207 (2001) 60-65.

[21] D.J. Nesbitt, M.A. Suhm, *Phys. Chem. Chem. Phys.* 12 (2010) 8151.

[22] W. Siebrand, D.F. Williams, *J. Chem. Phys.* 49 (1968) 1860-71.

[23] B.R. Henry, *Acc. Chem. Res.* 10 (1977) 207-13.

[24] B.R. Henry, W. Siebrand, *J. Chem. Phys.* 49 (1968) 5369-76.

[25] M.S. Child, L. Halonen, *Adv. Chem. Phys.* 57 (1984) 1-58.

[26] P. Jensen, *Wiley Interdiscip. Rev. Comput. Mol. Sci.* 2 (2012) 494-512.

[27] G. Herzberg, J.W.T. Spinks, Molecular Spectra and Molecular Structure. 2nd ed. (1950).

[28] X. Wang, D.S. Perry, *J. Chem. Phys.* 109 (1998) 10795-10805.

[29] M. Born, R. Oppenheimer, *Ann. Phys. (Berlin, Ger.)* 84 (1927) 457-84.

[30] P. Hamm, G. Stock, *Mol. Phys.* 111 (2013) 2046-2056.

[31] T.N. Clasp, D.S. Perry, *J. Chem. Phys.* 125 (2006) 104313/1-104313/9.

[32] B. Fehrensen, D. Luckhaus, M. Quack, M. Willeke, T.R. Rizzo, *J. Chem. Phys.* 119 (2003) 5534-5544.

[33] W. Domcke, D.R. Yarkony, *Annu. Rev. Phys. Chem.* 63 (2012) 325-352.

[34] J.W. Zwanziger, E.R. Grant, *J. Chem. Phys.* 87 (1987) 2954-64.

[35] J. Guo, R. Eng, T. Carrington, S.V. Filseth, *J. Chem. Phys.* 112 (2000) 8904-8909.

[36] R.G. McKinlay, J.M. Zurek, M.J. Paterson, *Adv. Inorg. Chem.* 62 (2010) 351-390.

[37] S.F. Fischer, E.C. Lim, *Chem. Phys. Lett.* 26 (1974) 312-17.

[38] S. Matsika, *Rev. Comput. Chem.* 23 (2007) 83-124.

[39] M. Bixon, J. Jortner, *J. Chem. Phys.* 48 (1968) 715-26.

[40] M.J. Paterson, M.J. Bearpark, M.A. Robb, L. Blancafort, G.A. Worth, *Phys. Chem. Chem. Phys.* 7 (2005) 2100-2115.

[41] D.R. Yarkony, *Rev. Mod. Phys.* 68 (1996) 985-1013.

[42] J.V. Neumann, E.P. Wigner, *Physik,* 30 (1929).

[43] P. Hamm, G. Stock, *Phys. Rev. Lett.* 109 (2012) 173201/1-173201/5.

[44] S. Sardar, S. Mukherjee, A.K. Paul, S. Adhikari, *Chem. Phys.* 416 (2013) 11-20.

[45] H.C. Longuet-Higgins, U. Opik, M.H.L. Pryce, R.A. Sack, *Proc. R. Soc. Lond, A* 244 (1958).

[46] G. Herzberg, H.C. Longuet-Higgins, *Discuss. Faraday Soc.,* 35 (1963).

[47] C.A. Mead, D.G. Truhlar, *J. Chem. Phys.* 70 (1979) 2284-96.

[48] M.V. Berry, *Proc. R. Soc. Lond, A* 392 (1984) 45-57.

[49] D.C. Clary, *Science (Washington, DC, U. S.)* 309 (2005) 1195-1196.

[50] M.B. Dawadi, C. Michael Lindsay, A. Chirokolava, D.S. Perry, L.-H. Xu, *J. Chem. Phys.* 138 (2013) 104305/1-104305/9.

[51] M.B. Dawadi, R.S. Bhatta, D.S. Perry, *J. Phys. Chem. A* 117 (2013) 13356-13367.

[52] M.B. Dawadi, D.S. Perry, *J. Chem. Phys.* 140 (2014) 161101/1-161101/4.

[53] X. Wang, Y. Ma, D.S. Perry, O.V. Boyarkin, T.R. Rizzo, *Book of Abstracts, 215th ACS National Meeting, Dallas, March 29-April 2* (1998) PHYS-085.

[54] A. Chirokolava, D.S. Perry, O.V. Boyarkin, M. Schmid, T.R. Rizzo, *J. Mol. Spectrosc.* 211 (2002) 221-227.

[55] L.-H. Xu, X. Wang, T.J. Cronin, D.S. Perry, G.T. Fraser, A.S. Pine, *J. Mol. Spectrosc.* 185 (1997) 158-172.

[56] A. Chirokolava, D.S. Perry, L.-H. Xu, *J. Mol. Spectrosc.* 203 (2000) 320-329.

[57] D. Kaur, A.M. De Souza, J. Wanna, S.A. Hammad, L. Mercorelli, D.S. Perry, *Appl. Opt.* 29 (1990) 119-24.

[58] K.K. Lehmann, G. Scoles, B.H. Pate, *Annu. Rev. Phys. Chem.* 45 (1994) 241-74.

[59] P. Zalicki, R.N. Zare, *J. Chem. Phys.* 102 (1995) 2708-17.

[60] G. Berden, R. Peeters, G. Meijer, *Int. Rev. Phys. Chem.* 19 (2000) 565-607.

[61] K.K. Lehmann, (Princeton University, USA). US Patent, (1996).

[62] L. Bozec, A. Hammiche, M.J. Tobin, J.M. Chalmers, N.J. Everall, H.M. Pollock, *Meas. Sci. Technol.* 13 (2002) 1217-1222.

[63] W.D. Duncan, G.P. Williams, *Appl. Opt.* 22 (1983) 2914-23.

[64] G.L. Carr, M.C. Martin, W.R. McKinney, K. Jordan, G.R. Neil, G.P. Williams, *Nature (London, U. K.)* 420 (2002) 153-156.

[65] S. Nasu, *Hyperfine Interact.* 128 (2000) 101-113.

[66] L. Vaccari, G. Birada, G. Grenci, S. Pacor, L. Businaro, *J. Phys. Conf. Ser.* 359 (2012) 012007/1-012007/10.

[67] K. Wille, *Rep. Prog. Phys.* 54 (1991) 1005-68.

[68] T. May, T. Ellis, R. Reininger, *Nucl. Instrum. Methods Phys. Res., Sect. A* 582 (2007) 111-113.

[69] C.P. Tripp, R.A. McFarlane, *Appl. Spectrosc.* 48 (1994) 1138-42.

[70] T. May, D. Appadoo, T. Ellis, R. Reininger, *AIP Conf. Proc.* 879 (2007) 579-582.

[71] G. Moruzzi, R.J. Murphy, R.M. Lees, A. Predoi-Cross, B.E. Billinghurst, *Mol. Phys.* 108 (2010) 2343-2353.

[72] T. Zaporozan, Z. Chen, J. van Wijngaarden, *J. Mol. Spectrosc.* 264 (2010) 105-110.

[73] R.M. Lees, L.-H. Xu, B.E. Billinghurst, D.R.T. Appadoo, *J. Mol. Struct.* 993 (2011) 269-276.

[74] G. Moruzzi, R.J. Murphy, J. Vos, R.M. Lees, A. Predoi-Cross, B.E. Billinghurst, *J. Mol. Spectrosc.* 268 (2011) 211-220.

[75] Z. Kisiel, M. Winnewisser, B.P. Winnewisser, F.C. De Lucia, D.W. Tokaryk, B.E. Billinghurst, *J. Phys. Chem. A* 117 (2013) 13815-13824.

[76] R.M. Lees, L.-H. Xu, B.E. Billinghurst, *Can. J. Phys.* 91 (2013) 949-956.

[77] http://exshare.lightsource.ca/farir/Pages/default.aspx.

[78] U. Merker, H.K. Srivastava, A. Callegari, K.K. Lehmann, G. Scoles, *Phys. Chem. Chem. Phys.* 1 (1999) 2427-2433.

[79] N. Ohashi, J.T. Hougen, *J. Mol. Spectrosc.* 121 (1987) 474-501.

[80] N. Ohashi, K. Takagi, J.T. Hougen, W.B. Olson, W.J. Lafferty, *J. Mol. Spectrosc.* 126 (1987) 443-59.

[81] L. Sztraka, S. Alanko, M. Koivusaari, *Acta Chim. Hung.* 130 (1993) 887-900.

[82] M. Oda, N. Ohashi, J.T. Hougen, *J. Mol. Spectrosc.* 142 (1990) 57-84.

[83] N. Ohashi, Y. Toriyama, *J. Mol. Spectrosc.* 165 (1994) 265-76.

[84] V.V. Ilyushin, E.A. Alekseev, S. F.Dyubko, R. A. Motiyenko, J.T. Hougen, *J. Mol. Spectrosc.* 229 (2005) 170-187.

[85] M. Kreglewski, G. Wlodarczak, *J. Mol. Spectrosc.* 156 (1992) 383-9.

[86] V. Ilyushin, F.J. Lovas, *J. Phys. Chem. Ref. Data* 36 (2007) 1141-1276.

[87] V.V. Ilyushin, E.A. Alekseev, Y.-C. Chou, Y.-C. Hsu, J.T. Hougen, F.J. Lovas, L.B. Picraux, *J. Mol. Spectrosc.* 251 (2008) 56-63.

[88] R.M. Lees, Z.-D. Sun, B.E. Billinghurst, *J. Chem. Phys.* 135 (2011) 104306/1-104306/9.

[89] I. Gulaczyk, W. Lodyga, M. Kreglewski, V.-M. Horneman, *Mol. Phys.* 108 (2010) 2389-2394.

[90] L. Sztraka, S. Alanko, M. Koivusaari, *J. Mol. Struct.* 410-411 (1997) 391-395.

[91] Y.-C. Chou, I.C. Chen, J.T. Hougen, *J. Chem. Phys.* 120 (2004) 2255-2269.

[92] M. Halonen, L. Halonen, *J. Phys. Chem. A.* 110 (2006) 7554-7559.

[93] I. Gulaczyk, M. Kreglewski, V.-M. Horneman, *J. Mol. Spectrosc.* 270 (2011) 70-74.

[94] O.V. Boyarkin, T.R. Rizzo, D.S. Perry, *J. Chem. Phys.* 110 (1999) 11359-11367.

[95] S. Twagirayezu, D.S. Perry, J.L. Neill, M.T. Muckle, *J. Mol. Spectrosc.* 262 (2010) 65-68.

[96] S. Twagirayezu, X. Wang, D.S. Perry, J.L. Neill, M.T. Muckle, B.H. Pate, L.-H. Xu, *J. Phys. Chem. A* 115 (2011) 9748-9763.

[97] D.S. Perry, *J. Phys. Chem. A* 112 (2008) 215-223.

[98] J. Castillo-Chara, E.L. Sibert, III, *J. Chem. Phys.* 119 (2003) 11671-11681.

[99] A. Ainetschian, G.T. Fraser, J. Ortigoso, B.H. Pate, *J. Chem. Phys.* 100 (1994) 729-32.

[100] M.S. Malghani, R.M. Lees, J.W.C. Johns, *Int. J. Infrared Millimeter Waves* 8 (1987) 803-25.

[101] J.T. Hougen, *J. Mol. Spectrosc.* 181 (1997) 287-296.

[102] T. Shimanouchi, Tables of Molecular Vibrational Frequencies Consolidated Volume I, National Bureau of Standards, 1-160, (1972).

[103] N. Ohashi, S. Tsunekawa, K. Takagi, J.T. Hougen, *J. Mol. Spectrosc.* 137 (1989) 33-46.

[104] L. Sztraka, *Acta Phys. Hung.* 55 (1984) 135-60.

[105] J.T. Hougen, I. Kleiner, M. Godefroid, *J. Mol. Spectrosc.* 163 (1994) 559-86.

[106] N. Ohashi, K. Takagi, J.T. Hougen, W.B. Olson, W.J. Lafferty, *J. Mol. Spectrosc.* 132 (1988) 242-60.

[107] C.H. Townes, A.L. Schawlow, Microwave spectroscopy, Dover Publications, Inc. New York, (1975).

[108] M.A. Mekhtiev, P.D. Godfrey, J.T. Hougen, *J. Mol. Spectrosc.* 194 (1999) 171-178.

[109] S.M. Lederman, J.H. Runnels, R.A. Marcus, *J. Phys. Chem.* 87 (1983) 4364-7.

[110] W.D. Lawrance, A.E.W. Knight, *J. Phys. Chem.* 89 (1985) 917-25.

[111] K.K. Lehmann, *J. Phys. Chem.* 95 (1991) 7556-57.

[112] W.D. Lawrance, A.E.W. Knight, *J. Phys. Chem.* 92 (1988) 5900-8.

[113] D.G. Burkhard, D.M. Dennison, *J. Mol. Spectrosc.* 3 (1959) 299-334.

[114] L.-H. Xu, J.T. Hougen, *J. Mol. Spectrosc.* 173 (1995) 540-51.

[115] R.H. Hunt, W.N. Shelton, W.B. Cook, O.N. Bignall, J.W. Mirick, F.A. Flaherty, *J. Mol. Spectrosc.* 149 (1991) 252-6.

[116] Y.-C. Chou, J.T. Hougen, *J. Chem. Phys.* 124 (2006) 074319/1-074319/10.

[117] R.M. Lees, L.-H. Xu, *Phys. Rev. Lett.* 84 (2000) 3815-3818.

[118] R.M. Lees, L.-H. Xu, A.K. Kristoffersen, M. Lock, B.P. Winnewisser, J.W.C. Johns, *Can. J. Phys.* 79 (2001) 435-447.

[119] M. Abbouti Temsamani, L.-H. Xu, R.M. Lees, *J. Mol. Spectrosc.* 218 (2003) 220-234.

[120] F. Lattanzi, C. Di Lauro, *Mol. Phys.* 103 (2005) 697-708.

[121] L. Halonen, *J. Chem. Phys.* 106 (1997) 7931-7945.

[122] E.L. Sibert, III, J. Castillo-Chara, *J. Chem. Phys.* 122 (2005) 194306/1-194306/11.

[123] L.-H. Xu, R.M. Lees, J.T. Hougen, *J. Chem. Phys.* 110 (1999) 3835-3841.

[124] L.-H. Xu, *J. Chem. Phys.* 113 (2000) 3980-3989.

[125] J.T. Hougen, *J. Mol. Spectrosc.* 288 (2013) 14-17.

[126] R.S. Bhatta, A. Gao, D.S. Perry, *J. Mol. Struct. THEOCHEM* 941 (2010) 22-29.

[127] V.V. Ilyushin, E.A. Cloessner, Y.-C. Chou, L.B. Picraux, J.T. Hougen, R. Lavrich, *J. Chem. Phys.* 133 (2010) 184307/1-184307/9.

[128] Y.G. Smeyers, M. Villa, *Chem. Phys. Lett.* 324 (2000) 273-278.

[129] M. Tsuboi, A.Y. Hirakawa, T. Ino, T. Sasaki, K. Tamagake, *J. Chem. Phys.* 41 (1964) 2721-34.

[130] M. Oda, N. Ohashi, *J. Mol. Spectrosc.* 138 (1989) 246-50.

[131] V.V. Ilyushin, P. Jansen, M.G. Kozlov, S.A. Levshakov, I. Kleiner, W. Ubachs, H.L. Bethlem, *arXiv.org, e-Print Arch., Phys.* (2012).

[132] I. Gulaczyk, M. Kreglewski, *J. Mol. Spectrosc.* 256 (2009) 86-90.

[133] M. Kreglewski, *J. Mol. Spectrosc.* 133 (1989) 10-21.

[134] M. Kreglewski, F. Winther, *J. Mol. Spectrosc.* 156 (1992) 261-91.

[135] T. Shimanouchi, *J. Phys. Chem. Ref. Data* 1 (1972) 189-216.

[136] M.J. Frish, et al. , Gaussian 09, Revision B.0.1; Gaussian, Inc: Wallingford, CT, 2009.

[137] A.P. Scott, L. Radom, *J. Phys. Chem.* 100 (1996) 16502-16513.

[138] V. Haenninen, L. Halonen, *Mol. Phys.* 101 (2003) 2907-2916.

[139] N. Ohashi, H. Shimada, W.B. Olson, K. Kawaguchi, *J. Mol. Spectrosc.* 152 (1992) 298-306.

[140] A.M. De Souza, D.S. Perry, *J. Phys. Chem.* 90 (1986) 4508-13.

[141] T.J. Sears, P.M. Johnson, J. BeeBe-Wang, *J. Chem. Phys.* 111 (1999) 9213-9221.

[142] L.-H. Xu, J.T. Jougen, *J. Mol. Spectrosc.* 169 (1995) 396-409.

[143] H.R. Duebal, F.F. Crim, *J. Chem. Phys.* 83 (1985) 3863-72.

[144] T.M. Ticich, M.D. Likar, H.R. Duebal, L.J. Butler, F.F. Crim, *J. Chem. Phys.* 87 (1987) 5820-9.

[145] L.-H. Xu, J.T. Hougen, R.M. Lees, J.M. Bowman, X. Huang, S. Carter, *J. Mol. Spectrosc.* 299 (2014) 11-16.

[146] L.-H. Xu, J.T. Hougen, R.M. Lees, *J. Mol. Spectrosc.* 293-294 (2013) 38-59.

[147] L.-H. Xu, J.T. Hougen, J.M. Fisher, R.M. Lees, *J. Mol. Spectrosc.* 260 (2010) 88-104.

[148] B.E. Applegate, T.A. Barckholtz, T.A. Miller, *Chem. Soc. Rev.* 32 (2003) 38-49.

[149] J.D. Coe, T.J. Matinez, *J. Am. Chem. Soc.* 127 (2005) 4560-4561.

[150] G.O. Soerensen, T. Pedersen, *Stud. Phys. Theor. Chem.* 23 (1983) 219-36.

[151] G.O. Sorensen, T. Pedersen, H. Dreizler, A. Guarnieri, A.P. Cox, *J. Mol. Struct.* 97 (1983) 77-82.

[152] M. Halonen, L. Halonen, A. Callegari, K.K. Lehmann, *J. Phys. Chem. A* 102 (1998) 9124-9128.

[153] D. Cavagnat, L. Lespade, *J. Chem. Phys.* 106 (1997) 7946-7957.

[154] E. Tannenbaum, R.D. Johnson, R.J. Myers, W.D. Gwinn, *J. Chem. Phys.* 22 (1954) 949.

[155] E. Tannenbaum, R.J. Myers, W.D. Gwinn, *J. Chem. Phys.* 25 (1956) 42-7.

[156] A.P. Cox, S. Waring, *J. Chem. Soc., Faraday Trans. 2* 68 (1972) 1060-71.

[157] F. Rohart, *J. Mol. Spectrosc.* 57 (1975) 301-11.

[158] E.J. Slingerland, E.G.E. Jahngen, T.M. Goyette, R.H. Giles, W.E. Nixon, *J. Quant. Spectrosc. Radiat. Transfer* 112 (2011) 2323-2329.

[159] A.J. Wells, E.B. Wilson, Jr., *J. Chem. Phys.* 9 (1941) 314-18.

[160] W.J. Jones, N. Sheppard, *Proc. R. Soc. London, Ser. A* 304 (1968) 139-59.

[161] A. Hazra, P.N. Ghosh, R.J. Kshirsagar, *J. Mol. Spectrosc.* 164 (1994) 20-6.

[162] C. Pal, A. Hazra, P.N. Ghosh, *J. Mol. Struct.* 407 (1997) 165-170.

[163] C.C. Lin, J.D. Swalen, *Rev. Mod. Phys.* 31 (1959) 841-92.

[164] D.C. McKean, R.A. Watt, *J. Mol. Spectrosc.* 61 (1976) 184-202.

[165] D.C. Smith, C.-Y. Pan, J.R. Nielsen, *J. Chem. Phys.* 18 (1950) 706-12.

[166] V.V. Ilyushin, Z. Kisiel, L. Pszczokowski, H. Maeder, J.T. Hougen, *J. Mol. Spectrosc.* 259 (2010) 26-38.

[167] V.V. Ilyushin, Private communication (2013).

[168] C.F. Neese, in: t. An Interactive Loomis-Wood Package, 56th OSU International Symposium on Molecular Spectroscopy, (2001).

[169] L. Degliumberto, D.S. Perry, W. Heiserman, R. Cook, H. Mettee, R.L. Sams, G.O. Soerensen, 61th OSU International Symposium on Molecular Spectroscopy, (2006).

APPENDICES

APPENDIX A

FLOW CHAT OF LABVIEW PROGRAM

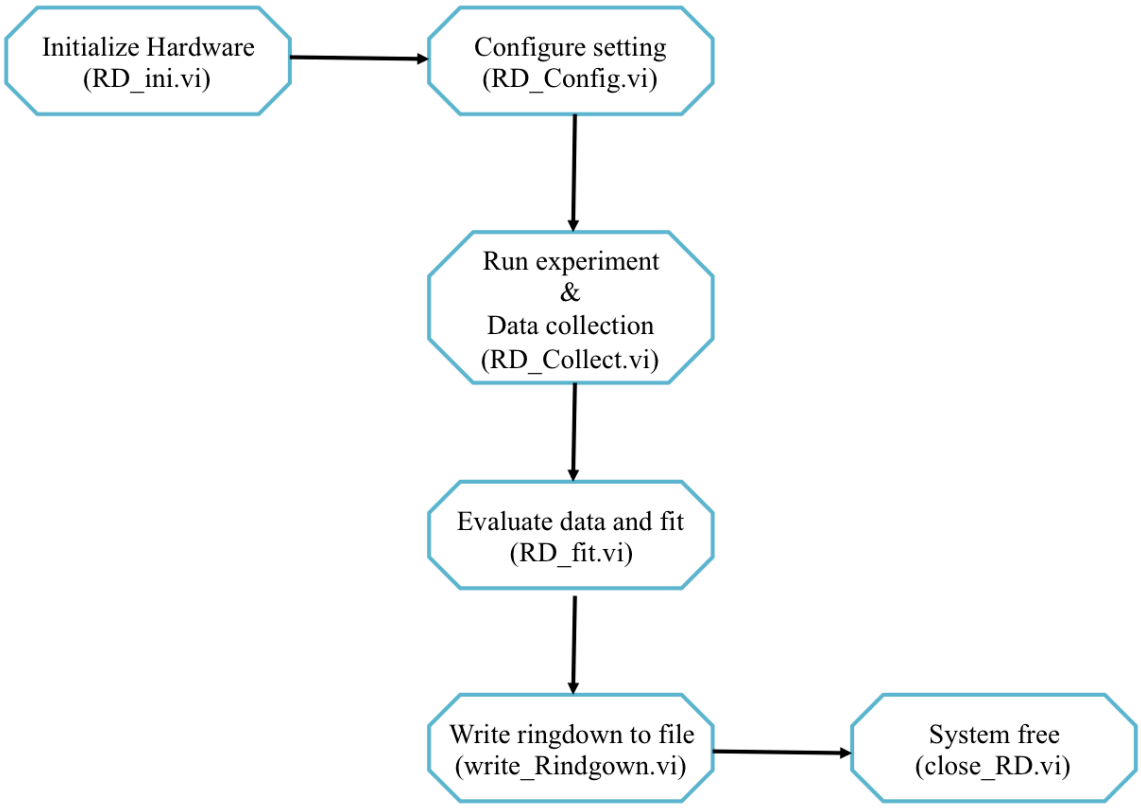

This flow chats indicates the structures of all subroutines for data acquisition, fast fitting algorithm and saving the ring-down time to a specified data folder.

APPENDIX B

A LABVIEW BLOCK DIAGRAM FOR THE REPRESENTATION OF DATA ACQUISITION AND FAST FIT ALTORITHM

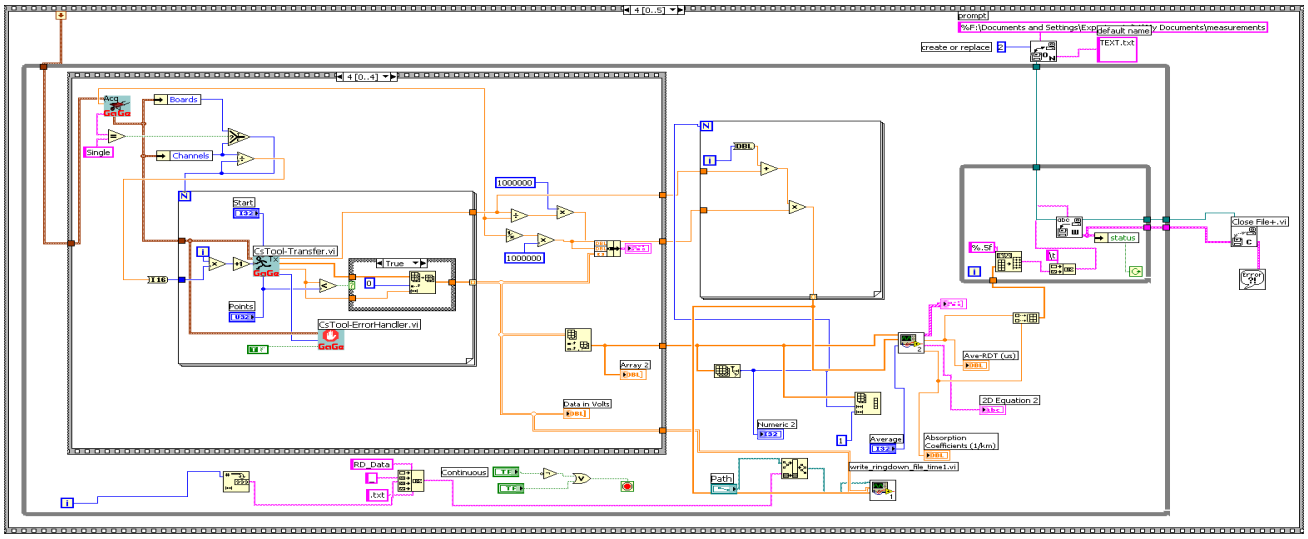

Available at Callisto: C:\Documents and Settings \ Cavityringdown\My Documents\Labview Programs\Development\mahesh Ringdown check3.vi

APPENDIX C

A LABVIEW FRONT PANEL FOR THE REPRESENTATION OF DATA ACQUISITION AND FAST FIT ALTORITHM

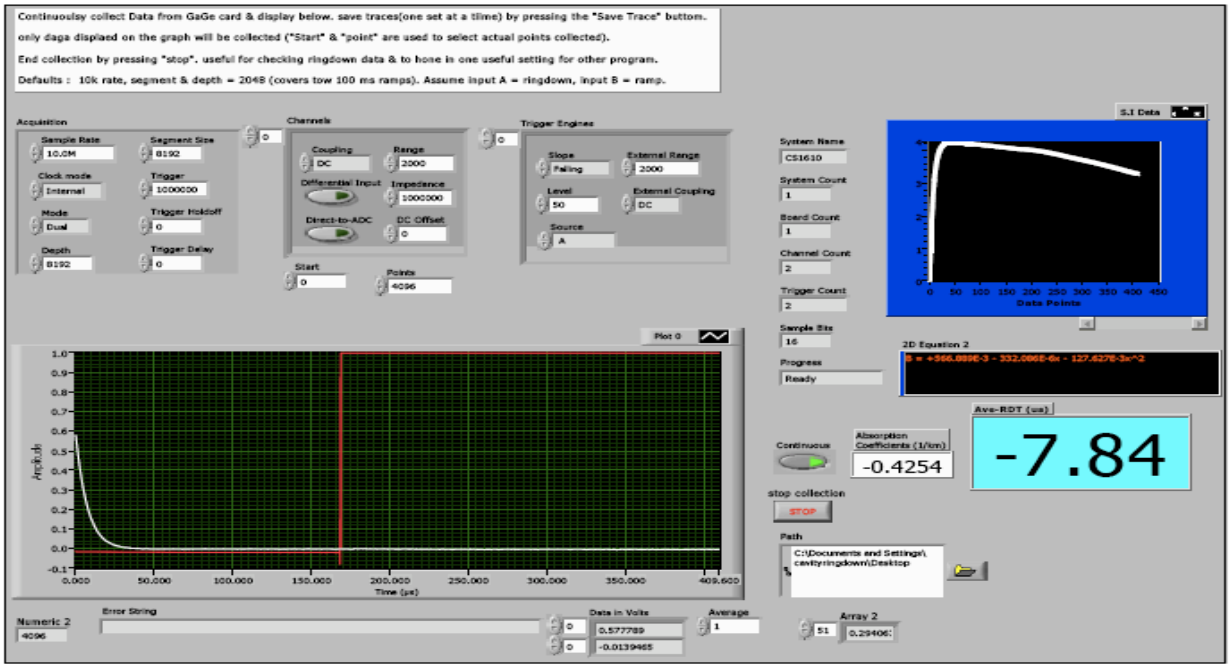

Available at Callisto: C:\Documents and Settings \ Cavityringdown\My Documents\Labview Programs\Development\mahesh Ringdown check3.vi

APPENDIX D

SLIT-JET SPECTRUM OF CH_3NH_2: TRANSITIONS IN THE ASYMMETRIC CH-STRETCH REGION

Wavenumber cm^{-1}	Relative intensity	Wavenumber cm^{-1}	Relative intensity
2965.00895	11	2978.00284	6
2965.05438	5	2978.01336	25
2965.06368	16	2978.0282	7
2965.07541	2	2978.02919	40
2965.08608	12	2978.03872	7
2965.12298	4	2978.04338	7
2965.14115	10	2978.04758	4
2965.14641	30	2978.05330	7
2965.15092	4	2978.06906	6
2965.16183	9	2978.09128	16
2965.17771	20	2978.09376	18
2965.19578	3	2978.11041	8
2965.31752	5	2978.11622	5
2965.32365	19	2978.12237	4
2965.34745	7	2978.12689	3
2965.40126	3	2978.14419	6
2965.41355	3	2978.15126	6
2965.41625	3	2978.16886	5
2965.44625	6	2978.17161	12
2965.49237	9	2978.18897	11
2965.55366	4	2978.19517	6
2965.58063	3	2978.20528	4
2965.61528	3	2978.2157	8
2965.6432	9	2978.22052	15
2965.65173	7	2978.22708	1
2965.70837	4	2978.23896	15
2965.73152	45	2978.24607	12
2965.77418	3	2978.24877	6
2965.81625	11	2978.25251	8
2965.84407	8	2978.2627	19
2965.85931	9	2978.27515	8
2965.88107	24	2978.28253	13
2965.9234	10	2978.28684	18
2965.95388	20	2978.30319	11
2965.96684	34	2978.30812	4

Wavenumber cm^{-1}	Relative intensity	Wavenumber cm^{-1}	Relative intensity
2965.98167	5	2978.32093	23
2966.02515	20	2978.3379	7
2966.03004	9	2978.34553	26
2966.04087	9	2978.35374	22
2966.04435	7	2978.38405	19
2966.06225	2	2978.39536	6
2966.06491	7	2978.3998	6
2966.07121	7	2978.41603	13
2966.08411	3	2978.43633	11
2966.09592	9	2978.48769	9
2966.10491	2	2978.49752	8
2966.12139	24	2978.53321	7
2966.1306	2	2978.56579	8
2966.19263	5	2978.5695	14
2966.22757	10	2978.62121	17
2966.2904	52	2978.683	16
2966.45364	32	2978.71567	5
2966.47048	17	2978.75647	4
2966.49044	5	2978.79792	22
2966.50722	19	2978.85762	7
2966.51942	3	2978.96081	3
2966.57427	3	2978.96776	3
2966.58715	10	2978.97072	12
2966.6159	6	2978.98010	50
2966.64037	8	2979.05706	14
2966.66438	26	2979.07564	4
2966.67476	4	2979.14327	5
2966.696	4	2979.22944	5
2966.71998	1	2979.24564	6
2966.73334	3	2979.2497	4
2966.74336	3	2979.25269	29
2966.75002	7	2979.28626	2
2966.76373	21	2979.29075	4
2966.77002	7	2979.2936	2
2966.78371	21	2979.38142	8
2966.8264	5	2979.40137	6
2966.83759	8	2979.47238	27
2966.8473	11	2979.56971	5
2966.8501	2	2979.60388	58
2966.85564	11	2979.62990	3
2966.86775	11	2979.65297	19
2966.8756	11	2979.69650	8
2966.88337	11	2979.70393	47
2966.90875	7	2979.73922	2
2966.99752	3	2979.74313	5

Wavenumber cm^{-1}	Relative intensity	Wavenumber cm^{-1}	Relative intensity
2967.01497	2	2979.80031	2
2967.04831	2	2979.80571	7
2967.06138	4	2979.82714	3
2967.09740	6	2979.83345	11
2967.14306	9	2979.8456	4
2967.14698	3	2979.86918	3
2967.15523	4	2979.87422	3
2967.15778	4	2979.90753	2
2967.16203	7	2979.92775	4
2967.19347	22	2979.97203	3
2967.20975	2	2980.04099	60
2967.26477	2	2980.09911	10
2967.28222	2	2980.10281	8
2967.30244	1	2980.16657	4
2967.31495	8	2980.20948	6
2967.32099	2	2980.21496	8
2967.33066	3	2980.21883	42
2967.33537	1	2980.22657	9
2967.34662	3	2980.2634	17
2967.36355	20	2980.29125	4
2967.37161	2	2980.33642	12
2967.38486	5	2980.39563	27
2967.39298	6	2980.40584	117
2967.39646	2	2980.438	18
2967.40014	3	2980.46351	9
2967.4041	18	2980.46822	4
2967.40811	7	2980.48309	26
2967.4172	1	2980.53395	18
2967.42458	6	2980.55626	22
2967.43004	3	2980.63881	4
2967.4361	1	2980.67262	9
2967.44121	24	2980.68947	10
2967.44554	7	2980.70406	11
2967.45134	7	2980.73928	19
2967.4648	4	2980.74998	32
2967.47395	3	2980.76921	13
2967.48038	5	2980.77878	9
2967.48348	21	2980.86921	12
2967.50989	7	2980.8788	18
2967.51368	12	2980.92912	48
2967.52025	6	2981.07231	22
2967.52786	15	2981.0749	21
2967.53352	11	2981.13777	37
2967.53829	6	2981.16508	6
2967.54683	2	2981.17600	10
2967.55456	5	2981.20199	56

Wavenumber cm^{-1}	Relative intensity	Wavenumber cm^{-1}	Relative intensity
2967.56338	13	2981.25322	6
2967.57501	18	2981.28426	8
2967.58086	8	2981.32987	22
2967.59725	2	2981.35772	33
2967.74211	2	2981.42076	13
2967.74598	2	2981.44574	14
2967.75367	4	2981.51868	43
2967.75812	3	2981.52548	15
2967.76443	2	2981.59613	15
2967.76804	4	2981.6354	10
2967.77728	2	2981.66847	40
2967.78634	2	2981.70453	9
2967.8098	50	2981.73597	6
2967.82782	2	2981.76814	7
2967.84751	13	2981.78551	11
2967.85599	3	2981.78866	11
2967.86993	2	2981.80543	11
2967.88411	2	2981.84097	4
2967.88963	2	2981.85113	97
2967.90595	5	2981.94544	13
2967.93691	7	2982.05765	12
2967.94272	1	2982.06365	10
2967.94544	1	2982.14943	19
2967.95376	2	2982.18570	7
2967.96176	22	2982.20533	20
2967.96662	2	2982.22084	33
2967.97878	16	2982.23715	22
2967.98218	2	2982.24924	13
2968.01225	13	2982.25258	27
2968.05212	4	2982.26712	3
2968.06815	2	2982.27458	16
2968.08121	2	2982.34294	10
2968.09563	12	2982.3607	4
2968.09824	4	2982.39088	44
2968.14368	3	2982.39539	5
2968.15038	2	2982.52873	9
2968.16001	10	2982.53686	9
2968.18617	18	2982.62962	29
2968.19971	25	2982.63379	27
2968.2162	6	2982.63887	10
2968.24148	5	2982.64299	18
2968.24917	5	2982.65007	17
2968.31327	12	2982.66550	18
2968.32299	7	2982.70353	41
2968.32568	20	2982.78271	7
2968.33478	8	2982.83459	8

Wavenumber cm^{-1}	Relative intensity	Wavenumber cm^{-1}	Relative intensity
2968.34092	6	2982.84669	32
2968.34945	3	2982.86695	4
2968.37404	10	2982.87565	57
2968.39114	17	2982.91108	15
2968.39877	10	2982.94946	5
2968.4073	2	2982.95767	21
2968.43466	11	2982.96193	9
2968.45207	19	2982.9729	5
2968.49796	17	2982.97742	7
2968.50828	4	2982.97954	23
2968.53832	4	2982.99114	30
2968.56378	4	2982.99612	16
2968.57614	3	2983.02842	46
2968.58683	16	2983.05194	5
2968.59814	5	2983.05451	5
2968.62146	11	2983.07159	59
2968.63129	20	2983.07542	4
2968.64022	5	2983.08601	43
2968.67	3	2983.10267	66
2968.69367	16	2983.12287	54
2968.69891	4	2983.12842	7
2968.70742	3	2983.15510	69
2968.74539	3	2983.17477	9
2968.75967	9	2983.17871	7
2968.76407	5	2983.18433	5
2968.77369	10	2983.19153	9
2968.77955	3	2983.20137	7
2968.80253	2	2983.21055	75
2968.80588	5	2983.23503	6
2968.81522	5	2983.23503	6
2968.8347	23	2983.25352	86
2968.84937	4	2983.26747	13
2968.85326	3	2983.27401	13
2968.87373	5	2983.28453	99
2968.89364	10	2983.30549	72
2968.90673	14	2983.31155	6
2968.91246	5	2983.32881	5
2968.92456	6	2983.34743	17
2968.93369	13	2983.37860	11
2968.94887	3	2983.38458	11
2968.95339	8	2983.39455	20
2968.97614	5	2983.40114	23
2968.98388	10	2983.41822	18
2968.9892	3	2983.42541	15
2969.00341	7	2983.50295	55
2969.01758	9	2983.51134	19

Wavenumber cm^{-1}	Relative intensity	Wavenumber cm^{-1}	Relative intensity
2969.03008	4	2983.53283	3
2969.03873	3	2983.53915	5
2969.06232	9	2983.56233	8
2969.07645	4	2983.58924	75
2969.09361	8	2983.60152	24
2969.11454	3	2983.62034	12
2969.1348	3	2983.63813	5
2969.15069	6	2983.65407	81
2969.16184	9	2983.65689	19
2969.19615	4	2983.69271	84
2969.23018	5	2983.70677	51
2969.24064	2	2983.71681	5
2969.25151	12	2983.74985	8
2969.29587	6	2983.75592	7
2969.3108	4	2983.76975	19
2969.32716	4	2983.79113	10
2969.33216	4	2983.79588	5
2969.33959	13	2983.81815	6
2969.3518	4	2983.82285	11
2969.35623	31	2983.82335	17
2969.36428	7	2983.82724	17
2969.38585	8	2983.82792	14
2969.40592	7	2983.84069	6
2969.42188	9	2983.87628	33
2969.44954	5	2983.88146	30
2969.469	10	2983.89663	17
2969.47538	16	2983.92648	8
2969.48143	7	2983.93182	9
2969.49572	12	2983.97242	6
2969.518	12	2984.12625	20
2969.53176	17	2984.13526	18
2969.53804	12	2984.17749	
2969.54102	5	2984.20881	20
2969.54907	11	2984.30022	8
2969.56051	3	2984.35408	33
2969.56975	10	2984.38562	63
2969.59471	14	2984.42793	12
2969.60958	4	2984.46238	27
2969.63346	15	2984.47796	7
2969.67825	4	2984.66419	4
2969.68647	3	2984.67509	6
2969.72201	10	2984.73382	5
2969.74572	11	2984.85893	5
2969.77872	6	2984.93552	4
2969.80659	4	2984.96760	4
2969.8118	6	2985.0321	2

Wavenumber cm^{-1}	Relative intensity	Wavenumber cm^{-1}	Relative intensity
2969.81465	3	2985.03909	3
2969.8339	5	2985.04169	10
2969.83893	3	2985.04836	10
2969.87606	4	2985.06881	4
2969.92289	4	2985.08625	3
2969.95624	3	2985.16755	1
2969.96904	3	2985.17632	2
2970.01315	3	2985.19950	6
2970.04782	2	2985.21913	4
2970.07405	4	2985.23354	5
2970.09848	3	2985.25372	5
2970.11178	2	2985.25748	15
2970.1224	2	2985.26723	5
2970.13229	2	2985.28203	2
2970.14187	5	2985.31053	2
2970.16976	4	2985.39071	2
2970.19511	7	2985.49593	4
2970.22069	3	2985.52919	2
2970.22356	3	2985.53548	5
2970.23825	3	2985.54049	2
2970.26738	3	2985.59738	4
2970.28026	1	2985.60851	3
2970.28681	3	2985.6248	2
2970.29595	1	2985.64219	3
2970.30402	7	2985.67845	10
2970.31339	6	2985.71854	3
2970.31862	22	2985.73638	2
2970.32411	40	2985.78829	12
2970.33705	1	2985.83205	2
2970.34425	1	2985.84506	2
2970.3468	13	2985.85056	13
2970.35694	9	2985.85522	5
2970.36671	1	2985.88600	36
2970.37334	13	2985.89342	10
2970.38015	1	2985.95953	13
2970.38419	18	2985.96856	3
2970.39213	12	2985.97521	1
2970.40098	1	2985.98888	1
2970.40943	4	2986.0184	3
2970.41786	10	2986.03927	1
2970.42107	10	2986.06898	1
2970.42943	10	2986.11244	1
2970.43404	6	2986.11872	15
2970.43964	13	2986.15211	2
2970.45654	24	2986.17789	6
2970.46268	2	2986.19836	5

Wavenumber cm^{-1}	Relative intensity	Wavenumber cm^{-1}	Relative intensity
2970.46858	8	2986.21215	6
2970.47738	26	2986.23081	1
2970.48416	3	2986.30052	39
2970.48482	4	2986.38029	3
2970.48926	1	2986.38475	2
2970.49842	17	2986.44675	6
2970.50284	7	2986.45074	2
2970.50566	1	2986.47329	1
2970.51522	12	2986.50433	3
2970.54884	14	2986.56917	2
2970.57879	28	2986.62849	2
2970.60951	22	2986.63147	1
2970.62348	7	2986.65566	4
2970.65214	11	2986.66010	10
2970.69565	12	2986.73911	4
2970.71751	10	2986.76083	3
2970.73039	5	2986.77746	3
2970.74503	2	2986.82997	13
2970.75275	2	2986.88374	1
2970.76094	6	2986.91037	1
2970.77564	3	2986.97385	11
2970.80135	3	2986.99854	2
2970.81122	1	2987.02018	1
2970.83163	1	2987.05799	2
2970.84076	1	2987.06158	6
2970.8498	1	2987.06537	4
2970.85826	3	2987.07184	2
2970.86538	2	2987.07631	3
2970.88916	7	2987.09871	2
2970.91088	44	2987.12036	2
2970.96028	4	2987.19466	6
2970.98819	5	2987.23040	2
2970.99552	9	2987.24778	1
2970.99896	21	2987.27119	1
2971.01784	8	2987.35414	3
2971.02052	1	2987.37273	2
2971.03847	1	2987.39716	2
2971.04193	1	2987.40552	4
2971.04584	1	2987.42692	1
2971.05773	2	2987.43728	2
2971.06863	2	2987.44883	2
2971.09094	3	2987.48018	1
2971.10588	5	2987.50915	4
2971.12299	3	2987.53720	2
2971.1379	2	2987.54702	3
2971.14342	2	2987.56089	2

Wavenumber cm^{-1}	Relative intensity	Wavenumber cm^{-1}	Relative intensity
2971.15695	4	2987.57938	3
2971.16218	1	2987.60385	6
2971.1655	1	2987.61745	12
2971.1878	2	2987.6201	2
2971.20969	1	2987.62712	18
2971.2228	1	2987.63237	16
2971.23157	2	2987.63946	21
2971.23899	3	2987.65161	8
2971.26836	4	2987.65569	6
2971.27936	2	2987.68931	6
2971.28662	2	2987.74687	3
2971.29061	4	2987.82150	54
2971.32386	16	2987.84511	3
2971.34977	3	2987.87054	1
2971.38263	4	2987.90094	4
2971.40231	35	2987.97457	2
2971.43518	8	2987.98575	3
2971.452	3	2987.99059	1
2971.48601	52	2988.05105	2
2971.51486	52	2988.09450	2
2971.5657	5	2988.11397	7
2971.59517	1	2988.11713	10
2971.62705	1	2988.15841	14
2971.63896	9	2988.16334	5
2971.65003	3	2988.18765	27
2971.66162	1	2988.20510	38
2971.67814	1	2988.21488	36
2971.70098	2	2988.25075	5
2971.70292	1	2988.27398	1
2971.71233	3	2988.27877	4
2971.7198	1	2988.30642	24
2971.72271	1	2988.41201	2
2971.73163	1	2988.42107	2
2971.7358	1	2988.45616	2
2971.74383	6	2988.4663	7
2971.78141	10	2988.52262	2
2971.78748	2	2988.52757	5
2971.79365	15	2988.57179	3
2971.80629	2	2988.57871	1
2971.82681	3	2988.59181	5
2971.83044	14	2988.61331	2
2971.84088	1	2988.61610	2
2971.84703	1	2988.63561	3
2971.85089	18	2988.66855	34
2971.87241	44	2988.67967	10
2971.88062	15	2988.70155	34

Wavenumber cm^{-1}	Relative intensity	Wavenumber cm^{-1}	Relative intensity
2971.89294	2	2988.74443	37
2971.90768	6	2988.74940	4
2971.91503	5	2988.75963	4
2971.93003	12	2988.78971	8
2971.94451	1	2988.80837	39
2971.95375	13	2988.85097	58
2971.95647	1	2988.86326	79
2971.95996	13	2988.87043	82
2971.96506	7	2988.88658	6
2971.97323	24	2988.8897	81
2971.98055	19	2988.89283	16
2971.98485	36	2988.8992	85
2971.99297	26	2988.90642	13
2972.00345	33	2988.91364	2
2972.00676	6	2988.92649	1
2972.01782	9	2988.93095	65
2972.02196	24	2988.94076	3
2972.02815	2	2988.94501	40
2972.04348	8	2988.97308	2
2972.04602	8	2988.98248	49
2972.06894	16	2988.99012	38
2972.076	3	2988.99831	66
2972.08669	3	2989.03855	44
2972.09195	4	2989.05863	72
2972.11587	35	2989.06234	18
2972.12337	15	2989.08052	4
2972.12959	30	2989.11161	12
2972.13311	4	2989.11377	30
2972.13692	6	2989.11652	5
2972.14403	3	2989.13056	4
2972.19369	3	2989.14776	45
2972.22768	7	2989.15379	3
2972.24911	3	2989.17800	16
2972.25235	2	2989.20579	17
2972.29902	4	2989.25764	21
2972.32154	4	2989.2797	4
2972.33971	27	2989.29224	2
2972.34976	3	2989.30255	1
2972.41542	9	2989.31276	2
2972.42902	9	2989.33127	3
2972.46663	20	2989.35485	4
2972.48031	68	2989.36012	47
2972.51682	40	2989.36975	5
2972.52027	5	2989.37927	9
2972.58543	3	2989.39415	2
2972.58873	3	2989.40167	1

Wavenumber cm^{-1}	Relative intensity	Wavenumber cm^{-1}	Relative intensity
2972.61131	4	2989.41026	3
2972.64736	6	2989.4769	3
2972.66855	4	2989.48292	2
2972.7118	5	2989.50598	2
2972.78292	6	2989.54343	2
2972.80715	4	2989.55128	5
2972.80997	4	2989.55693	2
2972.82447	3	2989.56476	2
2972.83395	6	2989.58365	4
2972.84013	5	2989.59151	2
2972.86214	24	2989.6284	2
2972.91956	11	2989.65515	2
2972.93325	14	2989.68369	2
2972.98837	5	2989.69387	26
2973.02086	39	2989.72569	5
2973.05535	12	2989.78543	4
2973.06608	2	2989.79399	26
2973.07726	9	2989.86059	2
2973.10230	4	2989.91600	2
2973.12039	8	2989.92413	1
2973.1351	2	2989.96174	3
2973.19961	4	2989.99919	3
2973.22571	1	2990.02636	1
2973.25283	8	2990.10851	4
2973.27923	4	2990.11470	23
2973.28191	3	2990.14753	4
2973.30897	8	2990.16685	4
2973.3384	8	2990.28506	3
2973.3445	22	2990.28726	34
2973.3567	4	2990.32245	72
2973.4241	21	2990.32987	24
2973.43443	40	2990.37065	2
2973.45754	6	2990.39681	31
2973.466	19	2990.54208	2
2973.47999	10	2990.57789	6
2973.48805	14	2990.58487	15
2973.50847	3	2990.61345	2
2973.51740	10	2990.71645	1
2973.52584	27	2990.72169	3
2973.52907	12	2990.73924	9
2973.54333	3	2990.76983	1
2973.55153	33	2990.81971	1
2973.5624	3	2990.89578	1
2973.569	10	2990.91506	35
2973.58037	30	2990.93023	1
2973.59099	3	2990.96167	2

Wavenumber cm^{-1}	Relative intensity	Wavenumber cm^{-1}	Relative intensity
2973.59497	4	2990.99872	2
2973.60148	6	2991.00359	2
2973.61922	3	2991.16299	32
2973.62284	13	2991.20087	1
2973.63132	5	2991.20932	5
2973.64759	29	2991.26917	1
2973.6722	17	2991.29527	1
2973.67652	29	2991.29921	22
2973.68021	4	2991.45483	1
2973.68949	2	2991.45976	1
2973.74979	8	2991.47819	2
2973.76436	8	2991.57121	30
2973.79067	6	2991.64058	1
2973.80914	6	2991.65927	2
2973.80992	3	2991.69975	1
2973.84463	21	2991.73239	2
2973.85437	2	2991.74797	51
2973.86122	5	2991.77923	88
2973.88351	16	2991.82147	15
2973.88795	2	2991.85625	37
2973.89166	3	2991.93785	3
2973.9427	3	2991.9969	5
2973.97979	55	2992.05340	15
2974.06025	3	2992.11596	1
2974.09191	3	2992.12438	2
2974.13152	8	2992.20978	1
2974.16426	10	2992.2206	1
2974.17079	3	2992.30982	7
2974.19139	2	2992.48527	21
2974.24537	3	2992.58636	1
2974.29715	13	2992.60067	2
2974.34452	9	2992.62378	29
2974.37366	25	2992.62726	1
2974.42195	19	2992.70759	4
2974.43166	3	2992.80892	6
2974.51045	3	2992.82554	10
2974.52184	7	2992.86735	1
2974.53297	3	2992.94709	1
2974.54097	28	2992.95486	1
2974.61934	4	2992.96412	1
2974.63663	4	2993.01449	32
2974.63982	3	2993.05981	2
2974.64404	6	2993.19559	58
2974.66191	3	2993.22485	87
2974.71579	1	2993.30689	39
2974.75146	11	2993.32544	10

Wavenumber cm^{-1}	Relative intensity	Wavenumber cm^{-1}	Relative intensity
2974.77074	6	2993.39321	4
2974.77978	11	2993.40062	6
2974.81287	14	2993.46222	2
2974.83155	4	2993.51711	12
2974.83494	4	2993.56873	2
2974.84662	31	2993.58133	4
2974.8588	3	2993.72311	1
2974.8744	32	2993.7384	1
2974.93164	13	2993.84181	2
2974.98438	21	2993.85525	1
2975.01067	8	2993.90061	4
2975.01502	37	2993.91936	3
2975.03124	8	2993.97713	3
2975.04452	3	2994.03977	2
2975.05154	8	2994.04875	6
2975.06506	23	2994.06361	11
2975.07188	21	2994.07157	23
2975.07782	9	2994.09822	11
2975.09616	33	2994.13632	13
2975.10311	25	2994.14317	2
2975.1137	24	2994.14621	5
2975.12532	11	2994.16477	11
2975.13555	4	2994.18094	1
2975.14161	11	2994.18753	12
2975.15614	7	2994.20720	3
2975.16647	16	2994.21097	2
2975.17253	5	2994.21997	21
2975.18549	13	2994.22305	3
2975.1957	11	2994.22886	2
2975.2155	7	2994.23238	2
2975.22093	8	2994.24130	31
2975.22345	9	2994.24919	32
2975.22961	7	2994.25271	10
2975.23214	7	2994.29231	6
2975.23667	10	2994.31109	13
2975.23962	7	2994.31890	5
2975.24714	9	2994.34351	8
2975.25565	27	2994.35250	12
2975.25866	9	2994.3531	12
2975.26359	7	2994.36612	22
2975.26689	15	2994.37425	6
2975.27419	15	2994.38835	12
2975.2785	2	2994.40372	2
2975.28556	18	2994.43103	2
2975.29235	3	2994.43653	11
2975.29895	4	2994.43996	15

Wavenumber cm^{-1}	Relative intensity	Wavenumber cm^{-1}	Relative intensity
2975.30804	17	2994.48200	6
2975.33352	9	2994.48388	6
2975.35050	30	2994.49393	17
2975.36371	5	2994.51562	1
2975.36706	19	2994.53505	26
2975.40374	3	2994.55750	8
2975.41145	4	2994.56678	34
2975.43155	27	2994.57667	30
2975.4401	3	2994.58106	2
2975.50108	41	2994.58589	2
2975.58558	4	2994.58942	29
2975.59542	11	2994.61713	50
2975.60223	14	2994.63259	75
2975.60901	12	2994.65803	7
2975.67057	10	2994.66032	101
2975.67467	5	2994.67756	51
2975.68419	6	2994.68104	32
2975.70903	8	2994.74226	55
2975.77762	4	2994.74838	49
2975.79951	17	2994.76233	16
2975.90074	8	2994.76664	3
2975.97045	5	2994.78345	7
2976.00223	13	2994.79354	18
2976.01468	2	2994.79935	2
2976.01974	3	2994.82663	59
2976.02347	2	2994.84512	11
2976.04655	4	2994.85692	12
2976.06098	3	2994.88151	16
2976.07377	19	2994.91106	2
2976.0936	2	2994.92823	27
2976.09713	3	2994.96363	8
2976.11572	2	2994.96885	14
2976.12082	2	2995.04641	13
2976.12960	5	2995.07338	5
2976.13566	3	2995.15263	3
2976.13935	3	2995.15919	4
2976.15063	5	2995.16363	4
2976.18414	34	2995.17217	5
2976.25826	4	2995.18597	3
2976.26090	10	2995.20539	2
2976.27107	4	2995.21198	3
2976.39053	12	2995.21861	4
2976.39744	19	2995.25312	4
2976.57128	19	2995.50339	24
2976.58255	11	2995.63135	5
2976.58634	15	2995.71364	6

Wavenumber cm^{-1}	Relative intensity	Wavenumber cm^{-1}	Relative intensity
2976.59495	23	2995.75834	2
2976.60909	6	2995.82895	3
2976.61471	18	2995.88328	23
2976.61853	4	2995.9011	4
2976.66568	18	2995.90454	5
2976.69661	8	2996.05943	59
2976.71194	16	2996.08700	82
2976.71597	6	2996.18181	38
2976.72558	4	2996.29076	2
2976.73349	23	2996.30675	9
2976.73872	7	2996.37989	2
2976.74833	30	2996.41068	6
2976.75352	10	2996.91538	8
2976.76208	3	2996.96274	6
2976.76832	6	2996.99206	5
2976.78703	9	2997.15191	26
2976.7948	9	2997.18152	26
2976.81331	12	2997.21665	76
2976.82065	6	2997.29947	11
2976.8311	4	2997.31861	3
2976.86567	22	2997.32798	26
2976.87588	5	2997.33498	2
2976.87855	3	2997.35520	2
2976.88892	2	2997.3846	2
2976.89857	2	2997.47714	22
2976.90317	7	2997.50533	30
2976.913	15	2997.52540	69
2976.93271	2	2997.57669	70
2976.94657	7	2997.60636	75
2976.96575	14	2997.74719	27
2976.97244	2	2997.84098	6
2976.98147	2	2998.01486	1
2976.98444	3	2998.0443	2
2977.00587	2	2998.04718	1
2977.01166	3	2998.20183	4
2977.02264	4	2998.30385	5
2977.04316	9	2998.40075	5
2977.04906	32	2998.48873	4
2977.0543	8	2998.61603	19
2977.07362	8	2998.70460	72
2977.08421	8	2998.71004	5
2977.10941	7	2998.7601	1
2977.18795	1	2998.81643	20
2977.1935	3	2998.8251	1
2977.19748	2	2998.83813	4
2977.20313	7	2998.8445	1

Wavenumber cm^{-1}	Relative intensity	Wavenumber cm^{-1}	Relative intensity
2977.20876	3	2998.8743	1
2977.21568	8	2998.8804	2
2977.21914	2	2998.88657	11
2977.22608	1	2998.8935	4
2977.24379	1	2998.91568	13
2977.24706	2	2999.02693	59
2977.25415	1	2999.04658	56
2977.26808	8	2999.13576	53
2977.27145	2	2999.18641	3
2977.27404	2	2999.24912	18
2977.28398	2	2999.62849	5
2977.29235	1	2999.66137	4
2977.29549	1	2999.66616	2
2977.29873	2	2999.81667	3
2977.30151	1	2999.92935	2
2977.30544	3	2999.99206	3
2977.31263	2	3000.06885	14
2977.31608	2	3000.11047	1
2977.31897	13	3000.11608	3
2977.32321	2	3000.12382	3
2977.32673	1	3000.13712	3
2977.32993	2	3000.14019	4
2977.33295	2	3000.14516	6
2977.33549	1	3000.14955	8
2977.33864	1	3000.15293	8
2977.34374	3	3000.16182	12
2977.35139	17	3000.17241	3
2977.3629	3	3000.18266	34
2977.37042	18	3000.24807	13
2977.37587	12	3000.28923	5
2977.3819	4	3000.29789	13
2977.38673	2	3000.30620	6
2977.39092	24	3000.31929	6
2977.39403	2	3000.33293	2
2977.41909	2	3000.37227	2
2977.42492	2	3000.37818	3
2977.45006	4	3000.3969	4
2977.45747	2	3000.42495	5
2977.45997	2	3000.43617	6
2977.47008	3	3000.44071	3
2977.48752	2	3000.50606	37
2977.51411	4	3000.54844	34
2977.52174	4	3000.55733	4
2977.56665	7	3000.57927	5
2977.57279	71	3000.59565	6
2977.57793	7	3000.61346	7

Wavenumber cm^{-1}	Relative intensity	Wavenumber cm^{-1}	Relative intensity
2977.58786	8	3000.61704	2
2977.61597	11	3000.68541	38
2977.62504	10	3000.71153	2
2977.64814	11	3000.72006	3
2977.65189	15	3000.72971	3
2977.66290	12	3000.73279	2
2977.67413	2	3000.73593	3
2977.69110	14	3000.76706	13
2977.70569	23	3000.82969	3
2977.71365	3	3000.84945	2
2977.74388	2	3000.87403	2
2977.74961	30	3000.88214	2
2977.75554	15	3000.96581	2
2977.76791	2	3000.99282	3
2977.77494	11	3001.05168	3
2977.78264	30	3001.15628	2
2977.78662	21	3001.20792	2
2977.7975	1	3001.49948	3
2977.80043	2	3001.50840	9
2977.80621	4	3001.64743	19
2977.80938	2	3001.68643	2
2977.82361	7	3001.71763	3
2977.82915	14	3001.75179	6
2977.83406	2	3001.76191	8
2977.83905	3	3001.80901	9
2977.8502	2	3001.95420	23
2977.85354	1	3001.98481	6
2977.86091	28	3002.08948	17
2977.87169	3	3002.25475	22
2977.87521	1	3002.30744	8
2977.87952	22	3002.4865	4
2977.88619	8	3002.92355	5
2977.88939	3	3003.10090	11
2977.89539	3	3003.16177	3
2977.90021	10	3003.16969	2
2977.90548	2	3003.37637	5
2977.90855	4	3003.38854	13
2977.91124	1	3003.57098	4
2977.91732	2	3003.63211	7
2977.92333	14	3003.84238	12
2977.94292	9	3003.87424	4
2977.94475	8	3003.94038	3
2977.94754	4	3004.36611	7
2977.95506	12	3004.48406	2
2977.95753	22	3004.54618	5
2977.98072	5	3004.59899	55

APPENDIX E

SLIT-JET SPECTRUM OF CH_3NH_2: ASSIGNED A-SYMMETRY TRANSITIONS

Substate identifier	Excited state			Ground state			Wavenumber cm^{-1}	Relative intensity
	J'	K'	$^{twrv}\Gamma'$	J''	K''	$^{twrv}\Gamma''$		
100	0	0	A2	1	1	A1	2981.66847	36
100	1	0	A1	1	1	A2	2983.12287	54
100	1	0	A1	2	1	A2	2980.21883	42
100	2	0	A2	1	1	A1	2986.11872	15
100	2	0	A2	2	1	A1	2983.10267	66
100	2	0	A2	3	1	A1	2978.79792	22
100	3	0	A1	2	1	A2	2987.63946	22
100	3	0	A1	3	1	A2	2983.07159	59
100	3	0	A1	4	1	A2	2977.39092	24
100	4	0	A2	3	1	A1	2989.17800	16
100	4	0	A2	4	1	A1	2983.02842	46
100	4	0	A2	5	1	A1	2976.00223	13
100	5	0	A1	4	1	A2	2990.73924	9
100	5	0	A1	5	1	A2	2982.97954	23
100	5	0	A1	6	1	A2	2974.63663	4
100	6	0	A2	5	1	A1	2992.30982	7
100	6	0	A2	6	1	A1	2982.91108	15
100	6	0	A2	7	1	A1	2973.28191	3
100	7	0	A1	6	1	A2	2993.90061	4
100	7	0	A1	7	1	A2	2982.83459	8
100	1	1	A2	0	0	A1	2990.39681	31
110	1	1	A2	2	0	A1	2985.95953	12
110	1	1	A2	2	2	A1	2974.75146	11
110	2	1	A1	1	0	A2	2991.85625	37
110	2	1	A1	3	0	A2	2984.46238	27
110	2	1	A1	2	2	A2	2977.69110	14
110	2	1	A1	3	2	A2	2973.25283	8
110	3	1	A2	2	0	A1	2993.30689	39
110	3	1	A2	4	0	A1	2982.95767	21
110	3	1	A2	3	2	A1	2977.66292	12
110	4	1	A1	3	0	A2	2994.74838	49
110	4	1	A1	5	0	A2	2981.44574	14
110	4	1	A1	3	2	A2	2983.53915	5
110	3	1	A2	4	2	A1	2971.74383	6

Substate identifier	Excited state			Ground state			Wavenumber cm^{-1}	Relative intensity
	J'	K'	${}^{twrv}\Gamma'$	J''	K''	${}^{twrv}\Gamma''$		
110	4	1	A1	4	2	A2	2977.62504	10
110	4	1	A1	4	2	A2	2,970.2227	3
110	5	1	A2	4	0	A1	2996.18181	38
110	5	1	A2	6	0	A1	2979.92775	4
110	5	1	A2	4	2	A1	2984.96760	4
110	5	1	A2	5	2	A1	2977.57793	7
110	6	1	A1	5	2	A2	2986.38475	2
110	6	1	A1	6	2	A2	2977.52174	4
111	1	1	A1	1	0	A2	2988.94501	40
111	1	1	A1	2	2	A2	2974.77978	11
111	2	1	A2	2	0	A1	2988.98248	49
111	2	1	A2	2	2	A1	2977.77494	10
111	2	1	A2	3	2	A1	2973.3384	8
111	3	1	A1	3	0	A2	2989.03855	44
111	3	1	A1	2	2	A2	2982.26712	3
111	3	1	A1	3	2	A2	2977.82915	14
111	3	1	A1	4	2	A2	2971.91503	5
111	4	1	A2	4	0	A1	2989.11377	30
111	4	1	A2	3	2	A1	2983.81815	6
111	4	1	A2	4	2	A1	2977.90021	10
111	5	1	A1	5	0	A2	2989.20579	17
111	5	1	A1	5	2	A2	2977.98390	8
111	6	1	A2	6	0	A1	2989.33127	3
120	2	2	A1	3	1	A2	2989.68369	2
120	2	2	A1	2	1	A2	2994.25271	10
120	2	2	A1	1	1	A2	2997.15191	26
120	2	2	A2	3	3	A1	2968.16001	10
120	3	2	A2	3	1	A1	2994.31109	13
120	3	2	A2	2	1	A1	2998.61603	19
120	3	2	A1	3	3	A2	2972.61131	4
120	3	2	A2	4	3	A1	2966.696	4
120	4	2	A1	4	1	A2	2994.38835	12
120	4	2	A1	5	1	A2	2986.62849	2
120	4	2	A1	3	1	A2	3000.06885	14
120	5	2	A1	5	3	A2	2972.64736	6
120	6	2	A1	5	1	A2	3002.92355	5
120	6	2	A1	6	1	A2	2994.58106	2
121	2	2	A2	1	1	A1	2997.18152	26
120	5	2	A2	5	1	A1	2994.48200	6
120	5	2	A2	4	1	A1	3001.50840	9
120	5	2	A2	4	3	A1	2980.04099	60

Substate identifier	Excited state			Ground state			Wavenumber cm^{-1}	Relative intensity
	J'	K'	${}^{twrv}\Gamma'$	J''	K''	${}^{twrv}\Gamma''$		
121	2	2	A2	2	1	A1	2994.16477	11
121	2	2	A2	3	1	A1	2989.86059	2
121	3	2	A1	3	1	A2	2994.13632	13
121	3	2	A1	4	1	A2	2988.45616	2
121	4	2	A2	3	1	A1	3000.24807	13
121	4	2	A2	4	1	A1	2994.09822	11
121	4	2	A2	5	1	A1	2987.07184	2
121	5	2	A1	4	1	A2	3001.80901	9
121	5	2	A1	5	1	A2	2994.04875	6
121	6	2	A2	5	1	A1	3003.37637	5
121	6	2	A1	6	1	A2	2993.97713	3
121	6	2	A1	6	3	A2	2972.66855	4

APPENDIX F

SLIT-JET SPECTRUM OF CH_3NH_2: ASSIGNED B-SYMMETRY TRANSITIONS

Substate identifier	Excited state			Ground state			Wavenumber	Relative intensity
	J'	K'	${}^{twrv}\Gamma'$	J''	K''	${}^{twrv}\Gamma''$	cm^{-1}	
200	0	0	B2	1	1	B1	2981.85113	97
200	1	0	B1	1	1	B2	2983.30550	71
200	1	0	B1	2	1	B2	2980.40584	117
200	2	0	B2	1	1	B1	2986.30052	39
200	2	0	B2	2	1	B1	2983.28453	99
200	2	0	B2	3	1	B1	2978.98010	50
200	3	0	B1	2	1	B2	2987.82150	54
200	3	0	B1	3	1	B2	2983.25352	86
200	3	0	B1	4	1	B2	2977.57279	71
200	4	0	B2	3	1	B1	2989.36012	47
200	4	0	B2	4	1	B1	2983.21055	75
200	4	0	B2	5	1	B1	2976.18414	34
200	5	0	B1	4	1	B2	2990.91506	35
200	5	0	B1	5	1	B2	2983.15510	69
200	5	0	B1	6	1	B2	2974.81287	14
200	6	0	B2	5	1	B1	2992.48527	21
200	6	0	B2	6	1	B1	2983.08601	43
200	6	0	B2	7	1	B1	2973.45754	6
200	7	0	B1	6	1	B2	2994.06361	11
200	7	0	B1	7	1	B2	2982.99612	16
200	8	0	B2	7	1	B1	2995.63135	5
200	8	0	B2	8	1	B2	2982.86695	4
210	1	1	B2	0	0	B1	2990.32245	72
210	1	1	B2	2	0	B1	2985.88600	36
210	1	1	B2	2	2	B1	2974.84662	31
210	2	1	B1	1	0	B2	2991.77923	88
210	2	1	B1	3	0	B2	2984.38562	63
210	2	1	B1	2	2	B2	2977.78264	30
210	2	1	B1	3	2	B2	2973.3445	22
210	3	1	B2	2	0	B1	2993.22485	87
210	3	1	B2	4	0	B1	2982.87565	57
210	3	1	B2	2	2	B1	2982.18570	7
210	3	1	B2	3	2	B1	2977.74961	30
210	3	1	B2	4	2	B1	2971.83044	14
210	4	1	B1	3	0	B2	2994.66032	101

Substate identifier	Excited state			Ground state			Wavenumber	Relative intensity
	J'	K'	${}^{twrv}\Gamma'$	J''	K''	${}^{twrv}\Gamma''$	cm^{-1}	
210	4	1	B1	5	0	B2	2981.35772	33
210	4	1	B1	3	2	B2	2983.62034	12
210	4	1	B1	4	2	B2	2977.70569	23
210	4	1	B1	5	2	B2	2970.30402	7
210	5	1	B2	4	0	B1	2996.08700	82
210	5	1	B2	6	0	B1	2979.83345	11
210	5	1	B2	4	2	B1	2985.04169	10
210	5	1	B2	5	2	B1	2977.65189	15
210	5	1	B2	6	2	B1	2968.76407	5
210	6	1	B1	5	0	B2	2997.50533	30
210	6	1	B1	7	0	B2	2978.30319	11
210	6	1	B1	5	2	B2	2986.45074	2
210	6	1	B1	6	2	B2	2977.58786	8
210	6	1	B1	7	2	B2	2967.20975	2
210	7	1	B2	6	0	B1	2998.91568	13
210	7	1	B2	8	0	B1	2976.76832	6
210	7	1	B2	7	2	B1	2977.51411	4
210	8	1	B1	7	0	B2	3000.31929	6
210	8	1	B1	9	0	B2	2975.23214	7
211	1	1	B1	1	0	B2	2988.87043	82
211	1	1	B1	2	2	B2	2974.8744	32
211	2	1	B2	2	0	B1	2988.8992	85
211	2	1	B2	3	2	B1	2973.4241	21
211	2	1	B2	2	2	B1	2977.86091	28
211	3	1	B1	3	0	B2	2988.99831	66
211	3	1	B1	3	2	B2	2977.95753	22
211	4	1	B2	4	0	B1	2989.05863	72
211	4	1	B2	4	2	B1	2978.01336	25
211	5	1	B1	5	0	B2	2989.14776	45
211	5	1	B1	5	2	B2	2978.09376	18
211	6	1	B2	6	0	B1	2989.25764	21
211	6	1	B2	6	2	B1	2978.18897	11
211	7	1	B1	7	2	B2	2978.30812	4
211	7	1	B1	7	0	B2	2989.40167	1
211	3	1	B2	4	2	B1	[n]2971.97323	24
211	4	1	B2	5	2	B1	[n]2970.54884	14
220	2	2	B2	2	1	B1	2994.58942	29
220	2	2	B2	3	3	B1	2968.32568	20
220	3	2	B1	4	3	B2	2966.86775	11
220	3	2	B1	4	1	B2	2988.88658	6
220	3	2	B1	3	1	B2	2994.56678	34
220	2	2	B2	3	1	B1	2997.60636	75
220	2	2	B2	1	1	B1	2990.28506	3
220	3	2	B1	3	3	B2	2972.78292	6

Substate identifier	Excited state			Ground state			Wavenumber cm^{-1}	Relative intensity
	J'	K'	${}^{twrv}\Gamma'$	J''	K''	${}^{twrv}\Gamma''$		
220	3	2	B1	2	1	B2	2999.13576	53
220	4	2	B1	4	3	B2	2972.80997	4
220	4	2	B2	5	1	B1	2987.50915	4
220	4	2	B2	4	1	B1	2994.53505	26
220	4	2	B2	3	1	B1	3000.68541	38
220	5	2	B1	5	1	B2	2994.49393	17
220	5	2	B1	6	1	B2	2986.15211	2
220	5	2	B1	4	1	B2	3002.25475	22
220	6	2	B1	6	1	B2	2995.04641	13
220	6	2	B1	5	1	B2	3003.38854	13
220	7	2	B2	7	1	B1	2995.17217	5
220	7	2	B2	6	1	B1	3004.80038	7
221	2	2	B1	3	1	B2	2990.10851	4
221	2	2	B1	2	1	B2	2994.67756	51
221	2	2	B1	1	1	B2	2997.57669	70
221	3	2	B2	4	1	B1	2988.59181	5
221	3	2	B2	2	1	B1	2999.04658	56
221	3	2	B2	3	1	B1	2994.74226	55
221	4	2	B1	5	1	B2	2987.06537	4
221	4	2	B2	4	3	B1	2972.80715	4
221	4	2	B1	3	1	B2	3000.50606	37
221	4	2	B1	4	1	B2	2994.82663	59
221	5	2	B2	5	1	B1	2994.92823	27
221	5	2	B2	4	1	B1	3001.95420	23
221	5	2	B2	6	1	B1	2985.52919	2

[n] Lines excluded from the fit to :

$$\nu(J',K',i) = \nu_o(J',K',i) + B_{eff}(J',K',i)J(J+1) - D_{eff}(J',K',i)J^2(J+1)^2$$

APPENDIX G

SLIT-JET SPECTRUM OF CH_3NH_2: ASSIGNED E_1-SYMMETRY TRANSITIONS

Substate	Excited state			Ground state			Wavenumber	Relative
identifier	J'	$\|K'\|$	${}^{twrv}\Gamma'$	J''	$\|K''\|$	${}^{twrv}\Gamma''$	cm^{-1}	intensity
300	1	0	E1+1	1	1	E1+1	2983.65689	19
300	1	0	E1+1	2	1	E1+1	2980.68947	10
300	1	0	E1+1	1	1	E1-1	2983.82724	17
300	1	0	E1+1	2	1	E1-1	2980.8788	18
300	2	0	E1+1	1	1	E1+1	2986.56917	2
300	2	0	E1+1	2	1	E1+1	2983.60152	24
300	2	0	E1+1	1	1	E1-1	2986.73911	4
300	2	0	E1+1	2	1	E1-1	2983.79113	10
300	2	0	E1+1	3	1	E1-1	2979.38142	8
300	3	0	E1+1	2	1	E1+1	2987.97457	2
300	3	0	E1+1	3	1	E1+1	2983.51134	19
300	3	0	E1+1	2	1	E1-1	2988.16334	5
300	3	0	E1+1	3	1	E1-1	2983.75592	7
300	3	0	E1+1	4	1	E1-1	2977.88619	8
300	4	0	E1+1	4	1	E1+1	2983.37860	11
300	4	0	E1+1	3	1	E1-1	2989.58365	4
300	4	0	E1+1	4	1	E1-1	2983.71681	5
300	4	0	E1+1	5	1	E1-1	2976.39053	12
301	0	0	E1+1	1	1	E1+1	2982.24924	13
301	1	0	E1+1	1	1	E1-1	2983.87628	33
301	1	0	E1+1	1	1	E1+1	2983.70677	51
301	1	0	E1+1	2	1	E1+1	2980.73928	19
301	2	0	E1+1	2	1	E1-1	2983.88146	30
301	2	0	E1+1	1	1	E1-1	2986.82997	13
301	2	0	E1+1	3	1	E1-1	2979.47238	27
301	2	0	E1+1	1	1	E1+1	2986.66010	10
301	2	0	E1+1	2	1	E1+1	2983.69271	84
301	2	0	E1+1	3	1	E1+1	2979.22944	5
301	3	0	E1+1	3	1	E1-1	2983.89663	17
301	3	0	E1+1	2	1	E1-1	2988.30642	24
301	3	0	E1+1	4	1	E1-1	2978.02919	40
301	3	0	E1+1	2	1	E1+1	2988.11713	10
301	3	0	E1+1	3	1	E1+1	2983.65407	81
301	4	0	E1+1	3	1	E1-1	2989.79399	26
301	4	0	E1+1	4	1	E1-1	2983.92648	8
301	4	0	E1+1	3	1	E1+1	2989.55128	5

Substate identifier	Excited state			Ground state			Wavenumber	Relative intensity
	J'	$\|K'\|$	${}^{twrv}\Gamma'$	J''	$\|K''\|$	${}^{twrv}\Gamma''$	cm^{-1}	
301	4	0	E1+1	5	1	E1+1	2976.12960	5
301	4	0	E1+1	4	1	E1+1	2983.58924	75
301	5	0	E1+1	5	1	E1-1	2983.97242	6
301	5	0	E1+1	4	1	E1-1	2991.29921	22
301	5	0	E1+1	6	1	E1-1	2975.18549	13
301	5	0	E1+1	5	1	E1+1	2983.50295	55
301	6	0	E1+1	5	1	E1-1	2992.82554	10
301	6	0	E1+1	7	1	E1-1	2973.79067	6
301	6	0	E1+1	6	1	E1+1	2983.40114	23
301	7	0	E1+1	6	1	E1-1	2994.35250	12
301	7	0	E1+1	7	1	E1+1	2983.26747	13
301	8	0	E1+1	7	1	E1-1	2995.90454	5
301	8	0	E1+1	8	1	E1+1	2983.12842	7
302	0	0	E1+1	1	1	E1+1	2980.16657	4
302	0	0	E1+1	1	1	E1-1	2980.33642	12
302	1	0	E1+1	1	1	E1-1	2981.80543	11
302	1	0	E1+1	2	1	E1-1	2978.85762	7
302	1	0	E1+1	1	1	E1+1	2981.6354	10
302	2	0	E1+1	1	1	E1-1	2984.73382	5
302	2	0	E1+1	2	1	E1-1	2981.78551	11
302	2	0	E1+1	3	1	E1-1	2977.37587	12
302	2	0	E1+1	2	1	E1+1	2981.59613	15
302	3	0	E1+1	2	1	E1-1	2986.17789	6
302	3	0	E1+1	3	1	E1-1	2981.76814	7
302	3	0	E1+1	4	1	E1-1	2975.90074	8
302	3	0	E1+1	2	1	E1+1	[n]2985.98888	1
302	3	0	E1+1	4	1	E1+1	[n]2977.6911	14
302	3	0	E1+1	3	1	E1+1	2981.52548	15
302	4	0	E1+1	3	1	E1-1	2987.60385	6
302	4	0	E1+1	4	1	E1-1	2981.73597	6
410	1	1	E1-1	2	2	E1-1	2975.35050	30
410	1	1	E1-1	0	0	E1+1	2990.32987	24
410	1	1	E1-1	1	0	E1+1	2988.85097	58
410	1	1	E1-1	2	0	E1+1	2985.89342	10
410	2	1	E1-1	2	2	E1-1	2978.32093	23
410	2	1	E1-1	3	2	E1-1	2973.88351	16
410	2	1	E1-1	1	0	E1+1	2991.82147	15
410	2	1	E1-1	2	0	E1+1	2988.86326	79
410	2	1	E1-1	3	0	E1+1	2984.42793	12
410	2	1	E1-1	2	2	E1+1	2978.0282	7
410	2	1	E1-1	3	2	E1+1	2973.59099	3
410	3	1	E1-1	2	2	E1-1	2982.78271	7
410	3	1	E1-1	3	2	E1-1	2978.34553	26
410	3	1	E1-1	4	2	E1-1	2972.42902	9
410	3	1	E1-1	2	0	E1+1	2993.32544	10
410	3	1	E1-1	3	0	E1+1	2988.8897	81

Substate identifier	Excited state			Ground state			Wavenumber	Relative intensity
	J'	$\|K'\|$	${}^{twrv}\Gamma'$	J''	$\|K''\|$	${}^{twrv}\Gamma''$	cm^{-1}	
410	3	1	E1-1	4	0	E1+1	2982.97742	7
410	3	1	E1-1	3	2	E1+1	2978.05330	7
410	3	1	E1-1	4	2	E1+1	2972.13692	6
410	4	1	E1-1	3	2	E1-1	2984.30022	8
410	4	1	E1-1	4	2	E1-1	2978.38405	19
410	4	1	E1-1	5	2	E1-1	2970.98819	5
410	4	1	E1-1	4	0	E1+1	2988.93095	65
410	4	1	E1-1	4	2	E1+1	2978.09128	16
410	4	1	E1-1	5	2	E1+1	2970.69565	12
410	5	1	E1-1	4	2	E1-1	2985.83205	2
410	5	1	E1-1	5	2	E1-1	2978.43633	11
410	5	1	E1-1	6	2	E1-1	2969.56051	3
410	5	1	E1-1	5	0	E1+1	2988.99012	38
410	5	1	E1-1	5	2	E1+1	2978.14419	6
410	6	1	E1-1	5	2	E1-1	2987.37273	2
410	6	1	E1-1	6	2	E1-1	2978.49752	8
410	6	1	E1-1	7	2	E1-1	2968.14368	3
410	6	1	E1-1	6	0	E1+1	2989.06234	18
410	6	1	E1-1	6	2	E1+1	2978.20528	4
310	1	1	E1+1	1	0	E1+1	2988.80837	40
310	1	1	E1+1	0	0	E1+1	2990.28726	34
310	1	1	E1+1	2	0	E1+1	2985.85056	13
310	1	1	E1+1	2	2	E1+1	2975.01502	37
310	1	1	E1+1	2	2	E1-1	2975.30804	17
310	2	1	E1+1	2	0	E1+1	2988.78971	8
310	2	1	E1+1	1	0	E1+1	2991.74797	51
310	2	1	E1+1	3	0	E1+1	2984.35408	33
310	2	1	E1+1	3	2	E1+1	2973.51740	10
310	2	1	E1+1	2	2	E1+1	2977.95506	12
310	2	1	E1+1	3	2	E1-1	2973.80914	6
310	2	1	E1+1	2	2	E1-1	2978.24607	12
310	3	1	E1+1	4	0	E1+1	2982.84669	32
310	4	1	E1+1	5	2	E1+1	2970.48416	3
310	4	1	E1+1	4	2	E1+1	2977.87952	22
310	4	1	E1+1	3	2	E1+1	2983.79588	5
310	4	1	E1+1	4	2	E1-1	2978.17161	12
310	4	1	E1+1	5	2	E1-1	2970.77564	3
310	5	1	E1+1	6	0	E1+1	2979.80571	7
310	3	1	E1+1	3	0	E1+1	2988.75963	4
310	3	1	E1+1	2	0	E1+1	2993.19559	58
310	3	1	E1+1	4	2	E1+1	2972.00676	6
310	3	1	E1+1	3	2	E1+1	2977.92333	14
310	3	1	E1+1	2	2	E1+1	2982.3607	4
310	3	1	E1+1	3	2	E1-1	2978.2157	8
310	3	1	E1+1	4	2	E1-1	2972.29902	4
310	4	1	E1+1	5	0	E1+1	2981.32987	22

Substate identifier	Excited state			Ground state			Wavenumber	Relative intensity
	J'	$\|K'\|$	${}^{twrv}\Gamma'$	J''	$\|K''\|$	${}^{twrv}\Gamma''$	cm^{-1}	
310	4	1	E1+1	3	0	E1+1	2994.63259	75
311	4	1	E1+1	3	2	E1+1	2983.23503	6
311	5	1	E1+1	4	0	E1+1	2995.50339	24
311	5	1	E1+1	5	0	E1+1	2988.11397	7
311	5	1	E1+1	6	0	E1+1	2979.2497	4
311	5	1	E1+1	6	2	E1+1	2968.39114	17
311	5	1	E1+1	5	2	E1+1	2977.26808	8
311	5	1	E1+1	4	2	E1+1	2984.66419	4
311	6	1	E1+1	5	0	E1+1	2996.91538	8
311	6	1	E1+1	6	0	E1+1	2988.05105	2
311	6	1	E1+1	7	0	E1+1	2977.71365	3
311	6	1	E1+1	7	2	E1+1	2966.83759	8
311	6	1	E1+1	6	2	E1+1	2977.1935	3
310	5	1	E1+1	4	0	E1+1	2996.05943	59
310	5	1	E1+1	6	2	E1+1	2968.94887	3
310	5	1	E1+1	5	2	E1+1	2977.82361	7
310	5	1	E1+1	4	2	E1+1	2985.21913	4
310	5	1	E1+1	5	2	E1-1	2978.11622	5
310	5	1	E1+1	6	2	E1-1	2969.24064	2
310	6	1	E1+1	5	0	E1+1	2997.47714	22
310	6	1	E1+1	7	0	E1+1	2978.27515	8
310	6	1	E1+1	6	2	E1+1	2977.75554	15
310	6	1	E1+1	7	2	E1+1	2967.40014	3
310	6	1	E1+1	5	2	E1+1	2986.63147	1
310	6	1	E1+1	6	2	E1-1	2978.04758	4
310	7	1	E1+1	6	0	E1+1	2998.88657	11
310	7	1	E1+1	8	0	E1+1	2976.73872	7
310	8	1	E1+1	7	0	E1+1	3000.28923	5
311	1	1	E1+1	1	0	E1+1	2988.21488	36
311	1	1	E1+1	0	0	E1+1	2989.69387	26
311	1	1	E1+1	2	2	E1+1	2974.42195	19
311	1	1	E1+1	2	0	E1+1	2985.25748	15
311	2	1	E1+1	2	0	E1+1	2988.20510	38
311	2	1	E1+1	1	0	E1+1	2991.16299	32
311	2	1	E1+1	3	0	E1+1	2983.76975	19
311	2	1	E1+1	3	2	E1+1	2972.93325	14
311	2	1	E1+1	2	2	E1+1	2977.37042	18
311	3	1	E1+1	4	0	E1+1	2982.27458	16
311	3	1	E1+1	2	0	E1+1	2992.62378	29
311	3	1	E1+1	3	2	E1+1	2977.35139	17
311	4	1	E1+1	5	2	E1+1	2969.92289	4
311	4	1	E1+1	4	2	E1+1	2977.31897	13
311	3	1	E1+1	2	2	E1+1	2981.78866	11
311	3	1	E1+1	4	2	E1+1	2971.43518	8
311	4	1	E1+1	3	0	E1+1	2994.07157	23
311	4	1	E1+1	4	0	E1+1	2988.15841	14

Substate identifier	Excited state			Ground state			Wavenumber	Relative intensity
	J'	$\|K'\|$	${}^{twrv}\Gamma'$	J''	$\|K''\|$	${}^{twrv}\Gamma''$	cm^{-1}	
311	4	1	E1+1	5	0	E1+1	2980.76921	13
311	7	1	E1+1	6	0	E1+1	2998.30385	5
311	8	1	E1+1	7	0	E1+1	2999.66137	4
311	3	1	E1+1	3	0	E1+1	2988.18765	27
411	1	1	E1-1	2	2	E1-1	2974.71579	13
411	2	1	E1-1	2	2	E1-1	2977.66290	12
411	2	1	E1-1	3	2	E1-1	2973.22571	1
411	3	1	E1-1	3	2	E1-1	2977.64814	11
411	3	1	E1-1	4	2	E1-1	2971.73163	1
411	3	1	E1-1	2	2	E1-1	2982.05765	12
411	4	1	E1-1	4	2	E1-1	2977.61597	11
411	4	1	E1-1	3	2	E1-1	2983.53283	3
411	4	1	E1-1	5	2	E1-1	2970.22069	3
411	5	1	E1-1	5	2	E1-1	2977.56665	7
411	5	1	E1-1	4	2	E1-1	2984.93552	4
420	6	2	E1-1	6	1	E1-1	[n]2977.5156	4
420	2	2	E1-1	3	3	E1-1	2968.37404	10
420	3	2	E1-1	3	1	E1-1	2994.61713	50
420	4	2	E1-1	5	3	E1-1	2965.4462	4
420	4	2	E1-1	4	3	E1-1	2972.84013	5
420	4	2	E1-1	5	1	E1-1	2987.35414	3
420	4	2	E1-1	4	1	E1-1	2994.68104	32
420	4	2	E1-1	3	1	E1-1	3000.54844	34
420	4	2	E1-1	3	1	E1+1	3000.30620	6
420	4	2	E1-1	4	1	E1+1	2994.34351	8
420	4	2	E1-1	5	1	E1+1	2986.88374	1
420	5	2	E1-1	6	1	E1-1	2985.97521	1
420	5	2	E1-1	5	1	E1-1	2994.76233	16
420	5	2	E1-1	4	1	E1-1	3002.08948	17
420	5	2	E1-1	4	1	E1+1	3001.75179	6
420	4	2	E1-1	5	3	E1-1	[n]2965.32365	19
420	5	2	E1-1	5	1	E1+1	2994.29231	6
420	6	2	E1-1	6	1	E1-1	2994.84512	11
420	6	2	E1-1	5	1	E1-1	3003.63211	7
420	2	2	E1-1	3	1	E1-1	2990.16685	4
420	2	2	E1-1	2	1	E1-1	2994.57667	30
420	2	2	E1-1	1	1	E1-1	2997.52540	63
420	3	2	E1-1	3	1	E1+1	2994.37425	6
420	3	2	E1-1	4	1	E1+1	2988.41201	2
420	2	2	E1-1	1	1	E1+1	2997.35520	2
420	2	2	E1-1	3	1	E1+1	2989.92413	1
420	2	2	E1-1	3	3	E1-1	2968.75967	9
420	3	2	E1-1	4	3	E1-1	2966.90875	7
420	3	2	E1-1	3	3	E1-1	2972.82447	3

Substate identifier	Excited state			Ground state			Wavenumber	Relative intensity
	J'	$\|K'\|$	$^{twrv}\Gamma'$	J''	$\|K''\|$	$^{twrv}\Gamma''$	cm^{-1}	
420	3	2	E1-1	4	1	E1-1	2988.74940	4
420	6	2	E1-1	5	1	E1-1	3003.16177	3
420	6	2	E1-1	6	1	E1+1	2994.20720	3
420	7	2	E1-1	7	3	E1-1	[n]2972.83395	6
420	3	2	E1-1	2	1	E1-1	2999.02693	59
420	3	2	E1-1	2	1	E1+1	2998.83813	4
320	2	2	E1+1	3	1	E1+1	2989.78543	4
320	2	2	E1+1	1	1	E1+1	2997.21665	76
320	2	2	E1+1	2	1	E1+1	2994.24919	32
320	2	2	E1+1	3	3	E1+1	2968.62146	11
320	4	2	E1+1	5	1	E1+1	2986.76083	3
320	4	2	E1+1	4	3	E1+1	2973.10230	4
320	4	2	E1+1	5	3	E1+1	2965.70837	4
320	4	2	E1+1	5	1	E1-1	2987.23040	2
320	4	2	E1+1	3	1	E1-1	3000.42495	5
320	4	2	E1+1	4	1	E1-1	2994.55750	8
320	3	2	E1+1	4	1	E1+1	2988.27877	4
320	3	2	E1+1	3	1	E1+1	2994.24130	31
320	3	2	E1+1	2	1	E1+1	2998.70460	72
320	3	2	E1+1	3	3	E1+1	2973.07726	9
320	3	2	E1+1	4	3	E1+1	2967.16203	7
320	3	2	E1+1	2	1	E1-1	2998.8935	4
320	3	2	E1+1	4	1	E1-1	2988.61610	2
320	3	2	E1+1	3	1	E1-1	2994.48388	6
320	4	2	E1+1	4	1	E1+1	2994.21997	21
320	4	2	E1+1	3	1	E1+1	3000.18266	34
320	5	2	E1+1	5	1	E1+1	2994.18753	12
320	5	2	E1+1	6	1	E1+1	2985.23354	5
320	5	2	E1+1	4	1	E1+1	3001.64743	19
320	5	2	E1+1	5	3	E1+1	2973.1351	2
320	5	2	E1+1	4	1	E1-1	3001.98481	6
320	5	2	E1+1	5	1	E1-1	2994.65803	7
320	6	2	E1+1	6	1	E1+1	2994.14621	5
320	6	2	E1+1	5	1	E1+1	3003.10090	11
320	6	2	E1+1	5	1	E1-1	3003.57098	4
320	6	2	E1+1	6	1	E1-1	2994.78345	7
320	7	2	E1+1	6	1	E1+1	3004.54618	5
320	2	2	E1+1	2	1	E1-1	[n]2994.43653	11
320	2	2	E1+1	3	1	E1-1	[n]2990.02636	1
320	2	2	E1+1	1	1	E1-1	[n]2997.3846	2

[n] Lines excluded from the fit to :

$$\nu(J',K',i) = \nu_o(J',K',i) + B_{eff}(J',K',i)J(J+1) - D_{eff}(J',K',i)J^2(J+1)^2$$

APPENDIX H

SLIT-JET SPECTRUM OF CH_3NH_2: ASSIGNED E_2-SYMMETRY TRANSITIONS

Substate identifier	Excited state J'	$\|K'\|$	$^{tw\tau v}\Gamma'$	Ground state J''	$\|K''\|$	$^{tw\tau v}\Gamma''$	Wavenumber cm^{-1}	Relative intensity
500	0	0	E2+1	1	1	E2-1	2981.17600	10
500	0	0	E2+1	1	1	E2+1	2980.77878	9
500	1	0	E2+1	1	1	E2-1	2982.65007	17
500	1	0	E2+1	1	1	E2+1	2982.25258	27
500	1	0	E2+1	2	1	E2-1	2979.69650	8
500	1	0	E2+1	2	1	E2+1	2979.29075	4
500	2	0	E2+1	1	1	E2-1	2985.59738	4
500	2	0	E2+1	1	1	E2+1	2982.23715	22
500	2	0	E2+1	2	1	E2-1	2982.64299	18
500	2	0	E2+1	1	1	E2+1	2985.19950	6
500	2	0	E2+1	3	1	E2+1	2977.78662	21
500	2	0	E2+1	3	1	E2-1	2978.22052	15
500	3	0	E2+1	2	1	E2-1	2987.06158	6
500	3	0	E2+1	3	1	E2+1	2982.20533	20
500	3	0	E2+1	3	1	E2-1	2982.63887	10
500	3	0	E2+1	2	1	E2+1	2986.65566	4
500	3	0	E2+1	4	1	E2+1	2976.26090	10
500	3	0	E2+1	4	1	E2-1	2976.75352	10
500	4	0	E2+1	3	1	E2-1	2988.52757	5
500	4	0	E2+1	4	1	E2+1	2982.14943	19
500	4	0	E2+1	4	1	E2-1	2982.64299	18
500	4	0	E2+1	4	1	E2+1	2988.09450	2
500	5	0	E2+1	4	1	E2-1	2989.99919	3
500	5	0	E2+1	4	1	E2+1	2989.50598	2
500	5	0	E2+1	4	1	E2+1	2982.06365	10
501	0	0	E2+1	1	1	E2-1	2982.34294	10
501	0	0	E2+1	1	1	E2+1	2981.94544	13
501	1	0	E2+1	1	1	E2-1	2983.82285	11
501	1	0	E2+1	1	1	E2+1	2983.42541	15
501	1	0	E2+1	2	1	E2-1	2980.86921	12
501	1	0	E2+1	2	1	E2+1	2980.46351	9
501	2	0	E2+1	1	1	E2-1	2986.77746	3
501	2	0	E2+1	1	1	E2+1	2986.38029	3
501	2	0	E2+1	2	1	E2-1	2983.82335	17
501	2	0	E2+1	2	1	E2+1	2983.41822	18
501	2	0	E2+1	3	1	E2-1	2979.40137	6

Substate identifier	Excited state			Ground state			Wavenumber cm^{-1}	Relative intensity
	J'	$\|K'\|$	$^{tw}\Gamma'$	J''	$\|K''\|$	$^{tw}\Gamma''$		
501	2	0	E2+1	3	1	E2+1	2978.97072	12
501	3	0	E2+1	2	1	E2-1	2988.25075	5
501	3	0	E2+1	2	1	E2+1	2987.84511	3
501	3	0	E2+1	3	1	E2-1	2983.82792	14
501	3	0	E2+1	3	1	E2+1	2983.39455	20
501	3	0	E2+1	4	1	E2-1	2977.94292	9
501	3	0	E2+1	4	1	E2+1	2977.45006	4
501	4	0	E2+1	3	1	E2-1	2989.72569	5
501	4	0	E2+1	3	1	E2+1	2989.29224	2
501	4	0	E2+1	4	1	E2-1	2983.84069	6
501	4	0	E2+1	4	1	E2+1	2983.34743	17
501	5	0	E2+1	4	1	E2-1	2991.20932	5
501	5	0	E2+1	4	1	E2+1	2990.71645	1
501	5	0	E2+1	5	1	E2+1	2983.27401	13
501	5	0	E2+1	6	1	E2-1	2975.06506	23
501	6	0	E2+1	5	1	E2-1	2992.70759	4
501	6	0	E2+1	6	1	E2+1	2983.17477	9
501	7	0	E2+1	6	1	E2-1	2994.22305	3
501	7	0	E2+1	7	1	E2+1	2983.05194	5
501	8	0	E2+1	7	1	E2-1	2995.75834	2
610	1	1	E2-1	2	2	E2-1	2975.07782	9
610	1	1	E2-1	0	0	E2+1	2990.14753	4
610	1	1	E2-1	1	0	E2+1	2988.66855	34
610	1	1	E2-1	2	2	E2+1	2975.13555	4
610	2	1	E2-1	2	2	E2-1	2978.06906	6
610	2	1	E2-1	3	2	E2-1	2973.63132	5
610	2	1	E2-1	1	0	E2+1	2991.65927	2
610	2	1	E2-1	2	0	E2+1	2988.70155	34
610	2	1	E2-1	2	2	E2+1	2978.12689	3
610	2	1	E2-1	3	2	E2+1	2973.68949	2
610	3	1	E2-1	3	2	E2-1	2978.11041	8
610	3	1	E2-1	4	2	E2-1	2972.19369	3
610	3	1	E2-1	3	0	E2+1	2988.74443	37
610	3	1	E2-1	3	2	E2+1	2978.16886	5
610	3	1	E2-1	4	2	E2+1	2972.25235	2
610	4	1	E2-1	4	2	E2-1	2978.16886	5
610	4	1	E2-1	4	2	E2+1	2978.22708	1
610	4	1	E2-1	5	2	E2+1	2970.83163	1
610	4	1	E2-1	3	2	E2+1	[n]2984.13526	18
510	1	1	E2+1	2	2	E2-1	2975.04452	3
510	1	1	E2+1	0	0	E2+1	2990.11470	23
510	1	1	E2+1	1	0	E2+1	2988.63561	3
510	1	1	E2+1	2	0	E2+1	2985.67845	10
510	1	1	E2+1	2	2	E2+1	2975.10311	25
510	2	1	E2+1	2	2	E2-1	2977.98072	5
510	2	1	E2+1	3	2	E2-1	2973.54333	3

Substate identifier	Excited state			Ground state			Wavenumber cm^{-1}	Relative intensity
	J'	$\|K'\|$	${}^{tw}{}^{rv}\Gamma'$	J''	$\|K''\|$	${}^{tw}{}^{tv}\Gamma''$		
510	2	1	E2+1	1	0	E2+1	2991.57121	30
510	2	1	E2+1	3	0	E2+1	2984.17749	20
510	2	1	E2+1	2	0	E2+1	2988.61331	2
510	2	1	E2+1	2	2	E2+1	2978.03872	7
510	2	1	E2+1	3	2	E2+1	2973.60148	6
510	3	1	E2+1	3	2	E2-1	2977.94475	8
510	3	1	E2+1	4	2	E2-1	2972.02815	2
510	3	1	E2+1	2	0	E2+1	2993.01449	32
510	3	1	E2+1	4	0	E2+1	2982.66550	18
510	3	1	E2+1	3	0	E2+1	2988.57871	1
510	3	1	E2+1	3	2	E2+1	2978.00284	6
510	3	1	E2+1	4	2	E2+1	2972.08669	3
510	4	1	E2+1	4	2	E2-1	2977.88939	3
510	4	1	E2+1	3	0	E2+1	2994.43996	15
510	4	1	E2+1	5	0	E2+1	2981.13777	37
510	4	1	E2+1	4	2	E2+1	2977.94754	4
510	5	1	E2+1	5	2	E2-1	2977.8502	2
510	5	1	E2+1	6	0	E2+1	2979.62990	3
510	5	1	E2+1	4	0	E2+1	2995.88328	23
510	5	1	E2+1	5	2	E2+1	2977.90855	4
511	1	1	E2+1	2	0	E2+1	2984.67509	6
511	1	1	E2+1	0	0	E2+1	2989.11161	12
511	1	1	E2+1	1	0	E2+1	2987.63237	16
511	2	1	E2+1	3	0	E2+1	2983.19153	9
511	2	1	E2+1	1	0	E2+1	2990.58487	15
511	2	1	E2+1	2	0	E2+1	2987.62712	18
511	3	1	E2+1	4	0	E2+1	2981.70453	9
511	3	1	E2+1	2	0	E2+1	2992.05340	15
511	3	1	E2+1	3	0	E2+1	2987.61745	12
511	3	1	E2+1	2	2	E2-1	2981.42076	13
511	4	1	E2+1	5	0	E2+1	2980.21496	8
511	4	1	E2+1	3	0	E2+1	2993.51711	12
511	4	1	E2+1	4	0	E2+1	2987.60385	6
511	4	1	E2+1	5	2	E2-1	2969.56975	10
511	4	1	E2+1	4	2	E2-1	2976.96575	14
511	5	1	E2+1	4	0	E2+1	2994.96885	14
511	5	1	E2+1	5	0	E2+1	2987.57938	3
511	5	1	E2+1	6	0	E2+1	2978.71567	5
611	1	1	E2-1	2	2	E2-1	2974.06025	3
611	1	1	E2-1	1	0	E2+1	2987.65161	8
611	1	1	E2-1	0	0	E2+1	2989.13056	4
611	2	1	E2-1	2	2	E2-1	2977.02264	4
611	2	1	E2-1	3	2	E2-1	2972.58543	3
611	2	1	E2-1	2	0	E2+1	2987.65569	6
611	2	1	E2-1	1	0	E2+1	2990.61345	2
611	3	1	E2-1	3	2	E2-1	2977.0543	8

Substate identifier	Excited state			Ground state			Wavenumber cm^{-1}	Relative intensity
	J'	$\|K'\|$	${}^{tw}{}^{rv}\Gamma'$	J''	$\|K''\|$	${}^{tw}{}^{tv}\Gamma''$		
611	3	1	E2-1	4	2	E2-1	2971.1379	2
611	3	1	E2-1	3	0	E2+1	2987.68931	6
611	3	1	E2-1	2	0	E2+1	2992.12438	2
611	4	1	E2-1	4	2	E2-1	2977.10941	7
611	4	1	E2-1	4	0	E2+1	2987.74687	3
611	5	1	E2-1	5	2	E2-1	2977.20313	7
620	2	2	E2-1	3	3	E2-1	2968.50828	4
620	2	2	E2-1	3	1	E2-1	2990.37065	2
620	2	2	E2-1	2	1	E2-1	2994.79354	18
620	2	2	E2-1	1	1	E2-1	2997.74719	27
620	2	2	E2-1	3	3	E2+1	2968.58683	16
620	3	2	E2-1	3	3	E2-1	2972.98837	5
620	3	2	E2-1	4	3	E2-1	2967.04831	2
620	3	2	E2-1	4	1	E2-1	2988.94076	3
620	3	2	E2-1	2	1	E2-1	2999.24912	18
620	3	2	E2-1	3	1	E2-1	2994.82625	16
620	4	2	E2-1	5	1	E2-1	2987.53720	2
620	4	2	E2-1	4	1	E2-1	2994.88151	16
620	4	2	E2-1	3	1	E2-1	3000.76706	13
620	4	2	E2-1	3	1	E2+1	3000.33293	2
620	4	2	E2-1	4	1	E2+1	2994.38835	12
620	5	2	E2-1	5	1	E2-1	2994.96363	8
620	5	2	E2-1	4	1	E2-1	3002.30744	8
620	6	2	E2-1	6	1	E2-1	2995.07338	5
620	6	2	E2-1	5	1	E2-1	3003.87424	4
620	7	2	E2-1	7	1	E2-1	2995.21198	3
520	2	2	E2+1	1	1	E2+1	2997.32798	26
520	2	2	E2+1	2	1	E2+1	2994.36612	22
520	2	2	E2+1	3	1	E2+1	2989.91600	2
520	2	2	E2+1	3	3	E2+1	2968.56378	3
520	3	2	E2+1	4	1	E2+1	2988.42107	2
520	3	2	E2+1	2	1	E2+1	2998.81643	20
520	3	2	E2+1	3	1	E2+1	2994.36612	22
520	3	2	E2+1	4	3	E2+1	2967.09740	6
520	3	2	E2+1	3	1	E2-1	2994.79935	2
520	3	2	E2+1	4	1	E2-1	2988.91364	2
520	4	2	E2+1	5	1	E2+1	2986.91037	1
520	4	2	E2+1	3	1	E2+1	3000.29789	13
520	5	2	E2+1	4	1	E2+1	3001.76191	8
520	5	2	E2+1	5	1	E2+1	2994.31890	5
520	5	2	E2+1	5	1	E2-1	2994.91106	2
520	6	2	E2+1	6	1	E2+1	2994.22886	2
520	6	2	E2+1	5	1	E2+1	3003.16969	2
520	4	2	E2+1	4	1	E2+1	[n]2994.3531	12

[n] Lines excluded from the fit to :
$$\nu(J',K',i) = \nu_o(J',K',i) + B_{eff}(J',K',i)J(J+1) - D_{eff}(J',K',i)J^2(J+1)^2$$

APPENDIX I

DEPERTURBED COUPLING MATRIX ELEMENTS SHOWING ANHARMONIC INTERACTIONS

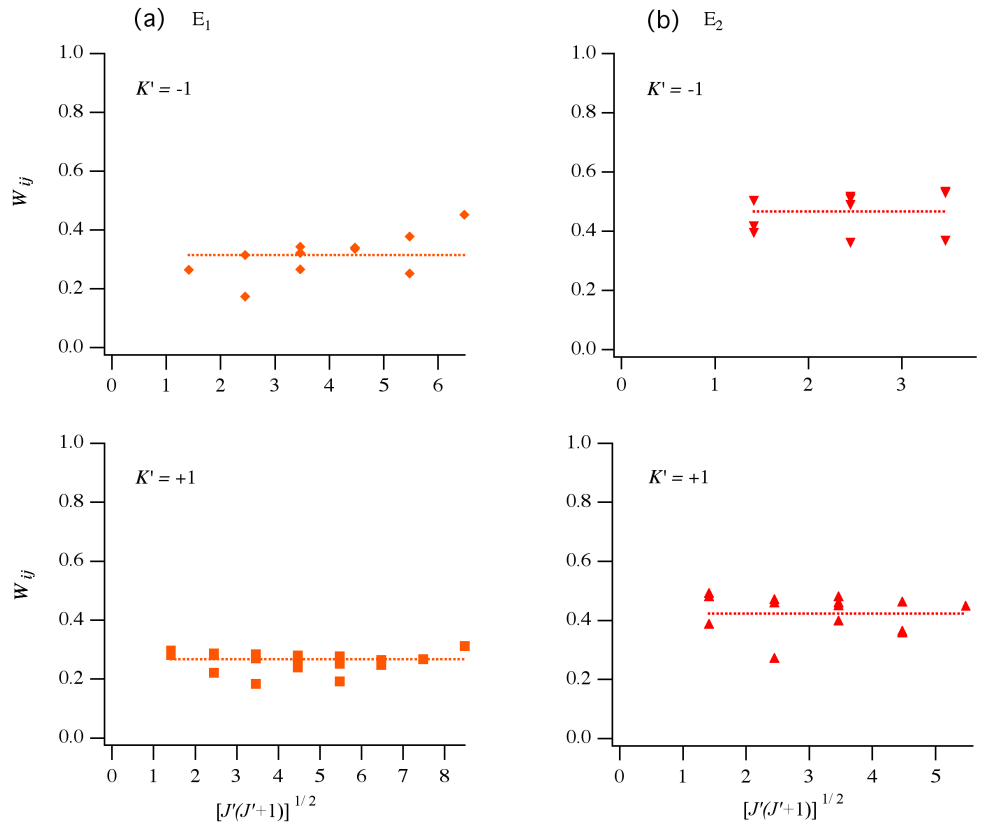

Excited state coupling matrix elements (W_{ij}) for (a) the $|K'| = 1$ E_1 species and (b) the $|K'| = 1$ E_2 species as a function of $[J'(J'+1)]^{½}$. The horizontal lines are the average values, which are given in Table 3.3.

APPENDIX J

ACTIONS OF THE G_{12} GROUP OPERATIONS ON QUANTITIES NEEDED FOR MODEL I AND MODEL II

class	operation		τ	α	$e^{i\alpha}$	$\cos\alpha$	q_1	q_2	q_3
$\boldsymbol{e}$	E	$\boldsymbol{e}$	τ	α	$e^{i\alpha}$	$\cos\alpha$	q_1	q_2	q_3
$\boldsymbol{a}$	(123)(45)	$\boldsymbol{a}$	$-\tau$	$\alpha-\frac{\pi}{3}$	$\varepsilon^{-1}e^{i\alpha}$	$\cos(\alpha-\frac{\pi}{3})$	q_2	q_3	q_1
$\boldsymbol{a^2}$	(132)	$\boldsymbol{a^2}$	τ	$\alpha-\frac{2\pi}{3}$	$\varepsilon^{-2}e^{i\alpha}$	$\cos(\alpha-\frac{2\pi}{3})$	q_3	q_1	q_2
$\boldsymbol{a^3}$	(45)	$\boldsymbol{a^3}$	$-\tau$	$\alpha-\pi$	$\varepsilon^{-3}e^{i\alpha}$	$\cos(\alpha-\pi)$	q_1	q_2	q_3
$\boldsymbol{a^2}$	(123)	$\boldsymbol{a^4}$	τ	$\alpha-\frac{4\pi}{3}$	$\varepsilon^{-4}e^{i\alpha}$	$\cos(\alpha-\frac{4\pi}{3})$	q_2	q_3	q_1
$\boldsymbol{a}$	(132)(45)	$\boldsymbol{a^5}$	$-\tau$	$\alpha-\frac{5\pi}{3}$	$\varepsilon^{-5}e^{i\alpha}$	$\cos(\alpha-\frac{5\pi}{3})$	q_3	q_1	q_2
$\boldsymbol{a^2b}$	(23)(45)*	$\boldsymbol{b}$	τ	$-\alpha$	$e^{-i\alpha}$	$\cos\alpha$	q_1	q_3	q_2
$\boldsymbol{ab}$	(12)*	$\boldsymbol{ab}$	$-\tau$	$-\alpha+\frac{\pi}{3}$	$\varepsilon^{+1}e^{-i\alpha}$	$\cos(\alpha-\frac{\pi}{3})$	q_2	q_1	q_3
$\boldsymbol{a^2b}$	(13)(45)*	$\boldsymbol{a^2b}$	τ	$-\alpha+\frac{2\pi}{3}$	$\varepsilon^{+2}e^{-i\alpha}$	$\cos(\alpha-\frac{2\pi}{3})$	q_3	q_2	q_1
$\boldsymbol{ab}$	(23)*	$\boldsymbol{a^3b}$	$-\tau$	$-\alpha+\pi$	$\varepsilon^{+3}e^{-i\alpha}$	$\cos(\alpha-\pi)$	q_1	q_3	q_2
$\boldsymbol{a^2b}$	(12)(45)*	$\boldsymbol{a^4b}$	τ	$-\alpha+\frac{4\pi}{3}$	$\varepsilon^{+4}e^{-i\alpha}$	$\cos(\alpha-\frac{4\pi}{3})$	q_2	q_1	q_3
$\boldsymbol{ab}$	(13)*	$\boldsymbol{a^5b}$	$-\tau$	$-\alpha+\frac{5\pi}{3}$	$\varepsilon^{+5}e^{-i\alpha}$	$\cos(\alpha-\frac{5\pi}{3})$	q_3	q_2	q_1

$\varepsilon=\exp(\pi i/3)$

APPENDIX K

AN ALTERNATE SET OF MODEL II PARAMETERS FIT TO THE VIBRATIONAL FREQUENCIES IN TABLE 4.1 WITH μ CONSTRAINED TO BE 0

Experimental	5-MT-d4	CH_3NH_2	2-MMA	CH_3OH
ω [b]	2950.3 [c], 2962.6 [d]	2922.3	2947.2 [c], 2957.4 [d]	2933.7
λ [b]	-28.6 [c], -20.6 [d]	-50.8	-26.5 [c], -18.5 [d]	-43.7
λ' [b]	-12.9 [c], -16.8 [d]	13.1	-9.1 [c], -14.4 [d]	-19.9
$\lvert\lambda'\rvert / (\lvert h_{2v}\rvert + \lvert h_{3v}\rvert)$	408 [c], 532 [d]	97.2	12.9 [d], 20.4 [d]	6.6

[b] Model II parameters fit to ν_2, ν_3 and ν_x with μ constrained to be 0.

[c] MP2/ 6-311++G(3df,2p) vibrational frequencies[136] scaled by 0.943[137] and the corresponding fit parameters ω, λ and λ'.

[d] B3LYP/ 6-311++G(3df,2p) vibrational frequencies[136] scaled by 0.967[137] and the corresponding fit parameters ω, λ and λ'.

APPENDIX L

VIBRATIONAL FREQUENCIES AND FORCE CONSTANT OF METHANOL

CALCULATED AT B3LYP/6-31+G(2d,p)

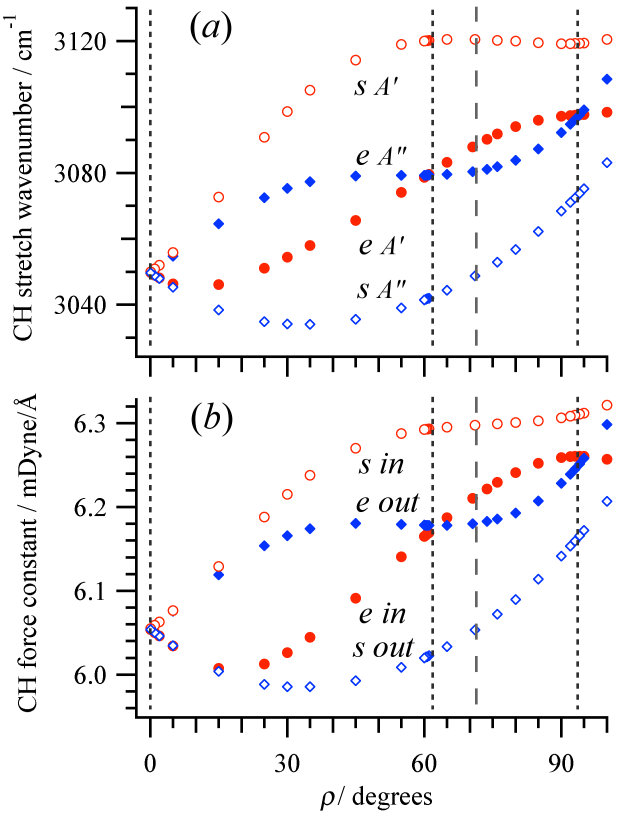

Methanol vibrational frequencies (a) and for the two asymmetric CH stretch vibrations (ν_2 A′ and ν_9 A″) and harmonic force constants (b) for individual CH bonds computed at B3LYP/6-31+G(2d,p) OPT=(Z-matrix, tight) for eclipsed (e) and staggered conformers (s). The figure and its labeling may be compared directly to the MP2 data in Figure 5.1.

APPENDIX M

VIBRATIONAL FREQUENCIES (cm^{-1}) AND FORCE CONSTANTS (mDyne/Å) FOR THE C_s GEOMETRIES OF CH_3OH

γ degrees	ρ degrees	A' (ν_2) cm^{-1}	Res.[a]	A" (ν_9) cm^{-1}	Res.[a]	Force const. in-plane CH-bond	Force const. out-of-plane CH bond
(i) Eclipsed conformations							
0.0	0.0	3139.30	0.0	3139.32	0.0	6.42	6.42
0.0	0.1	3139.23	0.0	3139.40	0.0	6.42	6.42
0.0	1.0	3138.51	0.0	3140.17	0.0	6.41	6.42
0.0	2.0	3137.81	0.0	3141.06	0.0	6.41	6.43
0.0	5.0	3136.25	-0.1	3143.86	0.0	6.40	6.44
0.0	15.0	3136.33	-0.3	3153.74	0.0	6.39	6.48
0.0	25.0	3141.51	-0.4	3162.01	-0.3	6.40	6.52
0.0	35.0	3148.38	-0.7	3166.85	-0.8	6.43	6.54
0.0	45.0	3155.55	-1.0	3168.49	-1.1	6.47	6.55
0.0	55.0	3162.72	-0.9	3168.11	-0.9	6.51	6.54
0.0	60.0	3166.22	-0.7	3167.64	-0.7	6.53	6.54
0.0	60.4	3166.49	-0.7	3167.61	-0.6	6.53	6.54
0.0	60.7	3166.70	-0.7	3167.58	-0.6	6.53	6.54
0.0	61.0	3166.90	-0.6	3167.56	-0.6	6.53	6.54
0.0	61.8	3167.44	-0.6	3167.49	-0.6	6.53	6.54
0.0	61.9	3167.48	-0.6	3167.49	-0.6	6.53	6.54
0.0	61.9	3167.51	-0.6	3167.48	-0.6	6.53	6.54
0.0	62.0	3167.58	-0.6	3167.47	-0.6	6.53	6.54
0.0	65.0	3169.55	-0.5	3167.25	-0.4	6.54	6.54
0.0	70.0	3172.56	-0.2	3167.14	-0.2	6.56	6.54
0.0	71.0	3173.07	-0.2	3167.16	-0.2	6.56	6.54
0.0	71.5	3173.32	-0.2	3167.18	-0.2	6.56	6.54
0.0	73.7	3174.60	0.1	3167.37	-0.1	6.57	6.54
0.0	76.0	3175.46	0.0	3167.64	-0.1	6.57	6.54

γ degrees	ρ degrees	A' (ν_2) cm^{-1}	Res.[a]	A" (ν_9) cm^{-1}	Res.[a]	Force const. in-plane CH-bond	Force const. out-of-plane CH bond
0.0	80.0	3176.81	0.1	3168.53	0.0	6.58	6.54
0.0	85.0	3177.65	0.1	3170.51	0.0	6.59	6.55
0.0	90.0	3177.49	0.0	3173.67	0.0	6.59	6.56
0.0	92.0	3177.17	0.0	3175.34	0.0	6.59	6.57
0.0	93.0	3176.97	0.0	3176.28	0.0	6.59	6.57
0.0	93.6	3176.84	0.0	3176.85	0.0	6.59	6.58
0.0	94.0	3176.75	0.0	3177.28	0.0	6.59	6.58
0.0	95.0	3176.50	0.0	3178.35	0.0	6.59	6.59
0.0	100.0	3175.21	0.0	3184.89	-0.1	6.58	6.61
(ii) Staggered conformations							
180.0	0.0	3139.32	0.0	3139.30	0.0	6.42	6.42
180.0	0.1	3139.40	0.0	3139.23	0.0	6.42	6.42
180.0	1.0	3140.20	0.0	3138.48	0.0	6.42	6.41
180.0	2.0	3141.18	0.0	3137.68	0.0	6.43	6.41
180.0	5.0	3144.62	-0.1	3135.49	0.0	6.44	6.40
180.0	15.0	3160.04	-0.1	3130.47	0.2	6.50	6.38
180.0	25.0	3176.54	0.5	3128.59	0.4	6.55	6.37
180.0	35.0	3189.28	0.9	3128.98	0.6	6.60	6.37
180.0	45.0	3196.95	0.9	3130.87	0.8	6.63	6.38
180.0	55.0	3200.40	0.7	3133.75	0.8	6.64	6.39
180.0	60.0	3201.01	0.6	3135.52	0.7	6.64	6.40
180.0	60.4	3201.04	0.6	3135.67	0.7	6.64	6.40
180.0	60.7	3201.05	0.6	3135.79	0.7	6.64	6.40
180.0	61.0	3201.07	0.6	3135.90	0.6	6.64	6.40
180.0	61.8	3201.10	0.6	3136.22	0.6	6.64	6.40
180.0	61.9	3201.10	0.6	3136.23	0.6	6.64	6.41
180.0	61.9	3201.10	0.6	3136.25	0.6	6.64	6.41
180.0	62.0	3201.11	0.6	3136.30	0.6	6.64	6.41
180.0	65.0	3201.11	0.5	3137.53	0.5	6.64	6.41
180.0	70.0	3200.84	0.3	3139.80	0.2	6.64	6.42
180.0	71.4	3200.72	0.3	3140.50	0.1	6.64	6.43
180.0	73.7	3200.39	0.1	3142.12	0.4	6.64	6.43
180.0	76.0	3200.21	0.1	3142.95	-0.1	6.64	6.44
180.0	80.0	3199.65	0.0	3145.36	-0.2	6.64	6.45
180.0	85.0	3198.90	-0.1	3148.76	-0.2	6.64	6.47
180.0	90.0	3198.20	-0.1	3152.70	-0.1	6.64	6.48
180.0	92.0	3197.97	0.0	3154.44	0.0	6.64	6.49

180.0	93.0	3197.87	0.0	3155.36	0.0	6.64	6.50
180.0	93.6	3197.82	0.0	3155.90	0.0	6.64	6.50
180.0	94.0	3197.78	0.0	3156.29	0.1	6.64	6.50
180.0	95.0	3197.71	0.0	3157.26	0.1	6.64	6.51
180.0	100.0	3197.72	0.1	3162.55	0.0	6.65	6.53

[a] Residuals: *Ab initio* vibrational frequencies for the two asymmetric CH stretch of methanol minus model calculation.

APPENDIX N

VIBRATIONAL FREQUENCIES (cm^{-1}) FOR NON-C_s GEOMETRIES OF CH_3OH

γ degrees	ρ degrees	Upper cm^{-1}	Res.[a]	Lower cm^{-1}	Res.[a]
(a) IRC, non-projected frequencies[b]					
0.0	71.0	3173.07	-0.2	3167.16	-0.2
2.0	71.0	3173.35	-0.3	3166.92	0.0
4.3	71.0	3174.10	-0.7	3166.13	0.3
6.7	71.0	3175.36	-0.9	3165.05	0.7
9.0	71.0	3176.55	-1.4	3163.81	1.1
11.3	71.0	3178.09	-1.5	3162.53	1.5
13.7	71.0	3179.45	-1.8	3161.14	1.7
16.0	71.0	3181.08	-1.8	3159.81	2.0
18.3	71.1	3182.52	-2.0	3158.33	2.2
20.7	71.1	3184.15	-1.9	3156.97	2.4
23.0	71.1	3185.62	-2.0	3155.47	2.4
25.3	71.1	3187.22	-1.8	3154.11	2.5
27.7	71.2	3188.67	-1.8	3152.62	2.3
30.0	71.2	3190.18	-1.6	3151.29	2.3
32.3	71.2	3191.54	-1.5	3149.85	2.1
34.7	71.2	3192.94	-1.2	3148.60	2.0
37.0	71.3	3194.16	-1.1	3147.26	1.7
39.3	71.3	3195.39	-0.8	3146.16	1.6
41.6	71.3	3196.42	-0.7	3144.96	1.3
44.0	71.3	3197.43	-0.4	3144.02	1.1
46.3	71.4	3198.27	-0.3	3143.07	0.8
48.6	71.4	3199.04	-0.1	3142.32	0.6
50.9	71.4	3199.62	0.0	3141.65	0.4
53.3	71.4	3200.12	0.1	3141.16	0.3
55.6	71.4	3200.47	0.2	3140.78	0.2
57.9	71.4	3200.72	0.3	3140.48	0.1
60.0	71.4	3200.72	0.3	3140.51	0.1

γ degrees	ρ degrees	Upper cm^{-1}	Res.[a]	Lower cm^{-1}	Res.[a]
(b) POPT-MEP, non-projected frequencies[c]					
0.0	71.0	3173.07	-0.2	3167.16	-0.2
1.0	71.0	3173.18	-0.2	3167.06	-0.2
2.0	71.0	3173.49	-0.2	3166.77	-0.2
2.9	71.0	3173.94	-0.1	3166.34	-0.2
3.9	71.0	3174.50	-0.1	3165.80	-0.2
5.9	71.0	3175.80	0.0	3164.57	-0.3
8.8	71.0	3177.98	0.2	3162.53	-0.3
11.8	71.0	3180.27	0.4	3160.42	-0.3
14.7	71.0	3182.58	0.6	3158.31	-0.4
17.6	71.0	3184.88	0.9	3156.24	-0.4
20.6	71.1	3187.11	1.1	3154.21	-0.5
23.5	71.1	3189.25	1.4	3152.25	-0.5
26.4	71.2	3191.27	1.6	3150.37	-0.6
29.3	71.2	3193.17	1.8	3148.58	-0.8
32.3	71.2	3194.88	1.9	3146.92	-0.9
35.2	71.3	3196.43	2.0	3145.40	-1.0
38.1	71.3	3197.78	2.1	3144.02	-1.1
41.0	71.3	3198.92	2.1	3142.83	-1.1
43.9	71.3	3199.83	2.0	3141.84	-1.1
46.9	71.4	3200.51	1.8	3141.06	-1.0
49.8	71.4	3200.98	1.6	3140.51	-0.9
52.7	71.4	3201.19	1.3	3140.20	-0.7
55.6	71.4	3201.17	0.9	3140.14	-0.4
58.6	71.4	3200.92	0.5	3140.32	-0.1
59.1	71.4	3200.86	0.4	3140.38	0.0
59.4	71.4	3200.82	0.4	3140.42	0.0
59.9	71.4	3200.74	0.3	3140.49	0.1
60.0	71.4	3200.72	0.3	3140.50	0.1
(c) IRC, projected frequencies[d]					
0.0	71.0	3173.61	0.3	3166.57	-0.6
2.0	71.0	3173.74	0.1	3166.45	-0.4
4.3	71.0	3174.23	-0.6	3166.00	0.3
6.7	71.0	3175.06	-1.2	3165.24	1.0
9.0	71.0	3176.18	-1.7	3164.21	1.6
11.3	71.0	3177.54	-2.0	3162.96	2.0

γ degrees	ρ degrees	Upper cm^{-1}	Res.[a]	Lower cm^{-1}	Res.[a]
13.7	71.0	3179.09	-2.1	3161.55	2.2
16.0	71.0	3180.75	-2.1	3160.02	2.3
18.3	71.1	3182.46	-2.0	3158.44	2.3
20.7	71.1	3184.18	-1.8	3156.86	2.3
23.0	71.1	3185.86	-1.7	3155.30	2.3
25.3	71.1	3187.46	-1.5	3153.80	2.2
27.7	71.2	3188.98	-1.4	3152.38	2.2
30.0	71.2	3190.39	-1.3	3151.03	2.1
32.3	71.2	3191.72	-1.2	3149.75	2.1
34.7	71.2	3192.96	-1.1	3148.53	2.0
37.0	71.3	3194.12	-1.0	3147.37	1.9
39.3	71.3	3195.21	-0.9	3146.26	1.7
41.6	71.3	3196.24	-0.8	3145.21	1.6
44.0	71.3	3197.20	-0.6	3144.21	1.3
46.3	71.4	3198.09	-0.4	3143.27	1.1
48.6	71.4	3198.89	-0.2	3142.43	0.8
50.9	71.4	3199.58	0.0	3141.69	0.5
53.3	71.4	3200.14	0.2	3141.09	0.3
55.6	71.4	3200.55	0.4	3140.65	0.1
57.9	71.4	3200.80	0.5	3140.39	0.0
60.0	71.4	3200.87	0.5	3140.31	0.0
(d) POPT[e]					
1.0	61.9	3168.37	-0.5	3166.59	-0.6
2.0	61.9	3169.25	-0.5	3165.72	-0.7
2.9	61.9	3170.15	-0.4	3164.86	-0.7
3.9	61.9	3171.04	-0.3	3163.99	-0.8
4.9	61.9	3171.93	-0.3	3163.14	-0.8
1.0	93.6	3177.49	0.1	3176.20	-0.1
2.0	93.6	3178.14	0.2	3175.55	-0.2
3.0	93.6	3178.80	0.3	3174.91	-0.3
4.0	93.6	3179.45	0.4	3174.25	-0.4
5.0	93.6	3180.09	0.5	3173.61	-0.5
30.0	0.0	3139.32	0.0	3139.31	0.0
30.0	0.1	3139.40	0.0	3139.23	0.0
30.0	1.0	3140.19	0.0	3138.50	0.0
30.0	2.0	3141.12	0.0	3137.75	0.0

γ degrees	ρ degrees	Upper cm^{-1}	Res.[a]	Lower cm^{-1}	Res.[a]
30.0	5.0	3144.26	0.0	3135.85	0.0
30.0	15.0	3157.34	0.0	3132.96	0.0
30.0	25.0	3170.92	0.4	3133.42	-0.3
30.0	35.0	3181.48	0.9	3135.40	-0.8
30.0	45.0	3188.04	1.2	3138.27	-1.0
30.0	55.0	3191.36	1.4	3141.86	-0.8
30.0	60.0	3192.22	1.4	3143.85	-0.6
30.0	60.4	3192.28	1.4	3144.01	-0.6
30.0	60.7	3192.32	1.4	3144.14	-0.6
30.0	61.0	3192.35	1.4	3144.26	-0.5
30.0	61.8	3192.45	1.4	3144.59	-0.5
30.0	61.9	3192.45	1.4	3144.61	-0.5
30.0	61.9	3192.46	1.4	3144.63	-0.5
30.0	62.0	3192.47	1.4	3144.67	-0.5
30.0	65.0	3192.76	1.4	3145.93	-0.4
30.0	70.0	3193.10	1.4	3148.08	-0.4
30.0	70.9	3193.15	1.4	3148.47	-0.4
30.0	71.4	3193.17	1.4	3148.69	-0.4
30.0	73.7	3193.27	1.4	3149.69	-0.4
30.0	76.0	3193.36	1.4	3150.70	-0.5
30.0	80.0	3193.47	1.5	3152.50	-0.8
30.0	85.0	3193.60	1.7	3154.86	-1.3
30.0	90.0	3193.81	2.1	3157.47	-1.9
30.0	95.0	3194.34	2.6	3160.53	-2.6
30.0	100.0	3195.72	2.7	3164.22	-3.0

[a] Residuals: *Ab initio* vibrational frequencies minus model calculation.

[b] 12-dimensional (non-projected) normal mode analyses along the path of steepest descent from the torsional saddle point (intrinsic reaction coordinate,"IRC") to the global minimum.

[c]12-dimensional normal mode analyses at partially optimized geometries ("POPT") at a series of fixed torsional angles along the minimum energy path (MEP).

[d] 11-dimensional (projected) normal mode analyses along the path of steepest descent

from the torsional saddle point ("IRC") to the global mimimum. Data here are obtained from the Fourier expansion coefficients given in Table 5 of *Xu* et al.(Ref. [147]).

[e] Partially optimized non-C_s geometries in the vicinity of the conical intersections and at $\gamma = 30^{\circ}$.

APPENDIX O

SYNCHROTRON BASED FTIR SPECTRUM OF CH_3NO_2: ASSIGNED *Ka* =1,3,5,7 TRANSITIONS FOR THE *m′*= 0 STATE WITH TWO DIFFERENT QUANTUM NUMBERS LABELING AND CORRESPONDING SYMMETRIES

Excited state					Ground state [a]					Ground state [b]					Wavenumber	
m′	*Γ′*	*J′*	*Ka′*	*Kc′*	*m″*	*Γ″*	*J″*	*Ka″*	*Kc″*	*m″*	*Γ″*	*J″*	*Ka″*	*Kc″*	cm^{-1}	Intensity
0	A2	1	1	1	0	A1	0	0	0	0	A'1	0	0	0	475.9891	0.200
0	A1	1	1	0	0	A2	1	0	1	0	A'2	1	0	1	475.6093	0.051
0	A1	2	1	2	0	A2	1	0	1	0	A'2	1	0	1	476.3900	0.076
0	A2	1	1	1	0	A1	2	0	2	0	A'1	2	0	2	474.4395	0.030
0	A2	2	1	1	0	A1	2	0	2	0	A'1	2	0	2	475.8705	0.070
0	A2	3	1	3	0	A1	2	0	2	0	A'1	2	0	2	476.7596	0.046
0	A2	3	3	1	0	A1	2	0	2	0	A'1	2	0	2	478.6884	0.277
0	A1	1	1	0	0	A2	2	2	1	0	A'2	2	2	1	473.8297	0.098
0	A2	1	1	1	0	A1	2	2	0	0	A'1	2	2	0	473.5676	0.070
0	A2	2	1	1	0	A1	2	2	0	0	A'1	2	2	0	474.9991	0.037
0	A1	2	1	2	0	A2	2	2	1	0	A'2	2	2	1	474.6100	0.200
0	A1	3	1	2	0	A2	2	2	1	0	A'2	2	2	1	476.8878	0.014
0	A2	3	1	3	0	A1	2	2	0	0	A'1	2	2	0	475.8873	0.025
0	A1	3	3	0	0	A2	2	2	1	0	A'2	2	2	1	477.9750	0.178
0	A2	3	3	1	0	A1	2	2	0	0	A'1	2	2	0	477.8170	0.188
0	A1	2	1	2	0	A2	3	0	3	0	A'2	3	0	3	474.0024	0.099
0	A1	3	1	2	0	A2	3	0	3	0	A'2	3	0	3	476.2793	0.023
0	A1	4	1	4	0	A2	3	0	3	0	A'2	3	0	3	477.1323	0.182
0	A1	4	3	2	0	A2	3	0	3	0	A'2	3	0	3	479.6100	0.059
0	A2	2	1	1	0	A1	3	2	2	0	A'1	3	2	2	473.4497	0.038
0	A1	2	1	2	0	A2	3	2	1	0	A'2	3	2	1	472.6147	0.032
0	A2	3	1	3	0	A1	3	2	2	0	A'1	3	2	2	474.3380	0.013
0	A1	3	3	0	0	A2	3	2	1	0	A'2	3	2	1	475.9814	0.050
0	A2	3	3	1	0	A1	3	2	2	0	A'1	3	2	2	476.2687	0.046
0	A2	4	1	3	0	A1	3	2	2	0	A'1	3	2	2	477.4439	0.050
0	A2	4	3	1	0	A1	3	2	2	0	A'1	3	2	2	478.8100	0.139
0	A2	3	1	3	0	A1	4	0	4	0	A'1	4	0	4	473.6060	0.199
0	A2	4	1	3	0	A1	4	0	4	0	A'1	4	0	4	476.7122	0.016
0	A2	5	1	5	0	A1	4	0	4	0	A'1	4	0	4	477.5142	0.139
0	A2	5	3	3	0	A1	4	0	4	0	A'1	4	0	4	480.6664	0.113
0	A1	3	1	2	0	A2	4	2	3	0	A'2	4	2	3	473.1330	0.064
0	A2	3	1	3	0	A1	4	2	2	0	A'1	4	2	2	471.4710	0.332
0	A2	3	3	1	0	A1	4	2	2	0	A'1	4	2	2	473.3990	0.153
0	A1	4	1	4	0	A2	4	2	3	0	A'2	4	2	3	473.9845	0.068
0	A2	4	3	1	0	A1	4	2	2	0	A'1	4	2	2	475.9415	0.056
0	A1	4	3	2	0	A2	4	2	3	0	A'2	4	2	3	476.4630	0.054

Excited state					Ground state [a]					Ground state [b]						
m′	*Γ′*	*J′*	*Ka′*	*Kc′*	*m″*	*Γ″*	*J″*	*Ka″*	*Kc″*	*m″*	*Γ″*	*J″*	*Ka″*	*Kc″*	Wavenumber cm^{-1}	Intensity
0	A1	5	1	4	0	A2	4	2	3	0	A'2	4	2	3	477.9040	0.147
0	A2	5	1	5	0	A1	4	2	2	0	A'1	4	2	2	475.3781	0.074
0	A1	5	3	2	0	A2	4	2	3	0	A'2	4	2	3	479.8812	0.083
0	A2	5	3	3	0	A1	4	2	2	0	A'1	4	2	2	478.5310	0.088
0	A2	5	5	1	0	A1	4	2	2	0	A'1	4	2	2	481.1146	0.055
0	A1	3	3	0	0	A2	4	4	1	0	A'2	4	4	1	472.0080	0.195
0	A2	3	3	1	0	A1	4	4	0	0	A'1	4	4	0	471.9266	0.202
0	A2	4	3	1	0	A1	4	4	0	0	A'1	4	4	0	474.4700	0.050
0	A1	5	3	2	0	A2	4	4	1	0	A'2	4	4	1	477.6700	0.236
0	A2	5	3	3	0	A1	4	4	0	0	A'1	4	4	0	477.0577	0.132
0	A1	5	5	0	0	A2	4	4	1	0	A'2	4	4	1	479.6854	0.137
0	A2	5	5	1	0	A1	4	4	0	0	A'1	4	4	0	479.6412	0.115
0	A1	4	1	4	0	A2	5	0	5	0	A'2	5	0	5	473.2067	0.277
0	A1	5	1	4	0	A2	5	0	5	0	A'2	5	0	5	477.1250	0.125
0	A1	6	1	6	0	A2	5	0	5	0	A'2	5	0	5	477.8982	0.264
0	A1	6	3	4	0	A2	5	0	5	0	A'2	5	0	5	481.7964	0.148
0	A2	4	1	3	0	A1	5	2	4	0	A'1	5	2	4	472.7955	0.166
0	A1	4	1	4	0	A2	5	2	3	0	A'2	5	2	3	470.2120	0.101
0	A2	4	3	1	0	A1	5	2	4	0	A'1	5	2	4	474.1610	0.042
0	A1	4	3	2	0	A2	5	2	3	0	A'2	5	2	3	472.6890	0.214
0	A1	5	1	4	0	A2	5	2	3	0	A'2	5	2	3	474.1312	0.061
0	A2	5	1	5	0	A1	5	2	4	0	A'1	5	2	4	473.5983	0.212
0	A1	5	3	2	0	A2	5	2	3	0	A'2	5	2	3	476.1080	0.149
0	A2	5	3	3	0	A1	5	2	4	0	A'1	5	2	4	476.7488	0.108
0	A2	6	1	5	0	A1	5	2	4	0	A'1	5	2	4	478.3204	0.250
0	A2	6	3	3	0	A1	5	2	4	0	A'1	5	2	4	481.1380	0.146
0	A1	6	3	4	0	A2	5	2	3	0	A'2	5	2	3	478.8008	0.203
0	A1	6	5	2	0	A2	5	2	3	0	A'2	5	2	3	481.6424	0.399
0	A2	4	1	3	0	A1	5	4	2	0	A'1	5	4	2	470.1793	0.141
0	A2	4	3	1	0	A1	5	4	2	0	A'1	5	4	2	471.5468	0.177
0	A1	4	3	2	0	A2	5	4	1	0	A'2	5	4	1	471.1905	0.512
0	A1	5	3	2	0	A2	5	4	1	0	A'2	5	4	1	474.6114	0.046
0	A2	5	3	3	0	A1	5	4	2	0	A'1	5	4	2	474.1347	0.090
0	A1	5	5	0	0	A2	5	4	1	0	A'2	5	4	1	476.6281	0.057
0	A2	5	5	1	0	A1	5	4	2	0	A'1	5	4	2	476.7201	0.078
0	A2	6	3	3	0	A1	5	4	2	0	A'1	5	4	2	478.5240	0.194
0	A1	6	3	4	0	A2	5	4	1	0	A'2	5	4	1	477.3035	0.325
0	A2	6	5	1	0	A1	5	4	2	0	A'1	5	4	2	480.3449	0.091
0	A1	6	5	2	0	A2	5	4	1	0	A'2	5	4	1	480.1450	0.078
0	A2	5	1	5	0	A1	6	0	6	0	A'1	6	0	6	472.8075	0.153
0	A2	6	1	5	0	A1	6	0	6	0	A'1	6	0	6	477.5310	0.159
0	A2	7	1	7	0	A1	6	0	6	0	A'1	6	0	6	478.2813	0.314
0	A2	7	3	5	0	A1	6	0	6	0	A'1	6	0	6	482.9569	0.263
0	A1	5	1	4	0	A2	6	2	5	0	A'2	6	2	5	472.4260	0.080
0	A2	5	1	5	0	A1	6	2	4	0	A'1	6	2	4	468.9616	0.255
0	A1	5	3	2	0	A2	6	2	5	0	A'2	6	2	5	474.4038	0.090
0	A2	5	3	3	0	A1	6	2	4	0	A'1	6	2	4	472.1127	0.102
0	A2	6	1	5	0	A1	6	2	4	0	A'1	6	2	4	473.6840	0.244
0	A1	6	1	6	0	A2	6	2	5	0	A'2	6	2	5	473.1980	0.228
0	A2	6	3	3	0	A1	6	2	4	0	A'1	6	2	4	476.5010	0.043

Excited state					Ground state [a]					Ground state [b]						
m′	*Γ′*	*J′*	*Ka′*	*Kc′*	*m″*	*Γ″*	*J″*	*Ka″*	*Kc″*	*m″*	*Γ″*	*J″*	*Ka″*	*Kc″*	Wavenumber cm^{-1}	Intensity
0	A1	6	3	4	0	A2	6	2	5	0	A'2	6	2	5	477.0957	0.070
0	A1	7	1	6	0	A2	6	2	5	0	A'2	6	2	5	478.7110	0.112
0	A2	7	1	7	0	A1	6	2	4	0	A'1	6	2	4	474.4341	0.027
0	A1	7	3	4	0	A2	6	2	5	0	A'2	6	2	5	482.4270	0.128
0	A2	7	3	5	0	A1	6	2	4	0	A'1	6	2	4	479.1103	0.129
0	A2	7	5	3	0	A1	6	2	4	0	A'1	6	2	4	482.3789	0.574
0	A1	5	1	4	0	A2	6	4	3	0	A'2	6	4	3	469.2429	0.222
0	A1	5	3	2	0	A2	6	4	3	0	A'2	6	4	3	471.2215	0.329
0	A2	5	3	3	0	A1	6	4	2	0	A'1	6	4	2	470.2316	0.063
0	A2	5	5	1	0	A1	6	4	2	0	A'1	6	4	2	472.8165	0.080
0	A2	6	3	3	0	A1	6	4	2	0	A'1	6	4	2	474.6209	0.140
0	A1	6	3	4	0	A2	6	4	3	0	A'2	6	4	3	473.9138	0.149
0	A2	6	5	1	0	A1	6	4	2	0	A'1	6	4	2	476.4426	0.048
0	A1	6	5	2	0	A2	6	4	3	0	A'2	6	4	3	476.7543	0.076
0	A1	7	3	4	0	A2	6	4	3	0	A'2	6	4	3	479.2441	0.145
0	A2	7	3	5	0	A1	6	4	2	0	A'1	6	4	2	477.2293	0.108
0	A1	7	5	2	0	A2	6	4	3	0	A'2	6	4	3	481.1573	0.104
0	A2	7	5	3	0	A1	6	4	2	0	A'1	6	4	2	480.5026	0.081
0	A2	7	7	1	0	A1	6	4	2	0	A'1	6	4	2	484.0668	0.071
0	A1	5	3	2	0	A2	6	6	1	0	A'2	6	6	1	468.1770	0.086
0	A1	5	5	0	0	A2	6	6	1	0	A'2	6	6	1	470.1950	0.094
0	A2	5	5	1	0	A1	6	6	0	0	A'1	6	6	0	470.1659	0.115
0	A2	6	5	1	0	A1	6	6	0	0	A'1	6	6	0	473.7913	0.032
0	A1	6	5	2	0	A2	6	6	1	0	A'2	6	6	1	473.7118	0.127
0	A1	7	5	2	0	A2	6	6	1	0	A'2	6	6	1	478.1143	0.130
0	A2	7	5	3	0	A1	6	6	0	0	A'1	6	6	0	477.8512	0.310
0	A1	7	7	0	0	A2	6	6	1	0	A'2	6	6	1	481.4536	0.151
0	A2	7	7	1	0	A1	6	6	0	0	A'1	6	6	0	481.4162	0.099
0	A1	6	1	6	0	A2	7	0	7	0	A'2	7	0	7	472.4081	0.142
0	A1	7	1	6	0	A2	7	0	7	0	A'2	7	0	7	477.9190	0.139
0	A1	8	1	8	0	A2	7	0	7	0	A'2	7	0	7	478.6632	0.399
0	A1	8	3	6	0	A2	7	0	7	0	A'2	7	0	7	484.1253	0.109
0	A2	6	1	5	0	A1	7	2	6	0	A'1	7	2	6	472.0450	0.161
0	A1	6	1	6	0	A2	7	2	5	0	A'2	7	2	5	467.7472	0.134
0	A1	6	3	4	0	A2	7	2	5	0	A'2	7	2	5	471.6444	0.062
0	A1	7	1	6	0	A2	7	2	5	0	A'2	7	2	5	473.2578	0.079
0	A2	7	1	7	0	A1	7	2	6	0	A'1	7	2	6	472.7955	0.166
0	A1	7	3	4	0	A2	7	2	5	0	A'2	7	2	5	476.9750	0.054
0	A2	7	3	5	0	A1	7	2	6	0	A'1	7	2	6	477.4710	0.091
0	A2	8	1	7	0	A1	7	2	6	0	A'1	7	2	6	479.0975	0.391
0	A1	8	1	8	0	A2	7	2	5	0	A'2	7	2	5	474.0024	0.099
0	A2	8	3	5	0	A1	7	2	6	0	A'1	7	2	6	483.6811	0.328
0	A1	8	3	6	0	A2	7	2	5	0	A'2	7	2	5	479.4640	0.275
0	A1	8	5	4	0	A2	7	2	5	0	A'2	7	2	5	483.3365	0.346
0	A2	6	1	5	0	A1	7	4	4	0	A'1	7	4	4	468.1713	0.280
0	A2	6	3	3	0	A1	7	4	4	0	A'1	7	4	4	470.9900	0.165
0	A1	6	3	4	0	A2	7	4	3	0	A'2	7	4	3	469.0410	0.297
0	A2	6	5	1	0	A1	7	4	4	0	A'1	7	4	4	472.8129	0.080
0	A1	6	5	2	0	A2	7	4	3	0	A'2	7	4	3	471.8835	0.047
0	A2	7	3	5	0	A1	7	4	4	0	A'1	7	4	4	473.5983	0.212

Excited state					Ground state [a]					Ground state [b]						
m′	*Γ′*	*J′*	*Ka′*	*Kc′*	*m″*	*Γ″*	*J″*	*Ka″*	*Kc″*	*m″*	*Γ″*	*J″*	*Ka″*	*Kc″*	Wavenumber cm^{-1}	Intensity
0	A1	7	5	2	0	A2	7	4	3	0	A'2	7	4	3	476.2856	0.206
0	A2	7	5	3	0	A1	7	4	4	0	A'1	7	4	4	476.8722	0.056
0	A2	8	3	5	0	A1	7	4	4	0	A'1	7	4	4	479.8092	0.192
0	A1	8	3	6	0	A2	7	4	3	0	A'2	7	4	3	476.8619	0.110
0	A2	8	5	3	0	A1	7	4	4	0	A'1	7	4	4	482.2204	0.188
0	A1	8	5	4	0	A2	7	4	3	0	A'2	7	4	3	480.7347	0.213
0	A1	8	7	2	0	A2	7	4	3	0	A'2	7	4	3	484.3093	0.137
0	A2	6	3	3	0	A1	7	6	2	0	A'1	7	6	2	467.8293	0.328
0	A2	6	5	1	0	A1	7	6	2	0	A'1	7	6	2	469.6522	0.193
0	A1	6	5	2	0	A2	7	6	1	0	A'2	7	6	1	469.5488	0.210
0	A1	7	5	2	0	A2	7	6	1	0	A'2	7	6	1	473.9521	0.093
0	A2	7	5	3	0	A1	7	6	2	0	A'1	7	6	2	473.7118	0.127
0	A1	7	7	0	0	A2	7	6	1	0	A'2	7	6	1	477.2919	0.043
0	A2	7	7	1	0	A1	7	6	2	0	A'1	7	6	2	477.2756	0.243
0	A2	8	5	3	0	A1	7	6	2	0	A'1	7	6	2	479.0600	0.116
0	A1	8	5	4	0	A2	7	6	1	0	A'2	7	6	1	478.4005	0.198
0	A2	8	7	1	0	A1	7	6	2	0	A'1	7	6	2	482.0387	0.553
0	A1	8	7	2	0	A2	7	6	1	0	A'2	7	6	1	481.9747	0.175
0	A2	7	1	7	0	A1	8	0	8	0	A'1	8	0	8	472.0075	0.242
0	A2	8	1	7	0	A1	8	0	8	0	A'1	8	0	8	478.3085	0.324
0	A2	9	1	9	0	A1	8	0	8	0	A'1	8	0	8	479.0435	0.391
0	A2	9	3	7	0	A1	8	0	8	0	A'1	8	0	8	485.2954	0.588
0	A1	7	1	6	0	A2	8	2	7	0	A'2	8	2	7	471.6476	0.287
0	A2	7	1	7	0	A1	8	2	6	0	A'1	8	2	6	466.5480	0.184
0	A2	7	3	5	0	A1	8	2	6	0	A'1	8	2	6	471.2232	0.234
0	A2	8	1	7	0	A1	8	2	6	0	A'1	8	2	6	472.8499	0.187
0	A1	8	1	8	0	A2	8	2	7	0	A'2	8	2	7	472.3921	0.266
0	A2	8	3	5	0	A1	8	2	6	0	A'1	8	2	6	477.4326	0.083
0	A1	8	3	6	0	A2	8	2	7	0	A'2	8	2	7	477.8532	0.310
0	A1	9	1	8	0	A2	8	2	7	0	A'2	8	2	7	479.4834	0.212
0	A2	9	1	9	0	A1	8	2	6	0	A'1	8	2	6	473.5853	0.063
0	A1	9	3	6	0	A2	8	2	7	0	A'2	8	2	7	484.8868	0.305
0	A2	9	3	7	0	A1	8	2	6	0	A'1	8	2	6	479.8319	0.332
0	A2	9	5	5	0	A1	8	2	6	0	A'1	8	2	6	484.4205	0.363
0	A1	7	1	6	0	A2	8	4	5	0	A'2	8	4	5	467.0190	0.227
0	A1	7	3	4	0	A2	8	4	5	0	A'2	8	4	5	470.7360	0.109
0	A2	7	3	5	0	A1	8	4	4	0	A'1	8	4	4	467.7149	0.086
0	A1	7	5	2	0	A2	8	4	5	0	A'2	8	4	5	472.6508	0.131
0	A2	7	5	3	0	A1	8	4	4	0	A'1	8	4	4	470.9879	0.401
0	A2	8	3	5	0	A1	8	4	4	0	A'1	8	4	4	473.9248	0.057
0	A1	8	3	6	0	A2	8	4	5	0	A'2	8	4	5	473.2246	0.222
0	A2	8	5	3	0	A1	8	4	4	0	A'1	8	4	4	476.3367	0.104
0	A1	8	5	4	0	A2	8	4	5	0	A'2	8	4	5	477.0973	0.183
0	A1	9	3	6	0	A2	8	4	5	0	A'2	8	4	5	480.2580	0.274
0	A2	9	3	7	0	A1	8	4	4	0	A'1	8	4	4	476.3232	0.204
0	A1	9	5	4	0	A2	8	4	5	0	A'2	8	4	5	483.4958	0.488
0	A2	9	5	5	0	A1	8	4	4	0	A'1	8	4	4	480.9107	0.070
0	A2	9	7	3	0	A1	8	4	4	0	A'1	8	4	4	484.6307	0.090
0	A1	7	3	4	0	A2	8	6	3	0	A'2	8	6	3	467.2887	0.164
0	A1	7	5	2	0	A2	8	6	3	0	A'2	8	6	3	469.2011	0.400
0	A2	7	5	3	0	A1	8	6	2	0	A'1	8	6	2	468.8283	0.118
0	A2	7	7	1	0	A1	8	6	2	0	A'1	8	6	2	472.3921	0.266

Excited state					Ground state [a]					Ground state [b]						
m′	*Γ′*	*J′*	*Ka′*	*Kc′*	*m″*	*Γ″*	*J″*	*Ka″*	*Kc″*	*m″*	*Γ″*	*J″*	*Ka″*	*Kc″*	Wavenumber cm^{-1}	Intensity
0	A2	8	5	3	0	A1	8	6	2	0	A'1	8	6	2	474.1769	0.067
0	A1	8	5	4	0	A2	8	6	3	0	A'2	8	6	3	473.6493	0.139
0	A2	8	7	1	0	A1	8	6	2	0	A'1	8	6	2	477.1538	0.147
0	A1	8	7	2	0	A2	8	6	3	0	A'2	8	6	3	477.2233	0.108
0	A1	9	5	4	0	A2	8	6	3	0	A'2	8	6	3	480.0467	0.141
0	A2	9	5	5	0	A1	8	6	2	0	A'1	8	6	2	478.7524	0.063
0	A1	9	7	2	0	A2	8	6	3	0	A'2	8	6	3	482.6778	0.121
0	A2	9	7	3	0	A1	8	6	2	0	A'1	8	6	2	482.4715	0.089
0	A1	7	5	2	0	A2	8	8	1	0	A'2	8	8	1	465.0701	0.278
0	A1	7	7	0	0	A2	8	8	1	0	A'2	8	8	1	468.4091	0.232
0	A2	7	7	1	0	A1	8	8	0	0	A'1	8	8	0	468.3711	0.429
0	A1	8	7	2	0	A2	8	8	1	0	A'2	8	8	1	473.0922	0.032
0	A1	9	7	2	0	A2	8	8	1	0	A'2	8	8	1	478.5454	0.124
0	A2	9	7	3	0	A1	8	8	0	0	A'1	8	8	0	478.4512	0.208
0	A1	8	1	8	0	A2	9	0	9	0	A'2	9	0	9	471.6056	0.289
0	A1	9	1	8	0	A2	9	0	9	0	A'2	9	0	9	478.6979	0.491
0	A1	10	1	10	0	A2	9	0	9	0	A'2	9	0	9	479.4228	0.402
0	A1	10	3	8	0	A2	9	0	9	0	A'2	9	0	9	486.4584	0.046
0	A2	8	1	7	0	A1	9	2	8	0	A'1	9	2	8	471.2499	0.557
0	A1	8	1	8	0	A2	9	2	7	0	A'2	9	2	7	465.3534	0.067
0	A1	8	3	6	0	A2	9	2	7	0	A'2	9	2	7	470.8162	0.141
0	A1	9	1	8	0	A2	9	2	7	0	A'2	9	2	7	472.4447	0.190
0	A2	9	1	9	0	A1	9	2	8	0	A'1	9	2	8	471.9856	0.204
0	A1	9	3	6	0	A2	9	2	7	0	A'2	9	2	7	477.8490	0.158
0	A2	9	3	7	0	A1	9	2	8	0	A'1	9	2	8	478.2335	0.369
0	A2	10	1	9	0	A1	9	2	8	0	A'1	9	2	8	479.8703	0.299
0	A1	10	1	10	0	A2	9	2	7	0	A'2	9	2	7	473.1716	0.154
0	A2	10	3	7	0	A1	9	2	8	0	A'1	9	2	8	486.0948	0.516
0	A1	10	3	8	0	A2	9	2	7	0	A'2	9	2	7	480.2061	0.054
0	A1	10	5	6	0	A2	9	2	7	0	A'2	9	2	7	485.5649	0.284
0	A2	8	1	7	0	A1	9	4	6	0	A'1	9	4	6	465.8361	0.284
0	A2	8	3	5	0	A1	9	4	6	0	A'1	9	4	6	470.4215	0.173
0	A1	8	3	6	0	A2	9	4	5	0	A'2	9	4	5	466.3777	0.117
0	A2	8	5	3	0	A1	9	4	6	0	A'1	9	4	6	472.8333	0.069
0	A1	8	5	4	0	A2	9	4	5	0	A'2	9	4	5	470.2512	0.563
0	A1	9	3	6	0	A2	9	4	5	0	A'2	9	4	5	473.4112	0.126
0	A2	9	3	7	0	A1	9	4	6	0	A'1	9	4	6	472.8202	0.080
0	A2	9	5	5	0	A1	9	4	6	0	A'1	9	4	6	477.4074	0.252
0	A2	10	3	7	0	A1	9	4	6	0	A'1	9	4	6	480.6807	0.281
0	A2	10	5	5	0	A1	9	4	6	0	A'1	9	4	6	484.8728	0.152
0	A1	10	5	6	0	A2	9	4	5	0	A'2	9	4	5	481.1275	0.054
0	A1	10	7	4	0	A2	9	4	5	0	A'2	9	4	5	485.1773	0.226
0	A2	8	3	5	0	A1	9	6	4	0	A'1	9	6	4	466.4983	0.420
0	A2	8	5	3	0	A1	9	6	4	0	A'1	9	6	4	468.9103	0.152
0	A1	8	5	4	0	A2	9	6	3	0	A'2	9	6	3	467.8966	0.113
0	A2	8	7	1	0	A1	9	6	4	0	A'1	9	6	4	471.8895	0.198
0	A1	8	7	2	0	A2	9	6	3	0	A'2	9	6	3	471.4710	0.332
0	A1	9	5	4	0	A2	9	6	3	0	A'2	9	6	3	474.2942	0.109
0	A2	9	5	5	0	A1	9	6	4	0	A'1	9	6	4	473.4848	0.109
0	A1	9	7	2	0	A2	9	6	3	0	A'2	9	6	3	476.9247	0.116
0	A2	9	7	3	0	A1	9	6	4	0	A'1	9	6	4	477.2044	0.024
0	A2	10	5	5	0	A1	9	6	4	0	A'1	9	6	4	480.9507	0.128

Excited state					Ground state [a]					Ground state [b]						
m′	*Γ′*	*J′*	*Ka′*	*Kc′*	*m″*	*Γ″*	*J″*	*Ka″*	*Kc″*	*m″*	*Γ″*	*J″*	*Ka″*	*Kc″*	Wavenumber cm^{-1}	Intensity
0	A1	10	5	6	0	A2	9	6	3	0	A'2	9	6	3	478.7733	0.266
0	A2	10	7	3	0	A1	9	6	4	0	A'1	9	6	4	483.4524	0.203
0	A1	10	7	4	0	A2	9	6	3	0	A'2	9	6	3	482.8217	0.120
0	A2	8	5	3	0	A1	9	8	2	0	A'1	9	8	2	464.8429	0.336
0	A2	8	7	1	0	A1	9	8	2	0	A'1	9	8	2	467.8223	0.183
0	A1	8	7	2	0	A2	9	8	1	0	A'2	9	8	1	467.7764	0.116
0	A1	9	7	2	0	A2	9	8	1	0	A'2	9	8	1	473.2304	0.206
0	A2	9	7	3	0	A1	9	8	2	0	A'1	9	8	2	473.1381	0.178
0	A2	10	7	3	0	A1	9	8	2	0	A'1	9	8	2	479.3864	0.242
0	A1	10	7	4	0	A2	9	8	1	0	A'2	9	8	1	479.1281	0.371
0	A2	9	1	9	0	A1	10	1	10	0	A'1	10	0	10	471.2024	0.454
0	A2	10	1	9	0	A1	10	1	10	0	A'1	10	0	10	479.0867	0.341
0	A2	11	1	11	0	A1	10	1	10	0	A'1	10	0	10	479.8007	0.421
0	A2	11	3	9	0	A1	10	1	10	0	A'1	10	0	10	487.6226	0.174
0	A1	9	1	8	0	A2	10	2	9	0	A'2	10	2	9	470.8532	0.437
0	A2	9	1	9	0	A1	10	2	8	0	A'1	10	2	8	464.1604	0.075
0	A2	9	3	7	0	A1	10	2	8	0	A'1	10	2	8	470.4083	0.153
0	A2	10	1	9	0	A1	10	2	8	0	A'1	10	2	8	472.0435	0.254
0	A1	10	1	10	0	A2	10	2	9	0	A'2	10	2	9	471.5787	0.090
0	A2	10	3	7	0	A1	10	2	8	0	A'1	10	2	8	478.2689	0.060
0	A1	10	3	8	0	A2	10	2	9	0	A'2	10	2	9	478.6145	0.205
0	A1	11	1	10	0	A2	10	2	9	0	A'2	10	2	9	480.2557	0.230
0	A2	11	1	11	0	A1	10	2	8	0	A'1	10	2	8	472.7596	0.027
0	A1	11	3	8	0	A2	10	2	9	0	A'2	10	2	9	487.2371	0.308
0	A2	11	3	9	0	A1	10	2	8	0	A'1	10	2	8	480.5812	0.067
0	A2	11	5	7	0	A1	10	2	8	0	A'1	10	2	8	486.7358	0.104
0	A1	9	1	8	0	A2	10	4	7	0	A'2	10	4	7	464.6472	0.067
0	A1	9	3	6	0	A2	10	4	7	0	A'2	10	4	7	470.0508	0.288
0	A2	9	3	7	0	A1	10	4	6	0	A'2	10	4	6	465.1004	0.143
0	A1	9	5	4	0	A2	10	4	7	0	A'2	10	4	7	473.2887	0.060
0	A2	9	5	5	0	A1	10	4	6	0	A'1	10	4	6	469.6890	0.262
0	A2	10	3	7	0	A1	10	4	6	0	A'1	10	4	6	472.9628	0.085
0	A1	10	3	8	0	A2	10	4	7	0	A'2	10	4	7	472.4081	0.142
0	A2	10	5	5	0	A1	10	4	6	0	A'1	10	4	6	477.1538	0.147
0	A1	10	5	6	0	A2	10	4	7	0	A'2	10	4	7	477.7672	0.062
0	A1	11	3	8	0	A2	10	4	7	0	A'2	10	4	7	481.0315	0.172
0	A1	11	5	6	0	A2	10	4	7	0	A'2	10	4	7	486.1975	0.281
0	A2	11	5	7	0	A1	10	4	6	0	A'1	10	4	6	481.4298	0.058
0	A2	11	7	5	0	A1	10	4	6	0	A'1	10	4	6	485.9828	0.597
0	A1	9	3	6	0	A2	10	6	5	0	A'2	10	6	5	465.4973	0.099
0	A1	9	5	4	0	A2	10	6	5	0	A'2	10	6	5	468.7348	0.224
0	A2	9	5	5	0	A1	10	6	4	0	A'1	10	6	4	466.7029	0.321
0	A1	9	7	2	0	A2	10	6	5	0	A'2	10	6	5	471.3643	0.212
0	A2	9	7	3	0	A1	10	6	4	0	A'1	10	6	4	470.4233	0.147
0	A2	10	5	5	0	A1	10	6	4	0	A'1	10	6	4	474.1685	0.134
0	A1	10	5	6	0	A2	10	6	5	0	A'2	10	6	5	473.2124	0.126
0	A2	10	7	3	0	A1	10	6	4	0	A'1	10	6	4	476.6720	0.016
0	A1	10	7	4	0	A2	10	6	5	0	A'2	10	6	5	477.2627	0.147
0	A1	11	5	6	0	A2	10	6	5	0	A'2	10	6	5	481.6424	0.399
0	A2	11	5	7	0	A1	10	6	4	0	A'1	10	6	4	478.4441	0.117
0	A1	11	7	4	0	A2	10	6	5	0	A'2	10	6	5	484.4736	0.136
0	A2	11	7	5	0	A1	10	6	4	0	A'1	10	6	4	482.9967	0.318

Excited state					Ground state [a]					Ground state [b]						
m′	*Γ′*	*J′*	*Ka′*	*Kc′*	*m″*	*Γ″*	*J″*	*Ka″*	*Kc″*	*m″*	*Γ″*	*J″*	*Ka″*	*Kc″*	Wavenumber cm^{-1}	Intensity
0	A1	9	7	2	0	A2	10	8	3	0	A'2	10	8	3	467.2740	0.131
0	A2	9	7	3	0	A1	10	8	2	0	A'1	10	8	2	467.1605	0.063
0	A2	10	7	3	0	A1	10	8	2	0	A'1	10	8	2	473.4092	0.126
0	A1	10	7	4	0	A2	10	8	3	0	A'2	10	8	3	473.1716	0.154
0	A1	11	7	4	0	A2	10	8	3	0	A'2	10	8	3	480.3840	0.181
0	A2	11	7	5	0	A1	10	8	2	0	A'1	10	8	2	479.7341	0.102
0	A1	9	7	2	0	A2	10	10	1	0	A'2	10	10	1	461.9442	0.672
0	A1	10	1	10	0	A2	11	1	11	0	A'2	11	0	11	470.7975	0.283
0	A1	11	1	10	0	A2	11	1	11	0	A'2	11	0	11	479.4753	0.222
0	A1	12	1	12	0	A2	11	1	11	0	A'2	11	0	11	480.1770	0.326
0	A1	12	3	10	0	A2	11	1	11	0	A'2	11	0	11	488.7941	0.130
0	A2	10	1	9	0	A1	11	2	10	0	A'1	11	2	10	470.4571	0.137
0	A1	10	1	10	0	A2	11	2	9	0	A'2	11	2	9	462.9664	0.132
0	A2	10	3	7	0	A1	11	2	10	0	A'1	11	2	10	476.6825	0.108
0	A1	10	3	8	0	A2	11	2	9	0	A'2	11	2	9	470.0022	0.146
0	A1	11	1	10	0	A2	11	2	9	0	A'2	11	2	9	471.6254	0.554
0	A2	11	1	11	0	A1	11	2	10	0	A'1	11	2	10	471.1705	0.202
0	A1	11	3	8	0	A2	11	2	9	0	A'2	11	2	9	478.6248	0.080
0	A2	11	3	9	0	A1	11	2	10	0	A'1	11	2	10	478.9932	0.108
0	A2	12	1	11	0	A1	11	2	10	0	A'1	11	2	10	480.6407	0.250
0	A1	12	1	12	0	A2	11	2	9	0	A'2	11	2	9	472.3470	0.214
0	A2	12	3	9	0	A1	11	2	10	0	A'1	11	2	10	488.4486	0.462
0	A1	12	3	10	0	A2	11	2	9	0	A'2	11	2	9	480.9629	0.126
0	A1	12	5	8	0	A2	11	2	9	0	A'2	11	2	9	487.9085	0.275
0	A2	10	1	9	0	A1	11	4	8	0	A'1	11	4	8	463.4554	0.322
0	A2	10	3	7	0	A1	11	4	8	0	A'1	11	4	8	469.6833	0.502
0	A1	10	3	8	0	A2	11	4	7	0	A'2	11	4	7	463.8690	0.164
0	A1	10	5	6	0	A2	11	4	7	0	A'2	11	4	7	469.2282	0.195
0	A1	11	3	8	0	A2	11	4	7	0	A'2	11	4	7	472.4922	0.155
0	A2	11	3	9	0	A1	11	4	8	0	A'1	11	4	8	471.9935	0.294
0	A1	11	5	6	0	A2	11	4	7	0	A'2	11	4	7	477.6580	0.115
0	A2	11	5	7	0	A1	11	4	8	0	A'1	11	4	8	478.1504	0.245
0	A2	12	3	9	0	A1	11	4	8	0	A'1	11	4	8	481.4493	0.194
0	A2	12	5	7	0	A1	11	4	8	0	A'1	11	4	8	487.4639	0.241
0	A1	12	5	8	0	A2	11	4	7	0	A'2	11	4	7	481.7749	0.096
0	A1	12	7	6	0	A2	11	4	7	0	A'2	11	4	7	487.0081	0.158
0	A2	10	3	7	0	A1	11	6	6	0	A'1	11	6	6	464.3978	0.243
0	A2	10	5	5	0	A1	11	6	6	0	A'1	11	6	6	468.5877	0.132
0	A1	10	5	6	0	A2	11	6	5	0	A'2	11	6	5	465.3205	0.156
0	A2	10	7	3	0	A1	11	6	6	0	A'1	11	6	6	471.0905	0.323
0	A1	10	7	4	0	A2	11	6	5	0	A'2	11	6	5	469.3693	0.318
0	A1	11	5	6	0	A2	11	6	5	0	A'2	11	6	5	473.7498	0.138
0	A2	11	5	7	0	A1	11	6	6	0	A'1	11	6	6	472.8622	0.112
0	A1	11	7	4	0	A2	11	6	5	0	A'2	11	6	5	476.5819	0.091
0	A2	11	7	5	0	A1	11	6	6	0	A'1	11	6	6	477.4161	0.089
0	A2	12	5	7	0	A1	11	6	6	0	A'1	11	6	6	482.1757	0.056
0	A1	12	5	8	0	A2	11	6	5	0	A'2	11	6	5	477.8673	0.342
0	A2	12	7	5	0	A1	11	6	6	0	A'1	11	6	6	485.7634	0.117
0	A1	12	7	6	0	A2	11	6	5	0	A'2	11	6	5	483.0992	0.235
0	A2	10	5	5	0	A1	11	8	4	0	A'1	11	8	4	464.3161	0.108
0	A2	10	7	3	0	A1	11	8	4	0	A'1	11	8	4	466.8182	0.343

Excited state					Ground state [a]					Ground state [b]						
m′	*Γ′*	*J′*	*Ka′*	*Kc′*	*m″*	*Γ″*	*J″*	*Ka″*	*Kc″*	*m″*	*Γ″*	*J″*	*Ka″*	*Kc″*	Wavenumber cm^{-1}	Intensity
0	A1	10	7	4	0	A2	11	8	3	0	A'2	11	8	3	466.4676	0.137
0	A1	11	7	4	0	A2	11	8	3	0	A'2	11	8	3	473.6802	0.086
0	A2	11	7	5	0	A1	11	8	4	0	A'1	11	8	4	473.1448	0.176
0	A2	12	7	5	0	A1	11	8	4	0	A'1	11	8	4	481.4922	0.193
0	A1	12	7	6	0	A2	11	8	3	0	A'2	11	8	3	480.1995	0.204
0	A2	10	7	3	0	A1	11	10	2	0	A'1	11	10	2	461.6171	0.183
0	A2	11	1	11	0	A1	12	1	12	0	A'1	12	0	12	470.3916	0.305
0	A2	12	1	11	0	A1	12	1	12	0	A'1	12	0	12	479.8616	0.237
0	A2	13	1	13	0	A1	12	1	12	0	A'1	12	0	12	480.5522	0.366
0	A2	13	3	11	0	A1	12	1	12	0	A'1	12	0	12	489.9676	0.246
0	A1	11	1	10	0	A2	12	2	11	0	A'2	12	2	11	470.0585	0.218
0	A2	11	1	11	0	A1	12	2	10	0	A'1	12	2	10	461.7716	0.131
0	A1	11	3	8	0	A2	12	2	11	0	A'2	12	2	11	477.0391	0.064
0	A2	11	3	9	0	A1	12	2	10	0	A'1	12	2	10	469.5937	0.404
0	A2	12	1	11	0	A1	12	2	10	0	A'1	12	2	10	471.2433	0.200
0	A1	12	1	12	0	A2	12	2	11	0	A'2	12	2	11	470.7609	0.085
0	A2	12	3	9	0	A1	12	2	10	0	A'1	12	2	10	479.0505	0.082
0	A1	12	3	10	0	A2	12	2	11	0	A'2	12	2	11	479.3782	0.242
0	A1	13	1	12	0	A2	12	2	11	0	A'2	12	2	11	481.0392	0.169
0	A2	13	1	13	0	A1	12	2	10	0	A'1	12	2	10	471.9324	0.176
0	A1	13	3	10	0	A2	12	2	11	0	A'2	12	2	11	489.6130	0.184
0	A2	13	3	11	0	A1	12	2	10	0	A'1	12	2	10	481.3473	0.078
0	A2	13	5	9	0	A1	12	2	10	0	A'1	12	2	10	489.0805	0.253
0	A1	11	1	10	0	A2	12	4	9	0	A'2	12	4	9	462.2690	0.056
0	A1	11	3	8	0	A2	12	4	9	0	A'2	12	4	9	469.2501	0.378
0	A2	11	3	9	0	A1	12	4	8	0	A'1	12	4	8	462.6537	0.212
0	A2	11	5	7	0	A1	12	4	8	0	A'1	12	4	8	468.8109	0.198
0	A2	12	3	9	0	A1	12	4	8	0	A'1	12	4	8	472.1110	0.271
0	A1	12	3	10	0	A2	12	4	9	0	A'2	12	4	9	471.5883	0.244
0	A2	12	5	7	0	A1	12	4	8	0	A'1	12	4	8	478.1250	0.210
0	A1	12	5	8	0	A2	12	4	9	0	A'2	12	4	9	478.5324	0.076
0	A1	13	3	10	0	A2	12	4	9	0	A'2	12	4	9	481.8233	0.065
0	A2	13	3	11	0	A1	12	4	8	0	A'1	12	4	8	474.4104	0.115
0	A1	13	5	8	0	A2	12	4	9	0	A'2	12	4	9	488.6872	0.293
0	A2	13	5	9	0	A1	12	4	8	0	A'1	12	4	8	482.1416	0.109
0	A2	13	7	7	0	A1	12	4	8	0	A'1	12	4	8	488.1203	0.151
0	A1	11	3	8	0	A2	12	6	7	0	A'2	12	6	7	463.1792	0.286
0	A1	11	5	6	0	A2	12	6	7	0	A'2	12	6	7	468.3465	0.609
0	A2	11	5	7	0	A1	12	6	6	0	A'1	12	6	6	463.8914	0.215
0	A1	11	7	4	0	A2	12	6	7	0	A'2	12	6	7	471.1768	0.179
0	A2	11	7	5	0	A1	12	6	6	0	A'1	12	6	6	468.4458	0.273
0	A2	12	5	7	0	A1	12	6	6	0	A'1	12	6	6	473.2067	0.277
0	A1	12	5	8	0	A2	12	6	7	0	A'2	12	6	7	472.4633	0.126
0	A1	12	7	6	0	A2	12	6	7	0	A'2	12	6	7	477.6953	0.424
0	A1	13	5	8	0	A2	12	6	7	0	A'2	12	6	7	482.6162	0.227
0	A2	13	5	9	0	A1	12	6	6	0	A'1	12	6	6	477.2223	0.222
0	A1	13	7	6	0	A2	12	6	7	0	A'2	12	6	7	487.2084	0.242
0	A2	13	7	7	0	A1	12	6	6	0	A'1	12	6	6	483.2011	0.057
0	A1	11	5	6	0	A2	12	8	5	0	A'2	12	8	5	463.6969	0.050

Excited state					Ground state [a]					Ground state [b]						
m′	*Γ′*	*J′*	*Ka′*	*Kc′*	*m″*	*Γ″*	*J″*	*Ka″*	*Kc″*	*m″*	*Γ″*	*J″*	*Ka″*	*Kc″*	Wavenumber cm^{-1}	Intensity
0	A1	11	7	4	0	A2	12	8	5	0	A'2	12	8	5	466.5289	0.104
0	A2	11	7	5	0	A1	12	8	4	0	A'1	12	8	4	465.5762	0.186
0	A2	12	7	5	0	A1	12	8	4	0	A'1	12	8	4	473.9248	0.057
0	A1	12	7	6	0	A2	12	8	5	0	A'2	12	8	5	473.0474	0.094
0	A1	13	7	6	0	A2	12	8	5	0	A'2	12	8	5	482.5575	0.224
0	A2	13	7	7	0	A1	12	8	4	0	A'1	12	8	4	480.3335	0.127
0	A1	11	7	4	0	A2	12	10	3	0	A'2	12	10	3	461.4498	0.104
0	A1	12	1	12	0	A2	13	1	13	0	A'2	13	0	13	469.9842	0.331
0	A1	13	1	12	0	A2	13	1	13	0	A'2	13	0	13	480.2617	0.186
0	A1	14	1	14	0	A2	13	1	13	0	A'2	13	0	13	480.9258	0.471
0	A1	14	3	12	0	A2	13	1	13	0	A'2	13	0	13	491.1257	0.070
0	A2	12	1	11	0	A1	13	2	12	0	A'1	13	2	12	469.6601	0.156
0	A1	12	1	12	0	A2	13	2	11	0	A'2	13	2	11	460.5768	0.048
0	A2	12	3	9	0	A1	13	2	12	0	A'1	13	2	12	477.4657	0.152
0	A1	12	3	10	0	A2	13	2	11	0	A'2	13	2	11	469.1933	0.302
0	A1	13	1	12	0	A2	13	2	11	0	A'2	13	2	11	470.8532	0.437
0	A2	13	1	13	0	A1	13	2	12	0	A'1	13	2	12	470.3499	0.516
0	A1	13	3	10	0	A2	13	2	11	0	A'2	13	2	11	479.4279	0.088
0	A2	13	3	11	0	A1	13	2	12	0	A'1	13	2	12	479.7657	0.114
0	A2	14	1	13	0	A1	13	2	12	0	A'1	13	2	12	481.4345	0.120
0	A1	14	1	14	0	A2	13	2	11	0	A'2	13	2	11	471.5167	0.238
0	A2	14	3	11	0	A1	13	2	12	0	A'1	13	2	12	490.8029	0.182
0	A1	14	3	12	0	A2	13	2	11	0	A'2	13	2	11	481.7160	0.278
0	A1	14	5	10	0	A2	13	2	11	0	A'2	13	2	11	490.2472	0.128
0	A2	12	1	11	0	A1	13	4	10	0	A'1	13	4	10	461.0791	0.040
0	A2	12	3	9	0	A1	13	4	10	0	A'1	13	4	10	468.8867	0.460
0	A1	12	3	10	0	A2	13	4	9	0	A'2	13	4	9	461.4555	0.154
0	A1	12	5	8	0	A2	13	4	9	0	A'2	13	4	9	468.4017	0.367
0	A1	13	3	10	0	A2	13	4	9	0	A'2	13	4	9	471.6911	0.050
0	A2	13	3	11	0	A1	13	4	10	0	A'1	13	4	10	471.1858	0.146
0	A1	13	5	8	0	A2	13	4	9	0	A'2	13	4	9	478.5564	0.181
0	A2	13	5	9	0	A1	13	4	10	0	A'1	13	4	10	478.9171	0.058
0	A2	14	3	11	0	A1	13	4	10	0	A'1	13	4	10	482.2229	0.412
0	A1	14	3	12	0	A2	13	4	9	0	A'2	13	4	9	473.9795	0.141
0	A2	14	5	9	0	A1	13	4	10	0	A'1	13	4	10	489.8958	0.028
0	A1	14	5	10	0	A2	13	4	9	0	A'2	13	4	9	482.5097	0.207
0	A1	14	7	8	0	A2	13	4	9	0	A'2	13	4	9	489.2864	0.225
0	A2	12	3	9	0	A1	13	6	8	0	A'1	13	6	8	462.0179	0.049
0	A2	12	5	7	0	A1	13	6	8	0	A'1	13	6	8	468.0311	0.126
0	A1	12	5	8	0	A2	13	6	7	0	A'2	13	6	7	462.5290	0.157
0	A2	12	7	5	0	A1	13	6	8	0	A'1	13	6	8	471.6180	0.206
0	A1	12	7	6	0	A2	13	6	7	0	A'2	13	6	7	467.7620	0.068
0	A1	13	5	8	0	A2	13	6	7	0	A'2	13	6	7	472.6838	0.047
0	A2	13	5	9	0	A1	13	6	8	0	A'1	13	6	8	472.0475	0.083
0	A1	13	7	6	0	A2	13	6	7	0	A'2	13	6	7	477.2736	0.243
0	A2	13	7	7	0	A1	13	6	8	0	A'1	13	6	8	478.0279	0.173
0	A2	14	5	9	0	A1	13	6	8	0	A'1	13	6	8	483.0249	0.165
0	A1	14	5	10	0	A2	13	6	7	0	A'2	13	6	7	476.6384	0.057
0	A2	14	7	7	0	A1	13	6	8	0	A'1	13	6	8	488.6633	0.306
0	A1	14	7	8	0	A2	13	6	7	0	A'2	13	6	7	483.4138	0.138
0	A2	12	5	7	0	A1	13	8	6	0	A'1	13	8	6	462.8197	0.186
0	A2	12	7	5	0	A1	13	8	6	0	A'1	13	8	6	466.4080	0.277

Excited state					Ground state [a]					Ground state [b]						
m′	*Γ′*	*J′*	*Ka′*	*Kc′*	*m″*	*Γ″*	*J″*	*Ka″*	*Kc″*	*m″*	*Γ″*	*J″*	*Ka″*	*Kc″*	Wavenumber cm^{-1}	Intensity
0	A1	12	7	6	0	A2	13	8	5	0	A'2	13	8	5	464.4255	0.272
0	A1	13	7	6	0	A2	13	8	5	0	A'2	13	8	5	473.9390	0.153
0	A2	14	7	7	0	A1	13	8	6	0	A'1	13	8	6	483.4524	0.203
0	A1	14	7	8	0	A2	13	8	5	0	A'2	13	8	5	480.0780	0.162
0	A2	12	7	5	0	A1	13	10	4	0	A'1	13	10	4	461.3857	0.065
0	A2	13	1	13	0	A1	14	1	14	0	A'1	14	0	14	469.5753	0.348
0	A2	14	1	13	0	A1	14	1	14	0	A'1	14	0	14	480.6596	0.061
0	A2	15	1	15	0	A1	14	1	14	0	A'1	14	0	14	481.2981	0.512
0	A1	13	1	12	0	A2	14	2	13	0	A'2	14	2	13	469.2740	0.245
0	A2	13	1	13	0	A1	14	3	12	0	A'1	14	2	12	459.3797	0.090
0	A1	13	3	10	0	A2	14	2	13	0	A'2	14	2	13	477.8490	0.310
0	A2	13	3	11	0	A1	14	3	12	0	A'1	14	2	12	468.7946	0.115
0	A2	14	1	13	0	A1	14	3	12	0	A'1	14	2	12	470.4635	0.062
0	A1	14	1	14	0	A2	14	2	13	0	A'2	14	2	13	469.9379	0.195
0	A2	14	3	11	0	A1	14	3	12	0	A'1	14	2	12	479.8319	0.332
0	A1	14	3	12	0	A2	14	2	13	0	A'2	14	2	13	480.1374	0.217
0	A1	15	1	14	0	A2	14	2	13	0	A'2	14	2	13	481.8286	0.165
0	A2	15	1	15	0	A1	14	3	12	0	A'1	14	2	12	471.1021	0.067
0	A1	15	3	12	0	A2	14	2	13	0	A'2	14	2	13	491.9831	0.154
0	A2	15	3	13	0	A1	14	3	12	0	A'1	14	2	12	482.0848	0.364
0	A2	15	5	11	0	A1	14	3	12	0	A'1	14	2	12	491.4089	0.244
0	A1	13	1	12	0	A2	14	4	11	0	A'2	14	4	11	459.9035	0.059
0	A1	13	3	10	0	A2	14	4	11	0	A'2	14	4	11	468.4773	0.163
0	A2	13	3	11	0	A1	14	4	10	0	A'1	14	4	10	460.2632	0.335
0	A2	13	5	9	0	A1	14	4	10	0	A'1	14	4	10	467.9948	0.283
0	A2	14	3	11	0	A1	14	4	10	0	A'1	14	4	10	471.3011	0.195
0	A1	14	3	12	0	A2	14	4	11	0	A'2	14	4	11	470.7671	0.121
0	A2	14	5	9	0	A1	14	4	10	0	A'1	14	4	10	478.9723	0.125
0	A1	14	5	10	0	A2	14	4	11	0	A'2	14	4	11	479.2981	0.150
0	A1	15	3	12	0	A2	14	4	11	0	A'2	14	4	11	482.6138	0.082
0	A2	15	3	13	0	A1	14	4	10	0	A'1	14	4	10	473.5526	0.138
0	A1	15	5	10	0	A2	14	4	11	0	A'2	14	4	11	491.0875	0.072
0	A2	15	5	11	0	A1	14	4	10	0	A'1	14	4	10	482.8770	0.658
0	A2	15	7	9	0	A1	14	4	10	0	A'1	14	4	10	490.4646	0.259
0	A1	13	3	10	0	A2	14	6	9	0	A'2	14	6	9	460.8064	0.148
0	A1	13	5	8	0	A2	14	6	9	0	A'2	14	6	9	467.6714	0.132
0	A2	13	5	9	0	A1	14	6	8	0	A'1	14	6	8	461.2476	0.507
0	A1	13	7	6	0	A2	14	6	9	0	A'2	14	6	9	472.2607	0.063
0	A2	13	7	7	0	A1	14	6	8	0	A'1	14	6	8	467.2271	0.673
0	A2	14	5	9	0	A1	14	6	8	0	A'1	14	6	8	472.2253	0.156
0	A1	14	5	10	0	A2	14	6	9	0	A'2	14	6	9	471.6260	0.269
0	A2	14	7	7	0	A1	14	6	8	0	A'1	14	6	8	477.8636	0.159
0	A1	14	7	8	0	A2	14	6	9	0	A'2	14	6	9	478.4017	0.185
0	A1	15	5	10	0	A2	14	6	9	0	A'2	14	6	9	483.4178	0.269
0	A1	15	7	8	0	A2	14	6	9	0	A'2	14	6	9	490.0059	0.059
0	A2	15	7	9	0	A1	14	6	8	0	A'1	14	6	8	483.7181	0.169
0	A1	13	5	8	0	A2	14	8	7	0	A'2	14	8	7	461.7639	0.168
0	A1	13	7	6	0	A2	14	8	7	0	A'2	14	8	7	466.3527	0.125
0	A2	13	7	7	0	A1	14	8	6	0	A'1	14	8	6	463.0080	0.208
0	A2	14	7	7	0	A1	14	8	6	0	A'1	14	8	6	473.6450	0.073
0	A1	14	7	8	0	A2	14	8	7	0	A'2	14	8	7	472.4922	0.155
0	A1	15	7	8	0	A2	14	8	7	0	A'2	14	8	7	484.0978	0.159

Excited state					Ground state [a]					Ground state [b]						
m′	*Γ′*	*J′*	*Ka′*	*Kc′*	*m″*	*Γ″*	*J″*	*Ka″*	*Kc″*	*m″*	*Γ″*	*J″*	*Ka″*	*Kc″*	Wavenumber cm^{-1}	Intensity
0	A2	15	7	9	0	A1	14	8	6	0	A'1	14	8	6	479.4998	0.100
0	A1	13	7	6	0	A2	14	10	5	0	A'2	14	10	5	461.2487	0.324
0	A1	14	1	14	0	A2	15	1	15	0	A'2	15	0	15	469.1652	0.310
0	A1	15	1	14	0	A2	15	1	15	0	A'2	15	0	15	481.0566	0.179
0	A1	16	1	16	0	A2	15	1	15	0	A'2	15	0	15	481.6688	0.506
0	A1	16	3	14	0	A2	15	1	15	0	A'2	15	0	15	493.4420	0.071
0	A1	14	1	14	0	A2	15	3	13	0	A'2	15	2	13	458.1813	0.111
0	A2	14	3	11	0	A1	15	2	14	0	A'1	15	2	14	478.2547	0.118
0	A1	14	3	12	0	A2	15	3	13	0	A'2	15	2	13	468.3800	0.310
0	A1	15	1	14	0	A2	15	3	13	0	A'2	15	2	13	470.0715	0.073
0	A2	15	1	15	0	A1	15	2	14	0	A'1	15	2	14	469.5252	0.152
0	A1	15	3	12	0	A2	15	3	13	0	A'2	15	2	13	480.2271	0.087
0	A2	15	3	13	0	A1	15	2	14	0	A'1	15	2	14	480.5088	0.096
0	A2	16	1	15	0	A1	15	2	14	0	A'1	15	2	14	482.2269	0.412
0	A1	16	1	16	0	A2	15	3	13	0	A'2	15	2	13	470.6855	0.124
0	A2	16	3	13	0	A1	15	2	14	0	A'1	15	2	14	493.1639	0.117
0	A1	16	3	14	0	A2	15	3	13	0	A'2	15	2	13	482.4587	0.390
0	A1	16	5	12	0	A2	15	3	13	0	A'2	15	2	13	492.5776	0.182
0	A2	14	1	13	0	A1	15	4	12	0	A'1	15	4	12	458.7230	0.245
0	A2	14	3	11	0	A1	15	4	12	0	A'1	15	4	12	468.0947	0.245
0		14	3	12	0	A2	15	4	11	0	A'2	15	4	11	459.0562	0.079
0	A1	14	5	10	0	A2	15	4	11	0	A'2	15	4	11	467.5864	0.262
0	A1	15	3	12	0	A2	15	4	11	0	A'2	15	4	11	470.9015	0.159
0	A2	15	3	13	0	A1	15	4	12	0	A'1	15	4	12	470.3499	0.516
0	A1	15	5	10	0	A2	15	4	11	0	A'2	15	4	11	479.3782	0.119
0	A2	15	5	11	0	A1	15	4	12	0	A'1	15	4	12	479.6729	0.098
0	A2	16	3	13	0	A1	15	4	12	0	A'1	15	4	12	483.0046	0.318
0	A1	16	3	14	0	A2	15	4	11	0	A'2	15	4	11	473.1341	0.178
0	A2	16	5	11	0	A1	15	4	12	0	A'1	15	4	12	492.2837	0.118
0	A1	16	5	12	0	A2	15	4	11	0	A'2	15	4	11	483.2543	0.472
0	A1	16	7	10	0	A2	15	4	11	0	A'2	15	4	11	491.6375	0.087
0	A2	14	3	11	0	A1	15	6	10	0	A'1	15	6	10	459.6247	0.085
0	A2	14	5	9	0	A1	15	6	10	0	A'1	15	6	10	467.2968	0.229
0	A1	14	5	10	0	A2	15	6	9	0	A'2	15	6	9	460.0082	0.056
0	A2	14	7	7	0	A1	15	6	10	0	A'1	15	6	10	472.9345	0.095
0	A1	14	7	8	0	A2	15	6	9	0	A'2	15	6	9	466.7823	0.311
0	A1	15	5	10	0	A2	15	6	9	0	A'2	15	6	9	471.7970	0.328
0	A2	15	5	11	0	A1	15	6	10	0	A'1	15	6	10	471.2024	0.454
0	A1	15	7	8	0	A2	15	6	9	0	A'2	15	6	9	478.3876	0.182
0	A2	15	7	9	0	A1	15	6	10	0	A'1	15	6	10	478.7889	0.142
0	A2	16	5	11	0	A1	15	6	10	0	A'1	15	6	10	483.8140	0.602
0	A2	16	7	9	0	A1	15	6	10	0	A'1	15	6	10	491.2699	0.234
0	A1	16	7	10	0	A2	15	6	9	0	A'2	15	6	9	484.0573	0.153
0	A2	14	5	9	0	A1	15	8	8	0	A'1	15	8	8	460.6122	0.064
0	A2	14	7	7	0	A1	15	8	8	0	A'1	15	8	8	466.2516	0.222
0	A1	14	7	8	0	A2	15	8	7	0	A'2	15	8	7	461.4913	0.126
0	A1	15	7	8	0	A2	15	8	7	0	A'2	15	8	7	473.0954	0.155
0	A2	15	7	9	0	A1	15	8	8	0	A'1	15	8	8	472.1060	0.108
0	A2	16	7	9	0	A1	15	8	8	0	A'1	15	8	8	484.5874	0.454
0	A1	16	7	10	0	A2	15	8	7	0	A'2	15	8	7	478.7679	0.266
0	A2	14	7	7	0	A1	15	10	6	0	A'1	15	10	6	460.8745	0.332
0	A2	15	1	15	0	A1	16	1	16	0	A'1	16	0	16	468.7538	0.383

Excited state					Ground state [a]					Ground state [b]						
m′	*Γ′*	*J′*	*Ka′*	*Kc′*	*m″*	*Γ″*	*J″*	*Ka″*	*Kc″*	*m″*	*Γ″*	*J″*	*Ka″*	*Kc″*	Wavenumber cm^{-1}	Intensity
0	A2	16	1	15	0	A1	16	1	16	0	A'1	16	0	16	481.4555	0.512
0	A2	17	1	17	0	A1	16	1	16	0	A'1	16	0	16	482.0387	0.553
0	A1	15	1	14	0	A2	16	2	15	0	A'2	16	2	15	468.4974	0.095
0	A2	15	1	15	0	A1	16	3	14	0	A'1	16	2	14	456.9796	0.047
0	A1	15	3	12	0	A2	16	2	15	0	A'2	16	2	15	478.6526	0.253
0	A2	15	3	13	0	A1	16	3	14	0	A'1	16	2	14	467.9647	0.213
0	A2	16	1	15	0	A1	16	3	14	0	A'1	16	2	14	469.6833	0.043
0	A1	16	1	16	0	A2	16	2	15	0	A'2	16	2	15	469.1100	0.164
0	A2	16	3	13	0	A1	16	3	14	0	A'1	16	2	14	480.6203	0.097
0	A1	16	3	14	0	A2	16	2	15	0	A'2	16	2	15	480.8832	0.106
0	A1	17	1	16	0	A2	16	2	15	0	A'2	16	2	15	482.6255	0.399
0	A2	17	1	17	0	A1	16	3	14	0	A'1	16	2	14	470.2657	0.233
0	A1	17	3	14	0	A2	16	2	15	0	A'2	16	2	15	494.3519	0.083
0	A2	17	3	15	0	A1	16	3	14	0	A'1	16	2	14	482.8217	0.424
0	A2	17	5	13	0	A1	16	3	14	0	A'1	16	2	14	493.7323	0.142
0	A1	15	1	14	0	A2	16	4	13	0	A'2	16	4	13	457.5490	0.067
0	A1	15	3	12	0	A2	16	4	13	0	A'2	16	4	13	467.7031	0.389
0	A2	15	3	13	0	A1	16	4	12	0	A'1	16	4	12	457.8481	0.264
0	A2	15	5	11	0	A1	16	4	12	0	A'1	16	4	12	467.1733	0.304
0	A2	16	3	13	0	A1	16	4	12	0	A'1	16	4	12	470.5059	0.136
0	A2	16	5	11	0	A1	16	4	12	0	A'1	16	4	12	479.7862	0.218
0	A1	16	5	12	0	A2	16	4	13	0	A'2	16	4	13	480.0537	0.117
0	A1	17	3	14	0	A2	16	4	13	0	A'2	16	4	13	483.4044	0.124
0	A2	17	3	15	0	A1	16	4	12	0	A'1	16	4	12	472.7058	0.051
0	A1	17	5	12	0	A2	16	4	13	0	A'2	16	4	13	493.4634	0.207
0	A2	17	5	13	0	A1	16	4	12	0	A'1	16	4	12	483.6182	0.636
0	A2	17	7	11	0	A1	16	4	12	0	A'1	16	4	12	492.8183	0.153
0	A1	15	3	12	0	A2	16	6	11	0	A'2	16	6	11	458.4350	0.087
0	A1	15	7	8	0	A2	16	6	11	0	A'2	16	6	11	473.5003	0.081
0	A2	15	7	9	0	A1	16	6	10	0	A'1	16	6	10	466.3674	0.395
0	A2	16	5	11	0	A1	16	6	10	0	A'1	16	6	10	471.3907	0.382
0	A1	16	5	12	0	A2	16	6	11	0	A'2	16	6	11	470.7864	0.458
0	A2	16	7	9	0	A1	16	6	10	0	A'1	16	6	10	478.8486	0.176
0	A1	17	5	12	0	A2	16	6	11	0	A'2	16	6	11	484.1971	0.503
0	A1	17	7	10	0	A2	16	6	11	0	A'2	16	6	11	492.5021	0.341
0	A2	17	7	11	0	A1	16	6	10	0	A'1	16	6	10	484.4260	0.363
0	A1	15	7	8	0	A2	16	8	9	0	A'2	16	8	9	466.0096	0.051
0	A2	15	7	9	0	A1	16	8	8	0	A'1	16	8	8	460.0238	0.053
0	A2	16	7	9	0	A1	16	8	8	0	A'1	16	8	8	472.5045	0.049
0	A1	16	7	10	0	A2	16	8	9	0	A'2	16	8	9	471.6810	0.168
0	A1	17	7	10	0	A2	16	8	9	0	A'2	16	8	9	485.0123	0.404
0	A2	17	7	11	0	A1	16	8	8	0	A'1	16	8	8	478.0803	0.109
0	A1	15	7	8	0	A2	16	10	7	0	A'2	16	10	7	460.1534	0.046
0	A1	16	1	16	0	A2	17	1	17	0	A'2	17	0	17	468.3407	0.399
0	A1	17	1	16	0	A2	17	1	17	0	A'2	17	0	17	481.8560	0.348
0	A1	18	1	18	0	A2	17	1	17	0	A'2	17	0	17	482.4069	0.485
0	A1	18	3	16	0	A2	17	1	17	0	A'2	17	0	17	495.7563	0.080
0	A2	16	1	15	0	A1	17	2	16	0	A'1	17	2	16	468.1114	0.248
0	A2	16	3	13	0	A1	17	2	16	0	A'1	17	2	16	479.0486	0.350
0	A1	16	3	14	0	A2	17	3	15	0	A'2	17	2	15	467.5547	0.286
0	A1	17	1	16	0	A2	17	3	15	0	A'2	17	2	15	469.2959	0.134

Excited state					Ground state [a]					Ground state [b]						
m′	*Γ′*	*J′*	*Ka′*	*Kc′*	*m″*	*Γ″*	*J″*	*Ka″*	*Kc″*	*m″*	*Γ″*	*J″*	*Ka″*	*Kc″*	Wavenumber cm^{-1}	Intensity
0	A2	17	1	17	0	A1	17	2	16	0	A'1	17	2	16	468.6940	0.533
0	A1	17	3	14	0	A2	17	3	15	0	A'2	17	2	15	481.0235	0.271
0	A2	17	3	15	0	A1	17	2	16	0	A'1	17	2	16	481.2504	0.126
0	A2	18	1	17	0	A1	17	2	16	0	A'1	17	2	16	483.0233	0.370
0	A1	18	1	18	0	A2	17	3	15	0	A'2	17	2	15	469.8479	0.209
0	A2	18	3	15	0	A1	17	2	16	0	A'1	17	2	16	495.5416	0.062
0	A1	18	3	16	0	A2	17	3	15	0	A'2	17	2	15	483.1966	0.393
0	A1	18	5	14	0	A2	17	3	15	0	A'2	17	2	15	494.8910	0.088
0	A2	16	3	13	0	A1	17	4	14	0	A'1	17	4	14	467.3113	0.108
0	A1	16	3	14	0	A2	17	4	13	0	A'2	17	4	13	456.6476	0.194
0	A1	16	5	12	0	A2	17	4	13	0	A'2	17	4	13	466.7683	0.094
0	A1	17	3	14	0	A2	17	4	13	0	A'2	17	4	13	470.1174	0.449
0	A2	17	3	15	0	A1	17	4	14	0	A'1	17	4	14	469.5125	0.134
0	A1	17	5	12	0	A2	17	4	13	0	A'2	17	4	13	480.1770	0.326
0	A2	17	5	13	0	A1	17	4	14	0	A'1	17	4	14	480.4227	0.115
0	A2	18	3	15	0	A1	17	4	14	0	A'1	17	4	14	483.8034	0.113
0	A1	18	3	16	0	A2	17	4	13	0	A'2	17	4	13	472.2901	0.317
0	A2	18	5	13	0	A1	17	4	14	0	A'1	17	4	14	494.6440	0.061
0	A1	18	5	14	0	A2	17	4	13	0	A'2	17	4	13	483.9852	0.742
0	A1	18	7	12	0	A2	17	4	13	0	A'2	17	4	13	493.9897	0.122
0	A2	16	3	13	0	A1	17	6	12	0	A'1	17	6	12	457.2491	0.086
0	A2	16	5	11	0	A1	17	6	12	0	A'1	17	6	12	466.5289	0.104
0	A2	16	7	9	0	A1	17	6	12	0	A'1	17	6	12	473.9845	0.141
0	A1	16	7	10	0	A2	17	6	11	0	A'2	17	6	11	465.9541	0.219
0	A1	17	5	12	0	A2	17	6	11	0	A'2	17	6	11	470.9801	0.171
0	A2	17	5	13	0	A1	17	6	12	0	A'1	17	6	12	470.3614	0.037
0	A1	17	7	10	0	A2	17	6	11	0	A'2	17	6	11	479.2852	0.327
0	A2	17	7	11	0	A1	17	6	12	0	A'1	17	6	12	479.5629	0.231
0	A2	18	5	13	0	A1	17	6	12	0	A'1	17	6	12	484.5796	0.443
0	A1	18	5	14	0	A2	17	6	11	0	A'2	17	6	11	474.7879	0.051
0	A2	18	7	11	0	A1	17	6	12	0	A'1	17	6	12	493.7232	0.174
0	A2	16	5	11	0	A1	17	8	10	0	A'1	17	8	10	458.2257	0.129
0	A2	16	7	9	0	A1	17	8	10	0	A'1	17	8	10	465.6825	0.161
0	A1	16	7	10	0	A2	17	8	9	0	A'2	17	8	9	458.6594	0.062
0	A1	17	7	10	0	A2	17	8	9	0	A'2	17	8	9	471.9914	0.157
0	A2	17	7	11	0	A1	17	8	10	0	A'1	17	8	10	471.2591	0.107
0	A2	18	7	11	0	A1	17	8	10	0	A'1	17	8	10	485.4195	0.110
0	A1	18	7	12	0	A2	17	8	9	0	A'2	17	8	9	477.4971	0.121
0	A2	16	7	9	0	A1	17	10	8	0	A'1	17	10	8	459.1790	0.206
0	A2	17	1	17	0	A1	18	1	18	0	A'1	18	0	18	467.9263	0.752
0	A2	18	1	17	0	A1	18	1	18	0	A'1	18	0	18	482.2570	0.112
0	A2	19	1	19	0	A1	18	1	18	0	A'1	18	0	18	482.7737	0.402
0	A2	19	3	17	0	A1	18	1	18	0	A'1	18	0	18	496.9133	0.095
0	A1	17	1	16	0	A2	18	2	17	0	A'2	18	2	17	467.7261	0.278
0	A2	17	1	17	0	A1	18	3	16	0	A'1	18	2	16	454.5794	0.055
0	A1	17	3	14	0	A2	18	2	17	0	A'2	18	2	17	479.4542	0.356
0	A2	17	3	15	0	A1	18	3	16	0	A'1	18	2	16	467.1350	0.500
0	A2	18	1	17	0	A1	18	3	16	0	A'1	18	2	16	468.9087	0.268
0	A1	18	1	18	0	A2	18	2	17	0	A'2	18	2	17	468.2767	0.150
0	A2	18	3	15	0	A1	18	3	16	0	A'1	18	2	16	481.4272	0.113
0	A1	18	3	16	0	A2	18	2	17	0	A'2	18	2	17	481.6262	0.114
0	A1	19	1	18	0	A2	18	2	17	0	A'2	18	2	17	483.4162	0.342

Excited state					Ground state [a]					Ground state [b]						
m′	*Γ′*	*J′*	*Ka′*	*Kc′*	*m″*	*Γ″*	*J″*	*Ka″*	*Kc″*	*m″*	*Γ″*	*J″*	*Ka″*	*Kc″*	Wavenumber cm^{-1}	Intensity
0	A2	19	1	19	0	A1	18	3	16	0	A'1	18	2	16	469.4261	0.103
0	A1	19	3	16	0	A2	18	2	17	0	A'2	18	2	17	496.7363	0.051
0	A2	19	3	17	0	A1	18	3	16	0	A'1	18	2	16	483.5667	0.050
0	A2	19	5	15	0	A1	18	3	16	0	A'1	18	2	16	496.0501	0.056
0	A1	17	1	16	0	A2	18	4	15	0	A'2	18	4	15	455.2004	0.112
0	A1	17	3	14	0	A2	18	4	15	0	A'2	18	4	15	466.9279	0.189
0	A2	17	3	15	0	A1	18	5	14	0	A'1	18	4	14	455.4618	0.478
0	A1	17	5	12	0	A2	18	4	15	0	A'2	18	4	15	476.9879	0.221
0	A2	17	5	13	0	A1	18	5	14	0	A'1	18	4	14	466.3498	0.292
0	A2	18	3	15	0	A1	18	5	14	0	A'1	18	4	14	469.7304	0.105
0	A1	18	3	16	0	A2	18	4	15	0	A'2	18	4	15	469.1007	0.173
0	A2	18	5	13	0	A1	18	5	14	0	A'1	18	4	14	480.5700	0.047
0	A1	18	5	14	0	A2	18	4	15	0	A'2	18	4	15	480.7947	0.118
0	A1	19	3	16	0	A2	18	4	15	0	A'2	18	4	15	484.2103	0.511
0	A2	19	3	17	0	A1	18	5	14	0	A'1	18	4	14	471.8720	0.078
0	A1	19	5	14	0	A2	18	4	15	0	A'2	18	4	15	495.8251	0.046
0	A2	19	5	15	0	A1	18	5	14	0	A'1	18	4	14	484.3544	0.336
0	A2	19	7	13	0	A1	18	5	14	0	A'1	18	4	14	495.1429	0.096
0	A1	17	5	12	0	A2	18	6	13	0	A'2	18	6	13	466.1323	0.205
0	A2	17	7	11	0	A1	18	6	12	0	A'1	18	6	12	465.5535	0.196
0	A1	18	5	14	0	A2	18	6	13	0	A'2	18	6	13	469.9403	0.482
0	A2	18	7	11	0	A1	18	6	12	0	A'1	18	6	12	479.7130	0.197
0	A1	18	7	12	0	A2	18	6	13	0	A'2	18	6	13	479.9450	0.111
0	A1	19	5	14	0	A2	18	6	13	0	A'2	18	6	13	484.9690	0.182
0	A2	19	5	15	0	A1	18	6	12	0	A'1	18	6	12	474.3568	0.100
0	A1	19	7	12	0	A2	18	6	13	0	A'2	18	6	13	494.9203	0.171
0	A2	19	7	13	0	A1	18	6	12	0	A'1	18	6	12	485.1442	0.539
0	A1	17	5	12	0	A2	18	8	11	0	A'2	18	8	11	457.0188	0.165
0	A1	17	7	10	0	A2	18	8	11	0	A'2	18	8	11	465.3243	0.070
0	A2	17	7	11	0	A1	18	8	10	0	A'1	18	8	10	457.3839	0.659
0	A2	18	7	11	0	A1	18	8	10	0	A'1	18	8	10	471.5439	0.081
0	A1	18	7	12	0	A2	18	8	11	0	A'2	18	8	11	470.8295	0.162
0	A1	19	7	12	0	A2	18	8	11	0	A'2	18	8	11	485.8052	0.416
0	A2	19	7	13	0	A1	18	8	10	0	A'1	18	8	10	476.9750	0.054
0	A1	17	7	10	0	A2	18	10	9	0	A'2	18	10	9	458.0639	0.100
0	A1	18	1	18	0	A2	19	1	19	0	A'2	19	0	19	467.5115	0.395
0	A1	19	1	18	0	A2	19	1	19	0	A'2	19	0	19	482.6511	0.399
0	A1	20	1	20	0	A2	19	1	19	0	A'2	19	0	19	483.1393	0.549
0	A1	20	3	18	0	A2	19	1	19	0	A'2	19	0	19	498.0733	0.035
0	A2	18	1	17	0	A1	19	2	18	0	A'1	19	2	18	467.3406	0.234
0	A2	18	3	15	0	A1	19	2	18	0	A'1	19	2	18	479.8581	0.237
0	A1	18	3	16	0	A2	19	3	17	0	A'2	19	2	17	466.7259	0.207
0	A1	19	1	18	0	A2	19	3	17	0	A'2	19	2	17	468.5165	0.113
0	A2	19	1	19	0	A1	19	2	18	0	A'1	19	2	18	467.8582	0.140
0	A1	19	3	16	0	A2	19	3	17	0	A'2	19	2	17	481.8369	0.217
0	A2	19	3	17	0	A1	19	2	18	0	A'1	19	2	18	481.9999	0.204
0	A2	20	1	19	0	A1	19	2	18	0	A'1	19	2	18	483.8140	0.602
0	A1	20	1	20	0	A2	19	3	17	0	A'2	19	2	17	469.0048	0.087
0	A2	20	3	17	0	A1	19	2	18	0	A'1	19	2	18	497.9124	0.105
0	A1	20	3	18	0	A2	19	3	17	0	A'2	19	2	17	483.9381	0.373
0	A1	20	5	16	0	A2	19	3	17	0	A'2	19	2	17	497.2047	0.236
0	A2	18	3	15	0	A1	19	4	16	0	A'1	19	4	16	466.5452	0.236

Excited state					Ground state [a]					Ground state [b]						
m′	*Γ′*	*J′*	*Ka′*	*Kc′*	*m″*	*Γ″*	*J″*	*Ka″*	*Kc″*	*m″*	*Γ″*	*J″*	*Ka″*	*Kc″*	Wavenumber cm^{-1}	Intensity
0	A1	18	3	16	0	A2	19	5	15	0	A'2	19	4	15	454.2401	0.084
0	A2	18	5	13	0	A1	19	4	16	0	A'1	19	4	16	477.3847	0.299
0	A1	18	5	14	0	A2	19	5	15	0	A'2	19	4	15	465.9355	0.243
0	A1	19	3	16	0	A2	19	5	15	0	A'2	19	4	15	469.3515	0.101
0	A2	19	3	17	0	A1	19	4	16	0	A'1	19	4	16	468.6858	0.071
0	A1	19	5	14	0	A2	19	5	15	0	A'2	19	4	15	480.9661	0.505
0	A2	19	5	15	0	A1	19	4	16	0	A'1	19	4	16	481.1683	0.064
0	A2	20	3	17	0	A1	19	4	16	0	A'1	19	4	16	484.5985	0.258
0	A1	20	3	18	0	A2	19	5	15	0	A'2	19	4	15	471.4528	0.256
0	A2	20	5	15	0	A1	19	4	16	0	A'1	19	4	16	497.0191	0.081
0	A1	20	5	16	0	A2	19	5	15	0	A'2	19	4	15	484.7197	0.347
0	A1	20	7	14	0	A2	19	5	15	0	A'2	19	4	15	496.2920	0.050
0	A2	18	3	15	0	A1	19	6	14	0	A'1	19	6	14	454.8968	0.061
0	A2	18	5	13	0	A1	19	6	14	0	A'1	19	6	14	465.7374	0.551
0	A1	18	5	14	0	A2	19	6	13	0	A'2	19	6	13	455.1411	0.177
0	A1	18	7	12	0	A2	19	6	13	0	A'2	19	6	13	465.1449	0.207
0	A1	19	5	14	0	A2	19	6	13	0	A'2	19	6	13	470.1695	0.251
0	A1	19	7	12	0	A2	19	6	13	0	A'2	19	6	13	480.1196	0.206
0	A2	19	7	13	0	A1	19	6	14	0	A'1	19	6	14	480.3090	0.152
0	A2	20	5	15	0	A1	19	6	14	0	A'1	19	6	14	485.3724	0.442
0	A1	20	7	14	0	A2	19	6	13	0	A'2	19	6	13	485.4973	0.074
0	A2	18	5	13	0	A1	19	8	12	0	A'1	19	8	12	455.8176	0.102
0	A2	18	7	11	0	A1	19	8	12	0	A'1	19	8	12	464.9578	0.268
0	A1	18	7	12	0	A2	19	8	11	0	A'2	19	8	11	456.1370	0.163
0	A1	19	7	12	0	A2	19	8	11	0	A'2	19	8	11	471.1137	0.145
0	A2	20	7	13	0	A1	19	8	12	0	A'1	19	8	12	486.1937	0.185
0	A1	20	7	14	0	A2	19	8	11	0	A'2	19	8	11	476.4913	0.049
0	A2	18	7	11	0	A1	19	10	10	0	A'1	19	10	10	456.8852	0.301
0	A2	19	1	19	0	A1	20	1	20	0	A'1	20	0	20	467.0947	0.298
0	A2	20	1	19	0	A1	20	1	20	0	A'1	20	0	20	483.0511	0.549
0	A2	21	1	21	0	A1	20	1	20	0	A'1	20	0	20	483.5037	0.508
0	A1	19	1	18	0	A2	20	2	19	0	A'2	20	2	19	466.9500	0.203
0	A2	19	1	19	0	A1	20	3	18	0	A'1	20	2	18	452.1723	0.116
0	A1	19	3	16	0	A2	20	2	19	0	A'2	20	2	19	480.2691	0.279
0	A2	19	3	17	0	A1	20	3	18	0	A'1	20	2	18	466.3136	0.591
0	A2	20	1	19	0	A1	20	3	18	0	A'1	20	2	18	468.1294	0.332
0	A1	20	1	20	0	A2	20	2	19	0	A'2	20	2	19	467.4380	0.453
0	A2	20	3	17	0	A1	20	3	18	0	A'1	20	2	18	482.2269	0.412
0	A1	20	3	18	0	A2	20	2	19	0	A'2	20	2	19	482.3728	0.034
0	A1	21	1	20	0	A2	20	2	19	0	A'2	20	2	19	484.2103	0.511
0	A2	21	1	21	0	A1	20	3	18	0	A'1	20	2	18	468.5794	0.040
0	A2	21	3	19	0	A1	20	3	18	0	A'1	20	2	18	484.3046	0.044
0	A1	19	3	16	0	A2	20	4	17	0	A'2	20	4	17	466.1686	0.135
0	A2	19	3	17	0	A1	20	5	16	0	A'1	20	4	16	453.0398	0.387
0	A1	19	5	14	0	A2	20	4	17	0	A'2	20	4	17	477.7841	0.136
0	A2	19	5	15	0	A1	20	5	16	0	A'1	20	4	16	465.5226	0.393
0	A2	20	3	17	0	A1	20	5	16	0	A'1	20	4	16	468.9534	0.094
0	A1	20	3	18	0	A2	20	4	17	0	A'2	20	4	17	468.2712	0.268
0	A2	20	5	15	0	A1	20	5	16	0	A'1	20	4	16	481.3726	0.241
0	A1	20	5	16	0	A2	20	4	17	0	A'2	20	4	17	481.5371	0.043
0	A1	21	3	18	0	A2	20	4	17	0	A'2	20	4	17	484.9884	0.052
0	A2	21	3	19	0	A1	20	5	16	0	A'1	20	4	16	471.0320	0.192

Excited state					Ground state [a]					Ground state [b]						
m′	*Γ′*	*J′*	*Ka′*	*Kc′*	*m″*	*Γ″*	*J″*	*Ka″*	*Kc″*	*m″*	*Γ″*	*J″*	*Ka″*	*Kc″*	Wavenumber cm^{-1}	Intensity
0	A1	21	5	16	0	A2	20	4	17	0	A'2	20	4	17	498.2064	0.045
0	A2	21	5	17	0	A1	20	5	16	0	A'1	20	4	16	485.0757	0.606
0	A1	19	3	16	0	A2	20	6	15	0	A'2	20	6	15	453.7293	0.239
0	A1	19	5	14	0	A2	20	6	15	0	A'2	20	6	15	465.3446	0.087
0	A2	19	5	15	0	A1	20	6	14	0	A'1	20	6	14	453.9315	0.107
0	A2	19	7	13	0	A1	20	6	14	0	A'1	20	6	14	464.7201	0.097
0	A2	20	5	15	0	A1	20	6	14	0	A'1	20	6	14	469.7820	0.188
0	A1	20	5	16	0	A2	20	6	15	0	A'2	20	6	15	469.1006	0.173
0	A2	20	7	13	0	A1	20	6	14	0	A'1	20	6	14	480.5245	0.168
0	A1	20	7	14	0	A2	20	6	15	0	A'2	20	6	15	480.6730	0.310
0	A1	21	5	16	0	A2	20	6	15	0	A'2	20	6	15	485.7674	0.580
0	A2	21	5	17	0	A1	20	6	14	0	A'1	20	6	14	473.4942	0.233
0	A2	21	7	15	0	A1	20	6	14	0	A'1	20	6	14	485.8747	0.377
0	A1	19	7	12	0	A2	20	8	13	0	A'2	20	8	13	464.5710	0.333
0	A2	20	7	13	0	A1	20	8	12	0	A'1	20	8	12	470.6977	0.212
0	A1	20	7	14	0	A2	20	8	13	0	A'2	20	8	13	469.9477	0.335
0	A1	21	7	14	0	A2	20	8	13	0	A'2	20	8	13	486.5718	0.139
0	A2	21	7	15	0	A1	20	8	12	0	A'1	20	8	12	476.0492	0.127
0	A1	20	1	20	0	A2	21	1	21	0	A'2	21	0	21	466.6765	0.307
0	A1	21	1	20	0	A2	21	1	21	0	A'2	21	0	21	483.4501	0.203
0	A1	22	1	22	0	A2	21	1	21	0	A'2	21	0	21	483.8660	0.383
0	A2	20	1	19	0	A1	21	2	20	0	A'1	21	2	20	466.5649	0.134
0	A1	20	1	20	0	A2	21	2	19	0	A'2	21	2	19	450.9681	0.053
0	A2	20	3	17	0	A1	21	2	20	0	A'1	21	2	20	480.6625	0.110
0	A1	20	3	18	0	A2	21	3	19	0	A'2	21	2	19	465.9010	0.324
0	A1	21	1	20	0	A2	21	3	19	0	A'2	21	2	19	467.7360	0.419
0	A2	21	1	21	0	A1	21	2	20	0	A'1	21	2	20	467.0172	0.089
0	A1	21	3	18	0	A2	21	3	19	0	A'2	21	2	19	482.6193	0.077
0	A2	21	3	19	0	A1	21	2	20	0	A'1	21	2	20	482.7415	0.054
0	A2	22	1	21	0	A1	21	2	20	0	A'1	21	2	20	484.6133	0.223
0	A1	22	1	22	0	A2	21	3	19	0	A'2	21	2	19	468.1540	0.231
0	A2	22	3	19	0	A1	21	2	20	0	A'1	21	2	20	500.2650	0.025
0	A1	22	3	20	0	A2	21	3	19	0	A'2	21	2	19	484.6722	0.856
0	A2	20	1	19	0	A1	21	4	18	0	A'1	21	4	18	451.6754	0.188
0	A2	20	3	17	0	A1	21	4	18	0	A'1	21	4	18	465.7736	0.040
0	A2	20	5	15	0	A1	21	4	18	0	A'1	21	4	18	478.1932	0.188
0	A1	20	5	16	0	A2	21	5	17	0	A'2	21	4	17	465.1053	0.293
0	A1	21	3	18	0	A2	21	5	17	0	A'2	21	4	17	468.5569	0.186
0	A2	21	3	19	0	A1	21	4	18	0	A'1	21	4	18	467.8518	0.127
0	A1	21	5	16	0	A2	21	5	17	0	A'2	21	4	17	481.7739	0.096
0	A2	21	5	17	0	A1	21	4	18	0	A'1	21	4	18	481.9045	0.134
0	A2	22	3	19	0	A1	21	4	18	0	A'1	21	4	18	485.3784	0.392
0	A1	22	3	20	0	A2	21	5	17	0	A'2	21	4	17	470.6094	0.124
0	A1	22	5	18	0	A2	21	5	17	0	A'2	21	4	17	485.4472	0.280
0	A1	22	7	16	0	A2	21	5	17	0	A'2	21	4	17	498.6204	0.015
0	A2	20	3	17	0	A1	21	6	16	0	A'1	21	6	16	452.5451	0.059
0	A2	20	5	15	0	A1	21	6	16	0	A'1	21	6	16	464.9654	0.202
0	A1	20	7	14	0	A2	21	6	15	0	A'2	21	6	15	464.2959	0.567
0	A1	21	5	16	0	A2	21	6	15	0	A'2	21	6	15	469.3908	0.306
0	A2	21	5	17	0	A1	21	6	16	0	A'1	21	6	16	468.6769	0.127
0	A1	21	7	14	0	A2	21	6	15	0	A'2	21	6	15	480.9178	0.312
0	A2	21	7	15	0	A1	21	6	16	0	A'1	21	6	16	481.0566	0.179

Excited state					Ground state [a]					Ground state [b]						
m′	*Γ′*	*J′*	*Ka′*	*Kc′*	*m″*	*Γ″*	*J″*	*Ka″*	*Kc″*	*m″*	*Γ″*	*J″*	*Ka″*	*Kc″*	Wavenumber cm^{-1}	Intensity
0	A2	22	5	17	0	A1	21	6	16	0	A'1	21	6	16	486.1655	0.510
0	A1	22	5	18	0	A2	21	6	15	0	A'2	21	6	15	473.0633	0.054
0	A1	22	7	16	0	A2	21	6	15	0	A'2	21	6	15	486.2384	0.561
0	A2	20	7	13	0	A1	21	8	14	0	A'1	21	8	14	464.1845	0.156
0	A1	20	7	14	0	A2	21	8	13	0	A'2	21	8	13	453.6538	0.577
0	A1	21	7	14	0	A2	21	8	13	0	A'2	21	8	13	470.2763	0.161
0	A2	21	7	15	0	A1	21	8	14	0	A'1	21	8	14	469.5359	0.199
0	A2	22	7	15	0	A1	21	8	14	0	A'1	21	8	14	486.9803	0.090
0	A2	21	1	21	0	A1	22	1	22	0	A'1	22	0	22	466.2573	0.286
0	A2	22	1	21	0	A1	22	1	22	0	A'1	22	0	22	483.8528	0.072
0	A2	23	1	23	0	A1	22	1	22	0	A'1	22	0	22	484.2274	0.292
0	A1	21	1	20	0	A2	22	2	21	0	A'2	22	2	21	466.1776	0.591
0	A2	21	1	21	0	A1	22	3	20	0	A'1	22	2	20	449.7599	0.062
0	A1	21	3	18	0	A2	22	2	21	0	A'2	22	2	21	481.0566	0.179
0	A2	21	3	19	0	A1	22	3	20	0	A'1	22	2	20	465.4844	0.167
0	A2	22	1	21	0	A1	22	3	20	0	A'1	22	2	20	467.3556	0.419
0	A1	22	1	22	0	A2	22	2	21	0	A'2	22	2	21	466.5949	0.079
0	A2	22	3	19	0	A1	22	3	20	0	A'1	22	2	20	483.0105	0.059
0	A1	22	3	20	0	A2	22	2	21	0	A'2	22	2	21	483.1088	0.466
0	A1	23	1	22	0	A2	22	2	21	0	A'2	22	2	21	485.0089	0.614
0	A2	23	1	23	0	A1	22	3	20	0	A'1	22	2	20	467.7299	0.140
0	A1	23	3	20	0	A2	22	2	21	0	A'2	22	2	21	501.4485	0.023
0	A2	23	5	19	0	A1	22	3	20	0	A'1	22	2	20	500.6760	0.030
0	A1	21	1	20	0	A2	22	4	19	0	A'2	22	4	19	450.5017	0.213
0	A1	21	3	18	0	A2	22	4	19	0	A'2	22	4	19	465.3809	0.163
0	A2	21	3	19	0	A1	22	5	18	0	A'1	22	4	18	450.6329	0.143
0	A1	21	5	16	0	A2	22	4	19	0	A'2	22	4	19	478.5979	0.139
0	A2	21	5	17	0	A1	22	5	18	0	A'1	22	4	18	464.6865	0.231
0	A2	22	3	19	0	A1	22	5	18	0	A'1	22	4	18	468.1598	0.204
0	A1	22	3	20	0	A2	22	4	19	0	A'2	22	4	19	467.4308	0.158
0	A2	22	5	17	0	A1	22	5	18	0	A'1	22	4	18	482.1757	0.056
0	A1	22	5	18	0	A2	22	4	19	0	A'2	22	4	19	482.2699	0.361
0	A1	23	3	20	0	A2	22	4	19	0	A'2	22	4	19	485.7713	0.279
0	A2	23	3	21	0	A1	22	5	18	0	A'1	22	4	18	470.1832	0.202
0	A1	23	5	18	0	A2	22	4	19	0	A'2	22	4	19	500.5773	0.181
0	A2	23	5	19	0	A1	22	5	18	0	A'1	22	4	18	485.8247	0.045
0	A1	21	5	16	0	A2	22	6	17	0	A'2	22	6	17	464.5797	0.055
0	A2	21	5	17	0	A1	22	7	16	0	A'1	22	6	16	451.5116	0.049
0	A1	21	7	14	0	A2	22	6	17	0	A'2	22	6	17	476.1085	0.149
0	A2	21	7	15	0	A1	22	7	16	0	A'1	22	6	16	463.8914	0.215
0	A2	22	5	17	0	A1	22	7	16	0	A'1	22	6	16	468.9999	0.234
0	A1	22	5	18	0	A2	22	6	17	0	A'2	22	6	17	468.2529	0.201
0	A2	22	7	15	0	A1	22	7	16	0	A'1	22	6	16	481.3362	0.084
0	A1	22	7	16	0	A2	22	6	17	0	A'2	22	6	17	481.4272	0.113
0	A1	23	5	18	0	A2	22	6	17	0	A'2	22	6	17	486.5596	0.049
0	A2	23	7	17	0	A1	22	7	16	0	A'1	22	6	16	486.5996	0.349
0	A1	21	7	14	0	A2	22	8	15	0	A'2	22	8	15	463.7992	0.079
0	A2	22	7	15	0	A1	22	8	14	0	A'1	22	8	14	469.8933	0.165
0	A1	22	7	16	0	A2	22	8	15	0	A'2	22	8	15	469.1195	0.150
0	A1	23	7	16	0	A2	22	8	15	0	A'2	22	8	15	487.3862	0.466
0	A1	22	1	22	0	A2	23	1	23	0	A'2	23	0	23	465.8361	0.284
0	A1	23	1	22	0	A2	23	1	23	0	A'2	23	0	23	484.2520	0.249

Excited state					Ground state [a]					Ground state [b]						
m′	*Γ′*	*J′*	*Ka′*	*Kc′*	*m″*	*Γ″*	*J″*	*Ka″*	*Kc″*	*m″*	*Γ″*	*J″*	*Ka″*	*Kc″*	Wavenumber cm^{-1}	Intensity
0	A1	24	1	24	0	A2	23	1	23	0	A'2	23	0	23	484.5874	0.454
0	A2	22	1	21	0	A1	23	2	22	0	A'1	23	2	22	465.7959	0.140
0	A1	22	1	22	0	A2	23	3	21	0	A'2	23	2	21	448.5530	0.033
0	A2	22	3	19	0	A1	23	2	22	0	A'1	23	2	22	481.4555	0.512
0	A1	22	3	20	0	A2	23	3	21	0	A'2	23	2	21	465.0673	0.084
0	A1	23	1	22	0	A2	23	3	21	0	A'2	23	2	21	466.9671	0.092
0	A2	23	1	23	0	A1	23	2	22	0	A'1	23	2	22	466.1706	0.117
0	A1	23	3	20	0	A2	23	3	21	0	A'2	23	2	21	483.4073	0.100
0	A2	23	3	21	0	A1	23	2	22	0	A'1	23	2	22	483.4739	0.518
0	A2	24	1	23	0	A1	23	2	22	0	A'1	23	2	22	485.4075	0.856
0	A1	24	1	24	0	A2	23	3	21	0	A'2	23	2	21	467.3031	0.122
0	A1	24	3	22	0	A2	23	3	21	0	A'2	23	2	21	485.4033	0.320
0	A2	22	1	21	0	A1	23	4	20	0	A'1	23	4	20	449.3329	0.026
0	A2	22	3	19	0	A1	23	4	20	0	A'1	23	4	20	464.9862	0.171
0	A1	22	5	18	0	A2	23	5	19	0	A'2	23	4	19	464.2665	0.224
0	A1	23	3	20	0	A2	23	5	19	0	A'2	23	4	19	467.7679	0.156
0	A2	23	3	21	0	A1	23	4	20	0	A'1	23	4	20	467.0112	0.202
0	A1	23	5	18	0	A2	23	5	19	0	A'2	23	4	19	482.5742	0.202
0	A2	23	5	19	0	A1	23	4	20	0	A'1	23	4	20	482.6511	0.399
0	A2	24	3	21	0	A1	23	4	20	0	A'1	23	4	20	486.1655	0.510
0	A1	24	3	22	0	A2	23	5	19	0	A'2	23	4	19	469.7646	0.065
0	A1	24	5	20	0	A2	23	5	19	0	A'2	23	4	19	486.2064	0.227
0	A2	22	3	19	0	A1	23	6	18	0	A'1	23	6	18	450.1796	0.065
0	A2	22	5	17	0	A1	23	6	18	0	A'1	23	6	18	464.1965	0.086
0	A1	22	5	18	0	A2	23	7	17	0	A'2	23	6	17	450.2999	0.384
0	A1	22	7	16	0	A2	23	7	17	0	A'2	23	6	17	463.4741	0.101
0	A1	23	5	18	0	A2	23	7	17	0	A'2	23	6	17	468.6063	0.104
0	A2	23	5	19	0	A1	23	6	18	0	A'1	23	6	18	467.8439	0.239
0	A1	23	7	16	0	A2	23	7	17	0	A'2	23	6	17	481.7403	0.147
0	A2	23	7	17	0	A1	23	6	18	0	A'1	23	6	18	481.7964	0.148
0	A2	24	5	19	0	A1	23	6	18	0	A'1	23	6	18	486.9602	0.200
0	A1	24	7	18	0	A2	23	7	17	0	A'2	23	6	17	486.9525	0.238
0	A2	22	7	15	0	A1	23	8	16	0	A'1	23	8	16	463.4156	0.069
0	A1	23	7	16	0	A2	23	8	15	0	A'2	23	8	15	469.5148	0.091
0	A2	23	7	17	0	A1	23	8	16	0	A'1	23	8	16	468.6781	0.127
0	A2	24	7	17	0	A1	23	8	16	0	A'1	23	8	16	487.7573	0.467
0	A2	22	7	15	0	A1	23	10	14	0	A'1	23	10	14	452.0641	0.417
0	A2	23	1	23	0	A1	24	1	24	0	A'1	24	0	24	465.4141	0.331
0	A2	24	1	23	0	A1	24	1	24	0	A'1	24	0	24	484.6510	0.478
0	A2	25	1	25	0	A1	24	1	24	0	A'1	24	0	24	484.9466	0.498
0	A1	23	1	22	0	A2	24	2	23	0	A'2	24	2	23	465.4092	0.124
0	A2	23	1	23	0	A1	24	3	22	0	A'1	24	2	22	447.3442	0.020
0	A1	23	3	20	0	A2	24	2	23	0	A'2	24	2	23	481.8457	0.055
0	A2	23	3	21	0	A1	24	2	22	0	A'1	24	2	22	464.6472	0.319
0	A2	24	1	23	0	A1	24	3	22	0	A'1	24	2	22	466.5805	0.751
0	A1	24	1	24	0	A2	24	2	23	0	A'2	24	2	23	465.7449	0.121
0	A2	24	3	21	0	A1	24	3	22	0	A'1	24	2	22	483.8034	0.034
0	A1	24	3	22	0	A2	24	2	23	0	A'2	24	2	23	483.8455	0.105
0	A1	25	1	24	0	A2	24	2	23	0	A'2	24	2	23	485.8052	0.416
0	A2	25	1	25	0	A1	24	3	22	0	A'1	24	2	22	466.8751	0.180
0	A2	25	3	23	0	A1	24	3	22	0	A'1	24	2	22	485.7809	0.262
0	A1	23	3	20	0	A2	24	4	21	0	A'2	24	4	21	464.5974	0.252

Excited state					Ground state [a]					Ground state [b]						
m′	*Γ′*	*J′*	*Ka′*	*Kc′*	*m″*	*Γ″*	*J″*	*Ka″*	*Kc″*	*m″*	*Γ″*	*J″*	*Ka″*	*Kc″*	Wavenumber cm^{-1}	Intensity
0	A2	23	3	21	0	A1	24	5	20	0	A'1	24	4	20	448.2232	0.102
0	A1	23	5	18	0	A2	24	4	21	0	A'2	24	4	21	479.4033	0.284
0	A2	23	5	19	0	A1	24	5	20	0	A'1	24	4	20	463.8616	0.101
0	A2	24	3	21	0	A1	24	5	20	0	A'1	24	4	20	467.3763	0.100
0	A1	24	3	22	0	A2	24	4	21	0	A'2	24	4	21	466.5937	0.105
0	A2	24	5	19	0	A1	24	5	20	0	A'1	24	4	20	482.9791	0.277
0	A1	24	5	20	0	A2	24	4	21	0	A'2	24	4	21	483.0356	0.266
0	A1	25	3	22	0	A2	24	4	21	0	A'2	24	4	21	486.5570	0.044
0	A2	25	3	23	0	A1	24	5	20	0	A'1	24	4	20	469.3547	0.202
0	A2	25	5	21	0	A1	24	5	20	0	A'1	24	4	20	486.5481	0.247
0	A1	23	3	20	0	A2	24	6	19	0	A'2	24	6	19	449.0052	0.210
0	A1	23	5	18	0	A2	24	6	19	0	A'2	24	6	19	463.8112	0.093
0	A2	23	5	19	0	A1	24	7	18	0	A'2	24	6	18	449.1046	0.293
0	A1	23	7	16	0	A2	24	6	19	0	A'2	24	6	19	476.9457	0.105
0	A2	23	7	17	0	A1	24	7	18	0	A'1	24	6	18	463.0574	0.067
0	A2	24	5	19	0	A1	24	7	18	0	A'1	24	6	18	468.2233	0.124
0	A1	24	5	20	0	A2	24	6	19	0	A'2	24	6	19	467.4430	0.463
0	A2	24	7	17	0	A1	24	7	18	0	A'1	24	6	18	482.1363	0.283
0	A1	24	7	18	0	A2	24	6	19	0	A'2	24	6	19	482.1554	0.365
0	A2	25	7	19	0	A1	24	7	18	0	A'1	24	6	18	487.3436	0.133
0	A1	23	7	16	0	A2	24	8	17	0	A'2	24	8	17	463.0329	0.332
0	A2	24	7	17	0	A1	24	8	16	0	A'1	24	8	16	469.0824	0.158
0	A1	24	7	18	0	A2	24	8	17	0	A'2	24	8	17	468.2438	0.098
0	A1	25	7	18	0	A2	24	8	17	0	A'2	24	8	17	488.1258	0.332
0	A2	25	7	19	0	A1	24	8	16	0	A'1	24	8	16	474.2890	0.194
0	A1	24	1	24	0	A2	25	1	25	0	A'2	25	0	25	464.9907	0.349
0	A1	25	1	24	0	A2	25	1	25	0	A'2	25	0	25	485.0509	0.156
0	A1	26	1	26	0	A2	25	1	25	0	A'2	25	0	25	485.3032	0.497
0	A2	24	1	23	0	A1	25	2	24	0	A'1	25	2	24	465.0246	0.751
0	A2	24	3	21	0	A1	25	2	24	0	A'1	25	2	24	482.2509	0.342
0	A1	24	3	22	0	A2	25	3	23	0	A'2	25	2	23	464.2328	0.102
0	A1	25	1	24	0	A2	25	3	23	0	A'2	25	2	23	466.1928	0.157
0	A2	25	1	25	0	A1	25	2	24	0	A'1	25	2	24	465.3193	0.207
0	A1	25	3	22	0	A2	25	3	23	0	A'2	25	2	23	484.1971	0.503
0	A2	25	3	23	0	A1	25	2	24	0	A'1	25	2	24	484.2240	0.092
0	A2	26	1	25	0	A1	25	2	24	0	A'1	25	2	24	486.1975	0.281
0	A1	26	1	26	0	A2	25	3	23	0	A'2	25	2	23	466.4457	0.116
0	A1	26	3	24	0	A2	25	3	23	0	A'2	25	2	23	486.1655	0.510
0	A2	24	1	23	0	A1	25	4	22	0	A'1	25	4	22	446.9861	0.037
0	A2	24	3	21	0	A1	25	4	22	0	A'1	25	4	22	464.2087	0.395
0	A2	24	5	19	0	A1	25	4	22	0	A'1	25	4	22	479.8092	0.192
0	A1	24	5	20	0	A2	25	5	21	0	A'2	25	4	21	463.4610	0.196
0	A1	25	3	22	0	A2	25	5	21	0	A'2	25	4	21	466.9851	0.215
0	A2	25	3	23	0	A1	25	4	22	0	A'1	25	4	22	466.1860	0.091
0	A1	25	5	20	0	A2	25	5	21	0	A'2	25	4	21	483.3699	0.079
0	A2	25	5	21	0	A1	25	4	22	0	A'1	25	4	22	483.3779	0.421
0	A2	26	3	23	0	A1	25	4	22	0	A'1	25	4	22	486.9391	0.110
0	A1	26	3	24	0	A2	25	5	21	0	A'2	25	4	21	468.9534	0.094
0	A2	24	5	19	0	A1	25	6	20	0	A'1	25	6	20	463.4245	0.128
0	A2	24	7	17	0	A1	25	6	20	0	A'1	25	6	20	477.3391	0.011
0	A1	25	5	20	0	A2	25	7	19	0	A'2	25	6	19	467.8334	0.203
0	A2	25	5	21	0	A1	25	6	20	0	A'1	25	6	20	466.9951	0.149

Excited state					Ground state [a]					Ground state [b]						
m′	*Γ′*	*J′*	*Ka′*	*Kc′*	*m″*	*Γ″*	*J″*	*Ka″*	*Kc″*	*m″*	*Γ″*	*J″*	*Ka″*	*Kc″*	Wavenumber cm^{-1}	Intensity
0	A2	25	7	19	0	A1	25	6	20	0	A'1	25	6	20	482.5451	0.272
0	A2	26	5	21	0	A1	25	6	20	0	A'1	25	6	20	487.7394	0.138
0	A1	26	5	22	0	A2	25	7	19	0	A'2	25	6	19	471.3945	0.144
0	A2	24	7	17	0	A1	25	8	18	0	A'1	25	8	18	462.6433	0.209
0	A2	25	7	19	0	A1	25	8	18	0	A'1	25	8	18	467.8497	0.068
0	A2	25	1	25	0	A1	26	1	26	0	A'1	26	0	26	464.5663	0.320
0	A2	26	1	25	0	A1	26	1	26	0	A'1	26	0	26	485.4437	0.328
0	A2	27	1	27	0	A1	26	1	26	0	A'1	26	0	26	485.6591	0.392
0	A1	25	1	24	0	A2	26	2	25	0	A'2	26	2	25	464.6376	0.067
0	A2	25	1	25	0	A1	26	3	24	0	A'1	26	2	24	444.9211	0.097
0	A1	25	3	22	0	A2	26	2	25	0	A'2	26	2	25	482.6408	0.033
0	A2	25	3	23	0	A1	26	3	24	0	A'1	26	2	24	463.8268	0.179
0	A2	26	1	25	0	A1	26	3	24	0	A'1	26	2	24	464.2477	0.085
0	A2	26	1	25	0	A1	26	3	24	0	A'1	26	2	24	465.8015	0.234
0	A1	26	1	26	0	A2	26	2	25	0	A'2	26	2	25	464.8903	0.749
0	A2	26	3	23	0	A1	26	3	24	0	A'1	26	2	24	484.5796	0.443
0	A1	27	1	26	0	A2	26	2	25	0	A'2	26	2	25	486.5953	0.757
0	A2	27	1	27	0	A1	26	3	24	0	A'1	26	2	24	466.0141	0.100
0	A1	27	3	24	0	A2	26	2	25	0	A'2	26	2	25	506.1780	0.019
0	A2	27	3	25	0	A1	26	3	24	0	A'1	26	2	24	486.5500	0.167
0	A1	25	3	22	0	A2	26	4	23	0	A'2	26	4	23	463.8171	0.064
0	A1	25	5	20	0	A2	26	4	23	0	A'2	26	4	23	480.2048	0.086
0	A2	25	5	21	0	A1	26	5	22	0	A'1	26	4	22	463.0209	0.475
0	A2	26	3	23	0	A1	26	5	22	0	A'1	26	4	22	466.5805	0.751
0	A1	26	3	24	0	A2	26	4	23	0	A'2	26	4	23	465.7868	0.076
0	A2	26	5	21	0	A1	26	5	22	0	A'1	26	4	22	483.7649	0.256
0	A1	26	5	22	0	A2	26	4	23	0	A'2	26	4	23	483.7649	0.256
0	A1	27	3	24	0	A2	26	4	23	0	A'2	26	4	23	487.3543	0.074
0	A2	27	3	25	0	A1	26	5	22	0	A'1	26	4	22	468.5494	0.172
0	A2	27	5	23	0	A1	26	5	22	0	A'1	26	4	22	487.3009	0.108
0	A1	25	5	20	0	A2	26	6	21	0	A'2	26	6	21	463.0329	0.332
0	A1	25	7	18	0	A2	26	6	21	0	A'2	26	6	21	477.7171	0.098
0	A2	26	5	21	0	A1	26	7	20	0	A'1	26	6	20	467.4205	0.301
0	A1	26	5	22	0	A2	26	6	21	0	A'2	26	6	21	466.5937	0.105
0	A1	26	7	20	0	A2	26	6	21	0	A'2	26	6	21	482.9123	0.313
0	A1	27	5	22	0	A2	26	6	21	0	A'2	26	6	21	488.1491	0.430
0	A2	27	5	23	0	A1	26	7	20	0	A'1	26	6	20	470.9574	0.191
0	A2	27	7	21	0	A1	26	7	20	0	A'1	26	6	20	488.0708	0.051
0	A1	25	7	18	0	A2	26	8	19	0	A'2	26	8	19	462.2585	0.038
0	A2	26	7	19	0	A1	26	9	18	0	A'1	26	8	18	468.3317	0.612
0	A1	26	7	20	0	A2	26	8	19	0	A'2	26	8	19	467.4525	0.164
0	A1	27	7	20	0	A2	26	8	19	0	A'2	26	8	19	488.9900	0.132
0	A1	26	1	26	0	A2	27	1	27	0	A'2	27	0	27	464.1398	0.285
0	A1	27	1	26	0	A2	27	1	27	0	A'2	27	0	27	485.8435	0.082
0	A1	28	1	28	0	A2	27	1	27	0	A'2	27	0	27	486.0143	0.486
0	A1	26	1	26	0	A2	27	3	25	0	A'2	27	2	25	443.7080	0.018
0	A2	26	3	23	0	A1	27	2	26	0	A'1	27	2	26	483.0280	0.165
0	A1	27	1	26	0	A2	27	3	25	0	A'2	27	2	25	465.4130	0.201
0	A2	27	1	27	0	A1	27	2	26	0	A'1	27	2	26	464.4613	0.111
0	A1	27	3	24	0	A2	27	3	25	0	A'2	27	2	25	484.9954	0.439
0	A2	27	3	25	0	A1	27	2	26	0	A'1	27	2	26	484.9954	0.439
0	A2	28	1	27	0	A1	27	2	26	0	A'1	27	2	26	486.9906	0.114

Excited state					Ground state [a]					Ground state [b]						
m′	*Γ′*	*J′*	*Ka′*	*Kc′*	*m″*	*Γ″*	*J″*	*Ka″*	*Kc″*	*m″*	*Γ″*	*J″*	*Ka″*	*Kc″*	Wavenumber cm^{-1}	Intensity
0	A1	28	1	28	0	A2	27	3	25	0	A'2	27	2	25	465.5830	0.275
0	A1	28	3	26	0	A2	27	3	25	0	A'2	27	2	25	486.9249	0.269
0	A2	26	3	23	0	A1	27	4	24	0	A'1	27	4	24	463.4156	0.069
0	A2	26	5	21	0	A1	27	4	24	0	A'1	27	4	24	480.6027	0.311
0	A1	26	5	22	0	A2	27	5	23	0	A'2	27	4	23	462.6207	0.148
0	A1	27	3	24	0	A2	27	5	23	0	A'2	27	4	23	466.2098	0.061
0	A2	27	3	25	0	A1	27	4	24	0	A'1	27	4	24	465.3837	0.084
0	A1	27	5	22	0	A2	27	5	23	0	A'2	27	4	23	484.1760	0.080
0	A2	27	5	23	0	A1	27	4	24	0	A'1	27	4	24	484.1363	0.188
0	A2	28	3	25	0	A1	27	4	24	0	A'1	27	4	24	487.7514	0.575
0	A1	28	3	26	0	A2	27	5	23	0	A'2	27	4	23	468.1372	0.137
0	A1	28	5	24	0	A2	27	5	23	0	A'2	27	4	23	487.6662	0.286
0	A2	26	3	23	0	A1	27	6	22	0	A'1	27	6	22	445.4568	0.058
0	A2	26	5	21	0	A1	27	6	22	0	A'1	27	6	22	462.6433	0.209
0	A2	26	7	19	0	A1	27	6	22	0	A'1	27	6	22	478.1765	0.142
0	A1	26	7	20	0	A2	27	7	21	0	A'2	27	6	21	461.8115	0.051
0	A1	27	5	22	0	A2	27	7	21	0	A'2	27	6	21	467.0477	0.065
0	A2	27	5	23	0	A1	27	6	22	0	A'1	27	6	22	466.1776	0.591
0	A1	27	7	20	0	A2	27	7	21	0	A'2	27	6	21	483.3490	0.263
0	A2	27	7	21	0	A1	27	6	22	0	A'1	27	6	22	483.2944	0.398
0	A2	28	5	23	0	A1	27	6	22	0	A'1	27	6	22	488.5441	0.136
0	A1	28	5	24	0	A2	27	7	21	0	A'2	27	6	21	470.5365	0.066
0	A1	28	7	22	0	A2	27	7	21	0	A'2	27	6	21	488.4260	0.186
0	A1	26	7	20	0	A2	27	9	19	0	A'2	27	8	19	446.4676	0.066
0	A1	27	7	20	0	A2	27	9	19	0	A'2	27	8	19	468.0060	0.126
0	A2	27	7	21	0	A1	27	8	20	0	A'1	27	8	20	466.9932	0.083
0	A2	28	7	21	0	A1	27	8	20	0	A'1	27	8	20	489.3357	0.308
0	A1	28	7	22	0	A2	27	9	19	0	A'2	27	8	19	473.0831	0.110
0	A2	26	7	19	0	A1	27	10	18	0	A'1	27	10	18	447.3296	0.070
0	A2	27	1	27	0	A1	28	1	28	0	A'1	28	0	28	463.7123	0.249
0	A2	28	1	27	0	A1	28	1	28	0	A'1	28	0	28	486.2420	0.214
0	A2	29	1	29	0	A1	28	1	28	0	A'1	28	0	28	486.3666	0.425
0	A1	27	1	26	0	A2	28	2	27	0	A'2	28	2	27	463.8616	0.101
0	A2	27	1	27	0	A1	28	3	26	0	A'1	28	2	26	442.4945	0.025
0	A1	27	3	24	0	A2	28	2	27	0	A'2	28	2	27	483.4437	0.140
0	A2	27	3	25	0	A1	28	3	26	0	A'1	28	2	26	463.0289	0.273
0	A2	28	1	27	0	A1	28	3	26	0	A'1	28	2	26	465.0240	0.347
0	A1	28	1	28	0	A2	28	2	27	0	A'2	28	2	27	464.0306	0.141
0	A2	28	3	25	0	A1	28	3	26	0	A'1	28	2	26	485.3966	0.184
0	A1	28	3	26	0	A2	28	2	27	0	A'2	28	2	27	485.3724	0.442
0	A1	29	1	28	0	A2	28	2	27	0	A'2	28	2	27	487.3896	0.464
0	A2	29	1	29	0	A1	28	3	26	0	A'1	28	2	26	465.1484	0.201
0	A2	29	3	27	0	A1	28	3	26	0	A'1	28	2	26	487.2863	0.100
0	A1	27	3	24	0	A2	28	4	25	0	A'2	28	4	25	463.0471	0.130
0	A1	27	5	22	0	A2	28	4	25	0	A'2	28	4	25	481.0141	0.229
0	A2	27	5	23	0	A1	28	5	24	0	A'1	28	4	24	462.2085	0.056
0	A2	28	3	25	0	A1	28	5	24	0	A'1	28	4	24	465.8255	0.392
0	A1	28	3	26	0	A2	28	4	25	0	A'2	28	4	25	464.9750	0.036
0	A2	28	5	23	0	A1	28	5	24	0	A'1	28	4	24	484.5741	0.055
0	A1	28	5	24	0	A2	28	4	25	0	A'2	28	4	25	484.5037	0.202
0	A1	29	3	26	0	A2	28	4	25	0	A'2	28	4	25	488.1422	0.166
0	A2	29	3	27	0	A1	28	5	24	0	A'1	28	4	24	467.7149	0.086

Excited state					Ground state [a]					Ground state [b]						
m′	*Γ′*	*J′*	*Ka′*	*Kc′*	*m″*	*Γ″*	*J″*	*Ka″*	*Kc″*	*m″*	*Γ″*	*J″*	*Ka″*	*Kc″*	Wavenumber cm^{-1}	Intensity
0	A2	29	5	25	0	A1	28	5	24	0	A'1	28	4	24	488.0535	0.078
0	A1	27	5	22	0	A2	28	6	23	0	A'2	28	6	23	462.2703	0.084
0	A1	27	7	20	0	A2	28	6	23	0	A'2	28	6	23	478.5721	0.103
0	A2	27	7	21	0	A1	28	7	22	0	A'1	28	6	22	461.4089	0.324
0	A2	28	5	23	0	A1	28	7	22	0	A'1	28	6	22	466.6581	0.149
0	A1	28	5	24	0	A2	28	6	23	0	A'2	28	6	23	465.7608	0.201
0	A2	28	7	21	0	A1	28	7	22	0	A'1	28	6	22	483.7522	0.090
0	A1	28	7	22	0	A2	28	6	23	0	A'2	28	6	23	483.6494	0.172
0	A1	29	5	24	0	A2	28	6	23	0	A'2	28	6	23	488.8745	0.190
0	A2	29	5	25	0	A1	28	7	22	0	A'1	28	6	22	470.1377	0.130
0	A2	29	7	23	0	A1	28	7	22	0	A'1	28	6	22	488.7886	0.349
0	A1	27	5	22	0	A2	28	8	21	0	A'2	28	8	21	445.1857	0.094
0	A1	27	7	20	0	A2	28	8	21	0	A'2	28	8	21	461.4877	0.102
0	A2	27	7	21	0	A1	28	9	20	0	A'1	28	8	20	445.1627	0.238
0	A2	28	7	21	0	A1	28	9	20	0	A'1	28	8	20	467.5065	0.201
0	A1	28	7	22	0	A2	28	8	21	0	A'2	28	8	21	466.5649	0.534
0	A1	29	7	22	0	A2	28	8	21	0	A'2	28	8	21	489.7333	0.070
0	A2	29	7	23	0	A1	28	9	20	0	A'1	28	8	20	472.5418	0.245
0	A1	27	7	20	0	A2	28	10	19	0	A'2	28	10	19	446.2562	0.122
0	A1	28	1	28	0	A2	29	1	29	0	A'2	29	0	29	463.2840	0.281
0	A1	29	1	28	0	A2	29	1	29	0	A'2	29	0	29	486.6415	0.142
0	A1	30	1	30	0	A2	29	1	29	0	A'2	29	0	29	486.7185	0.375
0	A2	28	1	27	0	A1	29	2	28	0	A'1	29	2	28	463.4741	0.101
0	A1	28	1	28	0	A2	29	3	27	0	A'2	29	2	27	441.2790	0.026
0	A2	28	3	25	0	A1	29	2	28	0	A'1	29	2	28	483.8455	0.105
0	A1	28	3	26	0	A2	29	3	27	0	A'2	29	2	27	462.6207	0.148
0	A1	29	1	28	0	A2	29	3	27	0	A'2	29	2	27	464.6376	0.302
0	A2	29	1	29	0	A1	29	2	28	0	A'1	29	2	28	463.5988	0.179
0	A1	29	3	26	0	A2	29	3	27	0	A'2	29	2	27	485.7888	0.140
0	A2	29	3	27	0	A1	29	2	28	0	A'1	29	2	28	485.7373	0.808
0	A2	30	1	29	0	A1	29	2	28	0	A'1	29	2	28	487.7786	0.084
0	A1	30	1	30	0	A2	29	3	27	0	A'2	29	2	27	464.7142	0.077
0	A1	30	3	28	0	A2	29	3	27	0	A'2	29	2	27	487.6733	0.378
0	A2	28	3	25	0	A1	29	4	26	0	A'1	29	4	26	462.6626	0.079
0	A2	28	5	23	0	A1	29	4	26	0	A'1	29	4	26	481.4112	0.244
0	A1	28	5	24	0	A2	29	5	25	0	A'2	29	4	25	461.7987	0.427
0	A1	29	3	26	0	A2	29	5	25	0	A'2	29	4	25	465.4383	0.264
0	A2	29	3	27	0	A1	29	4	26	0	A'1	29	4	26	464.5523	0.086
0	A1	29	5	24	0	A2	29	5	25	0	A'2	29	4	25	484.9153	0.468
0	A2	29	5	25	0	A1	29	4	26	0	A'1	29	4	26	484.8919	0.317
0	A2	30	3	27	0	A1	29	4	26	0	A'1	29	4	26	488.5505	0.570
0	A1	30	3	28	0	A2	29	5	25	0	A'2	29	4	25	467.3229	0.068
0	A1	30	5	26	0	A2	29	5	25	0	A'2	29	4	25	488.4260	0.186
0	A2	28	5	23	0	A1	29	6	24	0	A'1	29	6	24	461.8869	0.166
0	A2	28	7	21	0	A1	29	6	24	0	A'1	29	6	24	478.9799	0.212
0	A1	28	7	22	0	A2	29	7	23	0	A'2	29	6	23	460.9798	0.218
0	A1	29	5	24	0	A2	29	7	23	0	A'2	29	6	23	466.2047	0.059
0	A2	29	5	25	0	A1	29	6	24	0	A'1	29	6	24	465.3667	0.130
0	A1	29	7	22	0	A2	29	7	23	0	A'2	29	6	23	484.1500	0.199
0	A1	30	5	26	0	A2	29	7	23	0	A'2	29	6	23	469.7187	0.158
0	A1	30	7	24	0	A2	29	7	23	0	A'2	29	6	23	489.0479	0.152
0	A1	28	7	22	0	A2	29	9	21	0	A'2	29	8	21	443.9475	0.158

Excited state					Ground state [a]					Ground state [b]						
m′	*Γ′*	*J′*	*Ka′*	*Kc′*	*m″*	*Γ″*	*J″*	*Ka″*	*Kc″*	*m″*	*Γ″*	*J″*	*Ka″*	*Kc″*	Wavenumber cm^{-1}	Intensity
0	A1	29	7	22	0	A2	29	9	21	0	A'2	29	8	21	467.1158	0.100
0	A2	29	7	23	0	A1	29	8	22	0	A'1	29	8	22	466.1431	0.095
0	A2	30	7	23	0	A1	29	8	22	0	A'1	29	8	22	490.1256	0.072
0	A1	30	7	24	0	A2	29	9	21	0	A'2	29	8	21	472.0166	0.256
0	A2	28	7	21	0	A1	29	10	20	0	A'1	29	10	20	444.9253	0.090
0	A2	29	1	29	0	A1	30	1	30	0	A'1	30	0	30	462.8536	0.463
0	A2	30	1	29	0	A1	30	1	30	0	A'1	30	0	30	487.0325	0.081
0	A2	31	1	31	0	A1	30	1	30	0	A'1	30	0	30	487.0688	0.460
0	A1	29	1	28	0	A2	30	2	29	0	A'2	30	2	29	463.0896	0.032
0	A1	29	3	26	0	A2	30	2	29	0	A'2	30	2	29	484.2396	0.279
0	A2	29	3	27	0	A1	30	3	28	0	A'1	30	2	28	462.2004	0.188
0	A2	30	1	29	0	A1	30	3	28	0	A'1	30	2	28	464.2408	0.045
0	A1	30	1	30	0	A2	30	2	29	0	A'2	30	2	29	463.1662	0.119
0	A2	30	3	27	0	A1	30	3	28	0	A'1	30	2	28	486.1975	0.281
0	A1	30	3	28	0	A2	30	2	29	0	A'2	30	2	29	486.1258	0.207
0	A2	31	1	31	0	A1	30	3	28	0	A'1	30	2	28	464.2786	0.109
0	A2	31	3	29	0	A1	30	3	28	0	A'1	30	2	28	488.9046	0.334
0	A1	29	3	26	0	A2	30	4	27	0	A'2	30	4	27	462.2703	0.139
0	A1	29	5	24	0	A2	30	4	27	0	A'2	30	4	27	481.7442	0.101
0	A2	29	5	25	0	A1	30	5	26	0	A'1	30	4	26	461.3857	0.065
0	A2	30	3	27	0	A1	30	5	26	0	A'1	30	4	26	465.0438	0.259
0	A1	30	3	28	0	A2	30	4	27	0	A'2	30	4	27	464.1555	0.167
0	A2	30	5	25	0	A1	30	5	26	0	A'1	30	4	26	485.4000	0.162
0	A1	30	5	26	0	A2	30	4	27	0	A'2	30	4	27	485.2595	0.198
0	A1	31	3	28	0	A2	30	4	27	0	A'2	30	4	27	488.9460	0.128
0	A2	31	3	29	0	A1	30	5	26	0	A'1	30	4	26	467.7502	0.115
0	A2	31	5	27	0	A1	30	5	26	0	A'1	30	4	26	488.7712	0.355
0	A1	29	5	24	0	A2	30	6	25	0	A'2	30	6	25	461.5074	0.477
0	A1	29	7	22	0	A2	30	6	25	0	A'2	30	6	25	479.4510	0.356
0	A2	29	7	23	0	A1	30	7	24	0	A'1	30	6	24	460.5670	0.058
0	A2	30	5	25	0	A1	30	7	24	0	A'1	30	6	24	465.9307	0.247
0	A1	30	5	26	0	A2	30	6	25	0	A'2	30	6	25	465.0210	0.347
0	A2	30	7	23	0	A1	30	7	24	0	A'1	30	6	24	484.5495	0.312
0	A1	30	7	24	0	A2	30	6	25	0	A'2	30	6	25	484.3516	0.323
0	A1	31	5	26	0	A2	30	6	25	0	A'2	30	6	25	489.8525	0.062
0	A2	31	5	27	0	A1	30	7	24	0	A'1	30	6	24	469.3006	0.145
0	A2	31	7	25	0	A1	30	7	24	0	A'1	30	6	24	489.5881	0.365
0	A1	29	5	24	0	A2	30	8	23	0	A'2	30	8	23	442.7748	0.075
0	A1	29	7	22	0	A2	30	8	23	0	A'2	30	8	23	460.7181	0.050
0	A2	30	7	23	0	A1	30	9	22	0	A'1	30	8	22	466.7215	0.161
0	A1	30	7	24	0	A2	30	8	23	0	A'2	30	8	23	465.6175	0.305
0	A1	31	7	24	0	A2	30	8	23	0	A'2	30	8	23	490.4204	0.101
0	A1	30	1	30	0	A2	31	1	31	0	A'2	31	0	31	462.4220	0.280
0	A1	31	1	30	0	A2	31	1	31	0	A'2	31	0	31	487.4179	0.429
0	A1	32	1	32	0	A2	31	1	31	0	A'2	31	0	31	487.4179	0.429
0	A2	30	1	29	0	A1	31	2	30	0	A'1	31	2	30	462.6948	0.559
0	A2	30	3	27	0	A1	31	2	30	0	A'1	31	2	30	484.6510	0.478
0	A1	30	3	28	0	A2	31	3	29	0	A'2	31	2	29	461.8045	0.154
0	A1	31	1	30	0	A2	31	3	29	0	A'2	31	2	29	463.8403	0.145
0	A2	31	1	31	0	A1	31	2	30	0	A'1	31	2	30	462.7310	0.198
0	A1	31	3	28	0	A2	31	3	29	0	A'2	31	2	29	486.5941	0.331
0	A2	32	1	31	0	A1	31	2	30	0	A'1	31	2	30	488.5634	0.230

Excited state					Ground state [a]					Ground state [b]						
m′	*Γ′*	*J′*	*Ka′*	*Kc′*	*m″*	*Γ″*	*J″*	*Ka″*	*Kc″*	*m″*	*Γ″*	*J″*	*Ka″*	*Kc″*	Wavenumber cm^{-1}	Intensity
0	A1	32	1	32	0	A2	31	3	29	0	A'2	31	2	29	463.8403	0.145
0	A1	32	3	30	0	A2	31	3	29	0	A'2	31	2	29	489.2651	0.452
0	A2	30	3	27	0	A1	31	4	28	0	A'1	31	4	28	461.8958	0.149
0	A2	30	5	25	0	A1	31	4	28	0	A'1	31	4	28	482.2509	0.342
0	A1	30	5	26	0	A2	31	5	27	0	A'2	31	4	27	460.9719	0.226
0	A1	31	3	28	0	A2	31	5	27	0	A'2	31	4	27	464.6584	0.211
0	A2	31	3	29	0	A1	31	4	28	0	A'1	31	4	28	464.6019	0.120
0	A1	31	5	26	0	A2	31	5	27	0	A'2	31	4	27	485.8032	0.083
0	A2	31	5	27	0	A1	31	4	28	0	A'1	31	4	28	485.6221	0.669
0	A2	32	3	29	0	A1	31	4	28	0	A'1	31	4	28	489.3401	0.091
0	A1	32	3	30	0	A2	31	5	27	0	A'2	31	4	27	467.3302	0.054
0	A1	32	5	28	0	A2	31	5	27	0	A'2	31	4	27	489.1372	0.124
0	A2	30	5	25	0	A1	31	6	26	0	A'1	31	6	26	461.1287	0.031
0	A2	30	7	23	0	A1	31	6	26	0	A'1	31	6	26	479.7488	0.125
0	A1	31	5	26	0	A2	31	7	25	0	A'2	31	6	25	465.6557	0.284
0	A2	31	5	27	0	A1	31	6	26	0	A'1	31	6	26	464.4992	0.106
0	A2	31	7	25	0	A1	31	6	26	0	A'1	31	6	26	484.7874	0.113
0	A2	32	5	27	0	A1	31	6	26	0	A'1	31	6	26	490.1519	0.304
0	A1	32	5	28	0	A2	31	7	25	0	A'2	31	6	25	468.9915	0.137
0	A1	32	7	26	0	A2	31	7	25	0	A'2	31	6	25	490.0505	0.324
0	A2	30	7	23	0	A1	31	8	24	0	A'1	31	8	24	460.3347	0.137
0	A1	31	7	24	0	A2	31	9	23	0	A'2	31	8	23	466.2307	0.039
0	A2	31	7	25	0	A1	31	8	24	0	A'1	31	8	24	465.3742	0.205
0	A2	32	7	25	0	A1	31	8	24	0	A'1	31	8	24	490.9768	0.288
0	A1	32	7	26	0	A2	31	9	23	0	A'2	31	8	23	471.3230	0.053
0	A2	31	1	31	0	A1	32	1	32	0	A'1	32	0	32	461.9891	0.308
0	A2	32	1	31	0	A1	32	1	32	0	A'1	32	0	32	487.8212	0.324
0	A2	33	1	33	0	A1	32	1	32	0	A'1	32	0	32	487.7654	0.555
0	A1	31	1	30	0	A2	32	2	31	0	A'2	32	2	31	462.2957	0.074
0	A1	31	3	28	0	A2	32	2	31	0	A'2	32	2	31	485.0483	0.302
0	A2	31	3	29	0	A1	32	3	30	0	A'1	32	2	30	462.2523	0.070
0	A2	32	1	31	0	A1	32	3	30	0	A'1	32	2	30	463.4585	0.322
0	A1	32	1	32	0	A2	32	2	31	0	A'2	32	2	31	462.2957	0.074
0	A2	32	3	29	0	A1	32	3	30	0	A'1	32	2	30	486.9906	0.114
0	A1	32	3	30	0	A2	32	2	31	0	A'2	32	2	31	487.7207	0.091
0	A1	33	1	32	0	A2	32	2	31	0	A'2	32	2	31	488.9575	0.058
0	A2	33	1	33	0	A1	32	3	30	0	A'1	32	2	30	463.4024	0.106
0	A2	33	3	31	0	A1	32	3	30	0	A'1	32	2	30	489.6387	0.147
0	A1	31	3	28	0	A2	32	4	29	0	A'2	32	4	29	461.5074	0.477
0	A1	31	5	26	0	A2	32	4	29	0	A'2	32	4	29	482.6530	0.254
0	A2	32	3	29	0	A1	32	5	28	0	A'1	32	4	28	464.2697	0.078
0	A1	32	3	30	0	A2	32	4	29	0	A'2	32	4	29	464.1796	0.121
0	A2	32	5	27	0	A1	32	5	28	0	A'1	32	4	28	486.2031	0.070
0	A1	32	5	28	0	A2	32	4	29	0	A'2	32	4	29	485.9878	0.076
0	A1	33	3	30	0	A2	32	4	29	0	A'2	32	4	29	489.7384	0.105
0	A2	33	3	31	0	A1	32	5	28	0	A'1	32	4	28	466.9183	0.151
0	A2	33	5	29	0	A1	32	5	28	0	A'1	32	4	28	489.4944	0.273
0	A1	31	5	26	0	A2	32	6	27	0	A'2	32	6	27	460.7511	0.096
0	A1	31	7	24	0	A2	32	6	27	0	A'2	32	6	27	480.0517	0.209
0	A2	31	7	25	0	A1	32	7	26	0	A'1	32	6	26	459.7514	0.653
0	A2	32	5	27	0	A1	32	7	26	0	A'1	32	6	26	465.1158	0.244
0	A1	32	5	28	0	A2	32	6	27	0	A'2	32	6	27	464.0865	0.257

Excited state					Ground state [a]					Ground state [b]						
m′	*Γ′*	*J′*	*Ka′*	*Kc′*	*m″*	*Γ″*	*J″*	*Ka″*	*Kc″*	*m″*	*Γ″*	*J″*	*Ka″*	*Kc″*	Wavenumber cm^{-1}	Intensity
0	A2	32	7	25	0	A1	32	7	26	0	A'1	32	6	26	485.3549	0.382
0	A1	32	7	26	0	A2	32	6	27	0	A'2	32	6	27	485.1458	0.235
0	A1	33	5	28	0	A2	32	6	27	0	A'2	32	6	27	490.5563	0.118
0	A2	33	5	29	0	A1	32	7	26	0	A'1	32	6	26	468.4078	0.130
0	A2	33	7	27	0	A1	32	7	26	0	A'1	32	6	26	490.2558	0.150
0	A1	31	7	24	0	A2	32	8	25	0	A'2	32	8	25	459.9478	0.096
0	A2	32	7	25	0	A1	32	9	24	0	A'1	32	8	24	465.9994	0.156
0	A1	32	7	26	0	A2	32	8	25	0	A'2	32	8	25	465.0423	0.230
0	A1	33	7	26	0	A2	32	8	25	0	A'2	32	8	25	491.4659	0.346
0	A2	33	7	27	0	A1	32	9	24	0	A'1	32	8	24	470.9015	0.159
0	A1	32	1	32	0	A2	33	1	33	0	A'2	33	0	33	461.5551	0.330
0	A1	33	1	32	0	A2	33	1	33	0	A'2	33	0	33	488.2179	0.408
0	A1	34	1	34	0	A2	33	1	33	0	A'2	33	0	33	488.1829	0.747
0	A2	32	1	31	0	A1	33	2	32	0	A'1	33	2	32	461.9146	0.139
0	A2	32	3	29	0	A1	33	2	32	0	A'1	33	2	32	485.4472	0.280
0	A1	32	3	30	0	A2	33	3	31	0	A'2	33	2	31	461.8307	0.121
0	A1	33	1	32	0	A2	33	3	31	0	A'2	33	2	31	463.0715	0.143
0	A2	33	1	33	0	A1	33	2	32	0	A'1	33	2	32	461.8583	0.074
0	A1	33	3	30	0	A2	33	3	31	0	A'2	33	2	31	487.3896	0.464
0	A2	33	3	31	0	A1	33	2	32	0	A'1	33	2	32	488.0957	0.177
0	A2	34	1	33	0	A1	33	2	32	0	A'1	33	2	32	489.3452	0.391
0	A1	34	1	34	0	A2	33	3	31	0	A'2	33	2	31	462.9620	0.023
0	A1	34	3	32	0	A2	33	3	31	0	A'2	33	2	31	490.0059	0.059
0	A2	32	3	29	0	A1	33	4	30	0	A'1	33	4	30	461.1198	0.221
0	A2	32	5	27	0	A1	33	4	30	0	A'1	33	4	30	483.0511	0.549
0	A1	32	5	28	0	A2	33	5	29	0	A'2	33	4	29	460.1350	0.155
0	A1	33	3	30	0	A2	33	5	29	0	A'2	33	4	29	463.8840	0.057
0	A1	33	5	28	0	A2	33	5	29	0	A'2	33	4	29	486.5996	0.349
0	A2	34	3	31	0	A1	33	4	30	0	A'1	33	4	30	490.1334	0.265
0	A1	34	3	32	0	A2	33	5	29	0	A'2	33	4	29	466.4983	0.420
0	A1	34	5	30	0	A2	33	5	29	0	A'2	33	4	29	489.8584	0.259
0	A2	32	5	27	0	A1	33	6	28	0	A'1	33	6	28	460.3667	0.121
0	A2	32	7	25	0	A1	33	6	28	0	A'1	33	6	28	480.6065	0.174
0	A1	33	5	28	0	A2	33	7	27	0	A'2	33	6	27	464.7405	0.259
0	A2	33	5	29	0	A1	33	6	28	0	A'1	33	6	28	463.6591	0.081
0	A1	33	7	26	0	A2	33	7	27	0	A'2	33	6	27	485.7531	0.127
0	A2	34	5	29	0	A1	33	6	28	0	A'1	33	6	28	490.9560	0.149
0	A1	34	5	30	0	A2	33	7	27	0	A'2	33	6	27	467.9948	0.283
0	A2	32	7	25	0	A1	33	8	26	0	A'1	33	8	26	459.5637	0.104
0	A1	33	7	26	0	A2	33	9	25	0	A'2	33	8	25	465.6979	0.213
0	A2	33	7	27	0	A1	33	8	26	0	A'1	33	8	26	464.4640	0.160
0	A2	34	7	27	0	A1	33	8	26	0	A'1	33	8	26	491.7072	0.188
0	A1	34	7	28	0	A2	33	9	25	0	A'2	33	8	25	470.5718	0.096
0	A2	33	1	33	0	A1	34	1	34	0	A'1	34	0	34	461.1198	0.221
0	A2	34	1	33	0	A1	34	1	34	0	A'1	34	0	34	488.6067	0.259
0	A2	35	1	35	0	A1	34	1	34	0	A'1	34	0	34	488.4564	0.465
0	A1	33	1	32	0	A2	34	2	33	0	A'2	34	2	33	461.5254	0.478
0	A2	33	3	31	0	A1	34	3	32	0	A'1	34	2	32	461.4199	0.398
0	A2	34	1	33	0	A1	34	3	32	0	A'1	34	2	32	462.6719	0.123
0	A1	34	1	34	0	A2	34	2	33	0	A'2	34	2	33	461.4199	0.398
0	A2	34	3	31	0	A1	34	3	32	0	A'1	34	2	32	487.7855	0.047
0	A1	34	3	32	0	A2	34	2	33	0	A'2	34	2	33	488.4652	0.421

Excited state					Ground state [a]					Ground state [b]						
m′	*Γ′*	*J′*	*Ka′*	*Kc′*	*m″*	*Γ″*	*J″*	*Ka″*	*Kc″*	*m″*	*Γ″*	*J″*	*Ka″*	*Kc″*	Wavenumber cm^{-1}	Intensity
0	A1	35	1	34	0	A2	34	2	33	0	A'2	34	2	33	489.7333	0.070
0	A2	35	1	35	0	A1	34	3	32	0	A'1	34	2	32	462.5210	0.129
0	A2	35	3	33	0	A1	34	3	32	0	A'1	34	2	32	490.3767	0.156
0	A1	33	3	30	0	A2	34	4	31	0	A'2	34	4	31	460.7355	0.224
0	A1	33	5	28	0	A2	34	4	31	0	A'2	34	4	31	483.4558	0.204
0	A2	33	5	29	0	A1	34	5	30	0	A'1	34	4	30	459.7069	0.525
0	A2	34	3	31	0	A1	34	5	30	0	A'1	34	4	30	463.4972	0.298
0	A1	34	3	32	0	A2	34	4	31	0	A'2	34	4	31	463.3521	0.194
0	A2	34	5	29	0	A1	34	5	30	0	A'1	34	4	30	487.0035	0.118
0	A1	34	5	30	0	A2	34	4	31	0	A'2	34	4	31	486.7105	0.343
0	A1	35	3	32	0	A2	34	4	31	0	A'2	34	4	31	490.5287	0.117
0	A2	35	3	33	0	A1	34	5	30	0	A'1	34	4	30	466.0871	0.144
0	A1	33	5	28	0	A2	34	6	29	0	A'2	34	6	29	459.9858	0.152
0	A1	33	7	26	0	A2	34	6	29	0	A'2	34	6	29	480.9999	0.231
0	A2	33	7	27	0	A1	34	7	28	0	A'1	34	6	28	458.9092	0.165
0	A2	34	5	29	0	A1	34	7	28	0	A'1	34	6	28	464.3580	0.230
0	A1	34	5	30	0	A2	34	6	29	0	A'2	34	6	29	463.2386	0.170
0	A2	34	7	27	0	A1	34	7	28	0	A'1	34	6	28	486.1516	0.164
0	A1	34	7	28	0	A2	34	6	29	0	A'2	34	6	29	485.8747	0.377
0	A1	35	5	30	0	A2	34	6	29	0	A'2	34	6	29	491.3535	0.214
0	A2	35	5	31	0	A1	34	7	28	0	A'1	34	6	28	467.5783	0.153
0	A2	35	7	29	0	A1	34	7	28	0	A'1	34	6	28	491.0067	0.089
0	A1	33	7	26	0	A2	34	8	27	0	A'2	34	8	27	459.1806	0.066
0	A2	34	7	27	0	A1	34	9	26	0	A'1	34	8	26	465.1684	0.308
0	A1	34	7	28	0	A2	34	8	27	0	A'2	34	8	27	464.0559	0.174
0	A2	35	7	29	0	A1	34	9	26	0	A'1	34	8	26	470.0230	0.145
0	A1	34	1	34	0	A2	35	1	35	0	A'2	35	0	35	460.6830	0.187
0	A1	35	1	34	0	A2	35	1	35	0	A'2	35	0	35	488.9963	0.419
0	A1	36	1	36	0	A2	35	1	35	0	A'2	35	0	35	488.8001	0.382
0	A2	34	1	33	0	A1	35	2	34	0	A'1	35	2	34	461.1307	0.183
0	A1	34	3	32	0	A2	35	3	33	0	A'2	35	2	33	461.0065	0.048
0	A1	35	1	34	0	A2	35	3	33	0	A'2	35	2	33	462.2747	0.079
0	A2	35	1	35	0	A1	35	2	34	0	A'1	35	2	34	460.9798	0.218
0	A1	35	3	32	0	A2	35	3	33	0	A'2	35	2	33	488.1829	0.747
0	A2	35	3	33	0	A1	35	2	34	0	A'1	35	2	34	488.8345	0.237
0	A2	36	1	35	0	A1	35	2	34	0	A'1	35	2	34	490.1297	0.195
0	A1	36	1	36	0	A2	35	3	33	0	A'2	35	2	33	462.0797	0.096
0	A1	36	3	34	0	A2	35	3	33	0	A'2	35	2	33	491.4528	0.209
0	A2	34	3	31	0	A1	35	4	32	0	A'1	35	4	32	460.3488	0.312
0	A2	34	5	29	0	A1	35	4	32	0	A'1	35	4	32	483.8566	0.346
0	A1	34	5	30	0	A2	35	5	31	0	A'2	35	4	31	459.2890	0.494
0	A1	35	3	32	0	A2	35	5	31	0	A'2	35	4	31	463.1111	0.175
0	A1	35	5	30	0	A2	35	5	31	0	A'2	35	4	31	487.4038	0.058
0	A2	35	5	31	0	A1	35	4	32	0	A'1	35	4	32	487.0785	0.123
0	A2	36	3	33	0	A1	35	4	32	0	A'1	35	4	32	490.9201	0.280
0	A1	36	3	34	0	A2	35	5	31	0	A'2	35	4	31	465.6792	0.129
0	A1	36	5	32	0	A2	35	5	31	0	A'2	35	4	31	490.5839	0.364
0	A2	34	5	29	0	A1	35	6	30	0	A'1	35	6	30	459.6018	0.581
0	A2	34	7	27	0	A1	35	6	30	0	A'1	35	6	30	481.3953	0.223
0	A1	34	7	28	0	A2	35	7	29	0	A'2	35	6	29	458.4928	0.560
0	A1	35	5	30	0	A2	35	7	29	0	A'2	35	6	29	463.9721	0.329
0	A2	35	5	31	0	A1	35	6	30	0	A'1	35	6	30	462.8229	0.149

Excited state					Ground state [a]					Ground state [b]						
m′	*Γ′*	*J′*	*Ka′*	*Kc′*	*m″*	*Γ″*	*J″*	*Ka″*	*Kc″*	*m″*	*Γ″*	*J″*	*Ka″*	*Kc″*	Wavenumber cm^{-1}	Intensity
0	A1	35	7	28	0	A2	35	7	29	0	A'2	35	6	29	486.5481	0.247
0	A2	35	7	29	0	A1	35	6	30	0	A'1	35	6	30	486.2514	0.171
0	A2	36	5	31	0	A1	35	6	30	0	A'1	35	6	30	491.7475	0.279
0	A1	36	5	32	0	A2	35	7	29	0	A'2	35	6	29	467.1523	0.092
0	A1	36	7	30	0	A2	35	7	29	0	A'2	35	6	29	491.3795	0.075
0	A2	34	7	27	0	A1	35	8	28	0	A'1	35	8	28	458.7937	0.096
0	A2	36	7	29	0	A1	35	8	28	0	A'1	35	8	28	492.5097	0.239
0	A1	36	7	30	0	A2	35	9	27	0	A'2	35	8	27	469.6166	0.225
0	A2	35	1	35	0	A1	36	1	36	0	A'1	36	0	36	460.2450	0.146
0	A2	36	1	35	0	A1	36	1	36	0	A'1	36	0	36	489.3934	0.123
0	A2	37	1	37	0	A1	36	1	36	0	A'1	36	0	36	489.1419	0.363
0	A1	35	1	34	0	A2	36	2	35	0	A'2	36	2	35	460.7355	0.047
0	A1	35	3	32	0	A2	36	2	35	0	A'2	36	2	35	486.6437	0.230
0	A2	35	3	33	0	A1	36	3	34	0	A'1	36	2	34	460.5930	0.253
0	A2	36	1	35	0	A1	36	3	34	0	A'1	36	2	34	461.8856	0.170
0	A1	36	1	36	0	A2	36	2	35	0	A'2	36	2	35	460.5393	0.118
0	A2	36	3	33	0	A1	36	3	34	0	A'1	36	2	34	488.5741	0.267
0	A1	36	3	34	0	A2	36	2	35	0	A'2	36	2	35	489.2131	0.078
0	A1	37	1	36	0	A2	36	2	35	0	A'2	36	2	35	490.5184	0.109
0	A2	37	1	37	0	A1	36	3	34	0	A'1	36	2	34	461.6343	0.041
0	A2	37	3	35	0	A1	36	3	34	0	A'1	36	2	34	491.1257	0.070
0	A1	35	3	32	0	A2	36	4	33	0	A'2	36	4	33	459.9646	0.237
0	A1	35	5	30	0	A2	36	4	33	0	A'2	36	4	33	484.2600	0.065
0	A2	35	5	31	0	A1	36	5	32	0	A'1	36	4	32	458.8757	0.219
0	A2	36	3	33	0	A1	36	5	32	0	A'1	36	4	32	462.7180	0.163
0	A1	36	3	34	0	A2	36	4	33	0	A'2	36	4	33	462.5335	0.156
0	A2	36	5	31	0	A1	36	5	32	0	A'1	36	4	32	487.7997	0.167
0	A1	36	5	32	0	A2	36	4	33	0	A'2	36	4	33	487.4398	0.155
0	A1	37	3	34	0	A2	36	4	33	0	A'2	36	4	33	491.3685	0.200
0	A2	37	3	35	0	A1	36	5	32	0	A'1	36	4	32	465.2675	0.052
0	A1	35	5	30	0	A2	36	6	31	0	A'2	36	6	31	459.2184	0.261
0	A1	35	7	28	0	A2	36	6	31	0	A'2	36	6	31	481.7964	0.148
0	A2	35	7	29	0	A1	36	7	30	0	A'1	36	6	30	458.0845	0.094
0	A2	36	5	31	0	A1	36	7	30	0	A'1	36	6	30	463.5814	0.164
0	A1	36	5	32	0	A2	36	6	31	0	A'2	36	6	31	462.3987	0.248
0	A2	36	7	29	0	A1	36	7	30	0	A'1	36	6	30	486.9466	0.049
0	A1	36	7	30	0	A2	36	6	31	0	A'2	36	6	31	486.6253	0.030
0	A1	37	5	32	0	A2	36	6	31	0	A'2	36	6	31	492.1356	0.078
0	A2	37	5	33	0	A1	36	7	30	0	A'1	36	6	30	466.7259	0.207
0	A2	37	7	31	0	A1	36	7	30	0	A'1	36	6	30	491.7403	0.227
0	A1	35	7	28	0	A2	36	8	29	0	A'2	36	8	29	458.4069	0.117
0	A1	37	7	30	0	A2	36	8	29	0	A'2	36	8	29	492.9166	0.225
0	A2	37	7	31	0	A1	36	9	28	0	A'1	36	8	28	469.1933	0.302
0	A1	36	1	36	0	A2	37	1	37	0	A'2	37	0	37	459.8060	0.162
0	A1	37	1	36	0	A2	37	1	37	0	A'2	37	0	37	489.7852	0.125
0	A1	38	1	38	0	A2	37	1	37	0	A'2	37	0	37	489.4824	0.431
0	A2	36	1	35	0	A1	37	2	36	0	A'1	37	2	36	460.3488	0.312
0	A2	36	3	33	0	A1	37	2	36	0	A'1	37	2	36	487.0373	0.420
0	A1	36	3	34	0	A2	37	3	35	0	A'2	37	2	35	460.1868	0.572
0	A1	37	1	36	0	A2	37	3	35	0	A'2	37	2	35	461.4913	0.126
0	A2	37	1	37	0	A1	37	2	36	0	A'1	37	2	36	460.0962	0.109
0	A1	37	3	34	0	A2	37	3	35	0	A'2	37	2	35	489.0223	0.221

Excited state					Ground state [a]					Ground state [b]						
m′	*Γ′*	*J′*	*Ka′*	*Kc′*	*m″*	*Γ″*	*J″*	*Ka″*	*Kc″*	*m″*	*Γ″*	*J″*	*Ka″*	*Kc″*	Wavenumber cm^{-1}	Intensity
0	A2	37	3	35	0	A1	37	2	36	0	A'1	37	2	36	489.5861	0.365
0	A2	38	1	37	0	A1	37	2	36	0	A'1	37	2	36	490.9119	0.054
0	A1	38	1	38	0	A2	37	3	35	0	A'2	37	2	35	461.1879	0.121
0	A1	38	3	36	0	A2	37	3	35	0	A'2	37	2	35	491.4922	0.183
0	A2	36	3	33	0	A1	37	4	34	0	A'1	37	4	34	459.6018	0.581
0	A2	36	5	31	0	A1	37	4	34	0	A'1	37	4	34	484.6651	0.166
0	A1	37	3	34	0	A2	37	5	33	0	A'2	37	4	33	462.3858	0.264
0	A2	37	3	35	0	A1	37	4	34	0	A'1	37	4	34	462.1323	0.119
0	A1	37	5	32	0	A2	37	5	33	0	A'2	37	4	33	488.1924	0.223
0	A2	37	5	33	0	A1	37	4	34	0	A'1	37	4	34	487.8101	0.193
0	A2	38	3	35	0	A1	37	4	34	0	A'1	37	4	34	491.7526	0.088
0	A1	38	3	36	0	A2	37	5	33	0	A'2	37	4	33	464.8556	0.026
0	A1	38	5	34	0	A2	37	5	33	0	A'2	37	4	33	491.5228	0.234
0	A2	36	5	31	0	A1	37	6	32	0	A'1	37	6	32	458.8315	0.029
0	A1	36	7	30	0	A2	37	7	31	0	A'2	37	6	31	457.6756	0.108
0	A1	37	5	32	0	A2	37	7	31	0	A'2	37	6	31	463.1846	0.152
0	A2	37	5	33	0	A1	37	6	32	0	A'1	37	6	32	461.9766	0.094
0	A1	37	7	30	0	A2	37	7	31	0	A'2	37	6	31	487.3543	0.136
0	A2	38	5	33	0	A1	37	6	32	0	A'1	37	6	32	492.5041	0.128
0	A1	38	5	34	0	A2	37	7	31	0	A'2	37	6	31	466.5154	0.274
0	A1	38	7	32	0	A2	37	7	31	0	A'2	37	6	31	492.1025	0.296
0	A2	36	7	29	0	A1	37	8	30	0	A'1	37	8	30	458.0206	0.077
0	A1	37	7	30	0	A2	37	9	29	0	A'2	37	8	29	464.0202	0.221
0	A2	37	7	31	0	A1	37	9	30	0	A'1	37	8	30	462.8141	0.181
0	A2	38	7	31	0	A1	37	8	30	0	A'1	37	8	30	493.3113	0.249
0	A1	38	7	32	0	A2	37	9	29	0	A'2	37	8	29	468.7687	0.104
0	A2	37	1	37	0	A1	38	1	38	0	A'1	38	0	38	459.3651	0.167
0	A2	38	1	37	0	A1	38	1	38	0	A'1	38	0	38	490.1807	0.026
0	A2	39	1	39	0	A1	38	1	38	0	A'1	38	0	38	489.8220	0.300
0	A1	37	1	36	0	A2	38	2	37	0	A'2	38	2	37	459.9554	0.126
0	A1	37	3	34	0	A2	38	2	37	0	A'2	38	2	37	487.4855	0.253
0	A2	37	3	35	0	A1	38	3	36	0	A'1	38	2	36	459.7762	0.429
0	A2	38	1	37	0	A1	38	3	36	0	A'1	38	2	36	461.1022	0.202
0	A1	38	1	38	0	A2	38	2	37	0	A'2	38	2	37	459.6521	0.213
0	A2	38	3	35	0	A1	38	3	36	0	A'1	38	2	36	489.3972	0.176
0	A1	38	3	36	0	A2	38	2	37	0	A'2	38	2	37	489.9559	0.144
0	A1	39	1	38	0	A2	38	2	37	0	A'2	38	2	37	491.2967	0.044
0	A2	39	1	39	0	A1	38	3	36	0	A'1	38	2	36	460.7437	0.224
0	A2	39	3	37	0	A1	38	3	36	0	A'1	38	2	36	491.8580	0.167
0	A1	37	3	34	0	A2	38	4	35	0	A'2	38	4	35	459.1887	0.163
0	A1	37	5	32	0	A2	38	4	35	0	A'2	38	4	35	484.9954	0.439
0	A2	37	5	33	0	A1	38	5	34	0	A'1	38	4	34	458.0469	0.669
0	A2	38	3	35	0	A1	38	5	34	0	A'1	38	4	34	461.9891	0.308
0	A1	38	3	36	0	A2	38	4	35	0	A'2	38	4	35	461.6603	0.087
0	A2	38	5	33	0	A1	38	5	34	0	A'1	38	4	34	488.5741	0.267
0	A1	38	5	34	0	A2	38	4	35	0	A'2	38	4	35	488.3266	0.130
0	A2	39	3	37	0	A1	38	4	34	0	A'1	38	4	34	464.4512	0.122
0	A2	39	5	35	0	A1	38	5	34	0	A'1	38	4	34	491.7744	0.121
0	A1	37	5	32	0	A2	38	6	33	0	A'2	38	6	33	458.4417	0.085
0	A1	37	7	30	0	A2	38	6	33	0	A'2	38	6	33	482.6118	0.082
0	A2	37	7	31	0	A1	38	7	32	0	A'1	38	6	32	457.2570	0.253
0	A2	38	5	33	0	A1	38	7	32	0	A'1	38	6	32	462.7695	0.139

Excited state					Ground state [a]					Ground state [b]						
m′	*Γ′*	*J′*	*Ka′*	*Kc′*	*m″*	*Γ″*	*J″*	*Ka″*	*Kc″*	*m″*	*Γ″*	*J″*	*Ka″*	*Kc″*	Wavenumber cm^{-1}	Intensity
0	A1	38	5	34	0	A2	38	6	33	0	A'2	38	6	33	461.7716	0.131
0	A2	38	7	31	0	A1	38	7	32	0	A'1	38	6	32	487.7573	0.467
0	A1	39	5	34	0	A2	38	6	33	0	A'2	38	6	33	493.0914	0.130
0	A2	39	5	35	0	A1	38	7	32	0	A'1	38	6	32	465.9695	0.134
0	A2	39	7	33	0	A1	38	6	32	0	A'1	38	6	32	492.4512	0.090
0	A1	37	7	30	0	A2	38	8	31	0	A'2	38	8	31	457.6442	0.078
0	A2	38	7	31	0	A1	38	9	30	0	A'1	38	8	30	463.6344	0.151
0	A1	38	7	32	0	A2	38	8	31	0	A'2	38	8	31	462.3907	0.135
0	A1	39	7	32	0	A2	38	8	31	0	A'2	38	8	31	493.7149	0.199
0	A2	39	7	33	0	A1	38	9	30	0	A'1	38	8	30	468.3285	0.356
0	A1	38	1	38	0	A2	39	1	39	0	A'2	39	0	39	458.9229	0.143
0	A1	39	1	38	0	A2	39	1	39	0	A'2	39	0	39	490.6088	0.690
0	A1	40	1	40	0	A2	39	1	39	0	A'2	39	0	39	490.1599	0.305
0	A2	38	1	37	0	A1	39	2	38	0	A'1	39	2	38	459.5670	0.290
0	A2	38	3	35	0	A1	39	3	37	0	A'1	39	2	37	487.8613	0.414
0	A1	38	3	36	0	A2	39	3	37	0	A'2	39	2	37	459.3617	0.049
0	A1	39	1	38	0	A2	39	2	37	0	A'2	39	2	37	460.7014	0.100
0	A2	39	1	39	0	A1	39	2	38	0	A'1	39	2	38	459.2075	0.090
0	A1	39	3	36	0	A2	39	3	37	0	A'2	39	2	37	489.7923	0.208
0	A2	39	3	37	0	A1	39	2	38	0	A'1	39	2	38	490.3227	0.192
0	A2	40	1	39	0	A1	39	2	38	0	A'1	39	2	38	491.6859	0.206
0	A1	40	1	40	0	A2	39	3	37	0	A'2	39	2	37	460.2957	0.438
0	A1	40	3	38	0	A2	39	3	37	0	A'2	39	2	37	492.2248	0.087
0	A2	38	3	35	0	A1	39	4	36	0	A'1	39	4	36	458.8082	0.168
0	A2	38	5	33	0	A1	39	4	36	0	A'1	39	4	36	485.3925	0.042
0	A1	38	5	34	0	A2	39	5	35	0	A'2	39	4	35	457.6458	0.103
0	A1	39	3	36	0	A2	39	5	35	0	A'2	39	4	35	461.4199	0.398
0	A2	39	3	37	0	A1	39	4	36	0	A'1	39	4	36	461.2672	0.054
0	A1	39	5	34	0	A2	39	5	35	0	A'2	39	4	35	488.9634	0.172
0	A2	39	5	35	0	A1	39	4	36	0	A'1	39	4	36	488.5924	0.062
0	A2	40	3	37	0	A1	39	4	36	0	A'1	39	4	36	492.5210	0.051
0	A1	40	3	38	0	A2	39	5	35	0	A'2	39	4	35	463.8403	0.145
0	A1	40	5	36	0	A2	39	5	35	0	A'2	39	4	35	491.9492	0.201
0	A2	38	5	33	0	A1	39	6	34	0	A'1	39	6	34	458.0469	0.669
0	A2	38	7	31	0	A1	39	6	34	0	A'1	39	6	34	483.0330	0.083
0	A1	38	7	32	0	A2	39	7	33	0	A'2	39	6	33	456.8414	0.062
0	A1	39	5	34	0	A2	39	7	33	0	A'2	39	6	33	462.5732	0.222
0	A2	39	5	35	0	A1	39	6	34	0	A'1	39	6	34	461.2476	0.507
0	A1	39	7	32	0	A2	39	7	33	0	A'2	39	6	33	488.1641	0.061
0	A1	40	5	36	0	A2	39	7	33	0	A'2	39	6	33	465.5585	0.139
0	A1	40	7	34	0	A2	39	7	33	0	A'2	39	6	33	492.9539	0.173
0	A2	38	7	31	0	A1	39	8	32	0	A'1	39	8	32	457.2609	0.126
0	A1	39	7	32	0	A2	39	9	31	0	A'2	39	8	31	463.2489	0.496
0	A2	39	7	33	0	A1	39	8	32	0	A'1	39	8	32	461.9557	0.322
0	A1	40	7	34	0	A2	39	9	31	0	A'2	39	8	31	468.0385	0.074
0	A2	39	1	39	0	A1	40	1	40	0	A'1	40	0	40	458.4796	0.174
0	A2	40	1	39	0	A1	40	1	40	0	A'1	40	0	40	490.9590	0.105
0	A2	41	1	41	0	A1	40	1	40	0	A'1	40	0	40	490.4956	0.366
0	A1	39	1	38	0	A2	40	2	39	0	A'2	40	2	39	459.1690	0.206
0	A1	39	3	36	0	A2	40	2	39	0	A'2	40	2	39	488.2586	0.218
0	A2	39	3	37	0	A1	40	3	38	0	A'1	40	2	38	458.9443	0.106
0	A2	40	1	39	0	A1	40	3	38	0	A'1	40	2	38	460.3083	0.134

Excited state					Ground state [a]					Ground state [b]						
m′	*Γ′*	*J′*	*Ka′*	*Kc′*	*m″*	*Γ″*	*J″*	*Ka″*	*Kc″*	*m″*	*Γ″*	*J″*	*Ka″*	*Kc″*	Wavenumber cm^{-1}	Intensity
0	A1	40	1	40	0	A2	40	2	39	0	A'2	40	2	39	458.7612	0.078
0	A2	40	3	37	0	A1	40	3	38	0	A'1	40	2	38	490.1954	0.095
0	A1	41	1	40	0	A2	40	2	39	0	A'2	40	2	39	492.0821	0.167
0	A2	41	1	41	0	A1	40	3	38	0	A'1	40	2	38	459.8450	0.246
0	A2	41	3	39	0	A1	40	3	38	0	A'1	40	2	38	492.5930	0.145
0	A1	39	3	36	0	A2	40	4	37	0	A'2	40	4	37	458.4254	0.197
0	A1	39	5	34	0	A2	40	4	37	0	A'2	40	4	37	485.9798	0.076
0	A2	40	3	37	0	A1	40	5	36	0	A'1	40	4	36	461.1608	0.143
0	A1	40	3	38	0	A2	40	4	37	0	A'2	40	4	37	460.8565	0.479
0	A1	41	3	38	0	A2	40	4	37	0	A'2	40	4	37	492.9378	0.120
0	A2	41	3	39	0	A1	40	5	36	0	A'1	40	4	36	463.5583	0.172
0	A1	39	5	34	0	A2	40	6	35	0	A'2	40	6	35	457.6501	0.059
0	A2	39	7	33	0	A1	40	7	34	0	A'1	40	6	34	456.4312	0.036
0	A2	40	5	35	0	A1	40	7	34	0	A'1	40	6	34	462.1031	0.058
0	A1	40	5	36	0	A2	40	6	35	0	A'2	40	6	35	460.6330	0.113
0	A2	40	7	33	0	A1	40	7	34	0	A'1	40	6	34	488.5559	0.204
0	A1	40	7	34	0	A2	40	6	35	0	A'2	40	6	35	488.0292	0.401
0	A1	39	7	32	0	A2	40	8	33	0	A'2	40	8	33	456.8818	0.060
0	A2	40	7	33	0	A1	40	9	32	0	A'1	40	8	32	462.8312	0.211
0	A1	40	7	34	0	A2	40	8	33	0	A'2	40	8	33	461.6726	0.049
0	A2	41	7	35	0	A1	40	9	32	0	A'1	40	8	32	467.5622	0.200
0	A1	40	1	40	0	A2	41	1	41	0	A'2	41	0	41	458.0352	0.105
0	A1	41	1	40	0	A2	41	1	41	0	A'2	41	0	41	491.3558	0.148
0	A1	42	1	42	0	A2	41	1	41	0	A'2	41	0	41	490.8317	0.364
0	A2	40	1	39	0	A1	41	2	40	0	A'1	41	2	40	458.7762	0.056
0	A2	40	3	37	0	A1	41	2	40	0	A'1	41	2	40	488.6633	0.306
0	A1	40	3	38	0	A2	41	3	39	0	A'2	41	2	39	458.5274	0.303
0	A1	41	1	40	0	A2	41	3	39	0	A'2	41	2	39	459.9189	0.032
0	A2	41	1	41	0	A1	41	2	40	0	A'1	41	2	40	458.3151	0.162
0	A1	41	3	38	0	A2	41	3	39	0	A'2	41	2	39	490.6088	0.690
0	A2	41	3	39	0	A1	41	2	40	0	A'1	41	2	40	491.0622	0.152
0	A2	42	1	41	0	A1	41	2	40	0	A'1	41	2	40	492.4772	0.143
0	A1	42	1	42	0	A2	41	3	39	0	A'2	41	2	39	459.3950	0.098
0	A2	40	3	37	0	A1	41	4	38	0	A'1	41	4	38	458.0469	0.669
0	A1	41	3	38	0	A2	41	5	37	0	A'2	41	4	37	460.7996	0.142
0	A2	41	3	39	0	A1	41	4	38	0	A'1	41	4	38	460.4442	0.122
0	A1	41	5	36	0	A2	41	5	37	0	A'2	41	4	37	489.7786	0.332
0	A2	42	3	39	0	A1	41	4	38	0	A'1	41	4	38	493.3333	0.214
0	A1	42	5	38	0	A2	41	5	37	0	A'2	41	4	37	492.8344	0.127
0	A2	40	5	35	0	A1	41	6	36	0	A'1	41	6	36	457.2721	0.480
0	A2	40	7	33	0	A1	41	6	36	0	A'1	41	6	36	483.7271	0.357
0	A1	42	5	38	0	A2	41	7	35	0	A'2	41	6	35	464.6251	0.287
0	A2	40	7	33	0	A1	41	8	34	0	A'1	41	8	34	456.4848	0.055
0	A2	41	7	35	0	A1	41	8	34	0	A'1	41	8	34	461.2162	0.018
0	A2	41	1	41	0	A1	42	1	42	0	A'1	42	0	42	457.5893	0.201
0	A2	42	1	41	0	A1	42	1	42	0	A'1	42	0	42	491.7526	0.088
0	A2	43	1	43	0	A1	42	1	42	0	A'1	42	0	42	491.1655	0.263
0	A1	41	1	40	0	A2	42	2	41	0	A'2	42	2	41	458.3891	0.113
0	A2	41	3	39	0	A1	42	3	40	0	A'1	42	2	40	458.1153	0.121
0	A2	42	1	41	0	A1	42	3	40	0	A'1	42	2	40	459.5317	0.091
0	A1	42	3	40	0	A2	42	2	41	0	A'2	42	2	41	491.4307	0.134
0	A1	43	1	42	0	A2	42	2	41	0	A'2	42	2	41	492.8646	0.151

Excited state					Ground state [a]					Ground state [b]						
m′	*Γ′*	*J′*	*Ka′*	*Kc′*	*m″*	*Γ″*	*J″*	*Ka″*	*Kc″*	*m″*	*Γ″*	*J″*	*Ka″*	*Kc″*	Wavenumber cm^{-1}	Intensity
0	A2	43	1	43	0	A1	42	3	40	0	A'1	42	2	40	458.9443	0.106
0	A1	41	3	38	0	A2	42	4	39	0	A'2	42	4	39	457.6768	0.113
0	A2	42	3	39	0	A1	42	5	38	0	A'1	42	4	38	460.4163	0.184
0	A1	42	3	40	0	A2	42	4	39	0	A'2	42	4	39	460.0296	0.136
0	A1	42	5	38	0	A2	42	4	39	0	A'2	42	4	39	489.7097	0.170
0	A1	43	3	40	0	A2	42	4	39	0	A'2	42	4	39	493.7363	0.142
0	A1	41	5	36	0	A2	42	6	37	0	A'2	42	6	37	456.8852	0.301
0	A1	42	1	42	0	A2	43	1	43	0	A'2	43	0	43	457.1420	0.095
0	A1	43	1	42	0	A2	43	1	43	0	A'2	43	0	43	492.1416	0.243
0	A1	44	1	44	0	A2	43	1	43	0	A'2	43	0	43	491.4980	0.268
0	A2	42	1	41	0	A1	43	2	42	0	A'1	43	2	42	458.0027	0.091
0	A2	42	3	39	0	A1	43	2	42	0	A'1	43	2	42	489.4745	0.347
0	A1	42	3	40	0	A2	43	3	41	0	A'2	43	2	41	457.7014	0.348
0	A1	43	1	42	0	A2	43	3	41	0	A'2	43	2	41	459.1345	0.223
0	A2	43	1	43	0	A1	43	2	42	0	A'1	43	2	42	457.4150	0.146
0	A1	43	3	40	0	A2	43	3	41	0	A'2	43	2	41	491.4069	0.067
0	A2	43	3	41	0	A1	43	2	42	0	A'1	43	2	42	491.7867	0.024
0	A2	44	1	43	0	A1	43	2	42	0	A'1	43	2	42	493.2750	0.408
0	A1	44	1	44	0	A2	43	3	41	0	A'2	43	2	41	458.4928	0.560
0	A1	44	3	42	0	A2	43	3	41	0	A'2	43	2	41	493.6918	0.137
0	A2	42	3	39	0	A1	43	4	40	0	A'1	43	4	40	457.2900	0.072
0	A1	43	3	40	0	A2	43	5	39	0	A'2	43	4	39	460.0379	0.109
0	A2	43	3	41	0	A1	43	4	40	0	A'1	43	4	40	459.6018	0.581
0	A1	43	5	38	0	A2	43	5	39	0	A'2	43	4	39	490.5665	0.278
0	A2	43	5	39	0	A1	43	4	40	0	A'1	43	4	40	490.0423	0.236
0	A2	44	3	41	0	A1	43	4	40	0	A'1	43	4	40	494.1265	0.063
0	A1	43	5	38	0	A2	43	7	37	0	A'2	43	6	37	460.8512	0.479
0	A2	43	5	39	0	A1	43	6	38	0	A'1	43	6	38	459.4951	0.058
0	A2	44	5	39	0	A1	43	6	38	0	A'1	43	6	38	494.8948	0.266
0	A2	43	1	43	0	A1	44	1	44	0	A'1	44	0	44	456.6936	0.119
0	A2	44	1	43	0	A1	44	1	44	0	A'1	44	0	44	492.5529	0.156
0	A2	45	1	45	0	A1	44	1	44	0	A'1	44	0	44	491.8288	0.230
0	A1	43	1	42	0	A2	44	2	43	0	A'2	44	2	43	457.6074	0.226
0	A1	43	3	40	0	A2	44	2	43	0	A'2	44	2	43	489.8798	0.428
0	A2	43	3	41	0	A1	44	3	42	0	A'1	44	2	42	457.2738	0.058
0	A2	44	1	43	0	A1	44	3	42	0	A'1	44	2	42	458.7612	0.078
0	A1	44	1	44	0	A2	44	2	43	0	A'2	44	2	43	456.9631	0.082
0	A2	44	3	41	0	A1	44	3	42	0	A'1	44	2	42	491.7984	0.089
0	A1	44	3	42	0	A2	44	2	43	0	A'2	44	2	43	492.1631	0.143
0	A1	45	1	44	0	A2	44	2	43	0	A'2	44	2	43	493.6668	0.113
0	A2	45	1	45	0	A1	44	3	42	0	A'1	44	2	42	458.0386	0.105
0	A2	45	3	43	0	A1	44	3	42	0	A'1	44	2	42	494.0651	0.069
0	A1	43	3	40	0	A2	44	4	41	0	A'2	44	4	41	456.9102	0.116
0	A2	43	5	39	0	A1	44	5	40	0	A'1	44	4	40	455.5632	0.647
0	A2	44	3	41	0	A1	44	5	40	0	A'1	44	4	40	459.6463	0.126
0	A1	44	3	42	0	A2	44	4	41	0	A'2	44	4	41	459.1944	0.304
0	A2	44	5	39	0	A1	44	5	40	0	A'1	44	4	40	490.9615	0.132
0	A1	44	5	40	0	A2	44	4	41	0	A'2	44	4	41	490.4169	0.174
0	A1	45	3	42	0	A2	44	4	41	0	A'2	44	4	41	494.4974	0.124
0	A2	45	3	43	0	A1	44	5	40	0	A'1	44	4	40	461.9136	0.163
0	A1	43	5	38	0	A2	44	6	39	0	A'2	44	6	39	456.1084	0.840
0	A1	44	5	40	0	A2	44	6	39	0	A'2	44	6	39	459.0884	0.071

Excited state					Ground state [a]					Ground state [b]						
m′	*Γ′*	*J′*	*Ka′*	*Kc′*	*m″*	*Γ″*	*J″*	*Ka″*	*Kc″*	*m″*	*Γ″*	*J″*	*Ka″*	*Kc″*	Wavenumber cm^{-1}	Intensity
0	A2	45	5	41	0	A1	44	7	38	0	A'1	44	6	38	463.4245	0.128
0	A1	44	1	44	0	A2	45	1	45	0	A'2	45	0	45	456.2437	0.085
0	A1	45	1	44	0	A2	45	1	45	0	A'2	45	0	45	492.9467	0.192
0	A1	46	1	46	0	A2	45	1	45	0	A'2	45	0	45	492.1586	0.285
0	A2	44	1	43	0	A1	45	2	44	0	A'1	45	2	44	457.2354	0.093
0	A2	44	3	41	0	A1	45	2	44	0	A'1	45	2	44	490.2719	0.144
0	A1	44	3	42	0	A2	45	3	43	0	A'2	45	2	43	456.8677	0.091
0	A1	45	1	44	0	A2	45	3	43	0	A'2	45	2	43	458.3703	0.071
0	A2	45	1	45	0	A1	45	2	44	0	A'1	45	2	44	456.5128	0.123
0	A1	45	3	42	0	A2	45	3	43	0	A'2	45	2	43	492.1710	0.056
0	A2	45	3	43	0	A1	45	2	44	0	A'1	45	2	44	492.5386	0.064
0	A2	46	1	45	0	A1	45	2	44	0	A'1	45	2	44	494.0466	0.118
0	A1	46	1	46	0	A2	45	3	43	0	A'2	45	2	43	457.5833	0.087
0	A1	46	3	44	0	A2	45	3	43	0	A'2	45	2	43	494.4964	0.141
0	A2	44	3	41	0	A1	45	4	42	0	A'1	45	4	42	456.5193	0.199
0	A2	44	5	39	0	A1	45	4	42	0	A'1	45	4	42	487.8342	0.459
0	A1	44	5	40	0	A2	45	5	41	0	A'2	45	4	41	455.1543	0.562
0	A2	45	3	43	0	A1	45	4	42	0	A'1	45	4	42	458.7843	0.068
0	A1	45	5	40	0	A2	45	5	41	0	A'2	45	4	41	491.3607	0.148
0	A2	45	5	41	0	A1	45	4	42	0	A'1	45	4	42	490.7937	0.251
0	A2	46	3	43	0	A1	45	4	42	0	A'1	45	4	42	494.8968	0.266
0	A1	46	3	44	0	A2	45	5	41	0	A'2	45	4	41	461.5606	0.081
0	A1	45	5	40	0	A2	45	7	39	0	A'2	45	6	39	460.0824	0.123
0	A2	45	5	41	0	A1	45	6	40	0	A'1	45	6	40	458.6823	0.205
0	A2	45	1	45	0	A1	46	1	46	0	A'1	46	0	46	455.7925	0.598
0	A2	46	1	45	0	A1	46	1	46	0	A'1	46	0	46	493.3285	0.167
0	A2	47	1	47	0	A1	46	1	46	0	A'1	46	0	46	492.4870	0.261
0	A1	45	1	44	0	A2	46	2	45	0	A'2	46	2	45	456.8453	0.058
0	A1	45	3	42	0	A2	46	2	45	0	A'2	46	2	45	490.6458	0.148
0	A2	45	3	43	0	A1	46	3	44	0	A'1	46	2	44	456.3859	0.561
0	A2	46	1	45	0	A1	46	3	44	0	A'1	46	2	44	457.9680	0.425
0	A1	46	3	44	0	A2	46	2	45	0	A'2	46	2	45	492.9702	0.148
0	A1	47	1	46	0	A2	46	2	45	0	A'2	46	2	45	494.4441	0.044
0	A2	47	1	47	0	A1	46	3	44	0	A'1	46	2	44	457.1248	0.108
0	A1	45	3	42	0	A2	46	4	43	0	A'2	46	4	43	456.1084	0.840
0	A2	45	5	41	0	A1	46	5	42	0	A'1	46	4	42	454.7485	0.163
0	A2	46	3	43	0	A1	46	5	42	0	A'1	46	4	42	458.8492	0.206
0	A2	46	5	41	0	A1	46	5	42	0	A'1	46	4	42	491.7526	0.088
0	A1	47	3	44	0	A2	46	4	43	0	A'2	46	4	43	495.2926	0.068
0	A2	47	3	45	0	A1	46	5	42	0	A'1	46	4	42	461.1608	0.143
0	A2	47	5	43	0	A1	46	5	42	0	A'1	46	4	42	494.6955	0.144
0	A1	45	5	40	0	A2	46	6	41	0	A'2	46	6	41	455.3378	0.267
0	A2	46	5	41	0	A1	46	7	40	0	A'1	46	6	40	459.6911	0.066
0	A1	46	5	42	0	A2	46	6	41	0	A'2	46	6	41	458.2938	0.371
0	A2	47	5	43	0	A1	46	7	40	0	A'1	46	6	40	462.6352	0.058
0	A1	46	1	46	0	A2	47	1	47	0	A'2	47	0	47	455.3407	0.243
0	A1	47	1	46	0	A2	47	1	47	0	A'2	47	0	47	493.7278	0.042
0	A1	48	1	48	0	A2	47	1	47	0	A'2	47	0	47	492.8138	0.238
0	A2	46	1	45	0	A1	47	2	46	0	A'1	47	2	46	456.4426	0.229
0	A2	46	3	43	0	A1	47	2	46	0	A'1	47	2	46	491.0465	0.306
0	A1	46	3	44	0	A2	47	3	45	0	A'2	47	2	45	456.1084	0.840
0	A1	47	1	46	0	A2	47	3	45	0	A'2	47	2	45	457.5811	0.126

Excited state					Ground state [a]					Ground state [b]						
m′	*Γ′*	*J′*	*Ka′*	*Kc′*	*m″*	*Γ″*	*J″*	*Ka″*	*Kc″*	*m″*	*Γ″*	*J″*	*Ka″*	*Kc″*	Wavenumber cm^{-1}	Intensity
0	A2	47	1	47	0	A1	47	2	46	0	A'1	47	2	46	455.6008	0.100
0	A1	47	3	44	0	A2	47	3	45	0	A'2	47	2	45	492.9689	0.259
0	A2	47	3	45	0	A1	47	2	46	0	A'1	47	2	46	493.3555	0.069
0	A2	48	1	47	0	A1	47	2	46	0	A'1	47	2	46	494.8464	0.220
0	A1	48	1	48	0	A2	47	3	45	0	A'2	47	2	45	456.6696	0.063
0	A1	48	3	46	0	A2	47	2	45	0	A'2	47	2	45	495.2499	0.053
0	A2	46	3	43	0	A1	47	4	44	0	A'1	47	4	44	455.7251	0.074
0	A2	46	5	41	0	A1	47	4	44	0	A'1	47	4	44	488.6324	0.614
0	A1	46	5	42	0	A2	47	5	43	0	A'2	47	4	43	454.3609	0.588
0	A1	47	3	44	0	A2	47	5	43	0	A'2	47	4	43	458.4650	0.062
0	A2	47	3	45	0	A1	47	4	44	0	A'1	47	4	44	458.0339	0.053
0	A1	47	5	42	0	A2	47	5	43	0	A'2	47	4	43	492.1339	0.126
0	A2	47	5	43	0	A1	47	4	44	0	A'1	47	4	44	491.5698	0.163
0	A1	48	3	46	0	A2	47	5	43	0	A'2	47	4	43	460.7467	0.099
0	A2	46	5	41	0	A1	47	6	42	0	A'1	47	6	42	454.9478	0.306
0	A1	47	5	42	0	A2	47	7	41	0	A'2	47	6	41	459.2890	0.494
0	A2	47	1	47	0	A1	48	1	48	0	A'1	48	0	48	454.8863	0.068
0	A2	48	1	47	0	A1	48	1	48	0	A'1	48	0	48	494.1312	0.118
0	A2	49	1	49	0	A1	48	1	48	0	A'1	48	0	48	493.1393	0.173
0	A1	47	3	44	0	A2	48	2	47	0	A'2	48	2	47	491.4445	0.187
0	A2	47	3	45	0	A1	48	3	46	0	A'1	48	2	46	455.7103	0.056
0	A1	48	1	48	0	A2	48	2	47	0	A'2	48	2	47	455.1450	0.255
0	A2	48	3	45	0	A1	48	3	46	0	A'1	48	2	46	493.3678	0.055
0	A1	49	1	48	0	A2	48	2	47	0	A'2	48	2	47	495.2433	0.092
0	A2	49	1	49	0	A1	48	3	46	0	A'1	48	2	46	456.2098	0.091
0	A1	47	3	44	0	A2	48	4	45	0	A'2	48	4	45	455.3407	0.243
0	A2	47	5	43	0	A1	48	5	44	0	A'1	48	4	44	453.9601	0.147
0	A2	48	3	45	0	A1	48	5	44	0	A'1	48	4	44	458.0819	0.080
0	A1	48	3	46	0	A2	48	4	45	0	A'2	48	4	45	457.6221	0.103
0	A1	48	5	44	0	A2	48	4	45	0	A'2	48	4	45	491.9531	0.386
0	A2	48	5	43	0	A1	48	7	42	0	A'1	48	6	42	458.9001	0.043
0	A1	48	5	44	0	A2	48	6	43	0	A'2	48	6	43	457.4886	0.081
0	A1	48	1	48	0	A2	49	1	49	0	A'2	49	0	49	454.4317	0.082
0	A1	49	1	48	0	A2	49	1	49	0	A'2	49	0	49	494.5297	0.079
0	A2	48	1	47	0	A1	49	2	48	0	A'1	49	2	48	455.6796	0.213
0	A2	48	3	45	0	A1	49	2	48	0	A'1	49	2	48	491.8457	0.200
0	A1	48	3	46	0	A2	49	3	47	0	A'2	49	2	47	455.2997	0.107
0	A1	49	1	48	0	A2	49	3	47	0	A'2	49	2	47	456.8159	0.149
0	A2	49	1	49	0	A1	49	2	48	0	A'1	49	2	48	454.6856	0.519
0	A2	50	1	49	0	A1	49	2	48	0	A'1	49	2	48	495.6369	0.069
0	A1	50	1	50	0	A2	49	3	47	0	A'2	49	2	47	455.7537	0.148
0	A2	48	3	45	0	A1	49	4	46	0	A'1	49	4	46	454.9585	0.060
0	A2	49	3	47	0	A1	49	4	46	0	A'1	49	4	46	457.1939	0.117
0	A2	48	5	43	0	A1	49	6	44	0	A'1	49	6	44	454.1571	0.114
0	A2	49	1	49	0	A1	50	1	50	0	A'1	50	0	50	453.9751	0.086
0	A2	50	1	49	0	A1	50	1	50	0	A'1	50	0	50	494.9247	0.171
0	A1	49	1	48	0	A2	50	2	49	0	A'2	50	2	49	455.2942	0.073
0	A2	49	3	47	0	A1	50	3	48	0	A'1	50	2	48	454.8732	0.431
0	A1	50	1	50	0	A2	50	2	49	0	A'2	50	2	49	454.2311	0.080

[a] The quantum number leveling and symmetry are according to Ref. [167].

[b] The corresponding leveling and symmetry of Ref. [167] are according to Refs. [19, 150,151].

APPENDIX P

MEASURED TRANSITIONS FREQUENCIES AND RESIDUALS FORM THE FIT OF GROUND STATE COMBINATION DIFFERENCES FOR THE NO_2-IN-PLANE ROCK BAND OF CH_3NO_2

Ground upper levels					Ground lower levels					Obs. Trans.	Obs.- calc.		
Γ'	m'	J'	Ka'	Kc'	Γ''	m''	J''	Ka''	Kc''	(cm^{-1})	(cm^{-1})	weight	Ifit
A2	0	2	2	1	A2	0	1	0	1	1.7802	0.00009	0.250	1
A2	0	2	2	1	A2	0	1	0	1	1.7810	0.00089	0.250	1
A1	0	2	2	0	A1	0	2	0	2	0.8716	-0.00006	0.250	1
A1	0	2	2	0	A1	0	2	0	2	0.8720	0.00034	0.250	1
A1	0	2	2	0	A1	0	2	0	2	0.8721	0.00044	0.250	1
A1	0	2	2	0	A1	0	2	0	2	0.8712	-0.00046	0.250	1
A2	0	3	0	3	A2	0	2	2	1	0.6063	-0.00098	0.250	1
A2	0	3	0	3	A2	0	2	2	1	0.6076	0.00032	0.250	1
A2	0	3	2	1	A2	0	3	0	3	1.3862	-0.00078	0.250	1
A2	0	3	2	1	A2	0	3	0	3	1.3881	0.00112	0.250	1
A2	0	3	2	1	A2	0	2	2	1	1.9942	-0.00009	0.250	1
A2	0	3	2	1	A2	0	2	2	1	1.9940	-0.00027	0.250	1
A1	0	3	2	2	A1	0	2	2	0	1.5493	-0.00033	0.250	1
A1	0	3	2	2	A1	0	2	2	0	1.5488	-0.00083	0.250	1
A1	0	3	2	2	A1	0	2	2	0	1.5497	0.00007	0.250	1
A1	0	3	2	2	A1	0	2	0	2	2.4213	0.00001	0.250	1
A1	0	4	0	4	A1	0	3	2	2	0.7331	0.00076	0.250	1
A1	0	4	0	4	A1	0	3	2	2	0.7329	0.00056	0.250	1
A2	0	4	2	3	A2	0	3	0	3	3.1469	-0.00019	0.250	1
A2	0	4	2	3	A2	0	3	0	3	3.1470	-0.00009	0.250	1
A1	0	4	2	2	A1	0	4	0	4	2.1364	0.00028	0.250	1
A1	0	4	2	2	A1	0	4	0	4	2.1361	-0.00002	0.250	1
A1	0	4	2	2	A1	0	4	0	4	2.1354	-0.00070	0.250	1
A1	0	4	2	2	A1	0	3	2	2	2.8695	0.00105	0.250	1
A1	0	4	2	2	A1	0	3	2	2	2.8692	0.00075	0.250	1
A2	0	4	2	3	A2	0	3	2	1	1.7590	-0.00110	0.250	1
A1	0	4	2	2	A1	0	3	2	2	2.8679	-0.00055	0.250	1
A2	0	4	4	1	A2	0	3	0	3	5.3596	-0.00058	0.250	1
A1	0	4	4	0	A1	0	3	2	2	4.3413	0.00035	0.250	1
A2	0	4	4	1	A2	0	3	2	1	3.9735	0.00030	0.250	1
A2	0	4	4	1	A2	0	4	2	3	2.2126	-0.00049	0.250	1
A1	0	4	4	0	A1	0	4	2	2	1.4721	-0.00039	0.250	1
A1	0	4	4	0	A1	0	4	2	2	1.4728	0.00031	0.250	1
A2	0	4	4	1	A2	0	4	2	3	2.2131	0.00001	0.250	1
A1	0	4	4	0	A1	0	4	2	2	1.4734	0.00090	0.250	1
A2	0	5	0	5	A2	0	4	2	3	0.7787	0.00001	0.250	1

Ground upper levels					Ground lower levels					Obs. Trans.	Obs.- calc. (cm^{-1})	weight	Ifit
Γ′	*m′*	*J′*	*Ka′*	*Kc′*	*Γ″*	*m″*	*J″*	*Ka″*	*Kc″*				
A2	0	5	0	5	A2	0	4	2	3	0.7790	0.00030	0.250	1
A2	0	5	2	3	A2	0	5	0	5	2.9947	-0.00048	0.250	1
A2	0	5	2	3	A2	0	5	0	5	2.9946	-0.00052	0.250	1
A2	0	5	2	3	A2	0	5	0	5	2.9956	0.00043	0.250	1
A2	0	5	2	3	A2	0	4	2	3	3.7734	-0.00047	0.250	1
A2	0	5	2	3	A2	0	4	2	3	3.7740	0.00015	0.250	1
A1	0	5	2	4	A1	0	4	2	2	1.7798	-0.00061	0.250	1
A1	0	5	2	4	A1	0	4	4	0	0.3090	0.00109	0.250	1
A2	0	5	2	3	A2	0	4	4	1	1.5610	0.00024	0.250	1
A1	0	5	4	2	A1	0	4	2	2	4.3954	0.00025	0.250	1
A2	0	5	4	1	A2	0	4	2	3	5.2708	0.00003	0.250	1
A1	0	5	4	2	A1	0	5	2	4	2.6143	-0.00044	0.250	1
A2	0	5	4	1	A2	0	5	2	3	1.4970	0.00012	0.250	1
A1	0	5	4	2	A1	0	5	2	4	2.6150	0.00026	0.250	1
A1	0	5	4	2	A1	0	5	2	4	2.6141	-0.00063	0.250	1
A2	0	5	4	1	A2	0	5	2	3	1.4970	0.00010	0.250	1
A2	0	5	4	1	A2	0	5	2	3	1.4973	0.00040	0.250	1
A1	0	5	4	2	A1	0	5	2	4	2.6140	-0.00074	0.250	1
A2	0	5	4	1	A2	0	5	2	3	1.4974	0.00051	0.250	1
A1	0	5	4	2	A1	0	4	4	0	2.9226	-0.00008	0.250	1
A1	0	5	4	2	A1	0	4	4	0	2.9226	-0.00005	0.250	1
A2	0	5	4	1	A2	0	4	4	1	3.0573	-0.00037	0.250	1
A1	0	6	0	6	A1	0	5	2	4	0.7908	0.00066	0.250	1
A1	0	6	0	6	A1	0	5	2	4	0.7894	-0.00074	0.250	1
A2	0	6	2	5	A2	0	5	0	5	4.7002	0.00069	0.250	1
A1	0	6	2	4	A1	0	6	0	6	3.8459	-0.00042	0.250	1
A1	0	6	2	4	A1	0	6	0	6	3.8470	0.00070	0.250	1
A1	0	6	2	4	A1	0	6	0	6	3.8472	0.00088	0.250	1
A1	0	6	2	4	A1	0	6	0	6	3.8466	0.00030	0.250	1
A1	0	6	2	4	A1	0	5	2	4	4.6367	0.00025	0.250	1
A2	0	6	2	5	A2	0	5	2	3	1.7044	0.00001	0.250	1
A1	0	6	2	4	A1	0	5	2	4	4.6364	-0.00004	0.250	1
A1	0	6	2	4	A1	0	5	4	2	2.0220	0.00029	0.250	1
A2	0	6	2	5	A2	0	5	4	1	0.2072	-0.00025	0.250	1
A2	0	6	2	5	A2	0	5	4	1	0.2078	0.00034	0.250	1
A1	0	6	2	4	A1	0	5	4	2	2.0230	0.00129	0.250	1
A2	0	6	4	3	A2	0	5	2	3	4.8875	0.00031	0.250	1
A1	0	6	4	2	A1	0	5	2	4	6.5172	-0.00021	0.250	1
A2	0	6	4	3	A2	0	6	2	5	3.1831	0.00030	0.250	1
A1	0	6	4	2	A1	0	6	2	4	1.8811	0.00013	0.250	1
A2	0	6	4	3	A2	0	6	2	5	3.1828	0.00000	0.250	1
A2	0	6	4	3	A2	0	6	2	5	3.1819	-0.00090	0.250	1
A1	0	6	4	2	A1	0	6	2	4	1.8801	-0.00087	0.250	1
A1	0	6	4	2	A1	0	6	2	4	1.8810	0.00002	0.250	1
A2	0	6	4	3	A2	0	6	2	5	3.1829	0.00010	0.250	1
A1	0	6	4	2	A1	0	6	2	4	1.8806	-0.00036	0.250	1
A1	0	6	4	2	A1	0	5	4	2	3.9036	0.00092	0.250	1
A2	0	6	4	3	A2	0	5	4	1	3.3907	0.00043	0.250	1
A1	0	6	4	2	A1	0	5	4	2	3.9023	-0.00037	0.250	1
A2	0	6	6	1	A2	0	5	4	1	6.4340	0.00061	0.250	1
A1	0	6	6	0	A1	0	5	4	2	6.5542	0.00058	0.250	1

Ground upper levels					Ground lower levels					Obs. Trans.	Obs.- calc.		
Γ′	*m′*	*J′*	*Ka′*	*Kc′*	*Γ″*	*m″*	*J″*	*Ka″*	*Kc″*	(cm^{-1})	(cm^{-1})	weight	Ifit
A2	0	6	6	1	A2	0	5	4	1	6.4331	-0.00029	0.250	1
A2	0	6	6	1	A2	0	6	4	3	3.0440	0.00086	0.250	1
A1	0	6	6	0	A1	0	6	4	2	2.6506	-0.00033	0.250	1
A2	0	6	6	1	A2	0	6	4	3	3.0425	-0.00063	0.250	1
A1	0	6	6	0	A1	0	6	4	2	2.6513	0.00038	0.250	1
A1	0	6	6	0	A1	0	6	4	2	2.6514	0.00046	0.250	1
A2	0	6	6	1	A2	0	6	4	3	3.0430	-0.00015	0.250	1
A1	0	6	6	0	A1	0	6	4	2	2.6509	-0.00003	0.250	1
A2	0	7	0	7	A2	0	6	2	5	0.7899	-0.00053	0.250	1
A2	0	7	0	7	A2	0	6	2	5	0.7899	-0.00049	0.250	1
A2	0	7	2	5	A2	0	7	0	7	4.6609	-0.00072	0.250	1
A2	0	7	2	5	A2	0	7	0	7	4.6628	0.00114	0.250	1
A2	0	7	2	5	A2	0	7	0	7	4.6608	-0.00082	0.250	1
A2	0	7	2	5	A2	0	7	0	7	4.6613	-0.00031	0.250	1
A2	0	7	2	5	A2	0	6	2	5	5.4508	-0.00125	0.250	1
A1	0	7	2	6	A1	0	6	2	4	1.6387	-0.00046	0.250	1
A1	0	7	2	6	A1	0	6	2	4	1.6386	-0.00056	0.250	1
A2	0	7	2	5	A2	0	6	4	3	2.2694	0.00014	0.250	1
A2	0	7	2	5	A2	0	6	4	3	2.2691	-0.00015	0.250	1
A1	0	7	4	4	A1	0	6	2	4	5.5116	0.00032	0.250	1
A1	0	7	4	4	A1	0	7	2	6	3.8726	0.00050	0.250	1
A2	0	7	4	3	A2	0	7	2	5	2.6034	0.00131	0.250	1
A1	0	7	4	4	A1	0	7	2	6	3.8723	0.00019	0.250	1
A1	0	7	4	4	A1	0	7	2	6	3.8727	0.00060	0.250	1
A2	0	7	4	3	A2	0	7	2	5	2.6020	-0.00010	0.250	1
A2	0	7	4	3	A2	0	7	2	5	2.6021	-0.00002	0.250	1
A1	0	7	4	4	A1	0	7	2	6	3.8719	-0.00023	0.250	1
A2	0	7	4	3	A2	0	7	2	5	2.6018	-0.00031	0.250	1
A2	0	7	4	3	A2	0	6	4	3	4.8718	0.00044	0.250	1
A1	0	7	4	4	A1	0	6	4	2	3.6310	0.00070	0.250	1
A2	0	7	4	3	A2	0	6	6	1	1.8283	0.00006	0.250	1
A1	0	7	4	4	A1	0	6	6	0	0.9784	-0.00098	0.250	1
A1	0	7	4	4	A1	0	6	6	0	0.9790	-0.00036	0.250	1
A2	0	7	4	3	A2	0	6	6	1	1.8287	0.00047	0.250	1
A1	0	7	6	2	A1	0	6	4	2	6.7916	0.00103	0.250	1
A1	0	7	6	2	A1	0	7	4	4	3.1607	0.00044	0.250	1
A2	0	7	6	1	A2	0	7	4	3	2.3347	0.00102	0.250	1
A1	0	7	6	2	A1	0	7	4	4	3.1607	0.00044	0.250	1
A1	0	7	6	2	A1	0	7	4	4	3.1604	0.00014	0.250	1
A2	0	7	6	1	A2	0	7	4	3	2.3335	-0.00015	0.250	1
A2	0	7	6	1	A2	0	7	4	3	2.3342	0.00051	0.250	1
A1	0	7	6	2	A1	0	7	4	4	3.1604	0.00014	0.250	1
A2	0	7	6	1	A2	0	7	4	3	2.3346	0.00090	0.250	1
A2	0	7	6	1	A2	0	6	6	1	4.1630	0.00108	0.250	1
A1	0	7	6	2	A1	0	6	6	0	4.1391	-0.00054	0.250	1
A1	0	7	6	2	A1	0	6	6	0	4.1397	0.00003	0.250	1
A2	0	7	6	1	A2	0	6	6	1	4.1618	-0.00006	0.250	1
A1	0	8	0	8	A1	0	7	2	6	0.7880	-0.00023	0.250	1
A1	0	8	0	8	A1	0	7	2	6	0.7890	0.00077	0.250	1
A1	0	8	2	6	A1	0	8	0	8	5.4595	0.00002	0.250	1
A1	0	8	2	6	A1	0	8	0	8	5.4586	-0.00088	0.250	1

Ground upper levels					Ground lower levels					Obs. Trans.	Obs.- calc.		
Γ′	*m′*	*J′*	*Ka′*	*Kc′*	*Γ″*	*m″*	*J″*	*Ka″*	*Kc″*	(cm^{-1})	(cm^{-1})	weight	Ifit
A1	0	8	2	6	A1	0	8	0	8	5.4582	-0.00128	0.250	1
A1	0	8	2	6	A1	0	8	0	8	5.4587	-0.00077	0.250	1
A1	0	8	2	6	A1	0	8	0	8	5.4583	-0.00118	0.250	1
A1	0	8	2	6	A1	0	8	0	8	5.4587	-0.00081	0.250	1
A1	0	8	2	6	A1	0	7	2	6	6.2475	-0.00021	0.250	1
A2	0	8	2	7	A2	0	7	2	5	1.6103	0.00010	0.250	1
A2	0	8	2	7	A2	0	7	2	5	1.6103	0.00011	0.250	1
A1	0	8	2	6	A1	0	7	4	4	2.3751	-0.00051	0.250	1
A1	0	8	2	6	A1	0	7	4	4	2.3766	0.00102	0.250	1
A2	0	8	4	5	A2	0	7	2	5	6.2393	0.00015	0.250	1
A2	0	8	4	5	A2	0	7	2	5	6.2390	-0.00015	0.250	1
A2	0	8	4	5	A2	0	8	2	7	4.6290	0.00005	0.250	1
A1	0	8	4	4	A1	0	8	2	6	3.5083	-0.00048	0.250	1
A2	0	8	4	5	A2	0	8	2	7	4.6286	-0.00036	0.250	1
A1	0	8	4	4	A1	0	8	2	6	3.5078	-0.00100	0.250	1
A1	0	8	4	4	A1	0	8	2	6	3.5087	-0.00007	0.250	1
A2	0	8	4	5	A2	0	8	2	7	4.6288	-0.00015	0.250	1
A1	0	8	4	4	A1	0	8	2	6	3.5098	0.00101	0.250	1
A1	0	8	4	4	A1	0	7	4	4	5.8834	-0.00098	0.250	1
A2	0	8	4	5	A2	0	7	4	3	3.6370	-0.00005	0.250	1
A1	0	8	4	4	A1	0	7	4	4	5.8843	-0.00011	0.250	1
A2	0	8	4	5	A2	0	7	4	3	3.6358	-0.00124	0.250	1
A2	0	8	4	5	A2	0	7	4	3	3.6373	0.00025	0.250	1
A1	0	8	4	4	A1	0	7	6	2	2.7239	-0.00024	0.250	1
A2	0	8	4	5	A2	0	7	6	1	1.3032	-0.00016	0.250	1
A1	0	8	4	4	A1	0	7	6	2	2.7233	-0.00082	0.250	1
A2	0	8	6	3	A2	0	8	4	5	3.4473	-0.00065	0.250	1
A1	0	8	6	2	A1	0	8	4	4	2.1596	-0.00008	0.250	1
A2	0	8	6	3	A2	0	8	4	5	3.4487	0.00074	0.250	1
A2	0	8	6	3	A2	0	8	4	5	3.4480	0.00006	0.250	1
A1	0	8	6	2	A1	0	8	4	4	2.1598	0.00010	0.250	1
A1	0	8	6	2	A1	0	8	4	4	2.1594	-0.00029	0.250	1
A2	0	8	6	3	A2	0	8	4	5	3.4491	0.00114	0.250	1
A1	0	8	6	2	A1	0	8	4	4	2.1592	-0.00048	0.250	1
A1	0	8	6	2	A1	0	7	6	2	4.8838	-0.00002	0.250	1
A2	0	8	6	3	A2	0	7	6	1	4.7514	0.00008	0.250	1
A1	0	8	6	2	A1	0	7	6	2	4.8849	0.00107	0.250	1
A2	0	8	8	1	A2	0	7	6	1	8.8820	-0.00071	0.250	1
A1	0	8	8	0	A1	0	7	6	2	8.9034	0.00007	0.250	1
A2	0	8	8	1	A2	0	7	6	1	8.8830	0.00028	0.250	1
A2	0	8	8	1	A2	0	8	6	3	4.1310	-0.00036	0.250	1
A1	0	8	8	0	A1	0	8	6	2	4.0196	0.00008	0.250	1
A2	0	8	8	1	A2	0	8	6	3	4.1311	-0.00026	0.250	1
A1	0	8	8	0	A1	0	8	6	2	4.0183	-0.00118	0.250	1
A1	0	8	8	0	A1	0	8	6	2	4.0203	0.00081	0.250	1
A2	0	8	8	1	A2	0	8	6	3	4.1324	0.00102	0.250	1
A2	0	9	0	9	A2	0	8	2	7	0.7865	0.00076	0.250	1
A2	0	9	0	9	A2	0	8	2	7	0.7855	-0.00024	0.250	1
A1	0	9	2	8	A1	0	8	0	8	7.0579	-0.00016	0.250	1
A2	0	9	2	7	A2	0	9	0	9	6.2522	0.00064	0.250	1
A2	0	9	2	7	A2	0	9	0	9	6.2522	0.00067	0.250	1

Ground upper levels					Ground lower levels					Obs. Trans.	Obs.- calc.		
Γ′	*m′*	*J′*	*Ka′*	*Kc′*	*Γ″*	*m″*	*J″*	*Ka″*	*Kc″*	(cm^{-1})	(cm^{-1})	weight	Ifit
A2	0	9	2	7	A2	0	9	0	9	6.2512	-0.00036	0.250	1
A2	0	9	2	7	A2	0	9	0	9	6.2523	0.00076	0.250	1
A2	0	9	2	7	A2	0	8	2	7	7.0373	-0.00001	0.250	1
A1	0	9	2	8	A1	0	8	2	6	1.5991	0.00052	0.250	1
A1	0	9	2	8	A1	0	8	2	6	1.5997	0.00112	0.250	1
A2	0	9	2	7	A2	0	8	4	5	2.4084	0.00006	0.250	1
A2	0	9	2	7	A2	0	8	4	5	2.4090	0.00065	0.250	1
A1	0	9	4	6	A1	0	8	2	6	7.0128	0.00078	0.250	1
A1	0	9	4	6	A1	0	8	2	6	7.0111	-0.00094	0.250	1
A1	0	9	4	6	A1	0	9	2	8	5.4137	0.00026	0.250	1
A2	0	9	4	5	A2	0	9	2	7	4.4385	0.00108	0.250	1
A1	0	9	4	6	A1	0	9	2	8	5.4133	-0.00015	0.250	1
A2	0	9	4	5	A2	0	9	2	7	4.4378	0.00039	0.250	1
A1	0	9	4	6	A1	0	9	2	8	5.4141	0.00065	0.250	1
A2	0	9	4	5	A2	0	9	2	7	4.4374	0.00000	0.250	1
A2	0	9	4	5	A2	0	8	4	5	6.8469	0.00115	0.250	1
A1	0	9	4	6	A1	0	8	4	4	3.5033	0.00006	0.250	1
A1	0	9	4	6	A1	0	8	4	4	3.5030	-0.00023	0.250	1
A2	0	9	4	5	A2	0	8	6	3	3.3981	0.00030	0.250	1
A1	0	9	4	6	A1	0	8	6	2	1.3436	0.00007	0.250	1
A1	0	9	4	6	A1	0	8	6	2	1.3439	0.00035	0.250	1
A1	0	9	6	4	A1	0	9	4	6	3.9232	0.00048	0.250	1
A2	0	9	6	3	A2	0	9	4	5	2.3546	-0.00004	0.250	1
A1	0	9	6	4	A1	0	9	4	6	3.9230	0.00026	0.250	1
A1	0	9	6	4	A1	0	9	4	6	3.9226	-0.00012	0.250	1
A2	0	9	6	3	A2	0	9	4	5	2.3542	-0.00043	0.250	1
A1	0	9	6	4	A1	0	9	4	6	3.9221	-0.00064	0.250	1
A2	0	9	6	3	A2	0	9	4	5	2.3556	0.00099	0.250	1
A2	0	9	6	3	A2	0	8	6	3	5.7527	0.00026	0.250	1
A1	0	9	6	4	A1	0	8	6	2	5.2666	0.00033	0.250	1
A2	0	9	6	3	A2	0	8	6	3	5.7525	0.00007	0.250	1
A2	0	9	6	3	A2	0	8	8	1	1.6212	0.00012	0.250	1
A1	0	9	6	4	A1	0	8	8	0	1.2460	-0.00079	0.250	1
A1	0	9	6	4	A1	0	8	8	0	1.2468	0.00001	0.250	1
A2	0	9	6	3	A2	0	8	8	1	1.6207	-0.00037	0.250	1
A1	0	9	8	2	A1	0	9	6	4	4.0674	0.00102	0.250	1
A2	0	9	8	1	A2	0	9	6	3	3.6946	-0.00016	0.250	1
A1	0	9	8	2	A1	0	9	6	4	4.0672	0.00082	0.250	1
A1	0	9	8	2	A1	0	9	6	4	4.0663	-0.00008	0.250	1
A2	0	9	8	1	A2	0	9	6	3	3.6943	-0.00046	0.250	1
A2	0	9	8	1	A2	0	9	6	3	3.6936	-0.00118	0.250	1
A1	0	9	8	2	A1	0	9	6	4	4.0660	-0.00041	0.250	1
A2	0	9	8	1	A2	0	8	8	1	5.3158	-0.00003	0.250	1
A1	0	9	8	2	A1	0	8	8	0	5.3132	0.00002	0.250	1
A2	0	10	2	9	A2	0	9	0	9	7.8447	0.00053	0.250	1
A2	0	10	2	9	A2	0	9	0	9	7.8441	-0.00007	0.250	1
A1	0	10	2	8	A1	0	10	1	10	7.0420	0.00032	0.250	1
A1	0	10	2	8	A1	0	10	1	10	7.0418	0.00012	0.250	1
A1	0	10	2	8	A1	0	10	1	10	7.0411	-0.00058	0.250	1
A1	0	10	2	8	A1	0	10	1	10	7.0414	-0.00029	0.250	1
A1	0	10	2	8	A1	0	9	2	8	7.8252	0.00016	0.250	1

Ground upper levels					Ground lower levels					Obs. Trans.	Obs.- calc.		
Γ′	*m′*	*J′*	*Ka′*	*Kc′*	*Γ″*	*m″*	*J″*	*Ka″*	*Kc″*	(cm^{-1})	(cm^{-1})	weight	Ifit
A2	0	10	2	9	A2	0	9	2	7	1.5925	-0.00011	0.250	1
A2	0	10	2	9	A2	0	9	2	7	1.5929	0.00029	0.250	1
A1	0	10	2	8	A1	0	9	2	8	7.8254	0.00036	0.250	1
A2	0	10	2	9	A2	0	9	2	7	1.5916	-0.00103	0.250	1
A1	0	10	2	8	A1	0	9	4	6	2.4119	0.00030	0.250	1
A1	0	10	2	8	A1	0	9	4	6	2.4118	0.00019	0.250	1
A2	0	10	4	7	A2	0	9	2	7	7.7982	0.00009	0.250	1
A2	0	10	4	7	A2	0	10	2	9	6.2060	0.00051	0.250	1
A1	0	10	4	6	A1	0	10	2	8	5.3079	0.00031	0.250	1
A2	0	10	4	7	A2	0	10	2	9	6.2064	0.00091	0.250	1
A2	0	10	4	7	A2	0	10	2	9	6.2056	0.00010	0.250	1
A1	0	10	4	6	A1	0	9	4	6	7.7198	0.00062	0.250	1
A2	0	10	4	7	A2	0	9	4	5	3.3604	-0.00030	0.250	1
A1	0	10	4	6	A1	0	9	6	4	3.7958	-0.00065	0.250	1
A2	0	10	4	7	A2	0	9	6	3	1.0055	-0.00057	0.250	1
A2	0	10	4	7	A2	0	9	6	3	1.0061	0.00003	0.250	1
A1	0	10	4	6	A1	0	9	6	4	3.7969	0.00045	0.250	1
A2	0	10	6	5	A2	0	10	4	7	4.5535	-0.00073	0.250	1
A1	0	10	6	4	A1	0	10	4	6	2.9861	0.00086	0.250	1
A2	0	10	6	5	A2	0	10	4	7	4.5539	-0.00034	0.250	1
A2	0	10	6	5	A2	0	10	4	7	4.5548	0.00057	0.250	1
A1	0	10	6	4	A1	0	10	4	6	2.9853	0.00009	0.250	1
A1	0	10	6	4	A1	0	10	4	6	2.9857	0.00048	0.250	1
A2	0	10	6	5	A2	0	10	4	7	4.5551	0.00087	0.250	1
A1	0	10	6	4	A1	0	10	4	6	2.9861	0.00085	0.250	1
A1	0	10	6	4	A1	0	9	6	4	6.7819	0.00022	0.250	1
A2	0	10	6	5	A2	0	9	6	3	5.5594	-0.00091	0.250	1
A1	0	10	6	4	A1	0	9	8	2	2.7148	-0.00051	0.250	1
A2	0	10	6	5	A2	0	9	8	1	1.8661	0.00059	0.250	1
A1	0	10	6	4	A1	0	9	8	2	2.7144	-0.00088	0.250	1
A2	0	10	8	3	A2	0	10	6	5	4.0914	0.00081	0.250	1
A1	0	10	8	2	A1	0	10	6	4	3.2628	0.00054	0.250	1
A2	0	10	8	3	A2	0	10	6	5	4.0903	-0.00029	0.250	1
A2	0	10	8	3	A2	0	10	6	5	4.0911	0.00051	0.250	1
A1	0	10	8	2	A1	0	10	6	4	3.2628	0.00053	0.250	1
A1	0	10	8	2	A1	0	10	6	4	3.2626	0.00033	0.250	1
A2	0	10	8	3	A2	0	10	6	5	4.0896	-0.00099	0.250	1
A1	0	10	8	2	A1	0	9	8	2	5.9776	0.00003	0.250	1
A2	0	10	8	3	A2	0	9	8	1	5.9564	0.00030	0.250	1
A2	0	10	8	3	A2	0	9	8	1	5.9565	0.00038	0.250	1
A2	0	10	10	1	A2	0	10	8	3	5.3298	-0.00101	0.250	1
A2	0	11	2	9	A2	0	11	1	11	7.8311	0.00016	0.250	1
A2	0	11	2	9	A2	0	11	1	11	7.8309	-0.00004	0.250	1
A2	0	11	2	9	A2	0	11	1	11	7.8300	-0.00094	0.250	1
A2	0	11	2	9	A2	0	11	1	11	7.8312	0.00027	0.250	1
A2	0	11	2	9	A2	0	10	2	9	8.6123	0.00024	0.250	1
A1	0	11	2	10	A1	0	10	2	8	1.5878	-0.00069	0.250	1
A1	0	11	2	10	A1	0	10	2	8	1.5891	0.00061	0.250	1
A2	0	11	2	9	A2	0	10	2	9	8.6113	-0.00076	0.250	1
A1	0	11	2	10	A1	0	10	2	8	1.5880	-0.00048	0.250	1
A2	0	11	2	9	A2	0	10	4	7	2.4059	-0.00067	0.250	1

Ground upper levels					Ground lower levels					Obs. Trans.	Obs.- calc.		
Γ′	*m′*	*J′*	*Ka′*	*Kc′*	*Γ″*	*m″*	*J″*	*Ka″*	*Kc″*	(cm^{-1})	(cm^{-1})	weight	Ifit
A2	0	11	2	9	A2	0	10	4	7	2.4067	0.00014	0.250	1
A1	0	11	4	8	A1	0	10	2	8	8.5864	-0.00026	0.250	1
A1	0	11	4	8	A1	0	11	2	10	6.9986	0.00043	0.250	1
A2	0	11	4	7	A2	0	11	2	9	6.1332	0.00045	0.250	1
A1	0	11	4	8	A1	0	11	2	10	6.9992	0.00104	0.250	1
A1	0	11	4	8	A1	0	11	2	10	6.9982	-0.00002	0.250	1
A2	0	11	4	7	A2	0	11	2	9	6.1326	-0.00015	0.250	1
A1	0	11	4	8	A1	0	11	2	10	6.9993	0.00113	0.250	1
A2	0	11	4	7	A2	0	11	2	9	6.1336	0.00086	0.250	1
A2	0	11	4	7	A2	0	10	4	7	8.5391	-0.00022	0.250	1
A1	0	11	4	8	A1	0	10	4	6	3.2795	0.00043	0.250	1
A2	0	11	4	7	A2	0	10	6	5	3.9842	-0.00089	0.250	1
A1	0	11	4	8	A1	0	10	6	4	0.2937	-0.00014	0.250	1
A2	0	11	4	7	A2	0	10	6	5	3.9844	-0.00068	0.250	1
A1	0	11	6	6	A1	0	10	4	6	8.5657	-0.00068	0.250	1
A1	0	11	6	6	A1	0	10	4	6	8.5661	-0.00024	0.250	1
A1	0	11	6	6	A1	0	11	4	8	5.2872	-0.00002	0.250	1
A2	0	11	6	5	A2	0	11	4	7	3.9077	-0.00004	0.250	1
A1	0	11	6	6	A1	0	11	4	8	5.2882	0.00093	0.250	1
A2	0	11	6	5	A2	0	11	4	7	3.9082	0.00045	0.250	1
A2	0	11	6	5	A2	0	11	4	7	3.9076	-0.00015	0.250	1
A1	0	11	6	6	A1	0	11	4	8	5.2882	0.00094	0.250	1
A2	0	11	6	5	A2	0	11	4	7	3.9089	0.00114	0.250	1
A2	0	11	6	5	A2	0	10	6	5	7.8919	-0.00093	0.250	1
A1	0	11	6	6	A1	0	10	6	4	5.5808	-0.00033	0.250	1
A2	0	11	6	5	A2	0	10	6	5	7.8934	0.00058	0.250	1
A1	0	11	6	6	A1	0	10	8	2	2.3189	0.00006	0.250	1
A1	0	11	6	6	A1	0	10	8	2	2.3180	-0.00084	0.250	1
A2	0	11	6	5	A2	0	10	8	3	3.8021	-0.00015	0.250	1
A1	0	11	8	4	A1	0	11	6	6	4.2716	-0.00035	0.250	1
A2	0	11	8	3	A2	0	11	6	5	2.9017	0.00034	0.250	1
A1	0	11	8	4	A1	0	11	6	6	4.2721	0.00012	0.250	1
A1	0	11	8	4	A1	0	11	6	6	4.2713	-0.00066	0.250	1
A2	0	11	8	3	A2	0	11	6	5	2.9017	0.00035	0.250	1
A2	0	11	8	3	A2	0	11	6	5	2.9012	-0.00019	0.250	1
A1	0	11	8	4	A1	0	11	6	6	4.2712	-0.00075	0.250	1
A2	0	11	8	3	A2	0	10	8	3	6.7040	0.00041	0.250	1
A1	0	11	10	2	A1	0	10	8	2	11.7921	0.00016	0.250	1
A1	0	11	10	2	A1	0	11	8	4	5.2011	-0.00002	0.250	1
A1	0	12	1	12	A1	0	11	2	10	0.7789	-0.00007	0.250	1
A1	0	12	1	12	A1	0	11	2	10	0.7791	0.00011	0.250	1
A1	0	12	2	10	A1	0	12	1	12	8.6200	0.00028	0.250	1
A1	0	12	2	10	A1	0	12	1	12	8.6190	-0.00072	0.250	1
A1	0	12	2	10	A1	0	12	1	12	8.6198	0.00008	0.250	1
A1	0	12	2	10	A1	0	12	1	12	8.6203	0.00058	0.250	1
A1	0	12	2	10	A1	0	11	2	10	9.3989	0.00021	0.250	1
A2	0	12	2	11	A2	0	11	2	9	1.5859	0.00077	0.250	1
A2	0	12	2	11	A2	0	11	2	9	1.5861	0.00097	0.250	1
A2	0	12	2	11	A2	0	11	2	9	1.5847	-0.00045	0.250	1
A1	0	12	2	10	A1	0	11	4	8	2.3998	-0.00071	0.250	1
A2	0	12	4	9	A2	0	11	2	9	9.3754	0.00036	0.250	1

Ground upper levels					Ground lower levels					Obs. Trans.	Obs.- calc.		
Γ′	*m′*	*J′*	*Ka′*	*Kc′*	*Γ″*	*m″*	*J″*	*Ka″*	*Kc″*	(cm^{-1})	(cm^{-1})	weight	Ifit
A2	0	12	4	9	A2	0	12	2	11	7.7895	-0.00041	0.250	1
A1	0	12	4	8	A1	0	12	2	10	6.9385	0.00001	0.250	1
A2	0	12	4	9	A2	0	12	2	11	7.7890	-0.00090	0.250	1
A2	0	12	4	9	A2	0	12	2	11	7.7899	-0.00001	0.250	1
A1	0	12	4	8	A1	0	12	2	10	6.9395	0.00101	0.250	1
A1	0	12	4	8	A1	0	12	2	10	6.9385	-0.00001	0.250	1
A2	0	12	4	9	A2	0	12	2	11	7.7897	-0.00021	0.250	1
A1	0	12	4	8	A1	0	12	2	10	6.9389	0.00041	0.250	1
A1	0	12	4	8	A1	0	11	4	8	9.3398	0.00078	0.250	1
A2	0	12	4	9	A2	0	11	4	7	3.2421	-0.00020	0.250	1
A1	0	12	4	8	A1	0	11	4	8	9.3383	-0.00071	0.250	1
A2	0	12	4	9	A2	0	11	4	7	3.2425	0.00020	0.250	1
A1	0	12	4	8	A1	0	11	6	6	4.0513	-0.00047	0.250	1
A1	0	12	4	8	A1	0	11	6	6	4.0507	-0.00106	0.250	1
A2	0	12	6	7	A2	0	11	4	7	9.3130	0.00083	0.250	1
A2	0	12	6	7	A2	0	11	4	7	9.3115	-0.00065	0.250	1
A2	0	12	6	7	A2	0	12	4	9	6.0709	0.00103	0.250	1
A1	0	12	6	6	A1	0	12	4	8	4.9195	0.00099	0.250	1
A2	0	12	6	7	A2	0	12	4	9	6.0691	-0.00076	0.250	1
A1	0	12	6	6	A1	0	12	4	8	4.9183	-0.00022	0.250	1
A1	0	12	6	6	A1	0	12	4	8	4.9193	0.00078	0.250	1
A2	0	12	6	7	A2	0	12	4	9	6.0710	0.00113	0.250	1
A1	0	12	6	6	A1	0	12	4	8	4.9192	0.00067	0.250	1
A1	0	12	6	6	A1	0	11	6	6	8.9708	0.00053	0.250	1
A2	0	12	6	7	A2	0	11	6	5	5.4033	-0.00110	0.250	1
A1	0	12	6	6	A1	0	11	8	4	4.6990	0.00069	0.250	1
A2	0	12	6	7	A2	0	11	8	3	2.5034	0.00036	0.250	1
A2	0	12	6	7	A2	0	11	8	3	2.5042	0.00114	0.250	1
A2	0	12	8	5	A2	0	12	6	7	4.6496	0.00086	0.250	1
A1	0	12	8	4	A1	0	12	6	6	2.8696	0.00053	0.250	1
A2	0	12	8	5	A2	0	12	6	7	4.6479	-0.00085	0.250	1
A2	0	12	8	5	A2	0	12	6	7	4.6479	-0.00083	0.250	1
A1	0	12	8	4	A1	0	12	6	6	2.8690	-0.00005	0.250	1
A2	0	12	8	5	A2	0	12	6	7	4.6487	-0.00008	0.250	1
A1	0	12	8	4	A1	0	11	8	4	7.5686	0.00122	0.250	1
A2	0	12	8	5	A2	0	11	8	3	7.1513	-0.00049	0.250	1
A1	0	12	8	4	A1	0	11	8	4	7.5674	-0.00001	0.250	1
A2	0	12	10	3	A2	0	12	8	5	5.0791	0.00000	0.250	1
A2	0	13	1	13	A2	0	12	2	11	0.7767	-0.00020	0.250	1
A2	0	13	1	13	A2	0	12	2	11	0.7775	0.00063	0.250	1
A2	0	13	1	13	A2	0	12	2	11	0.7774	0.00046	0.250	1
A2	0	13	2	11	A2	0	13	1	13	9.4074	-0.00077	0.250	1
A2	0	13	2	11	A2	0	13	1	13	9.4074	-0.00073	0.250	1
A2	0	13	2	11	A2	0	13	1	13	9.4091	0.00093	0.250	1
A2	0	13	2	11	A2	0	13	1	13	9.4082	0.00005	0.250	1
A2	0	13	2	11	A2	0	12	2	11	10.1841	-0.00097	0.250	1
A1	0	13	2	12	A1	0	12	2	10	1.5825	0.00032	0.250	1
A2	0	13	2	11	A2	0	12	2	11	10.1842	-0.00090	0.250	1
A1	0	13	2	12	A1	0	12	2	10	1.5826	0.00038	0.250	1
A1	0	13	2	12	A1	0	12	2	10	1.5825	0.00031	0.250	1
A2	0	13	2	11	A2	0	12	4	9	2.3950	-0.00015	0.250	1

Ground upper levels					Ground lower levels					Obs. Trans.	Obs.- calc.		
Γ′	*m′*	*J′*	*Ka′*	*Kc′*	*Γ″*	*m″*	*J″*	*Ka″*	*Kc″*	(cm^{-1})	(cm^{-1})	weight	Ifit
A2	0	13	2	11	A2	0	12	4	9	2.3950	-0.00012	0.250	1
A2	0	13	2	11	A2	0	12	4	9	2.3954	0.00026	0.250	1
A1	0	13	4	10	A1	0	12	2	10	10.1635	0.00065	0.250	1
A1	0	13	4	10	A1	0	13	2	12	8.5810	0.00033	0.250	1
A2	0	13	4	9	A2	0	13	2	11	7.7378	0.00115	0.250	1
A1	0	13	4	10	A1	0	13	2	12	8.5807	0.00002	0.250	1
A1	0	13	4	10	A1	0	13	2	12	8.5799	-0.00078	0.250	1
A2	0	13	4	9	A2	0	13	2	11	7.7368	0.00014	0.250	1
A2	0	13	4	9	A2	0	13	2	11	7.7365	-0.00014	0.250	1
A1	0	13	4	10	A1	0	13	2	12	8.5800	-0.00067	0.250	1
A2	0	13	4	9	A2	0	13	2	11	7.7375	0.00084	0.250	1
A2	0	13	4	9	A2	0	12	4	9	10.1328	0.00100	0.250	1
A1	0	13	4	10	A1	0	12	4	8	3.2243	-0.00004	0.250	1
A1	0	13	4	10	A1	0	12	4	8	3.2246	0.00025	0.250	1
A2	0	13	4	9	A2	0	12	6	7	4.0616	-0.00035	0.250	1
A2	0	13	4	9	A2	0	12	6	7	4.0619	-0.00002	0.250	1
A1	0	13	6	8	A1	0	13	4	10	6.8688	-0.00038	0.250	1
A2	0	13	6	7	A2	0	13	4	9	5.8727	0.00092	0.250	1
A1	0	13	6	8	A1	0	13	4	10	6.8696	0.00046	0.250	1
A2	0	13	6	7	A2	0	13	4	9	5.8726	0.00081	0.250	1
A2	0	13	6	7	A2	0	13	4	9	5.8713	-0.00048	0.250	1
A2	0	13	6	7	A2	0	13	4	9	5.8726	0.00084	0.250	1
A2	0	13	6	7	A2	0	12	6	7	9.9343	0.00057	0.250	1
A1	0	13	6	8	A1	0	12	6	6	5.1756	0.00059	0.250	1
A1	0	13	6	8	A1	0	12	6	6	5.1748	-0.00019	0.250	1
A2	0	13	6	7	A2	0	12	6	7	9.9324	-0.00132	0.250	1
A2	0	13	6	7	A2	0	12	8	5	5.2854	0.00041	0.250	1
A1	0	13	6	8	A1	0	12	8	4	2.3068	0.00087	0.250	1
A1	0	13	6	8	A1	0	12	8	4	2.3056	-0.00033	0.250	1
A2	0	13	6	7	A2	0	12	8	5	5.2839	-0.00108	0.250	1
A1	0	13	8	6	A1	0	13	6	8	5.2114	0.00094	0.250	1
A2	0	13	8	5	A2	0	13	6	7	3.3365	0.00097	0.250	1
A1	0	13	8	6	A1	0	13	6	8	5.2100	-0.00044	0.250	1
A1	0	13	8	6	A1	0	13	6	8	5.2114	0.00094	0.250	1
A2	0	13	8	5	A2	0	13	6	7	3.3346	-0.00093	0.250	1
A2	0	13	8	5	A2	0	13	6	7	3.3358	0.00027	0.250	1
A1	0	13	8	6	A1	0	13	6	8	5.2109	0.00045	0.250	1
A2	0	13	8	5	A2	0	12	8	5	8.6219	0.00138	0.250	0
A1	0	13	10	4	A1	0	12	8	4	12.5391	0.00029	0.250	1
A1	0	13	10	4	A1	0	13	8	6	5.0223	-0.00013	0.250	1
A1	0	14	1	14	A1	0	13	2	12	0.7746	-0.00028	0.250	1
A1	0	14	1	14	A1	0	13	2	12	0.7749	0.00003	0.250	1
A2	0	14	2	13	A2	0	13	1	13	10.9877	0.00002	0.250	1
A2	0	14	2	13	A2	0	13	2	11	1.5792	-0.00029	0.250	1
A2	0	14	2	13	A2	0	13	2	11	1.5788	-0.00071	0.250	1
A1	0	14	3	12	A1	0	14	1	14	10.1956	-0.00077	0.250	1
A1	0	14	3	12	A1	0	14	1	14	10.1961	-0.00026	0.250	1
A1	0	14	3	12	A1	0	14	1	14	10.1960	-0.00037	0.250	1
A1	0	14	3	12	A1	0	13	4	10	2.3912	0.00063	0.250	1
A1	0	14	3	12	A1	0	13	4	10	2.3910	0.00041	0.250	1
A2	0	14	4	11	A2	0	13	2	11	10.9497	-0.00043	0.250	1

Ground upper levels					Ground lower levels					Obs. Trans.	Obs.- calc.		
Γ′	*m′*	*J′*	*Ka′*	*Kc′*	*Γ″*	*m″*	*J″*	*Ka″*	*Kc″*	(cm^{-1})	(cm^{-1})	weight	Ifit
A2	0	14	4	11	A2	0	14	2	13	9.3705	-0.00014	0.250	1
A2	0	14	4	11	A2	0	14	2	13	9.3717	0.00108	0.250	1
A2	0	14	4	11	A2	0	14	2	13	9.3703	-0.00034	0.250	1
A2	0	14	4	11	A2	0	14	2	13	9.3696	-0.00099	0.250	1
A1	0	14	4	10	A1	0	14	3	12	8.5314	0.00000	0.250	1
A1	0	14	4	10	A1	0	14	3	12	8.5308	-0.00056	0.250	1
A1	0	14	4	10	A1	0	14	3	12	8.5322	0.00081	0.250	1
A1	0	14	4	10	A1	0	14	3	12	8.5319	0.00051	0.250	1
A1	0	14	4	10	A1	0	13	4	10	10.9226	0.00064	0.250	1
A2	0	14	4	11	A2	0	13	4	9	3.2138	0.00032	0.250	1
A2	0	14	4	11	A2	0	13	4	9	3.2124	-0.00110	0.250	1
A1	0	14	4	10	A1	0	13	6	8	4.0527	-0.00012	0.250	1
A1	0	14	4	10	A1	0	13	6	8	4.0526	-0.00018	0.250	1
A2	0	14	6	9	A2	0	13	4	9	10.8847	0.00047	0.250	1
A2	0	14	6	9	A2	0	14	4	11	7.6709	0.00015	0.250	1
A1	0	14	6	8	A1	0	14	4	10	6.7472	0.00017	0.250	1
A2	0	14	6	9	A2	0	14	4	11	7.6695	-0.00123	0.250	1
A2	0	14	6	9	A2	0	14	4	11	7.6721	0.00135	0.250	0
A1	0	14	6	8	A1	0	14	4	10	6.7470	-0.00007	0.250	1
A2	0	14	6	9	A2	0	14	4	11	7.6722	0.00142	0.250	0
A1	0	14	6	8	A1	0	14	4	10	6.7468	-0.00020	0.250	1
A1	0	14	6	8	A1	0	14	4	10	6.7462	-0.00083	0.250	1
A2	0	14	6	9	A2	0	14	4	11	7.6697	-0.00104	0.250	1
A1	0	14	6	8	A1	0	14	4	10	6.7465	-0.00055	0.250	1
A1	0	14	6	8	A1	0	13	6	8	10.7999	0.00005	0.250	1
A2	0	14	6	9	A2	0	13	6	7	5.0124	-0.00003	0.250	1
A2	0	14	6	9	A2	0	13	6	7	5.0124	-0.00005	0.250	1
A2	0	14	6	9	A2	0	13	6	7	5.0125	0.00000	0.250	1
A2	0	14	6	9	A2	0	13	6	7	5.0124	-0.00008	0.250	1
A1	0	14	6	8	A1	0	13	8	6	5.5894	0.00001	0.250	1
A2	0	14	6	9	A2	0	13	8	5	1.6782	0.00126	0.250	1
A2	0	14	6	9	A2	0	13	8	5	1.6763	-0.00063	0.250	1
A1	0	14	6	8	A1	0	13	8	6	5.5894	0.00005	0.250	1
A2	0	14	6	9	A2	0	13	8	5	1.6784	0.00143	0.250	1
A2	0	14	6	9	A2	0	13	8	5	1.6763	-0.00066	0.250	1
A1	0	14	6	8	A1	0	13	8	6	5.5888	-0.00057	0.250	1
A2	0	14	8	7	A2	0	14	6	9	5.9075	-0.00088	0.250	1
A1	0	14	8	6	A1	0	14	6	8	4.2191	0.00110	0.250	1
A2	0	14	8	7	A2	0	14	6	9	5.9080	-0.00035	0.250	1
A2	0	14	8	7	A2	0	14	6	9	5.9095	0.00114	0.250	1
A1	0	14	8	6	A1	0	14	6	8	4.2186	0.00058	0.250	1
A1	0	14	8	6	A1	0	14	6	8	4.2183	0.00029	0.250	1
A2	0	14	8	7	A2	0	14	6	9	5.9081	-0.00028	0.250	1
A1	0	14	8	6	A1	0	13	8	6	9.8085	0.00111	0.250	1
A2	0	14	8	7	A2	0	13	8	5	7.5863	0.00101	0.250	1
A2	0	14	10	5	A2	0	14	8	7	5.1040	0.00084	0.250	1
A2	0	15	1	15	A2	0	14	2	13	0.7727	-0.00019	0.250	1
A2	0	15	1	15	A2	0	14	2	13	0.7720	-0.00089	0.250	1
A1	0	15	2	14	A1	0	14	1	14	11.7729	-0.00047	0.250	1
A1	0	15	2	14	A1	0	14	1	14	11.7730	-0.00044	0.250	1
A1	0	15	2	14	A1	0	14	3	12	1.5768	-0.00021	0.250	1

Ground upper levels					Ground lower levels					Obs. Trans.	Obs.- calc.		
Γ′	*m′*	*J′*	*Ka′*	*Kc′*	*Γ″*	*m″*	*J″*	*Ka″*	*Kc″*	(cm^{-1})	(cm^{-1})	weight	Ifit
A1	0	15	2	14	A1	0	14	3	12	1.5769	-0.00013	0.250	1
A1	0	15	2	14	A1	0	14	3	12	1.5768	-0.00018	0.250	1
A1	0	15	2	14	A1	0	14	3	12	1.5769	-0.00009	0.250	1
A2	0	15	3	13	A2	0	15	1	15	10.9839	-0.00047	0.250	1
A2	0	15	3	13	A2	0	15	1	15	10.9851	0.00074	0.250	1
A2	0	15	3	13	A2	0	15	1	15	10.9838	-0.00057	0.250	1
A2	0	15	3	13	A2	0	15	1	15	10.9851	0.00070	0.250	1
A2	0	15	3	13	A2	0	15	1	15	10.9833	-0.00107	0.250	1
A2	0	15	3	13	A2	0	15	1	15	10.9833	-0.00109	0.250	1
A2	0	15	3	13	A2	0	14	2	13	11.7566	-0.00063	0.250	1
A2	0	15	3	13	A2	0	14	2	13	11.7566	-0.00066	0.250	1
A2	0	15	3	13	A2	0	14	4	11	2.3871	0.00046	0.250	1
A2	0	15	3	13	A2	0	14	4	11	2.3867	0.00005	0.250	1
A2	0	15	3	13	A2	0	14	4	11	2.3873	0.00063	0.250	1
A2	0	15	3	13	A2	0	14	4	11	2.3868	0.00012	0.250	1
A1	0	15	4	12	A1	0	15	2	14	10.1607	0.00069	0.250	1
A1	0	15	4	12	A1	0	15	2	14	10.1600	0.00001	0.250	1
A1	0	15	4	12	A1	0	15	2	14	10.1589	-0.00110	0.250	1
A1	0	15	4	12	A1	0	15	2	14	10.1593	-0.00069	0.250	1
A2	0	15	4	11	A2	0	15	3	13	9.3238	-0.00039	0.250	1
A2	0	15	4	11	A2	0	15	3	13	9.3256	0.00142	0.250	0
A2	0	15	4	11	A2	0	15	3	13	9.3246	0.00042	0.250	1
A2	0	15	4	11	A2	0	15	3	13	9.3233	-0.00089	0.250	1
A2	0	15	4	11	A2	0	14	4	11	11.7109	0.00007	0.250	1
A1	0	15	4	12	A1	0	14	4	10	3.2064	0.00075	0.250	1
A2	0	15	4	11	A2	0	14	6	9	4.0396	-0.00048	0.250	1
A2	0	15	4	11	A2	0	14	6	9	4.0396	-0.00050	0.250	1
A1	0	15	6	10	A1	0	14	4	10	11.6764	0.00045	0.250	1
A1	0	15	6	10	A1	0	14	4	10	11.6755	-0.00046	0.250	1
A1	0	15	6	10	A1	0	15	4	12	8.4700	-0.00030	0.250	1
A2	0	15	6	9	A2	0	15	4	11	7.5782	-0.00102	0.250	1
A1	0	15	6	10	A1	0	15	4	12	8.4705	0.00021	0.250	1
A2	0	15	6	9	A2	0	15	4	11	7.5794	0.00022	0.250	1
A1	0	15	6	10	A1	0	15	4	12	8.4697	-0.00060	0.250	1
A2	0	15	6	9	A2	0	15	4	11	7.5802	0.00098	0.250	1
A2	0	15	6	9	A2	0	14	6	9	11.6178	-0.00150	0.250	0
A1	0	15	6	10	A1	0	14	6	8	4.9285	-0.00040	0.250	1
A1	0	15	6	10	A1	0	14	6	8	4.9284	-0.00049	0.250	1
A2	0	15	6	9	A2	0	14	8	7	5.7099	-0.00103	0.250	1
A1	0	15	6	10	A1	0	14	8	6	0.7105	-0.00039	0.250	1
A1	0	15	6	10	A1	0	14	8	6	0.7109	0.00001	0.250	1
A2	0	15	6	9	A2	0	14	8	7	5.7102	-0.00073	0.250	1
A1	0	15	8	8	A1	0	15	6	10	6.6825	-0.00091	0.250	1
A1	0	15	8	8	A1	0	15	6	10	6.6846	0.00121	0.250	1
A2	0	15	8	7	A2	0	15	6	9	5.2910	0.00026	0.250	1
A1	0	15	8	8	A1	0	15	6	10	6.6829	-0.00049	0.250	1
A1	0	15	8	8	A1	0	15	6	10	6.6829	-0.00048	0.250	1
A2	0	15	8	7	A2	0	15	6	9	5.2912	0.00047	0.250	1
A2	0	15	8	7	A2	0	15	6	9	5.2901	-0.00065	0.250	1
A2	0	15	8	7	A2	0	14	8	7	11.0009	-0.00077	0.250	1
A1	0	15	8	8	A1	0	14	8	6	7.3934	-0.00088	0.250	1

Ground upper levels					Ground lower levels					Obs. Trans.	Obs.- calc.		
Γ′	*m′*	*J′*	*Ka′*	*Kc′*	*Γ″*	*m″*	*J″*	*Ka″*	*Kc″*	(cm^{-1})	(cm^{-1})	weight	Ifit
A1	0	15	10	6	A1	0	15	8	8	5.3771	0.00011	0.250	1
A1	0	16	1	16	A1	0	15	2	14	0.7714	0.00045	0.250	1
A1	0	16	1	16	A1	0	15	2	14	0.7714	0.00045	0.250	1
A2	0	16	2	15	A2	0	15	3	13	1.5741	-0.00059	0.250	1
A2	0	16	2	15	A2	0	15	3	13	1.5755	0.00081	0.250	1
A1	0	16	3	14	A1	0	16	1	16	11.7722	0.00001	0.250	1
A1	0	16	3	14	A1	0	16	1	16	11.7730	0.00079	0.250	1
A1	0	16	3	14	A1	0	15	4	12	2.3843	0.00114	0.250	1
A2	0	16	4	13	A2	0	16	2	15	10.9492	0.00030	0.250	1
A2	0	16	4	13	A2	0	16	2	15	10.9495	0.00060	0.250	1
A2	0	16	4	13	A2	0	16	2	15	10.9485	-0.00040	0.250	1
A2	0	16	4	13	A2	0	16	2	15	10.9478	-0.00106	0.250	1
A2	0	16	4	13	A2	0	15	3	13	12.5233	-0.00029	0.250	1
A1	0	16	4	12	A1	0	16	3	14	10.1166	0.00086	0.250	1
A1	0	16	4	12	A1	0	16	3	14	10.1144	-0.00132	0.250	1
A1	0	16	4	12	A1	0	16	3	14	10.1159	0.00015	0.250	1
A2	0	16	4	13	A2	0	15	4	11	3.1984	-0.00099	0.250	1
A2	0	16	4	13	A2	0	15	4	11	3.1994	-0.00001	0.250	1
A2	0	16	4	13	A2	0	15	4	11	3.2006	0.00119	0.250	1
A1	0	16	4	12	A1	0	15	6	10	4.0291	0.00050	0.250	1
A1	0	16	4	12	A1	0	15	6	10	4.0278	-0.00079	0.250	1
A2	0	16	6	11	A2	0	15	4	11	12.4665	-0.00022	0.250	1
A2	0	16	6	11	A2	0	15	4	11	12.4677	0.00099	0.250	1
A2	0	16	6	11	A2	0	16	4	13	9.2681	0.00077	0.250	1
A1	0	16	6	10	A1	0	16	4	12	8.3915	-0.00115	0.250	1
A2	0	16	6	11	A2	0	16	4	13	9.2673	-0.00002	0.250	1
A2	0	16	6	11	A2	0	16	4	13	9.2663	-0.00102	0.250	1
A1	0	16	6	10	A1	0	16	4	12	8.3923	-0.00036	0.250	1
A1	0	16	6	10	A1	0	15	6	10	12.4206	-0.00065	0.250	1
A2	0	16	6	11	A2	0	15	6	9	4.8865	-0.00100	0.250	1
A2	0	16	6	11	A2	0	15	6	9	4.8885	0.00096	0.250	1
A1	0	16	6	10	A1	0	15	8	8	5.7386	0.00074	0.250	1
A1	0	16	6	10	A1	0	15	8	8	5.7388	0.00096	0.250	1
A1	0	16	8	8	A1	0	16	6	10	6.3436	-0.00064	0.250	1
A2	0	16	8	9	A2	0	16	6	11	7.4907	0.00074	0.250	1
A1	0	16	8	8	A1	0	16	6	10	6.3441	-0.00013	0.250	1
A1	0	16	8	8	A1	0	16	6	10	6.3442	-0.00001	0.250	1
A2	0	16	8	9	A2	0	16	6	11	7.4898	-0.00015	0.250	1
A1	0	16	8	8	A1	0	15	8	8	12.0822	0.00010	0.250	1
A2	0	16	8	9	A2	0	15	8	7	7.0858	-0.00094	0.250	1
A2	0	16	8	9	A2	0	15	8	7	7.0869	0.00018	0.250	1
A2	0	16	10	7	A2	0	15	8	7	12.9420	-0.00029	0.250	1
A2	0	16	10	7	A2	0	16	8	9	5.8562	0.00065	0.250	1
A2	0	17	1	17	A2	0	16	2	15	0.7693	0.00028	0.250	1
A2	0	17	1	17	A2	0	16	2	15	0.7695	0.00048	0.250	1
A1	0	17	2	16	A1	0	16	1	16	13.3441	-0.00055	0.250	1
A1	0	17	2	16	A1	0	16	3	14	1.5719	-0.00055	0.250	1
A1	0	17	2	16	A1	0	16	3	14	1.5717	-0.00075	0.250	1
A2	0	17	3	15	A2	0	17	1	17	12.5606	0.00069	0.250	1
A2	0	17	3	15	A2	0	17	1	17	12.5601	0.00018	0.250	1
A2	0	17	3	15	A2	0	17	1	17	12.5590	-0.00091	0.250	1

Ground upper levels					Ground lower levels					Obs. Trans.	Obs.- calc.		
Γ′	*m′*	*J′*	*Ka′*	*Kc′*	*Γ″*	*m″*	*J″*	*Ka″*	*Kc″*	(cm^{-1})	(cm^{-1})	weight	Ifit
A2	0	17	3	15	A2	0	17	1	17	12.5597	-0.00022	0.250	1
A2	0	17	3	15	A2	0	16	2	15	13.3299	0.00097	0.250	1
A2	0	17	3	15	A2	0	16	4	13	2.3800	-0.00001	0.250	1
A2	0	17	3	15	A2	0	16	4	13	2.3809	0.00086	0.250	1
A1	0	17	4	14	A1	0	17	2	16	11.7373	-0.00016	0.250	1
A1	0	17	4	14	A1	0	17	2	16	11.7379	0.00045	0.250	1
A1	0	17	4	14	A1	0	17	2	16	11.7382	0.00074	0.250	1
A2	0	17	4	13	A2	0	17	3	15	10.9071	0.00076	0.250	1
A2	0	17	4	13	A2	0	17	3	15	10.9061	-0.00023	0.250	1
A2	0	17	4	13	A2	0	17	3	15	10.9065	0.00017	0.250	1
A2	0	17	4	13	A2	0	17	3	15	10.9058	-0.00054	0.250	1
A2	0	17	4	13	A2	0	16	4	13	13.2871	0.00075	0.250	1
A1	0	17	4	14	A1	0	16	4	12	3.1946	0.00040	0.250	1
A1	0	17	4	14	A1	0	16	4	12	3.1933	-0.00087	0.250	1
A1	0	17	4	14	A1	0	16	4	12	3.1955	0.00132	0.250	1
A2	0	17	4	13	A2	0	16	6	11	4.0181	-0.00094	0.250	1
A2	0	17	4	13	A2	0	16	6	11	4.0201	0.00108	0.250	1
A1	0	17	6	12	A1	0	17	2	16	21.7995	-0.00018	0.250	1
A1	0	17	6	12	A1	0	17	4	14	10.0622	-0.00002	0.250	1
A1	0	17	6	12	A1	0	17	4	14	10.0625	0.00027	0.250	1
A1	0	17	6	12	A1	0	17	4	14	10.0613	-0.00092	0.250	1
A2	0	17	6	11	A2	0	17	4	13	9.1969	-0.00068	0.250	1
A2	0	17	6	11	A2	0	17	4	13	9.1973	-0.00026	0.250	1
A1	0	17	6	12	A1	0	17	4	14	10.0621	-0.00015	0.250	1
A1	0	17	6	12	A1	0	16	6	10	4.8628	-0.00096	0.250	1
A2	0	17	6	11	A2	0	16	8	9	5.7269	0.00025	0.250	1
A2	0	17	6	11	A2	0	16	8	9	5.7271	0.00047	0.250	1
A1	0	17	8	10	A1	0	17	4	14	18.3657	0.00011	0.250	1
A2	0	17	8	9	A2	0	17	4	13	16.4926	-0.00012	0.250	1
A2	0	17	8	9	A2	0	17	4	13	16.4926	-0.00015	0.250	1
A2	0	17	8	9	A2	0	16	6	11	20.5119	0.00016	0.250	1
A2	0	17	8	9	A2	0	16	6	11	20.5119	0.00019	0.250	1
A1	0	17	8	10	A1	0	17	6	12	8.3032	-0.00016	0.250	1
A2	0	17	8	9	A2	0	17	6	11	7.2947	-0.00044	0.250	1
A1	0	17	8	10	A1	0	17	6	12	8.3020	-0.00136	0.250	1
A1	0	17	8	10	A1	0	17	6	12	8.3038	0.00044	0.250	1
A2	0	17	8	9	A2	0	17	6	11	7.2951	-0.00008	0.250	1
A1	0	17	8	10	A1	0	17	6	12	8.3020	-0.00133	0.250	1
A1	0	17	8	10	A1	0	17	6	12	8.3039	0.00050	0.250	1
A1	0	17	8	10	A1	0	17	6	12	8.3037	0.00034	0.250	1
A1	0	17	8	10	A1	0	16	8	8	6.8220	-0.00088	0.250	1
A1	0	17	8	10	A1	0	16	8	8	6.8228	-0.00009	0.250	1
A1	0	17	8	10	A1	0	16	8	8	6.8220	-0.00090	0.250	1
A1	0	17	10	8	A1	0	17	6	12	14.8055	-0.00157	0.250	0
A1	0	17	10	8	A1	0	17	8	10	6.5035	-0.00021	0.250	1
A1	0	18	1	18	A1	0	17	2	16	0.7677	0.00058	0.250	1
A1	0	18	1	18	A1	0	17	2	16	0.7663	-0.00083	0.250	1
A2	0	18	2	17	A2	0	17	3	15	1.5698	-0.00052	0.250	1
A2	0	18	2	17	A2	0	17	3	15	1.5712	0.00089	0.250	1
A1	0	18	3	16	A1	0	18	1	18	13.3476	0.00011	0.250	1
A1	0	18	3	16	A1	0	18	1	18	13.3469	-0.00059	0.250	1

Ground upper levels					Ground lower levels					Obs. Trans.	Obs.- calc.		
Γ′	*m′*	*J′*	*Ka′*	*Kc′*	*Γ″*	*m″*	*J″*	*Ka″*	*Kc″*	(cm^{-1})	(cm^{-1})	weight	Ifit
A1	0	18	3	16	A1	0	18	1	18	13.3483	0.00081	0.250	1
A1	0	18	3	16	A1	0	18	1	18	13.3466	-0.00090	0.250	1
A1	0	18	3	16	A1	0	17	2	16	14.1146	-0.00001	0.250	1
A1	0	18	3	16	A1	0	17	4	14	2.3775	0.00033	0.250	1
A1	0	18	3	16	A1	0	17	4	14	2.3762	-0.00094	0.250	1
A2	0	18	4	15	A2	0	18	2	17	12.5257	0.00001	0.250	1
A2	0	18	4	15	A2	0	18	2	17	12.5263	0.00062	0.250	1
A2	0	18	4	15	A2	0	18	2	17	12.5255	-0.00020	0.250	1
A2	0	18	4	15	A2	0	18	2	17	12.5260	0.00031	0.250	1
A2	0	18	4	15	A2	0	17	3	15	14.0955	-0.00051	0.250	1
A2	0	18	4	15	A2	0	17	4	13	3.1895	-0.00016	0.250	1
A2	0	18	4	15	A2	0	17	4	13	3.1894	-0.00028	0.250	1
A1	0	18	5	14	A1	0	18	3	16	11.6958	-0.00040	0.250	1
A1	0	18	5	14	A1	0	18	3	16	11.6968	0.00057	0.250	1
A1	0	18	5	14	A1	0	18	3	16	11.6957	-0.00050	0.250	1
A1	0	18	5	14	A1	0	17	4	14	14.0733	-0.00007	0.250	1
A1	0	18	5	14	A1	0	17	6	12	4.0116	0.00046	0.250	1
A2	0	18	6	13	A2	0	17	4	13	14.0450	-0.00018	0.250	1
A2	0	18	6	13	A2	0	18	4	15	10.8555	-0.00001	0.250	1
A2	0	18	6	13	A2	0	18	4	15	10.8556	0.00010	0.250	1
A2	0	18	6	13	A2	0	18	4	15	10.8544	-0.00110	0.250	1
A2	0	18	6	13	A2	0	18	4	15	10.8561	0.00062	0.250	1
A2	0	18	6	13	A2	0	18	4	15	10.8560	0.00051	0.250	1
A1	0	18	6	12	A1	0	18	5	14	9.9986	0.00078	0.250	1
A1	0	18	6	12	A1	0	18	5	14	9.9969	-0.00090	0.250	1
A1	0	18	6	12	A1	0	18	5	14	9.9976	-0.00022	0.250	1
A1	0	18	6	12	A1	0	18	5	14	9.9987	0.00090	0.250	1
A1	0	18	6	12	A1	0	18	5	14	9.9977	-0.00016	0.250	1
A1	0	18	6	12	A1	0	18	5	14	9.9986	0.00080	0.250	1
A1	0	18	6	12	A1	0	17	6	12	14.0102	0.00123	0.250	1
A2	0	18	6	13	A2	0	17	6	11	4.8478	0.00021	0.250	1
A2	0	18	6	13	A2	0	17	6	11	4.8476	-0.00002	0.250	1
A1	0	18	6	12	A1	0	17	8	10	5.7056	0.00001	0.250	1
A1	0	18	6	12	A1	0	17	8	10	5.7065	0.00089	0.250	1
A1	0	18	6	12	A1	0	17	8	10	5.7065	0.00093	0.250	1
A2	0	18	8	11	A2	0	17	6	11	13.9613	-0.00065	0.250	1
A1	0	18	8	10	A1	0	17	6	12	22.1790	-0.00048	0.250	1
A2	0	18	8	11	A2	0	17	6	11	13.9612	-0.00074	0.250	1
A1	0	18	8	10	A1	0	17	6	12	22.1790	-0.00051	0.250	1
A2	0	18	8	11	A2	0	18	6	13	9.1135	-0.00086	0.250	1
A1	0	18	8	10	A1	0	18	6	12	8.1696	-0.00093	0.250	1
A2	0	18	8	11	A2	0	18	6	13	9.1152	0.00084	0.250	1
A2	0	18	8	11	A2	0	18	6	13	9.1155	0.00115	0.250	1
A1	0	18	8	10	A1	0	18	6	12	8.1691	-0.00142	0.250	0
A1	0	18	8	10	A1	0	18	6	12	8.1692	-0.00133	0.250	0
A2	0	18	8	11	A2	0	18	6	13	9.1151	0.00074	0.250	1
A2	0	18	8	11	A2	0	18	6	13	9.1135	-0.00087	0.250	1
A1	0	18	8	10	A1	0	18	6	12	8.1696	-0.00089	0.250	1
A2	0	18	8	11	A2	0	18	6	13	9.1150	0.00063	0.250	1
A2	0	18	8	11	A2	0	18	6	13	9.1153	0.00099	0.250	1
A1	0	18	8	10	A1	0	18	6	12	8.1692	-0.00136	0.250	0

Ground upper levels					Ground lower levels					Obs. Trans.	Obs.- calc.		
Γ′	*m′*	*J′*	*Ka′*	*Kc′*	*Γ″*	*m″*	*J″*	*Ka″*	*Kc″*	(cm^{-1})	(cm^{-1})	weight	Ifit
A2	0	18	8	11	A2	0	18	6	13	9.1151	0.00076	0.250	1
A2	0	18	8	11	A2	0	17	8	9	6.6671	0.00026	0.250	1
A2	0	18	8	11	A2	0	17	8	9	6.6676	0.00077	0.250	1
A2	0	18	8	11	A2	0	17	8	9	6.6670	0.00016	0.250	1
A2	0	18	8	11	A2	0	17	8	9	6.6675	0.00070	0.250	1
A2	0	18	10	9	A2	0	17	8	9	13.9275	0.00006	0.250	1
A2	0	18	10	9	A2	0	17	8	9	13.9274	0.00002	0.250	1
A2	0	18	10	9	A2	0	18	8	11	7.2604	-0.00019	0.250	1
A2	0	18	10	9	A2	0	18	8	11	7.2604	-0.00017	0.250	1
A2	0	19	1	19	A2	0	18	2	17	0.7652	-0.00004	0.250	1
A2	0	19	1	19	A2	0	18	2	17	0.7651	-0.00010	0.250	1
A1	0	19	2	18	A1	0	18	3	16	1.5681	-0.00016	0.250	1
A1	0	19	2	18	A1	0	18	3	16	1.5679	-0.00035	0.250	1
A2	0	19	3	17	A2	0	19	1	19	14.1356	0.00065	0.250	1
A2	0	19	3	17	A2	0	19	1	19	14.1356	0.00060	0.250	1
A2	0	19	3	17	A2	0	19	1	19	14.1346	-0.00040	0.250	1
A2	0	19	3	17	A2	0	19	1	19	14.1345	-0.00045	0.250	1
A2	0	19	3	17	A2	0	19	1	19	14.1352	0.00024	0.250	1
A2	0	19	3	17	A2	0	18	2	17	14.9008	0.00061	0.250	1
A2	0	19	3	17	A2	0	18	2	17	14.9008	0.00065	0.250	1
A2	0	19	3	17	A2	0	18	4	15	2.3748	0.00030	0.250	1
A2	0	19	3	17	A2	0	18	4	15	2.3734	-0.00112	0.250	1
A1	0	19	4	16	A1	0	19	2	18	13.3137	0.00003	0.250	1
A1	0	19	4	16	A1	0	19	2	18	13.3129	-0.00077	0.250	1
A1	0	19	4	16	A1	0	19	2	18	13.3141	0.00043	0.250	1
A1	0	19	4	16	A1	0	19	2	18	13.3139	0.00023	0.250	1
A1	0	19	4	16	A1	0	18	3	16	14.8818	-0.00013	0.250	1
A1	0	19	4	16	A1	0	18	5	14	3.1852	-0.00050	0.250	1
A1	0	19	4	16	A1	0	18	5	14	3.1862	0.00050	0.250	1
A2	0	19	5	15	A2	0	19	3	17	12.4858	0.00028	0.250	1
A2	0	19	5	15	A2	0	19	3	17	12.4853	-0.00019	0.250	1
A2	0	19	5	15	A2	0	19	3	17	12.4850	-0.00049	0.250	1
A2	0	19	5	15	A2	0	18	4	15	14.8606	0.00059	0.250	1
A2	0	19	5	15	A2	0	18	6	13	4.0048	0.00031	0.250	1
A1	0	19	6	14	A1	0	19	4	16	11.6484	0.00090	0.250	1
A1	0	19	6	14	A1	0	19	4	16	11.6473	-0.00020	0.250	1
A1	0	19	6	14	A1	0	19	4	16	11.6471	-0.00040	0.250	1
A1	0	19	6	14	A1	0	19	4	16	11.6467	-0.00081	0.250	1
A1	0	19	6	14	A1	0	18	5	14	14.8336	0.00040	0.250	1
A2	0	19	6	13	A2	0	19	5	15	10.7944	-0.00067	0.250	1
A2	0	19	6	13	A2	0	19	5	15	10.7949	-0.00016	0.250	1
A2	0	19	6	13	A2	0	19	5	15	10.7947	-0.00037	0.250	1
A2	0	19	6	13	A2	0	18	6	13	14.7992	-0.00036	0.250	1
A1	0	19	6	14	A1	0	18	6	12	4.8357	0.00030	0.250	1
A1	0	19	6	14	A1	0	18	6	12	4.8356	0.00019	0.250	1
A2	0	19	6	13	A2	0	18	8	11	5.6846	-0.00062	0.250	1
A2	0	19	6	13	A2	0	18	8	11	5.6856	0.00039	0.250	1
A1	0	19	8	12	A1	0	18	6	12	14.7555	-0.00051	0.250	1
A1	0	19	8	12	A1	0	19	6	14	9.9198	-0.00081	0.250	1
A2	0	19	8	11	A2	0	19	6	13	9.0079	0.00034	0.250	1
A1	0	19	8	12	A1	0	19	6	14	9.9200	-0.00059	0.250	1

Ground upper levels					Ground lower levels					Obs. Trans.	Obs.- calc.		
Γ′	*m′*	*J′*	*Ka′*	*Kc′*	*Γ″*	*m″*	*J″*	*Ka″*	*Kc″*	(cm^{-1})	(cm^{-1})	weight	Ifit
A1	0	19	8	12	A1	0	19	6	14	9.9207	0.00008	0.250	1
A2	0	19	8	11	A2	0	18	8	11	14.6925	-0.00027	0.250	1
A1	0	19	8	12	A1	0	18	8	10	6.5861	0.00064	0.250	1
A1	0	19	8	12	A1	0	18	8	10	6.5867	0.00122	0.250	1
A1	0	19	10	10	A1	0	19	6	14	17.9926	-0.00047	0.250	1
A1	0	19	10	10	A1	0	19	8	12	8.0726	0.00013	0.250	1
A1	0	20	1	20	A1	0	19	2	18	0.7635	0.00012	0.250	1
A1	0	20	1	20	A1	0	19	2	18	0.7629	-0.00047	0.250	1
A2	0	20	2	19	A2	0	19	3	17	1.5665	0.00026	0.250	1
A2	0	20	2	19	A2	0	19	3	17	1.5668	0.00056	0.250	1
A1	0	20	3	18	A1	0	20	1	20	14.9224	0.00008	0.250	1
A1	0	20	3	18	A1	0	20	1	20	14.9217	-0.00063	0.250	1
A1	0	20	3	18	A1	0	20	1	20	14.9220	-0.00032	0.250	1
A1	0	20	3	18	A1	0	20	1	20	14.9218	-0.00053	0.250	1
A1	0	20	3	18	A1	0	19	2	18	15.6859	0.00021	0.250	1
A1	0	20	3	18	A1	0	19	4	16	2.3722	0.00018	0.250	1
A1	0	20	3	18	A1	0	19	4	16	2.3716	-0.00041	0.250	1
A2	0	20	4	17	A2	0	20	2	19	14.1018	0.00038	0.250	1
A2	0	20	4	17	A2	0	20	2	19	14.1005	-0.00095	0.250	1
A2	0	20	4	17	A2	0	20	2	19	14.1016	0.00017	0.250	1
A2	0	20	4	17	A2	0	20	2	19	14.1016	0.00014	0.250	1
A2	0	20	4	17	A2	0	19	3	17	15.6683	0.00064	0.250	1
A2	0	20	4	17	A2	0	19	5	15	3.1829	0.00073	0.250	1
A2	0	20	4	17	A2	0	19	5	15	3.1816	-0.00057	0.250	1
A1	0	20	5	16	A1	0	20	3	18	13.2738	-0.00053	0.250	1
A1	0	20	5	16	A1	0	20	3	18	13.2735	-0.00084	0.250	1
A1	0	20	5	16	A1	0	20	3	18	13.2751	0.00078	0.250	1
A1	0	20	5	16	A1	0	19	4	16	15.6460	-0.00035	0.250	1
A1	0	20	5	16	A1	0	19	6	14	3.9986	-0.00025	0.250	1
A1	0	20	5	16	A1	0	19	6	14	3.9998	0.00096	0.250	1
A2	0	20	6	15	A2	0	20	2	19	26.5398	-0.00011	0.250	1
A1	0	20	6	14	A1	0	20	3	18	24.8646	0.00020	0.250	1
A2	0	20	6	15	A2	0	20	4	17	12.4393	0.00083	0.250	1
A2	0	20	6	15	A2	0	20	4	17	12.4395	0.00102	0.250	1
A2	0	20	6	15	A2	0	20	4	17	12.4385	-0.00002	0.250	1
A2	0	20	6	15	A2	0	20	4	17	12.4390	0.00052	0.250	1
A1	0	20	6	14	A1	0	20	5	16	11.5911	0.00105	0.250	1
A1	0	20	6	14	A1	0	20	5	16	11.5906	0.00051	0.250	1
A1	0	20	6	14	A1	0	20	5	16	11.5905	0.00048	0.250	1
A1	0	20	6	14	A1	0	20	5	16	11.5894	-0.00065	0.250	1
A1	0	20	6	14	A1	0	19	6	14	15.5897	0.00079	0.250	1
A2	0	20	6	15	A2	0	19	6	13	4.8249	-0.00069	0.250	1
A2	0	20	6	15	A2	0	19	6	13	4.8252	-0.00039	0.250	1
A2	0	20	6	15	A2	0	19	6	13	4.8249	-0.00064	0.250	1
A1	0	20	6	14	A1	0	19	8	12	5.6682	-0.00010	0.250	1
A1	0	20	6	14	A1	0	19	8	12	5.6692	0.00088	0.250	1
A2	0	20	8	13	A2	0	20	6	15	10.7229	-0.00080	0.250	1
A1	0	20	8	12	A1	0	20	6	14	9.8259	-0.00043	0.250	1
A2	0	20	8	13	A2	0	20	6	15	10.7253	0.00160	0.250	0
A1	0	20	8	12	A1	0	20	6	14	9.8268	0.00048	0.250	1
A1	0	20	8	12	A1	0	20	6	14	9.8255	-0.00083	0.250	1

Ground upper levels					Ground lower levels					Obs. Trans.	Obs.- calc.		
Γ′	*m′*	*J′*	*Ka′*	*Kc′*	*Γ″*	*m″*	*J″*	*Ka″*	*Kc″*	(cm^{-1})	(cm^{-1})	weight	Ifit
A2	0	20	8	13	A2	0	20	6	15	10.7242	0.00049	0.250	1
A1	0	20	8	12	A1	0	19	8	12	15.4941	-0.00053	0.250	1
A2	0	20	8	13	A2	0	19	8	11	6.5427	0.00096	0.250	1
A2	0	20	10	11	A2	0	19	8	11	15.4376	-0.00029	0.250	1
A2	0	21	1	21	A2	0	20	2	19	0.7615	-0.00003	0.250	1
A2	0	21	1	21	A2	0	20	2	19	0.7616	0.00010	0.250	1
A1	0	21	2	20	A1	0	20	1	20	16.4855	-0.00110	0.250	1
A1	0	21	2	20	A1	0	20	3	18	1.5645	0.00020	0.250	1
A1	0	21	2	20	A1	0	20	3	18	1.5642	-0.00006	0.250	1
A2	0	21	3	19	A2	0	21	1	21	15.7084	-0.00118	0.250	1
A2	0	21	3	19	A2	0	21	1	21	15.7101	0.00053	0.250	1
A2	0	21	3	19	A2	0	21	1	21	15.7090	-0.00058	0.250	1
A2	0	21	3	19	A2	0	20	2	19	16.4699	-0.00121	0.250	1
A2	0	21	3	19	A2	0	20	4	17	2.3702	0.00052	0.250	1
A2	0	21	3	19	A2	0	20	4	17	2.3691	-0.00056	0.250	1
A1	0	21	4	18	A1	0	21	2	20	14.8895	0.00051	0.250	1
A1	0	21	4	18	A1	0	21	2	20	14.8889	-0.00009	0.250	1
A1	0	21	4	18	A1	0	21	2	20	14.8891	0.00009	0.250	1
A1	0	21	4	18	A1	0	21	2	20	14.8886	-0.00038	0.250	1
A1	0	21	4	18	A1	0	20	3	18	16.4540	0.00071	0.250	1
A1	0	21	4	18	A1	0	20	5	16	3.1798	0.00086	0.250	1
A2	0	21	5	17	A2	0	21	3	19	14.0621	-0.00064	0.250	1
A2	0	21	5	17	A2	0	21	3	19	14.0624	-0.00034	0.250	1
A2	0	21	5	17	A2	0	21	3	19	14.0629	0.00015	0.250	1
A2	0	21	5	17	A2	0	20	4	17	16.4323	-0.00012	0.250	1
A2	0	21	5	17	A2	0	20	6	15	3.9953	0.00138	0.250	1
A2	0	21	5	17	A2	0	20	6	15	3.9935	-0.00045	0.250	1
A1	0	21	6	16	A1	0	21	2	20	28.1174	-0.00021	0.250	1
A1	0	21	6	16	A1	0	21	4	18	13.2285	-0.00012	0.250	1
A1	0	21	6	16	A1	0	21	4	18	13.2278	-0.00081	0.250	1
A1	0	21	6	16	A1	0	21	4	18	13.2276	-0.00101	0.250	1
A2	0	21	6	15	A2	0	21	5	17	12.3825	-0.00028	0.250	1
A2	0	21	6	15	A2	0	21	5	17	12.3831	0.00032	0.250	1
A2	0	21	6	15	A2	0	21	5	17	12.3839	0.00114	0.250	1
A2	0	21	6	15	A2	0	21	5	17	12.3820	-0.00078	0.250	1
A2	0	21	6	15	A2	0	20	6	15	16.3778	0.00110	0.250	1
A1	0	21	6	16	A1	0	20	6	14	4.8166	-0.00088	0.250	1
A1	0	21	6	16	A1	0	20	6	14	4.8173	-0.00021	0.250	1
A2	0	21	6	15	A2	0	20	8	13	5.6518	-0.00120	0.250	1
A2	0	21	6	15	A2	0	20	8	13	5.6540	0.00102	0.250	1
A1	0	21	8	14	A1	0	20	6	14	16.3390	-0.00104	0.250	1
A1	0	21	8	14	A1	0	21	6	16	11.5224	-0.00017	0.250	1
A2	0	21	8	13	A2	0	21	6	15	10.6421	0.00106	0.250	1
A2	0	21	8	13	A2	0	21	6	15	10.6415	0.00045	0.250	1
A2	0	21	8	13	A2	0	21	6	15	10.6406	-0.00043	0.250	1
A1	0	21	8	14	A1	0	21	6	16	11.5222	-0.00035	0.250	1
A2	0	21	8	13	A2	0	20	8	13	16.2939	-0.00014	0.250	1
A1	0	21	8	14	A1	0	20	8	12	6.5132	-0.00054	0.250	1
A1	0	21	8	14	A1	0	20	8	12	6.5133	-0.00042	0.250	1
A1	0	21	10	12	A1	0	21	8	14	9.7166	0.00113	0.250	1
A1	0	22	1	22	A1	0	21	2	20	0.7599	0.00021	0.250	1
A1	0	22	1	22	A1	0	21	2	20	0.7605	0.00081	0.250	1

Ground upper levels					Ground lower levels					Obs. Trans.	Obs.- calc.		
Γ′	*m′*	*J′*	*Ka′*	*Kc′*	*Γ″*	*m″*	*J″*	*Ka″*	*Kc″*	(cm^{-1})	(cm^{-1})	weight	Ifit
A2	0	22	2	21	A2	0	21	3	19	1.5624	0.00000	0.250	1
A2	0	22	2	21	A2	0	21	3	19	1.5621	-0.00028	0.250	1
A1	0	22	3	20	A1	0	22	1	22	16.4974	0.00064	0.250	1
A1	0	22	3	20	A1	0	22	1	22	16.4972	0.00047	0.250	1
A1	0	22	3	20	A1	0	22	1	22	16.4975	0.00074	0.250	1
A1	0	22	3	20	A1	0	21	2	20	17.2573	0.00085	0.250	1
A1	0	22	3	20	A1	0	21	4	18	2.3682	0.00076	0.250	1
A1	0	22	3	20	A1	0	21	4	18	2.3679	0.00044	0.250	1
A2	0	22	4	19	A2	0	22	2	21	15.6759	-0.00047	0.250	1
A2	0	22	4	19	A2	0	22	2	21	15.6757	-0.00067	0.250	1
A2	0	22	4	19	A2	0	22	2	21	15.6766	0.00022	0.250	1
A2	0	22	4	19	A2	0	22	2	21	15.6772	0.00082	0.250	1
A2	0	22	4	19	A2	0	21	3	19	17.2383	-0.00047	0.250	1
A2	0	22	4	19	A2	0	21	5	17	3.1760	-0.00002	0.250	1
A2	0	22	4	19	A2	0	21	5	17	3.1755	-0.00051	0.250	1
A1	0	22	5	18	A1	0	22	3	20	14.8509	0.00010	0.250	1
A1	0	22	5	18	A1	0	22	3	20	14.8507	-0.00009	0.250	1
A1	0	22	5	18	A1	0	22	3	20	14.8516	0.00080	0.250	1
A1	0	22	5	18	A1	0	22	3	20	14.8513	0.00050	0.250	1
A1	0	22	5	18	A1	0	21	4	18	17.2191	0.00085	0.250	1
A1	0	22	5	18	A1	0	21	6	16	3.9904	0.00078	0.250	1
A1	0	22	5	18	A1	0	21	6	16	3.9898	0.00017	0.250	1
A2	0	22	6	17	A2	0	22	4	19	14.0167	-0.00131	0.250	1
A2	0	22	6	17	A2	0	22	4	19	14.0182	0.00019	0.250	1
A2	0	22	6	17	A2	0	22	4	19	14.0170	-0.00100	0.250	1
A2	0	22	6	17	A2	0	22	4	19	14.0177	-0.00030	0.250	1
A2	0	22	6	17	A2	0	21	5	17	17.1927	-0.00132	0.250	1
A2	0	22	6	17	A2	0	21	6	15	4.8111	-0.00014	0.250	1
A2	0	22	6	17	A2	0	21	6	15	4.8104	-0.00084	0.250	1
A1	0	22	7	16	A1	0	22	5	18	13.1756	-0.00078	0.250	1
A1	0	22	7	16	A1	0	22	5	18	13.1758	-0.00055	0.250	1
A1	0	22	7	16	A1	0	22	5	18	13.1777	0.00135	0.250	0
A1	0	22	7	16	A1	0	21	6	16	17.1653	-0.00067	0.250	1
A1	0	22	7	16	A1	0	21	6	16	17.1652	-0.00075	0.250	1
A1	0	22	7	16	A1	0	21	6	16	17.1656	-0.00038	0.250	1
A1	0	22	7	16	A1	0	21	8	14	5.6445	0.00109	0.250	1
A1	0	22	7	16	A1	0	21	8	14	5.6441	0.00066	0.250	1
A2	0	22	8	15	A2	0	21	6	15	17.1252	0.00018	0.250	1
A2	0	22	8	15	A2	0	22	6	17	12.3142	0.00043	0.250	1
A2	0	22	8	15	A2	0	22	6	17	12.3142	0.00042	0.250	1
A2	0	22	8	15	A2	0	22	6	17	12.3077	-0.00615	0.250	0
A1	0	22	8	14	A1	0	22	7	16	11.4429	-0.00052	0.250	1
A1	0	22	8	14	A1	0	22	7	16	11.4429	-0.00052	0.250	1
A2	0	22	8	15	A2	0	21	8	13	6.4838	-0.00025	0.250	1
A2	0	22	8	15	A2	0	21	8	13	6.4833	-0.00073	0.250	1
A2	0	22	10	13	A2	0	21	8	13	17.0337	-0.00074	0.250	1
A2	0	22	10	13	A2	0	22	8	15	10.5566	0.00618	0.250	0
A2	0	23	1	23	A2	0	22	2	21	0.7588	0.00093	0.250	1
A2	0	23	1	23	A2	0	22	2	21	0.7569	-0.00097	0.250	1
A1	0	23	2	22	A1	0	22	3	20	1.5597	-0.00082	0.250	1
A1	0	23	2	22	A1	0	22	3	20	1.5593	-0.00121	0.250	1
A2	0	23	3	21	A2	0	23	1	23	17.2831	-0.00074	0.250	1

Ground upper levels					Ground lower levels					Obs. Trans.	Obs.- calc.		
Γ′	*m′*	*J′*	*Ka′*	*Kc′*	*Γ″*	*m″*	*J″*	*Ka″*	*Kc″*	(cm^{-1})	(cm^{-1})	weight	Ifit
A2	0	23	3	21	A2	0	23	1	23	17.2849	0.00107	0.250	1
A2	0	23	3	21	A2	0	23	1	23	17.2843	0.00046	0.250	1
A2	0	23	3	21	A2	0	22	2	21	18.0419	0.00019	0.250	1
A2	0	23	3	21	A2	0	22	4	19	2.3655	0.00016	0.250	1
A2	0	23	3	21	A2	0	22	4	19	2.3640	-0.00131	0.250	1
A1	0	23	4	20	A1	0	23	2	22	16.4630	-0.00059	0.250	1
A1	0	23	4	20	A1	0	23	2	22	16.4639	0.00031	0.250	1
A1	0	23	4	20	A1	0	22	3	20	18.0227	-0.00141	0.250	0
A1	0	23	4	20	A1	0	22	5	18	3.1736	0.00028	0.250	1
A1	0	23	4	20	A1	0	22	5	18	3.1733	0.00000	0.250	1
A2	0	23	5	19	A2	0	23	3	21	15.6393	0.00079	0.250	1
A2	0	23	5	19	A2	0	23	3	21	15.6394	0.00085	0.250	1
A2	0	23	5	19	A2	0	23	3	21	15.6390	0.00047	0.250	1
A2	0	23	5	19	A2	0	23	3	21	15.6394	0.00089	0.250	1
A2	0	23	5	19	A2	0	22	4	19	18.0048	0.00095	0.250	1
A2	0	23	5	19	A2	0	22	4	19	18.0031	-0.00073	0.250	1
A2	0	23	5	19	A2	0	22	6	17	3.9864	0.00054	0.250	1
A2	0	23	5	19	A2	0	22	6	17	3.9854	-0.00044	0.250	1
A1	0	23	6	18	A1	0	23	4	20	14.8066	0.00001	0.250	1
A1	0	23	6	18	A1	0	23	4	20	14.8070	0.00040	0.250	1
A1	0	23	6	18	A1	0	23	4	20	14.8072	0.00057	0.250	1
A1	0	23	6	18	A1	0	22	5	18	17.9802	0.00029	0.250	1
A1	0	23	6	18	A1	0	22	5	18	17.9792	-0.00071	0.250	1
A1	0	23	6	18	A1	0	22	7	16	4.8031	-0.00045	0.250	1
A1	0	23	6	18	A1	0	22	7	16	4.8032	-0.00033	0.250	1
A2	0	23	7	17	A2	0	23	5	19	13.9666	-0.00014	0.250	1
A2	0	23	7	17	A2	0	23	5	19	13.9679	0.00114	0.250	1
A2	0	23	7	17	A2	0	23	5	19	13.9669	0.00014	0.250	1
A2	0	23	7	17	A2	0	22	6	17	17.9530	0.00040	0.250	1
A2	0	23	7	17	A2	0	22	8	15	5.6387	-0.00003	0.250	1
A2	0	23	7	17	A2	0	22	8	15	5.6392	0.00046	0.250	1
A1	0	23	8	16	A1	0	23	6	18	13.1174	-0.00028	0.250	1
A1	0	23	8	16	A1	0	23	6	18	13.1183	0.00061	0.250	1
A2	0	23	8	15	A2	0	23	7	17	12.2366	0.00043	0.250	1
A2	0	23	8	15	A2	0	23	7	17	12.2355	-0.00068	0.250	1
A2	0	23	8	15	A2	0	23	7	17	12.2353	-0.00086	0.250	1
A2	0	23	8	15	A2	0	22	8	15	17.8750	0.00008	0.250	1
A1	0	23	8	16	A1	0	22	8	14	6.4777	-0.00010	0.250	1
A1	0	23	10	14	A1	0	22	8	14	17.8292	0.00014	0.250	1
A1	0	23	10	14	A1	0	23	8	16	11.3515	0.00024	0.250	1
A1	0	24	1	24	A1	0	23	2	22	0.7565	0.00045	0.250	1
A2	0	24	2	23	A2	0	23	1	23	18.8428	0.00028	0.250	1
A2	0	24	2	23	A2	0	23	1	23	18.8425	-0.00002	0.250	1
A2	0	24	2	23	A2	0	23	3	21	1.5579	-0.00079	0.250	1
A2	0	24	2	23	A2	0	23	3	21	1.5582	-0.00048	0.250	1
A1	0	24	3	22	A1	0	24	1	24	18.0699	-0.00093	0.250	1
A1	0	24	3	22	A1	0	24	1	24	18.0705	-0.00034	0.250	1
A1	0	24	3	22	A1	0	24	1	24	18.0715	0.00067	0.250	1
A1	0	24	3	22	A1	0	23	2	22	18.8264	-0.00049	0.250	1
A1	0	24	3	22	A1	0	23	4	20	2.3627	-0.00059	0.250	1
A1	0	24	3	22	A1	0	23	4	20	2.3621	-0.00120	0.250	1
A2	0	24	4	21	A2	0	24	2	23	17.2503	-0.00036	0.250	1

Ground upper levels					Ground lower levels					Obs. Trans.	Obs.- calc.		
Γ′	*m′*	*J′*	*Ka′*	*Kc′*	*Γ″*	*m″*	*J″*	*Ka″*	*Kc″*	(cm^{-1})	(cm^{-1})	weight	Ifit
A2	0	24	4	21	A2	0	24	2	23	17.2507	0.00006	0.250	1
A2	0	24	4	21	A2	0	23	5	19	3.1705	-0.00030	0.250	1
A2	0	24	4	21	A2	0	23	5	19	3.1705	-0.00029	0.250	1
A1	0	24	5	20	A1	0	24	3	22	16.4267	0.00077	0.250	1
A1	0	24	5	20	A1	0	24	3	22	16.4271	0.00116	0.250	1
A1	0	24	5	20	A1	0	24	3	22	16.4262	0.00027	0.250	1
A1	0	24	5	20	A1	0	23	4	20	18.7894	0.00017	0.250	1
A1	0	24	5	20	A1	0	23	6	18	3.9823	-0.00034	0.250	1
A1	0	24	5	20	A1	0	23	6	18	3.9818	-0.00086	0.250	1
A2	0	24	6	19	A2	0	24	4	21	15.5922	-0.00086	0.250	1
A2	0	24	6	19	A2	0	24	4	21	15.5921	-0.00096	0.250	1
A2	0	24	6	19	A2	0	24	4	21	15.5926	-0.00046	0.250	1
A2	0	24	6	19	A2	0	23	5	19	18.7627	-0.00116	0.250	1
A2	0	24	6	19	A2	0	23	5	19	18.7630	-0.00088	0.250	1
A2	0	24	6	19	A2	0	23	7	17	4.7965	-0.00063	0.250	1
A1	0	24	7	18	A1	0	24	5	20	14.7555	-0.00037	0.250	1
A1	0	24	7	18	A1	0	24	5	20	14.7558	-0.00007	0.250	1
A1	0	24	7	18	A1	0	24	5	20	14.7546	-0.00128	0.250	1
A1	0	24	7	18	A1	0	23	6	18	18.7378	-0.00071	0.250	1
A1	0	24	7	18	A1	0	23	8	16	5.6207	-0.00013	0.250	1
A1	0	24	7	18	A1	0	23	8	16	5.6210	0.00016	0.250	1
A2	0	24	8	17	A2	0	24	6	19	13.9110	-0.00002	0.250	1
A2	0	24	8	17	A2	0	24	6	19	13.9116	0.00061	0.250	1
A1	0	24	8	16	A1	0	24	7	18	13.0550	0.00095	0.250	1
A1	0	24	8	16	A1	0	24	7	18	13.0539	-0.00015	0.250	1
A1	0	24	8	16	A1	0	24	7	18	13.0546	0.00054	0.250	1
A1	0	24	8	16	A1	0	23	8	16	18.6757	0.00082	0.250	1
A2	0	24	8	17	A2	0	23	8	15	6.4730	0.00108	0.250	1
A1	0	24	8	16	A1	0	23	8	16	18.6749	0.00001	0.250	1
A2	0	24	10	15	A2	0	23	8	15	18.6204	0.00127	0.250	1
A2	0	25	1	25	A2	0	24	2	23	0.7542	-0.00005	0.250	1
A2	0	25	1	25	A2	0	24	2	23	0.7543	0.00005	0.250	1
A1	0	25	2	24	A1	0	24	3	22	1.5565	-0.00037	0.250	1
A1	0	25	2	24	A1	0	24	3	22	1.5558	-0.00108	0.250	1
A2	0	25	3	23	A2	0	25	1	25	18.8581	0.00036	0.250	1
A2	0	25	3	23	A2	0	25	1	25	18.8575	-0.00024	0.250	1
A2	0	25	3	23	A2	0	24	4	21	2.3615	0.00014	0.250	1
A2	0	25	3	23	A2	0	24	4	21	2.3599	-0.00145	0.250	0
A1	0	25	4	22	A1	0	25	2	24	18.0379	0.00034	0.250	1
A1	0	25	4	22	A1	0	25	2	24	18.0384	0.00084	0.250	1
A1	0	25	4	22	A1	0	24	3	22	19.5944	-0.00003	0.250	1
A1	0	25	4	22	A1	0	24	5	20	3.1676	-0.00089	0.250	1
A1	0	25	4	22	A1	0	24	5	20	3.1691	0.00060	0.250	1
A2	0	25	5	21	A2	0	25	3	23	17.2129	-0.00013	0.250	1
A2	0	25	5	21	A2	0	25	3	23	17.2120	-0.00103	0.250	1
A2	0	25	5	21	A2	0	25	3	23	17.2119	-0.00114	0.250	1
A2	0	25	5	21	A2	0	24	4	21	19.5744	0.00000	0.250	1
A2	0	25	5	21	A2	0	24	6	19	3.9820	0.00068	0.250	1
A2	0	25	5	21	A2	0	24	6	19	3.9825	0.00116	0.250	1
A1	0	25	6	20	A1	0	25	4	22	16.3855	0.00029	0.250	1
A1	0	25	6	20	A1	0	25	4	22	16.3852	0.00003	0.250	1
A1	0	25	6	20	A1	0	25	4	22	16.3847	-0.00047	0.250	1

Ground upper levels					Ground lower levels					Obs. Trans.	Obs.- calc.		
Γ′	*m′*	*J′*	*Ka′*	*Kc′*	*Γ″*	*m″*	*J″*	*Ka″*	*Kc″*	(cm^{-1})	(cm^{-1})	weight	Ifit
A1	0	25	6	20	A1	0	24	5	20	19.5528	-0.00086	0.250	1
A1	0	25	6	20	A1	0	24	7	18	4.7988	0.00100	0.250	1
A1	0	25	6	20	A1	0	24	7	18	4.7984	0.00060	0.250	1
A2	0	25	7	19	A2	0	25	5	21	15.5407	0.00023	0.250	1
A2	0	25	7	19	A2	0	25	5	21	15.5365	-0.00397	0.250	0
A2	0	25	7	19	A2	0	25	5	21	15.5361	-0.00437	0.250	0
A2	0	25	7	19	A2	0	24	6	19	19.5219	0.00014	0.250	1
A2	0	25	7	19	A2	0	24	6	19	19.5223	0.00053	0.250	1
A2	0	25	7	19	A2	0	24	8	17	5.6107	-0.00015	0.250	1
A2	0	25	7	19	A2	0	24	8	17	5.6110	0.00022	0.250	1
A1	0	25	8	18	A1	0	25	6	20	14.6952	-0.00091	0.250	1
A1	0	25	8	18	A1	0	25	6	20	14.6958	-0.00031	0.250	1
A1	0	25	8	18	A1	0	25	6	20	14.6954	-0.00070	0.250	1
A1	0	25	8	18	A1	0	24	7	18	19.4940	0.00009	0.250	1
A1	0	25	8	18	A1	0	24	7	18	19.4930	-0.00092	0.250	1
A1	0	25	8	18	A1	0	24	8	16	6.4393	-0.00055	0.250	1
A1	0	26	1	26	A1	0	25	2	24	0.7538	0.00134	0.250	1
A2	0	26	2	25	A2	0	25	3	23	1.5552	0.00009	0.250	1
A1	0	26	3	24	A1	0	26	1	26	19.6452	0.00065	0.250	1
A1	0	26	3	24	A1	0	26	1	26	19.6450	0.00045	0.250	1
A1	0	26	3	24	A1	0	25	2	24	20.3982	0.00118	0.250	1
A1	0	26	3	24	A1	0	25	4	22	2.3582	-0.00128	0.250	1
A1	0	26	3	24	A1	0	25	4	22	2.3595	0.00002	0.250	1
A2	0	26	4	23	A2	0	26	2	25	18.8246	0.00029	0.250	1
A2	0	26	4	23	A2	0	26	2	25	18.8237	-0.00060	0.250	1
A2	0	26	4	23	A2	0	26	2	25	18.8243	0.00000	0.250	1
A2	0	26	4	23	A2	0	26	2	25	18.8237	-0.00061	0.250	1
A2	0	26	4	23	A2	0	25	3	23	20.3798	0.00037	0.250	1
A2	0	26	4	23	A2	0	25	5	21	3.1667	0.00028	0.250	1
A2	0	26	4	23	A2	0	25	5	21	3.1668	0.00038	0.250	1
A1	0	26	5	22	A1	0	26	3	24	17.9998	-0.00001	0.250	1
A1	0	26	5	22	A1	0	26	3	24	17.9991	-0.00074	0.250	1
A1	0	26	5	22	A1	0	26	3	24	18.0006	0.00079	0.250	1
A1	0	26	5	22	A1	0	25	4	22	20.3580	-0.00129	0.250	1
A1	0	26	5	22	A1	0	25	6	20	3.9742	0.00008	0.250	1
A1	0	26	5	22	A1	0	25	6	20	3.9745	0.00040	0.250	1
A2	0	26	6	21	A2	0	26	4	23	17.1725	0.00108	0.250	1
A2	0	26	6	21	A2	0	26	4	23	17.1719	0.00048	0.250	1
A2	0	26	6	21	A2	0	26	4	23	17.1712	-0.00022	0.250	1
A1	0	26	7	20	A1	0	26	5	22	16.3477	0.00000	0.250	1
A1	0	26	7	20	A1	0	25	6	20	20.3218	-0.00004	0.250	1
A1	0	26	7	20	A1	0	25	8	18	5.6258	0.00008	0.250	1
A1	0	26	7	20	A1	0	25	8	18	5.6258	0.00010	0.250	1
A1	0	26	7	20	A1	0	25	8	18	5.6258	0.00008	0.250	1
A1	0	26	7	20	A1	0	25	8	18	5.6258	0.00010	0.250	1
A1	0	26	9	18	A1	0	26	7	20	14.6214	-0.00022	0.250	1
A1	0	26	9	18	A1	0	26	7	20	14.6214	-0.00028	0.250	1
A2	0	27	1	27	A2	0	26	2	25	0.7505	-0.00019	0.250	1
A2	0	27	1	27	A2	0	26	2	25	0.7518	0.00111	0.250	1
A1	0	27	2	26	A1	0	26	3	24	1.5528	-0.00059	0.250	1
A2	0	27	3	25	A2	0	27	1	27	20.4318	0.00052	0.250	1
A2	0	27	3	25	A2	0	27	1	27	20.4305	-0.00077	0.250	1

Ground upper levels					Ground lower levels					Obs. Trans.	Obs.- calc.		
Γ′	*m′*	*J′*	*Ka′*	*Kc′*	*Γ″*	*m″*	*J″*	*Ka″*	*Kc″*	(cm^{-1})	(cm^{-1})	weight	Ifit
A2	0	27	3	25	A2	0	27	1	27	20.4313	0.00002	0.250	1
A2	0	27	3	25	A2	0	26	2	25	21.1823	0.00033	0.250	1
A2	0	27	3	25	A2	0	26	2	25	21.1823	0.00034	0.250	1
A2	0	27	3	25	A2	0	26	4	23	2.3576	-0.00010	0.250	1
A2	0	27	3	25	A2	0	26	4	23	2.3589	0.00125	0.250	1
A1	0	27	4	24	A1	0	27	2	26	19.6114	0.00051	0.250	1
A1	0	27	4	24	A1	0	27	2	26	19.6109	0.00000	0.250	1
A1	0	27	4	24	A1	0	26	5	22	3.1649	0.00045	0.250	1
A1	0	27	4	24	A1	0	26	5	22	3.1640	-0.00046	0.250	1
A2	0	27	5	23	A2	0	27	3	25	18.7857	-0.00047	0.250	1
A2	0	27	5	23	A2	0	27	3	25	18.7856	-0.00059	0.250	1
A2	0	27	5	23	A2	0	27	3	25	18.7871	0.00094	0.250	1
A2	0	27	5	23	A2	0	26	4	23	21.1438	-0.00002	0.250	1
A2	0	27	5	23	A2	0	26	4	23	21.1442	0.00035	0.250	1
A2	0	27	5	23	A2	0	26	4	23	21.1445	0.00066	0.250	1
A2	0	27	5	23	A2	0	26	6	21	3.9730	0.00058	0.250	1
A2	0	27	5	23	A2	0	26	6	21	3.9731	0.00070	0.250	1
A1	0	27	6	22	A1	0	27	4	24	17.9578	-0.00002	0.250	1
A1	0	27	6	22	A1	0	27	4	24	17.9594	0.00157	0.250	0
A1	0	27	6	22	A1	0	27	4	24	17.9587	0.00087	0.250	1
A1	0	27	6	22	A1	0	26	5	22	21.1227	0.00043	0.250	1
A1	0	27	6	22	A1	0	26	7	20	4.7747	0.00010	0.250	1
A1	0	27	6	22	A1	0	26	7	20	4.7744	-0.00011	0.250	1
A2	0	27	7	21	A2	0	27	5	23	17.1283	-0.00004	0.250	1
A2	0	27	7	21	A2	0	27	5	23	17.1297	0.00136	0.250	1
A2	0	27	7	21	A2	0	26	8	19	5.6267	0.00178	0.250	0
A2	0	27	7	21	A2	0	26	8	19	5.6266	0.00175	0.250	0
A1	0	27	8	20	A1	0	27	6	22	16.3014	-0.00618	0.250	0
A1	0	27	8	20	A1	0	27	6	22	16.3075	-0.00013	0.250	1
A1	0	27	8	20	A1	0	27	6	22	16.3079	0.00028	0.250	1
A1	0	27	8	20	A1	0	26	7	20	21.0819	-0.00021	0.250	1
A1	0	27	8	20	A1	0	26	9	18	6.4597	-0.00085	0.250	1
A1	0	27	8	20	A1	0	26	9	18	6.4602	-0.00032	0.250	1
A2	0	27	9	19	A2	0	27	7	21	15.4006	-0.00030	0.250	1
A2	0	27	9	19	A2	0	27	7	21	15.4006	-0.00026	0.250	1
A2	0	27	9	19	A2	0	27	7	21	15.4006	-0.00029	0.250	1
A2	0	27	9	19	A2	0	27	7	21	15.4006	-0.00026	0.250	1
A1	0	27	10	18	A1	0	27	8	20	14.5471	0.00858	0.250	0
A1	0	28	1	28	A1	0	27	2	26	0.7490	0.00008	0.250	1
A1	0	28	1	28	A1	0	27	2	26	0.7486	-0.00032	0.250	1
A2	0	28	2	27	A2	0	27	3	25	1.5514	-0.00029	0.250	1
A2	0	28	2	27	A2	0	27	3	25	1.5524	0.00072	0.250	1
A1	0	28	3	26	A1	0	28	1	28	21.2178	-0.00012	0.250	1
A1	0	28	3	26	A1	0	28	1	28	21.2180	0.00009	0.250	1
A1	0	28	3	26	A1	0	28	1	28	21.2182	0.00028	0.250	1
A1	0	28	3	26	A1	0	27	2	26	21.9668	-0.00004	0.250	1
A1	0	28	3	26	A1	0	27	2	26	21.9661	-0.00075	0.250	1
A1	0	28	3	26	A1	0	27	4	24	2.3552	-0.00075	0.250	1
A1	0	28	3	26	A1	0	27	4	24	2.3548	-0.00114	0.250	1
A2	0	28	4	25	A2	0	28	2	27	20.3966	-0.00075	0.250	1
A2	0	28	4	25	A2	0	28	2	27	20.3975	0.00014	0.250	1
A2	0	28	4	25	A2	0	27	3	25	21.9483	-0.00073	0.250	1

Ground upper levels					Ground lower levels					Obs. Trans.	Obs.- calc.		
Γ′	*m′*	*J′*	*Ka′*	*Kc′*	*Γ″*	*m″*	*J″*	*Ka″*	*Kc″*	(cm^{-1})	(cm^{-1})	weight	Ifit
A2	0	28	4	25	A2	0	27	5	23	3.1617	-0.00118	0.250	1
A1	0	28	5	24	A1	0	28	3	26	19.5711	-0.00062	0.250	1
A1	0	28	5	24	A1	0	28	3	26	19.5711	-0.00062	0.250	1
A1	0	28	5	24	A1	0	27	6	22	3.9691	-0.00074	0.250	1
A1	0	28	5	24	A1	0	27	6	22	3.9700	0.00014	0.250	1
A2	0	28	6	23	A2	0	28	4	25	18.7438	0.00048	0.250	1
A2	0	28	6	23	A2	0	28	4	25	18.7429	-0.00043	0.250	1
A2	0	28	6	23	A2	0	27	7	21	4.7774	-0.00044	0.250	1
A2	0	28	6	23	A2	0	27	7	21	4.7778	-0.00003	0.250	1
A1	0	28	7	22	A1	0	28	5	24	17.9151	0.00038	0.250	1
A1	0	28	7	22	A1	0	28	5	24	17.9160	0.00127	0.250	1
A1	0	28	7	22	A1	0	28	5	24	17.9158	0.00109	0.250	1
A1	0	28	7	22	A1	0	27	6	22	21.8842	-0.00036	0.250	1
A1	0	28	7	22	A1	0	27	6	22	21.8860	0.00141	0.250	0
A2	0	28	8	21	A2	0	28	6	23	17.0846	0.00168	0.250	0
A2	0	28	8	21	A2	0	28	6	23	17.0844	0.00149	0.250	1
A2	0	28	8	21	A2	0	28	6	23	17.0845	0.00160	0.250	0
A2	0	28	8	21	A2	0	27	7	21	21.8620	0.00123	0.250	1
A1	0	28	9	20	A1	0	28	7	22	16.2596	-0.00047	0.250	1
A1	0	28	9	20	A1	0	28	7	22	16.2598	-0.00031	0.250	1
A1	0	28	9	20	A1	0	28	7	22	16.2597	-0.00037	0.250	1
A2	0	29	1	29	A2	0	28	2	27	0.7466	-0.00056	0.250	1
A1	0	29	2	28	A1	0	28	1	28	22.7679	-0.00001	0.250	1
A1	0	29	2	28	A1	0	28	3	26	1.5499	-0.00010	0.250	1
A1	0	29	2	28	A1	0	28	3	26	1.5496	-0.00040	0.250	1
A2	0	29	3	27	A2	0	29	1	29	22.0050	0.00053	0.250	1
A2	0	29	3	27	A2	0	29	1	29	22.0039	-0.00057	0.250	1
A2	0	29	3	27	A2	0	29	1	29	22.0043	-0.00017	0.250	1
A2	0	29	3	27	A2	0	28	2	27	22.7516	-0.00003	0.250	1
A2	0	29	3	27	A2	0	28	2	27	22.7520	0.00035	0.250	1
A2	0	29	3	27	A2	0	28	4	25	2.3546	0.00033	0.250	1
A2	0	29	3	27	A2	0	28	4	25	2.3534	-0.00086	0.250	1
A1	0	29	4	26	A1	0	29	2	28	21.1829	-0.00076	0.250	1
A1	0	29	4	26	A1	0	29	2	28	21.1846	0.00096	0.250	1
A1	0	29	4	26	A1	0	28	5	24	3.1629	0.00097	0.250	1
A1	0	29	4	26	A1	0	28	5	24	3.1630	0.00108	0.250	1
A2	0	29	5	25	A2	0	29	3	27	20.3536	0.00015	0.250	1
A2	0	29	5	25	A2	0	29	3	27	20.3540	0.00052	0.250	1
A2	0	29	5	25	A2	0	29	3	27	20.3531	-0.00033	0.250	1
A2	0	29	5	25	A2	0	28	4	25	22.7077	0.00001	0.250	1
A2	0	29	5	25	A2	0	28	4	25	22.7078	0.00007	0.250	1
A2	0	29	5	25	A2	0	28	6	23	3.9643	-0.00007	0.250	1
A2	0	29	5	25	A2	0	28	6	23	3.9643	-0.00008	0.250	1
A1	0	29	6	24	A1	0	29	4	26	19.5261	-0.00034	0.250	1
A1	0	29	6	24	A1	0	29	4	26	19.5243	-0.00218	0.250	0
A1	0	29	6	24	A1	0	29	4	26	19.5252	-0.00126	0.250	1
A1	0	29	6	24	A1	0	28	5	24	22.6878	-0.00060	0.250	1
A1	0	29	6	24	A1	0	28	5	24	22.6872	-0.00121	0.250	1
A1	0	29	6	24	A1	0	28	7	22	4.7710	-0.00269	0.250	0
A2	0	29	7	23	A2	0	29	5	25	18.7043	0.00034	0.250	1
A2	0	29	7	23	A2	0	29	5	25	18.7040	0.00004	0.250	1
A2	0	29	7	23	A2	0	28	8	21	5.5851	-0.00031	0.250	1

Ground upper levels					Ground lower levels					Obs. Trans.	Obs.- calc.		
Γ′	*m′*	*J′*	*Ka′*	*Kc′*	*Γ″*	*m″*	*J″*	*Ka″*	*Kc″*	(cm^{-1})	(cm^{-1})	weight	Ifit
A2	0	29	7	23	A2	0	28	8	21	5.5852	-0.00020	0.250	1
A1	0	29	8	22	A1	0	29	6	24	17.8701	-0.00068	0.250	1
A1	0	29	8	22	A1	0	28	9	20	6.3847	0.00025	0.250	1
A1	0	29	8	22	A1	0	28	9	20	6.3854	0.00092	0.250	1
A2	0	29	9	21	A2	0	29	7	23	17.0323	0.00114	0.250	1
A2	0	29	9	21	A2	0	29	7	23	17.0306	-0.00053	0.250	1
A2	0	29	9	21	A2	0	29	7	23	17.0313	0.00015	0.250	1
A2	0	29	9	21	A2	0	28	8	21	22.6174	0.00083	0.250	1
A1	0	29	10	20	A2	0	28	8	21	16.1805	0.03336	0.250	0
A1	0	29	10	20	A1	0	28	9	20	22.5912	-0.00001	0.250	1
A1	0	30	1	30	A1	0	29	2	28	0.7452	-0.00021	0.250	1
A1	0	30	1	30	A1	0	29	2	28	0.7461	0.00068	0.250	1
A2	0	30	2	29	A2	0	29	3	27	1.5480	-0.00034	0.250	1
A2	0	30	2	29	A2	0	29	3	27	1.5480	-0.00035	0.250	1
A1	0	30	3	28	A1	0	30	1	30	22.7912	0.00027	0.250	1
A1	0	30	3	28	A1	0	30	1	30	22.7917	0.00075	0.250	1
A1	0	30	3	28	A1	0	30	1	30	22.7902	-0.00073	0.250	1
A1	0	30	3	28	A1	0	29	2	28	23.5364	0.00005	0.250	1
A1	0	30	3	28	A1	0	29	2	28	23.5364	0.00006	0.250	1
A1	0	30	3	28	A1	0	29	4	26	2.3518	-0.00090	0.250	1
A1	0	30	3	28	A1	0	29	4	26	2.3530	0.00031	0.250	1
A2	0	30	4	27	A2	0	30	2	29	21.9693	-0.00050	0.250	1
A2	0	30	4	27	A2	0	30	2	29	21.9698	-0.00001	0.250	1
A2	0	30	4	27	A2	0	29	5	25	3.1646	-0.00010	0.250	1
A2	0	30	4	27	A2	0	29	5	25	3.1643	-0.00044	0.250	1
A1	0	30	5	26	A1	0	30	3	28	21.1537	-0.00158	0.250	0
A1	0	30	5	26	A1	0	30	3	28	21.1544	-0.00091	0.250	1
A1	0	30	5	26	A1	0	29	6	24	3.9810	-0.00053	0.250	1
A1	0	30	5	26	A1	0	29	6	24	3.9815	-0.00001	0.250	1
A2	0	30	6	25	A2	0	30	4	27	20.2922	-0.00060	0.250	1
A1	0	30	7	24	A1	0	30	5	26	19.4686	-0.00088	0.250	1
A1	0	30	7	24	A1	0	30	5	26	19.4693	-0.00019	0.250	1
A1	0	30	7	24	A1	0	30	5	26	19.4706	0.00112	0.250	1
A1	0	30	7	24	A1	0	29	6	24	23.4496	-0.00141	0.250	0
A1	0	30	7	24	A1	0	29	6	24	23.4519	0.00089	0.250	1
A1	0	30	7	24	A1	0	29	6	24	23.4508	-0.00021	0.250	1
A1	0	30	7	24	A1	0	29	8	22	5.5801	-0.00009	0.250	1
A1	0	30	7	24	A1	0	29	8	22	5.5804	0.00024	0.250	1
A2	0	30	8	23	A2	0	29	7	23	23.4289	0.00037	0.250	1
A2	0	30	8	23	A2	0	29	7	23	23.4319	0.00335	0.250	0
A2	0	30	8	23	A2	0	29	7	23	23.4299	0.00137	0.250	1
A2	0	30	8	23	A2	0	29	7	23	23.4282	-0.00030	0.250	1
A2	0	30	8	23	A2	0	29	7	23	23.4285	0.00001	0.250	1
A2	0	30	8	23	A2	0	29	9	21	6.3968	-0.00061	0.250	1
A2	0	30	8	23	A2	0	29	9	21	6.3971	-0.00028	0.250	1
A1	0	30	9	22	A1	0	30	7	24	17.8280	0.00757	0.250	0
A1	0	30	9	22	A1	0	30	7	24	17.8273	0.00687	0.250	0
A1	0	30	9	22	A1	0	30	7	24	17.8280	0.00757	0.250	0
A1	0	30	9	22	A1	0	30	7	24	17.8273	0.00687	0.250	0
A1	0	30	9	22	A1	0	29	8	22	23.4041	0.00348	0.250	0
A1	0	30	9	22	A1	0	29	8	22	23.4003	-0.00032	0.250	1
A1	0	30	9	22	A1	0	29	8	22	23.4008	0.00014	0.250	1

Ground upper levels					Ground lower levels					Obs. Trans.	Obs.- calc.		
Γ′	*m′*	*J′*	*Ka′*	*Kc′*	*Γ″*	*m″*	*J″*	*Ka″*	*Kc″*	(cm^{-1})	(cm^{-1})	weight	Ifit
A2	0	31	1	31	A2	0	30	2	29	0.7442	0.00052	0.250	1
A1	0	31	2	30	A1	0	30	1	30	24.3377	0.00005	0.250	1
A1	0	31	2	30	A1	0	30	3	28	1.5460	-0.00070	0.250	1
A1	0	31	2	30	A1	0	30	3	28	1.5465	-0.00021	0.250	1
A1	0	31	2	30	A1	0	30	3	28	1.5476	0.00088	0.250	1
A2	0	31	3	29	A2	0	31	1	31	23.5771	-0.00020	0.250	1
A2	0	31	3	29	A2	0	30	2	29	24.3213	0.00032	0.250	1
A2	0	31	3	29	A2	0	30	2	29	24.3219	0.00092	0.250	1
A2	0	31	3	29	A2	0	30	2	29	24.3215	0.00052	0.250	1
A2	0	31	3	29	A2	0	30	4	27	2.3521	0.00093	0.250	1
A2	0	31	3	29	A2	0	30	4	27	2.3519	0.00074	0.250	1
A1	0	31	4	28	A1	0	31	2	30	22.7552	-0.00057	0.250	1
A1	0	31	4	28	A1	0	31	2	30	22.7557	-0.00005	0.250	1
A1	0	31	4	28	A1	0	31	2	30	22.7557	-0.00005	0.250	1
A1	0	31	4	28	A1	0	30	5	26	3.1480	0.00080	0.250	1
A2	0	31	5	27	A2	0	31	3	29	21.9357	0.00041	0.250	1
A2	0	31	5	27	A2	0	31	3	29	21.9349	-0.00034	0.250	1
A2	0	31	5	27	A2	0	30	4	27	24.2876	0.00118	0.250	1
A2	0	31	5	27	A2	0	30	4	27	24.2876	0.00116	0.250	1
A1	0	31	6	26	A1	0	31	4	28	21.1222	-0.00542	0.250	0
A1	0	31	6	26	A1	0	31	4	28	21.1229	-0.00471	0.250	0
A1	0	31	6	26	A1	0	30	7	24	4.8020	-0.00330	0.250	0
A1	0	31	6	26	A1	0	30	7	24	4.8014	-0.00390	0.250	0
A1	0	31	8	24	A1	0	31	6	26	19.4063	-0.00075	0.250	1
A1	0	31	8	24	A1	0	31	6	26	19.4141	0.00709	0.250	0
A1	0	31	8	24	A1	0	31	6	26	19.4065	-0.00049	0.250	1
A1	0	31	8	24	A1	0	30	7	24	24.2125	0.00014	0.250	1
A1	0	31	8	24	A1	0	30	7	24	24.2126	0.00023	0.250	1
A1	0	31	8	24	A1	0	30	7	24	24.2115	-0.00086	0.250	1
A1	0	31	8	24	A1	0	30	7	24	24.2124	0.00009	0.250	1
A2	0	31	9	23	A2	0	30	8	23	24.1915	0.00644	0.250	0
A2	0	31	9	23	A2	0	30	8	23	24.1857	0.00063	0.250	1
A2	0	31	9	23	A2	0	30	8	23	24.1848	-0.00023	0.250	1
A2	0	31	9	23	A2	0	30	8	23	24.1854	0.00030	0.250	1
A1	0	32	1	32	A1	0	31	2	30	0.7419	-0.00005	0.250	1
A1	0	32	1	32	A1	0	31	2	30	0.7422	0.00024	0.250	1
A2	0	32	2	31	A2	0	31	1	31	25.1222	-0.00022	0.250	1
A2	0	32	2	31	A2	0	31	3	29	1.5446	-0.00050	0.250	1
A1	0	32	3	30	A1	0	32	1	32	24.3621	-0.00148	0.250	0
A1	0	32	3	30	A1	0	32	1	32	24.3627	-0.00088	0.250	1
A1	0	32	3	30	A1	0	32	1	32	24.3630	-0.00058	0.250	1
A1	0	32	3	30	A1	0	31	2	30	25.1040	-0.00153	0.250	0
A1	0	32	3	30	A1	0	31	2	30	25.1053	-0.00021	0.250	1
A1	0	32	3	30	A1	0	31	4	28	2.3496	-0.00016	0.250	1
A1	0	32	3	30	A1	0	31	4	28	2.3495	-0.00028	0.250	1
A2	0	32	4	29	A2	0	32	2	31	23.5409	-0.00060	0.250	1
A2	0	32	4	29	A2	0	32	2	31	23.5411	-0.00042	0.250	1
A2	0	32	4	29	A2	0	31	5	27	3.1510	-0.00035	0.250	1
A2	0	32	4	29	A2	0	31	5	27	3.1502	-0.00122	0.250	1
A2	0	32	4	29	A2	0	31	5	27	3.1506	-0.00079	0.250	1
A1	0	32	5	28	A1	0	32	3	30	22.7209	0.00118	0.250	1
A1	0	32	5	28	A1	0	32	3	30	22.7204	0.00069	0.250	1

Ground upper levels					Ground lower levels					Obs. Trans.	Obs.- calc.		
Γ′	*m′*	*J′*	*Ka′*	*Kc′*	*Γ″*	*m″*	*J″*	*Ka″*	*Kc″*	(cm^{-1})	(cm^{-1})	weight	Ifit
A1	0	32	5	28	A1	0	31	4	28	25.0704	0.00093	0.250	1
A1	0	32	5	28	A1	0	31	6	26	3.9475	0.00564	0.250	0
A1	0	32	5	28	A1	0	31	6	26	3.9488	0.00693	0.250	0
A2	0	32	6	27	A2	0	32	4	29	21.9019	0.00076	0.250	1
A2	0	32	6	27	A2	0	32	4	29	21.9013	0.00015	0.250	1
A1	0	32	9	24	A1	0	32	7	26	19.3223	-0.00049	0.250	1
A1	0	32	9	24	A1	0	32	7	26	19.3227	-0.00012	0.250	1
A1	0	32	9	24	A1	0	32	7	26	19.3217	-0.00116	0.250	1
A1	0	32	9	24	A1	0	32	7	26	19.3220	-0.00079	0.250	1
A2	0	33	1	33	A2	0	32	2	31	0.7406	0.00037	0.250	1
A2	0	33	1	33	A2	0	32	2	31	0.7396	-0.00064	0.250	1
A1	0	33	2	32	A1	0	32	1	32	25.9066	-0.00054	0.250	1
A1	0	33	2	32	A1	0	32	3	30	1.5439	0.00034	0.250	1
A1	0	33	2	32	A1	0	32	3	30	1.5434	-0.00015	0.250	1
A1	0	33	2	32	A1	0	32	3	30	1.5441	0.00056	0.250	1
A2	0	33	3	31	A2	0	33	1	33	25.1512	0.00144	0.250	0
A2	0	33	3	31	A2	0	32	2	31	25.8900	0.00002	0.250	1
A2	0	33	3	31	A2	0	32	4	29	2.3489	0.00044	0.250	1
A2	0	33	3	31	A2	0	32	4	29	2.3488	0.00035	0.250	1
A1	0	33	4	30	A1	0	33	2	32	24.3274	0.00035	0.250	1
A1	0	33	4	30	A1	0	33	2	32	24.3284	0.00135	0.250	0
A1	0	33	4	30	A1	0	32	5	28	3.1499	-0.00098	0.250	1
A1	0	33	4	30	A1	0	32	5	28	3.1520	0.00113	0.250	1
A1	0	33	4	30	A1	0	32	5	28	3.1510	0.00012	0.250	1
A2	0	33	5	29	A2	0	33	3	31	23.5056	0.00110	0.250	0
A2	0	33	5	29	A2	0	33	3	31	23.5076	0.00312	0.250	1
A2	0	33	5	29	A2	0	32	4	29	25.8528	-0.00017	0.250	1
A2	0	33	5	29	A2	0	32	6	27	3.9515	-0.00032	0.250	1
A1	0	33	6	28	A1	0	33	4	30	22.6844	0.00052	0.250	1
A1	0	33	6	28	A1	0	33	4	30	22.6844	0.00055	0.250	1
A2	0	33	7	27	A2	0	33	5	29	21.8658	0.00006	0.250	0
A2	0	33	7	27	A2	0	33	5	29	21.8646	-0.00112	0.250	0
A2	0	33	7	27	A2	0	32	6	27	25.8163	-0.00119	0.250	1
A1	0	34	1	34	A1	0	33	2	32	0.7385	-0.00003	0.250	1
A1	0	34	1	34	A1	0	33	2	32	0.7385	0.00000	0.250	1
A1	0	34	1	34	A1	0	33	2	32	0.7381	-0.00043	0.250	1
A2	0	34	2	33	A2	0	33	1	33	26.6925	0.00075	0.250	1
A2	0	34	2	33	A2	0	33	1	33	26.6925	0.00075	0.250	1
A2	0	34	2	33	A2	0	33	3	31	1.5412	-0.00079	0.250	1
A2	0	34	2	33	A2	0	33	3	31	1.5421	0.00011	0.250	1
A2	0	34	2	33	A2	0	33	3	31	1.5410	-0.00099	0.250	1
A1	0	34	3	32	A1	0	34	1	34	25.9348	-0.00107	0.250	1
A1	0	34	3	32	A1	0	34	1	34	25.9354	-0.00045	0.250	1
A1	0	34	3	32	A1	0	34	1	34	25.9364	0.00055	0.250	1
A1	0	34	3	32	A1	0	33	2	32	26.6745	0.00010	0.250	1
A1	0	34	3	32	A1	0	33	4	30	2.3474	0.00008	0.250	1
A1	0	34	3	32	A1	0	33	4	30	2.3479	0.00057	0.250	1
A1	0	34	3	32	A1	0	33	4	30	2.3474	0.00007	0.250	1
A2	0	34	4	31	A2	0	34	2	33	25.1129	0.00066	0.250	1
A2	0	34	4	31	A2	0	34	2	33	25.1131	0.00087	0.250	1
A2	0	34	4	31	A2	0	33	3	31	26.6550	0.00078	0.250	1
A2	0	34	4	31	A2	0	33	5	29	3.1485	-0.00124	0.250	1

Ground upper levels					Ground lower levels					Obs. Trans.	Obs.- calc.		
Γ′	*m′*	*J′*	*Ka′*	*Kc′*	*Γ″*	*m″*	*J″*	*Ka″*	*Kc″*	(cm^{-1})	(cm^{-1})	weight	Ifit
A2	0	34	4	31	A2	0	33	5	29	3.1505	0.00073	0.250	1
A2	0	34	4	31	A2	0	33	5	29	3.1479	-0.00184	0.250	0
A1	0	34	5	30	A1	0	34	3	32	24.2883	-0.00077	0.250	1
A1	0	34	5	30	A1	0	34	3	32	24.2896	0.00054	0.250	1
A1	0	34	5	30	A1	0	33	4	30	26.6366	0.00019	0.250	1
A1	0	34	5	30	A1	0	33	6	28	3.9522	-0.00036	0.250	1
A1	0	34	5	30	A1	0	33	6	28	3.9525	-0.00004	0.250	1
A2	0	34	6	29	A2	0	34	4	31	23.4680	0.00005	0.250	1
A2	0	34	6	29	A2	0	33	7	27	4.7547	0.00273	0.250	0
A2	0	34	6	29	A2	0	33	7	27	4.7532	0.00123	0.250	1
A2	0	34	6	29	A1	0	33	8	26	5.5556	-0.10242	0.250	0
A1	0	34	7	28	A1	0	34	5	30	22.6455	0.00021	0.250	1
A1	0	34	7	28	A1	0	34	5	30	22.6455	0.00020	0.250	1
A1	0	34	7	28	A1	0	33	6	28	26.5979	0.00005	0.250	1
A2	0	34	8	27	A2	0	34	6	29	21.8288	0.00074	0.250	1
A2	0	34	8	27	A2	0	34	6	29	21.8289	0.00084	0.250	1
A2	0	35	1	35	A2	0	34	2	33	0.7382	0.00137	0.250	1
A2	0	35	1	35	A2	0	34	2	33	0.7369	0.00007	0.250	1
A2	0	35	1	35	A2	0	34	2	33	0.7370	0.00017	0.250	1
A1	0	35	2	34	A1	0	34	1	34	27.4760	-0.00033	0.250	1
A1	0	35	2	34	A1	0	34	3	32	1.5412	0.00074	0.250	1
A1	0	35	2	34	A1	0	34	3	32	1.5405	0.00003	0.250	1
A1	0	35	2	34	A1	0	34	3	32	1.5412	0.00074	0.250	1
A2	0	35	3	33	A2	0	35	1	35	26.7216	-0.00022	0.250	1
A2	0	35	3	33	A2	0	35	1	35	26.7201	-0.00177	0.250	1
A2	0	35	3	33	A2	0	34	2	33	27.4587	0.00004	0.250	1
A2	0	35	3	33	A2	0	34	4	31	2.3456	-0.00083	0.250	1
A2	0	35	3	33	A2	0	34	4	31	2.3458	-0.00064	0.250	1
A1	0	35	4	32	A1	0	35	2	34	25.8962	-0.00066	0.250	1
A1	0	35	4	32	A1	0	35	2	34	25.8964	-0.00047	0.250	1
A1	0	35	4	32	A1	0	34	5	30	3.1484	0.00014	0.250	1
A1	0	35	4	32	A1	0	34	5	30	3.1469	-0.00135	0.250	1
A1	0	35	4	32	A1	0	34	5	30	3.1483	0.00005	0.250	1
A2	0	35	5	31	A2	0	34	4	31	27.4195	-0.00016	0.250	1
A2	0	35	5	31	A2	0	34	6	29	3.9516	-0.00012	0.250	1
A2	0	35	5	31	A2	0	34	6	29	3.9517	-0.00001	0.250	1
A1	0	35	6	30	A1	0	35	4	32	24.2525	-0.00001	0.250	1
A1	0	35	6	30	A1	0	35	4	32	24.2519	-0.00052	0.250	1
A1	0	35	6	30	A1	0	34	7	28	4.7562	0.00076	0.250	1
A1	0	35	6	30	A1	0	34	7	28	4.7563	0.00090	0.250	1
A1	0	35	6	30	A1	0	34	7	28	4.7553	-0.00011	0.250	1
A2	0	35	7	29	A2	0	34	6	29	27.3804	0.00039	0.250	1
A1	0	36	1	36	A1	0	35	2	34	0.7348	-0.00034	0.250	1
A1	0	36	1	36	A1	0	35	2	34	0.7363	0.00116	0.250	1
A2	0	36	2	35	A2	0	35	1	35	28.2608	0.00000	0.250	1
A2	0	36	2	35	A2	0	35	1	35	28.2608	0.00000	0.250	1
A2	0	36	2	35	A2	0	35	3	33	1.5392	0.00022	0.250	1
A2	0	36	2	35	A2	0	35	3	33	1.5393	0.00032	0.250	1
A2	0	36	2	35	A2	0	35	3	33	1.5391	0.00010	0.250	1
A1	0	36	3	34	A1	0	36	1	36	27.5078	0.00008	0.250	1
A1	0	36	3	34	A1	0	36	1	36	27.5076	-0.00013	0.250	1
A1	0	36	3	34	A1	0	35	2	34	28.2415	-0.00136	0.250	1

Ground upper levels					Ground lower levels					Obs. Trans.	Obs.- calc.		
Γ′	*m′*	*J′*	*Ka′*	*Kc′*	*Γ″*	*m″*	*J″*	*Ka″*	*Kc″*	(cm^{-1})	(cm^{-1})	weight	Ifit
A1	0	36	3	34	A1	0	35	4	32	2.3451	-0.00089	0.250	1
A1	0	36	3	34	A1	0	35	4	32	2.3460	0.00001	0.250	1
A2	0	36	4	33	A2	0	36	2	35	26.6814	0.00107	0.250	1
A2	0	36	4	33	A2	0	36	2	35	26.6813	0.00091	0.250	1
A2	0	36	4	33	A2	0	35	5	31	3.1465	0.00040	0.250	1
A2	0	36	4	33	A2	0	35	5	31	3.1460	-0.00010	0.250	1
A2	0	36	4	33	A2	0	35	5	31	3.1457	-0.00041	0.250	1
A2	0	36	4	33	A2	0	35	5	31	3.1441	-0.00201	0.250	0
A1	0	36	5	32	A1	0	36	3	34	25.8561	-0.00046	0.250	1
A1	0	36	5	32	A1	0	36	3	34	25.8582	0.00165	0.250	0
A1	0	36	5	32	A1	0	35	4	32	28.2031	0.00055	0.250	1
A1	0	36	5	32	A1	0	35	4	32	28.2033	0.00075	0.250	1
A1	0	36	5	32	A1	0	35	6	30	3.9505	0.00044	0.250	1
A1	0	36	5	32	A1	0	35	6	30	3.9511	0.00102	0.250	1
A2	0	36	6	31	A2	0	36	4	33	25.0379	0.00040	0.250	1
A2	0	36	6	31	A2	0	36	4	33	25.0370	-0.00059	0.250	1
A2	0	36	6	31	A2	0	35	7	29	4.7553	-0.00007	0.250	1
A2	0	36	6	31	A2	0	35	7	29	4.7559	0.00054	0.250	1
A2	0	36	6	31	A2	0	35	7	29	4.7542	-0.00118	0.250	1
A1	0	36	7	30	A2	0	35	5	31	24.2188	-0.06671	0.250	0
A1	0	36	7	30	A1	0	36	5	32	24.2135	0.00107	0.250	1
A1	0	36	7	30	A1	0	35	6	30	28.1617	-0.00086	0.250	1
A1	0	36	7	30	A1	0	35	6	30	28.1617	-0.00083	0.250	1
A1	0	36	7	30	A1	0	35	8	28	5.5611	0.00050	0.250	1
A2	0	36	8	29	A2	0	36	6	31	23.3828	-0.00029	0.250	1
A2	0	36	8	29	A2	0	36	6	31	23.3891	0.00597	0.250	0
A2	0	36	8	29	A2	0	35	9	27	6.3504	-0.00056	0.250	1
A1	0	36	9	28	A1	0	36	7	30	22.5505	-0.00092	0.250	1
A1	0	36	9	28	A1	0	36	7	30	22.5503	-0.00110	0.250	1
A2	0	37	1	37	A2	0	36	2	35	0.7333	-0.00016	0.250	1
A2	0	37	1	37	A2	0	36	2	35	0.7332	-0.00025	0.250	1
A1	0	37	2	36	A1	0	36	1	36	29.0446	-0.00060	0.250	1
A1	0	37	2	36	A1	0	36	3	34	1.5368	-0.00068	0.250	1
A1	0	37	2	36	A1	0	36	3	34	1.5381	0.00062	0.250	1
A2	0	37	3	35	A2	0	37	1	37	28.2939	0.00036	0.250	1
A2	0	37	3	35	A2	0	37	1	37	28.2945	0.00097	0.250	1
A2	0	37	3	35	A2	0	36	2	35	29.0263	-0.00069	0.250	1
A2	0	37	3	35	A2	0	36	4	33	2.3467	0.00007	0.250	1
A2	0	37	3	35	A2	0	36	4	33	2.3462	-0.00043	0.250	1
A1	0	37	4	34	A1	0	37	2	36	27.4355	-0.02438	0.250	0
A1	0	37	4	34	A1	0	37	2	36	27.4605	0.00060	0.250	1
A1	0	37	4	34	A1	0	36	5	32	3.1387	-0.00212	0.250	0
A2	0	37	5	33	A2	0	37	3	35	26.6365	-0.00186	0.250	0
A2	0	37	5	33	A2	0	36	4	33	28.9849	-0.00009	0.250	1
A2	0	37	5	33	A2	0	36	4	33	28.9827	-0.00229	0.250	0
A2	0	37	5	33	A2	0	36	6	31	3.9475	0.00002	0.250	1
A2	0	37	7	31	A2	0	36	8	29	5.5606	-0.00136	0.250	1
A2	0	37	7	31	A2	0	36	8	29	5.5623	0.00032	0.250	1
A1	0	37	8	30	A1	0	37	6	32	24.1666	0.00016	0.250	1
A1	0	37	8	30	A1	0	37	6	32	24.1665	0.00007	0.250	1
A1	0	37	8	30	A1	0	36	9	28	6.3788	0.00990	0.250	0
A2	0	37	9	29	A2	0	37	7	31	23.3308	0.00085	0.250	1

Ground upper levels					Ground lower levels					Obs. Trans.	Obs.- calc.		
Γ′	*m′*	*J′*	*Ka′*	*Kc′*	*Γ″*	*m″*	*J″*	*Ka″*	*Kc″*	(cm^{-1})	(cm^{-1})	weight	Ifit
A2	0	37	9	29	A2	0	37	7	31	23.3305	0.00054	0.250	1
A1	0	38	1	38	A1	0	37	2	36	0.7311	-0.00069	0.250	1
A1	0	38	1	38	A1	0	37	2	36	0.7312	-0.00059	0.250	1
A2	0	38	2	37	A2	0	37	1	37	29.8298	0.00021	0.250	1
A2	0	38	2	37	A2	0	37	3	35	1.5359	-0.00015	0.250	1
A2	0	38	2	37	A2	0	37	3	35	1.5358	-0.00023	0.250	1
A2	0	38	2	37	A2	0	37	3	35	1.5363	0.00026	0.250	1
A1	0	38	3	36	A1	0	38	1	38	29.0785	-0.00073	0.250	1
A1	0	38	3	36	A1	0	38	1	38	29.0783	-0.00092	0.250	1
A1	0	38	3	36	A1	0	37	2	36	29.8099	-0.00114	0.250	1
A1	0	38	5	34	A1	0	38	3	36	27.4171	0.00087	0.250	1
A1	0	38	5	34	A1	0	38	3	36	27.4168	0.00056	0.250	1
A1	0	38	5	34	A1	0	37	4	34	29.7675	0.00013	0.250	1
A1	0	38	5	34	A1	0	37	6	32	3.9424	0.00058	0.250	1
A1	0	38	5	34	A1	0	37	6	32	3.9427	0.00086	0.250	1
A1	0	38	7	32	A1	0	38	5	34	25.7873	0.00155	0.250	1
A1	0	38	7	32	A1	0	38	5	34	25.7876	0.00186	0.250	1
A1	0	38	7	32	A1	0	37	6	32	29.7269	-0.00058	0.250	1
A1	0	38	7	32	A1	0	37	8	30	5.5614	0.00036	0.250	1
A1	0	38	7	32	A1	0	37	8	30	5.5614	0.00028	0.250	1
A2	0	38	8	31	A2	0	38	6	33	24.9506	-0.00064	0.250	1
A2	0	38	8	31	A2	0	38	6	33	24.9502	-0.00099	0.250	1
A2	0	38	8	31	A2	0	37	9	29	6.3760	0.00362	0.250	0
A2	0	38	8	31	A2	0	37	9	29	6.3747	0.00230	0.250	0
A1	0	38	9	30	A1	0	38	7	32	24.1229	0.01113	0.250	0
A1	0	38	9	30	A1	0	38	7	32	24.1227	0.01095	0.250	0
A2	0	39	1	39	A2	0	38	2	37	0.7292	-0.00093	0.250	1
A1	0	39	2	38	A1	0	38	1	38	30.6137	-0.00012	0.250	1
A1	0	39	2	38	A1	0	38	3	36	1.5352	0.00061	0.250	1
A1	0	39	2	38	A1	0	38	3	36	1.5362	0.00159	0.250	0
A2	0	39	3	37	A2	0	39	1	39	29.8642	-0.00062	0.250	1
A2	0	39	3	37	A2	0	38	2	37	30.5942	-0.00075	0.250	1
A2	0	39	3	37	A2	0	38	2	37	30.5953	0.00036	0.250	1
A1	0	39	4	36	A1	0	39	2	38	29.0555	-0.00090	0.250	1
A1	0	39	4	36	A1	0	38	3	36	30.5890	-0.00199	0.250	0
A1	0	39	4	36	A1	0	38	5	34	3.1749	0.00019	0.250	1
A1	0	39	4	36	A1	0	38	5	34	3.1750	0.00022	0.250	1
A1	0	39	4	36	A1	0	38	5	34	3.1753	0.00049	0.250	1
A1	0	39	6	34	A1	0	39	4	36	27.3551	-0.00118	0.250	0
A1	0	39	6	34	A1	0	38	7	32	4.7432	-0.00218	0.250	0
A1	0	39	6	34	A1	0	38	7	32	4.7433	-0.00208	0.250	0
A1	0	39	6	34	A1	0	38	7	32	4.7443	-0.00104	0.250	1
A2	0	39	7	33	A2	0	38	6	33	30.5095	-0.00029	0.250	1
A2	0	39	7	33	A2	0	38	8	31	5.5493	-0.00930	0.250	0
A2	0	39	7	33	A2	0	38	8	31	5.5508	-0.00778	0.250	0
A1	0	39	8	32	A1	0	39	6	34	25.7394	0.00055	0.250	1
A1	0	39	8	32	A1	0	38	9	30	6.3735	0.00106	0.250	0
A1	0	39	8	32	A1	0	38	9	30	6.3728	0.00036	0.250	1
A2	0	39	9	31	A2	0	39	7	33	24.8915	-0.00383	0.250	0
A2	0	39	9	31	A2	0	39	7	33	24.8915	-0.00379	0.250	0
A1	0	40	1	40	A1	0	39	2	38	0.7279	-0.00058	0.250	1
A2	0	40	2	39	A2	0	39	3	37	1.5324	-0.00083	0.250	1

Ground upper levels					Ground lower levels					Obs. Trans.	Obs.- calc.		
Γ′	*m′*	*J′*	*Ka′*	*Kc′*	*Γ″*	*m″*	*J″*	*Ka″*	*Kc″*	(cm^{-1})	(cm^{-1})	weight	Ifit
A2	0	40	2	39	A2	0	39	3	37	1.5337	0.00048	0.250	1
A2	0	40	2	39	A2	0	39	3	37	1.5345	0.00129	0.250	1
A1	0	40	3	38	A1	0	40	1	40	30.6507	0.00042	0.250	1
A1	0	40	3	38	A1	0	40	1	40	30.6506	0.00029	0.250	1
A1	0	40	3	38	A1	0	39	2	38	31.3784	-0.00040	0.250	1
A1	0	40	3	38	A1	0	39	4	36	2.3229	0.00050	0.250	1
A2	0	40	4	37	A2	0	40	2	39	29.8332	-0.00133	0.250	1
A2	0	40	4	37	A2	0	40	2	39	29.8338	-0.00072	0.250	1
A1	0	40	7	34	A1	0	40	5	36	27.2109	-0.00295	0.250	0
A1	0	40	7	34	A1	0	39	8	32	5.5535	0.00004	0.250	1
A1	0	40	7	34	A1	0	39	8	32	5.5535	0.00004	0.250	0
A2	0	40	8	33	A2	0	39	9	31	6.3671	-0.00363	0.250	0
A2	0	40	8	33	A2	0	39	9	31	6.3659	-0.00482	0.250	0
A2	0	41	1	41	A2	0	40	2	39	0.7260	-0.00083	0.250	1
A2	0	41	1	41	A2	0	40	2	39	0.7263	-0.00055	0.250	1
A1	0	41	2	40	A1	0	40	1	40	32.1828	0.00065	0.250	1
A1	0	41	2	40	A1	0	40	1	40	32.1819	-0.00022	0.250	1
A1	0	41	2	40	A1	0	40	3	38	1.5321	0.00023	0.250	1
A1	0	41	2	40	A1	0	40	3	38	1.5321	0.00026	0.250	1
A2	0	41	3	39	A2	0	41	1	41	31.4369	0.00120	0.250	1
A2	0	41	3	39	A2	0	41	1	41	31.4367	0.00101	0.250	1
A2	0	41	3	39	A2	0	40	2	39	32.1629	0.00038	0.250	1
A2	0	41	3	39	A2	0	40	4	37	2.3291	0.00109	0.250	1
A2	0	41	3	39	A2	0	40	4	37	2.3290	0.00100	0.250	1
A1	0	41	4	38	A1	0	41	2	40	30.6164	-0.00081	0.250	1
A1	0	41	4	38	A1	0	41	2	40	30.6180	0.00078	0.250	1
A1	0	42	1	42	A1	0	41	2	40	0.7258	0.00061	0.250	1
A1	0	42	1	42	A1	0	41	2	40	0.7246	-0.00059	0.250	1
A2	0	42	2	41	A2	0	41	1	41	32.9667	0.00051	0.250	1
A2	0	42	2	41	A2	0	41	3	39	1.5298	-0.00069	0.250	1
A2	0	42	2	41	A2	0	41	3	39	1.5322	0.00169	0.250	0
A2	0	42	2	41	A2	0	41	3	39	1.5304	-0.00007	0.250	1
A1	0	42	3	40	A1	0	42	1	42	32.2209	-0.00008	0.250	1
A1	0	42	3	40	A1	0	42	1	42	32.2212	0.00023	0.250	1
A1	0	42	3	40	A1	0	41	4	38	2.3289	-0.00004	0.250	1
A1	0	42	3	40	A1	0	41	4	38	2.3288	-0.00013	0.250	1
A2	0	42	4	39	A2	0	42	2	41	31.3998	-0.00110	0.250	1
A2	0	42	4	39	A2	0	42	2	41	31.4011	0.00019	0.250	1
A2	0	42	4	39	A2	0	41	5	37	3.1128	0.00043	0.250	1
A2	0	42	4	39	A2	0	41	5	37	3.1135	0.00117	0.250	1
A2	0	42	4	39	A2	0	41	5	37	3.1138	0.00144	0.250	1
A1	0	42	5	38	A1	0	42	3	40	30.5909	-0.00036	0.250	1
A1	0	42	5	38	A1	0	42	3	40	30.5907	-0.00056	0.250	1
A1	0	42	5	38	A1	0	41	4	38	32.9198	-0.00035	0.250	1
A2	0	43	1	43	A2	0	42	2	41	0.7239	0.00034	0.250	1
A2	0	43	1	43	A2	0	42	2	41	0.7230	-0.00057	0.250	1
A1	0	43	2	42	A1	0	42	1	42	33.7499	-0.00027	0.250	1
A1	0	43	2	42	A1	0	42	1	42	33.7505	0.00033	0.250	1
A1	0	43	2	42	A1	0	42	3	40	1.5290	-0.00018	0.250	1
A1	0	43	2	42	A1	0	42	3	40	1.5300	0.00079	0.250	1
A1	0	43	2	42	A1	0	42	3	40	1.5293	0.00010	0.250	1
A2	0	43	3	41	A2	0	43	1	43	33.0071	0.00097	0.250	1

Ground upper levels					Ground lower levels					Obs. Trans.	Obs.- calc.		
Γ′	*m′*	*J′*	*Ka′*	*Kc′*	*Γ″*	*m″*	*J″*	*Ka″*	*Kc″*	(cm^{-1})	(cm^{-1})	weight	Ifit
A2	0	43	3	41	A2	0	43	1	43	33.0052	-0.00094	0.250	1
A2	0	43	3	41	A2	0	42	2	41	33.7293	-0.00039	0.250	1
A2	0	43	3	41	A2	0	42	4	39	2.3282	-0.00058	0.250	1
A2	0	43	3	41	A2	0	42	4	39	2.3294	0.00061	0.250	1
A1	0	43	4	40	A1	0	43	2	42	32.1845	-0.00045	0.250	1
A1	0	43	4	40	A1	0	43	2	42	32.1849	-0.00002	0.250	1
A2	0	43	5	39	A2	0	42	4	39	33.6975	-0.00211	0.250	0
A1	0	44	1	44	A1	0	43	2	42	0.7214	-0.00053	0.250	1
A1	0	44	1	44	A1	0	43	2	42	0.7221	0.00017	0.250	1
A2	0	44	2	43	A2	0	43	1	43	34.5342	0.00014	0.250	1
A2	0	44	2	43	A2	0	43	1	43	34.5349	0.00083	0.250	1
A2	0	44	2	43	A2	0	43	3	41	1.5271	-0.00084	0.250	1
A2	0	44	2	43	A2	0	43	3	41	1.5297	0.00176	0.250	0
A2	0	44	2	43	A2	0	43	3	41	1.5287	0.00077	0.250	1
A1	0	44	3	42	A1	0	44	1	44	33.7917	0.00050	0.250	1
A1	0	44	3	42	A1	0	44	1	44	33.7902	-0.00099	0.250	1
A1	0	44	3	42	A1	0	43	2	42	34.5129	-0.00021	0.250	1
A1	0	44	3	42	A1	0	43	4	40	2.3280	-0.00019	0.250	1
A1	0	44	3	42	A1	0	43	4	40	2.3281	-0.00010	0.250	1
A2	0	44	4	41	A2	0	44	2	43	32.9696	0.00056	0.250	1
A2	0	44	4	41	A2	0	44	2	43	32.9687	-0.00035	0.250	1
A2	0	44	4	41	A2	0	43	5	39	3.1264	0.00025	0.250	1
A1	0	44	5	40	A1	0	44	3	42	32.1521	-0.00041	0.250	1
A1	0	44	5	40	A1	0	44	3	42	32.1515	-0.00102	0.250	1
A1	0	44	5	40	A1	0	43	4	40	34.4791	-0.00160	0.250	0
A1	0	44	5	40	A1	0	43	6	38	3.9166	0.00123	0.250	1
A1	0	44	5	40	A1	0	43	6	38	3.9164	0.00103	0.250	1
A2	0	45	1	45	A2	0	44	2	43	0.7210	0.00069	0.250	1
A2	0	45	1	45	A2	0	44	2	43	0.7194	-0.00091	0.250	1
A2	0	45	1	45	A2	0	44	2	43	0.7201	-0.00019	0.250	1
A1	0	45	2	44	A1	0	44	1	44	35.3175	-0.00043	0.250	1
A1	0	45	2	44	A1	0	44	1	44	35.3160	-0.00190	0.250	0
A1	0	45	2	44	A1	0	44	3	42	1.5258	-0.00093	0.250	1
A1	0	45	2	44	A1	0	44	3	42	1.5265	-0.00023	0.250	1
A1	0	45	2	44	A1	0	44	3	42	1.5258	-0.00092	0.250	1
A2	0	45	3	43	A2	0	45	1	45	34.5764	0.00027	0.250	1
A2	0	45	3	43	A2	0	45	1	45	34.5753	-0.00082	0.250	1
A2	0	45	3	43	A2	0	44	2	43	35.2954	-0.00104	0.250	1
A2	0	45	3	43	A2	0	44	4	41	2.3267	-0.00069	0.250	1
A2	0	45	3	43	A2	0	44	4	41	2.3264	-0.00097	0.250	1
A1	0	45	4	42	A1	0	45	2	44	33.7526	-0.00052	0.250	1
A1	0	45	4	42	A1	0	45	2	44	33.7543	0.00116	0.250	1
A1	0	45	4	42	A1	0	44	5	40	3.1270	-0.00034	0.250	1
A1	0	45	4	42	A1	0	44	5	40	3.1293	0.00195	0.250	0
A2	0	45	5	41	A2	0	45	3	43	32.9355	0.00040	0.250	1
A2	0	45	5	41	A2	0	45	3	43	32.9358	0.00071	0.250	1
A2	0	45	5	41	A2	0	44	4	41	35.2626	0.00014	0.250	1
A1	0	46	1	46	A1	0	45	2	44	0.7203	0.00161	0.250	0
A1	0	46	1	46	A1	0	45	2	44	0.7181	-0.00058	0.250	1
A2	0	46	2	45	A2	0	45	1	45	36.1014	-0.00028	0.250	1
A2	0	46	2	45	A2	0	45	1	45	36.1002	-0.00146	0.250	1
A2	0	46	2	45	A2	0	45	3	43	1.5250	-0.00055	0.250	1

Ground upper levels					Ground lower levels					Obs. Trans.	Obs.- calc.		
Γ′	m′	J′	Ka′	Kc′	Γ″	m″	J″	Ka″	Kc″	(cm^{-1})	(cm^{-1})	weight	Ifit
A2	0	46	2	45	A2	0	45	3	43	1.5252	-0.00035	0.250	1
A2	0	46	2	45	A2	0	45	3	43	1.5249	-0.00064	0.250	1
A2	0	46	2	45	A2	0	45	3	43	1.5262	0.00064	0.250	1
A1	0	46	3	44	A1	0	46	1	46	35.3605	-0.00041	0.250	1
A1	0	46	3	44	A1	0	46	1	46	35.3622	0.00128	0.250	1
A2	0	46	4	43	A2	0	46	2	45	34.5374	0.00022	0.250	1
A2	0	46	4	43	A2	0	45	5	41	3.1271	-0.00053	0.250	1
A2	0	46	4	43	A2	0	45	5	41	3.1271	-0.00056	0.250	1
A1	0	46	5	42	A1	0	46	3	44	33.7177	-0.00035	0.250	1
A1	0	46	5	42	A1	0	45	4	42	36.0452	0.00067	0.250	1
A2	0	46	6	41	A2	0	46	4	43	32.8958	0.00090	0.250	1
A2	0	46	6	41	A2	0	46	4	43	32.8942	-0.00071	0.250	1
A2	0	46	6	41	A2	0	45	7	39	4.7260	0.00011	0.250	1
A2	0	46	6	41	A2	0	45	7	39	4.7260	0.00014	0.250	1
A2	0	46	6	41	A2	0	45	7	39	4.7261	0.00025	0.250	1
A2	0	47	1	47	A2	0	46	2	45	0.7177	0.00063	0.250	1
A2	0	47	1	47	A2	0	46	2	45	0.7163	-0.00079	0.250	1
A1	0	47	2	46	A1	0	46	1	46	36.8859	0.00055	0.250	1
A1	0	47	2	46	A1	0	46	1	46	36.8862	0.00085	0.250	1
A1	0	47	2	46	A1	0	46	3	44	1.5254	0.00096	0.250	1
A1	0	47	2	46	A1	0	46	3	44	1.5247	0.00026	0.250	1
A1	0	47	2	46	A1	0	46	3	44	1.5240	-0.00043	0.250	1
A2	0	47	3	45	A2	0	47	1	47	36.1467	0.00116	0.250	1
A2	0	47	3	45	A2	0	47	1	47	36.1454	-0.00020	0.250	1
A2	0	47	3	45	A2	0	46	2	45	36.8618	-0.00083	0.250	1
A1	0	47	4	44	A1	0	47	2	46	35.3214	0.00031	0.250	1
A1	0	47	4	44	A1	0	47	2	46	35.3216	0.00049	0.250	1
A1	0	47	4	44	A1	0	46	5	42	3.1285	0.00098	0.250	1
A1	0	47	4	44	A1	0	46	5	42	3.1285	0.00100	0.250	1
A1	0	47	4	44	A1	0	46	5	42	3.1269	-0.00058	0.250	1
A2	0	47	5	43	A2	0	46	4	43	36.8271	0.00039	0.250	1
A2	0	47	5	43	A2	0	46	6	41	3.9329	0.00110	0.250	1
A2	0	47	7	41	A2	0	47	5	43	32.8449	0.00049	0.250	1
A2	0	47	7	41	A2	0	46	6	41	36.7764	0.00022	0.250	1
A1	0	48	1	48	A1	0	47	2	46	0.7145	-0.00095	0.250	1
A1	0	48	1	48	A1	0	47	2	46	0.7152	-0.00024	0.250	1
A2	0	48	2	47	A2	0	47	1	47	37.6688	-0.00017	0.250	1
A2	0	48	2	47	A2	0	47	3	45	1.5244	0.00102	0.250	1
A2	0	48	2	47	A2	0	47	3	45	1.5229	-0.00046	0.250	1
A1	0	48	3	46	A1	0	48	1	48	36.9294	-0.00068	0.250	1
A1	0	48	3	46	A1	0	48	1	48	36.9295	-0.00056	0.250	1
A1	0	48	3	46	A1	0	47	2	46	37.6452	-0.00031	0.250	1
A2	0	48	4	45	A2	0	48	2	47	36.1038	-0.00110	0.250	1
A2	0	48	4	45	A2	0	47	5	43	3.1277	0.00060	0.250	1
A2	0	48	4	45	A2	0	47	5	43	3.1255	-0.00153	0.250	0
A1	0	48	5	44	A1	0	48	3	46	35.2859	0.00137	0.250	1
A1	0	48	5	44	A1	0	47	4	44	37.6097	0.00075	0.250	1
A2	0	48	6	43	A2	0	47	7	41	4.7398	-0.00041	0.250	1
A1	0	48	7	42	A1	0	47	6	42	37.5581	0.00264	0.250	0
A2	0	49	1	49	A2	0	48	2	47	0.7133	-0.00053	0.250	1
A2	0	49	1	49	A2	0	48	2	47	0.7136	-0.00024	0.250	1
A1	0	49	2	48	A1	0	48	1	48	38.4516	-0.00092	0.250	1

Ground upper levels					Ground lower levels					Obs. Trans.	Obs.- calc.		
Γ′	*m′*	*J′*	*Ka′*	*Kc′*	*Γ″*	*m″*	*J″*	*Ka″*	*Kc″*	(cm^{-1})	(cm^{-1})	weight	Ifit
A1	0	49	2	48	A1	0	48	1	48	38.4537	0.00118	0.250	1
A1	0	49	2	48	A1	0	48	3	46	1.5222	-0.00025	0.250	1
A1	0	49	2	48	A1	0	48	3	46	1.5221	-0.00037	0.250	1
A1	0	49	2	48	A1	0	48	3	46	1.5242	0.00174	0.250	0
A1	0	49	2	48	A1	0	48	3	46	1.5230	0.00055	0.250	1
A2	0	49	3	47	A2	0	49	1	49	37.7138	-0.00054	0.250	1
A1	0	49	4	46	A1	0	49	2	48	36.8872	-0.00129	0.250	1
A1	0	49	4	46	A1	0	49	2	48	36.8885	-0.00001	0.250	1
A2	0	49	5	45	A2	0	48	4	45	38.3931	0.00194	0.250	0
A1	0	50	1	50	A1	0	49	2	48	0.7105	-0.00171	0.250	0
A1	0	50	1	50	A1	0	49	2	48	0.7122	-0.00001	0.250	1
A2	0	50	2	49	A2	0	49	1	49	39.2355	-0.00051	0.250	1
A2	0	50	2	49	A2	0	49	3	47	1.5217	0.00003	0.250	1
A2	0	50	2	49	A2	0	49	3	47	1.5226	0.00093	0.250	1

APPENDIX Q

CONSTANT INPUT PARAMETERS USED IN SIX-FOLD TORSION-ROTATION PROGRAM (Ref. [166]) FOR FITTING COMBINATION DIFFERENCES FOR BOTH GROUND AND UPPER STATES OF NO_2-IN-PLANE ROCK BAND

Operators	Parameters	Value / cm^{-1}
$(\frac{1}{2})(1+\cos 6\alpha)$	V_6	1.04982227
P_α^2	F	5.561461
$P_\alpha P_a$	$-2\rho F$	-0.8859943
$P_\alpha^2 P^2$	F_J	-0.6139×10^{-5}
$(\frac{1}{2})(P_a P_b + P_b P_a)\cos 3\alpha$	V_{3zx}	0.42671×10^{-2}
$P_\alpha P_a P^2$	ρ_J	0.35820×10^{-5}
$(\frac{1}{2})\{P_a,(P_b^2 - P_c^2)\}P_\alpha$	ρ_{xy}	0.37737×10^{-5}
$P_\alpha^4 P^2$	F_{mJ}	0.9335206×10^{-9}
$P_\alpha^4 P_a^2$	F_{mK}	-0.254305×10^{-7}
$P_\alpha^3 P_a$	ρ_m	0.286490×10^{-4}
$P_\alpha^3 P_a P^2$	ρ_{mJ}	-0.548142×10^{-9}
$P_\alpha P_a^3$	ρ_k	-0.172395×10^{-5}
$P_a^2 \cos 6\alpha$	V_{6K}	0.345360×10^{-4}
$P_\alpha^3 P_a^3$	ρ_{mK}	0.239863×10^{-8}
$P_\alpha^2 P_a^2$	F_K	0.687859×10^{-6}

$P_\alpha^5 P_a$	ρ_{mm}	0.137515×10^{-6}
$P^2 \cos 6\alpha$	V_{6J}	-0.944831×10^{-5}
$(P_b^2 - P_c^2)\cos 6\alpha$	V_{6xy}	0.421867×10^{-5}
P_α^4	F_m	-0.178197×10^{-3}
$P_b P_\alpha \cos 3\alpha$	D_{3alfax}	0.0276539
$2P_\alpha^2(P_b^2 - P_c^2)$	F_{xy}	-0.397658×10^{-5}
$\left\{P_a^3, P_b\right\}\cos 3\alpha$	V_{3zx}	-0.468819×10^{-7}
$\left\{P_a P_b^2 (P_b^2 - P_c^2)\right\}\cos 3\alpha$	V_{3zxxy}	-0.347572×10^{-7}
$P^2 P_a^2 P_\alpha^2$	F_{JK}	0.771371×10^{-10}
$P_a^3 P_b \cos 3\alpha$	V_{3zxk}	-0.468819×10^{-7}
$P_a^2 P_b P_\alpha \cos 3\alpha$	$D_{3alfaxK}$	0.698270×10^{-6}
$P^2 P_a^3 P_\alpha$	ρ_{JK}	$-0.322975 \times 10^{-10}$
$P^4 P_a P_\alpha$	ρ_{JJ}	$-0.700111 \times 10^{-11}$
P_α^6	F_{mm}	-0.340610×10^{-6}
$P^2 P_b P_\alpha \cos 3\alpha$	D_{3alfaJ}	-0.203205×10^{-6}
$(\frac{1}{2})(P_b P_c + P_c P_b)\sin 6\alpha$	D_{3xy}	0.355161×10^{-5}
$P_\alpha \left\{P_a, (P_b^2 - P_c^2)\right\}$	$\rho_{x^2y^2}$	0.937670×10^{-10}

APPENDIX R

MEASURED TRANSITIONS FREQUENCIES AND RESIDUALS FROM THE FIT OF UPPER STATE COMBINATION DIFFERENCES FOR THE NO_2-IN-PLANE ROCK BAND OF CH_3NO_2

Upper state					Lower state					Obs. Trans.	Obs.- calc.	
m′	*Γ′*	*J′*	*Ka′*	*Kc′*	*m″*	*Γ″*	*J″*	*Ka″*	*Kc″*	(cm^{-1})	(cm^{-1})	Ifit
0	B1	2	1	2	0	B1	1	1	0	0.7818	-0.004	1
0	B1	2	1	2	0	B1	1	1	0	0.7810	-0.005	1
0	B2	3	1	3	0	B2	2	1	1	0.8887	-0.008	1
0	B2	3	1	3	0	B2	2	1	1	0.8886	-0.008	1
0	B2	3	1	3	0	B2	2	1	1	0.8891	-0.007	1
0	B1	4	1	4	0	B1	3	1	2	0.8760	0.002	1
0	B1	4	1	4	0	B1	3	1	2	0.8699	-0.005	1
0	B2	5	1	5	0	B2	4	1	3	0.8255	-0.004	1
0	B2	5	1	5	0	B2	4	1	3	0.8242	-0.005	1
0	B2	5	1	5	0	B2	4	1	3	0.8254	-0.004	1
0	B2	7	1	7	0	B2	6	1	5	0.7928	-0.014	1
0	B2	2	1	1	0	B2	1	1	1	1.4082	-0.003	1
0	B2	2	1	1	0	B2	1	1	1	1.4078	-0.003	1
0	B1	3	1	2	0	B1	2	1	2	2.2542	-0.005	1
0	B1	3	1	2	0	B1	2	1	2	2.2529	-0.006	1
0	B2	4	1	3	0	B2	3	1	3	3.0940	-0.010	1
0	B2	4	1	3	0	B2	3	1	3	3.0955	-0.008	1
0	B2	4	1	3	0	B2	3	1	3	3.0938	-0.010	1
0	B1	5	1	4	0	B1	4	1	4	3.9183	0.003	1
0	B1	5	1	4	0	B1	4	1	4	3.9183	0.003	1
0	B2	6	1	5	0	B2	5	1	5	4.7221	0.010	1
0	B2	6	1	5	0	B2	5	1	5	4.7235	0.012	1
0	B2	6	1	5	0	B2	5	1	5	4.7224	0.011	1
0	B1	7	1	6	0	B1	6	1	6	5.5111	0.007	1
0	B1	7	1	6	0	B1	6	1	6	5.5130	0.009	1
0	B1	7	1	6	0	B1	6	1	6	5.5130	0.009	1
0	B2	8	1	7	0	B2	7	1	7	6.3019	0.005	1
0	B2	8	1	7	0	B2	7	1	7	6.3010	0.005	1
0	B2	8	1	7	0	B2	7	3	5	1.6265	0.008	1
0	B1	9	1	8	0	B1	8	1	8	7.0923	0.003	1
0	B1	9	1	8	0	B1	8	1	8	7.0923	0.003	1
0	B1	9	1	8	0	B1	8	1	8	7.0913	0.002	1

Upper state					Lower state					Obs. Trans.	Obs.- calc.	
m′	*Γ′*	*J′*	*Ka′*	*Kc′*	*m″*	*Γ″*	*J″*	*Ka″*	*Kc″*	(cm^{-1})	(cm^{-1})	Ifit
0	B2	10	1	9	0	B2	9	1	9	7.8847	0.000	1
0	B2	10	1	9	0	B2	9	1	9	7.8843	0.000	1
0	B2	10	1	9	0	B2	9	1	9	7.8845	0.000	1
0	B1	11	1	10	0	B1	10	1	10	8.6770	-0.004	1
0	B1	11	1	10	0	B1	10	1	10	8.6778	-0.003	1
0	B1	11	1	10	0	B1	10	1	10	8.6780	-0.003	1
0	B2	12	1	11	0	B2	11	1	11	9.4700	-0.009	1
0	B1	13	1	12	0	B1	12	1	12	10.2775	-0.003	1
0	B1	13	1	12	0	B1	12	1	12	10.2764	-0.004	1
0	B2	14	1	13	0	B2	13	1	13	11.0838	0.001	1
0	B2	14	1	13	0	B2	13	1	13	11.0843	0.001	1
0	B2	14	1	13	0	B2	13	1	13	11.0846	0.001	1
0	B1	15	1	14	0	B1	14	1	14	11.8902	0.001	1
0	B1	15	1	14	0	B1	14	1	14	11.8914	0.002	1
0	B2	16	1	15	0	B2	15	1	15	12.7037	0.006	1
0	B2	16	1	15	0	B2	15	1	15	12.7017	0.004	1
0	B1	17	1	16	0	B1	16	1	16	13.5155	0.006	1
0	B1	17	1	16	0	B1	16	1	16	13.5153	0.006	1
0	B1	17	1	16	0	B1	16	1	16	13.5158	0.007	1
0	B2	18	1	17	0	B2	17	1	17	14.3307	0.007	1
0	B2	18	1	17	0	B2	17	1	17	14.3293	0.006	1
0	B1	19	1	18	0	B1	18	1	18	15.1396	0.000	1
0	B1	19	1	18	0	B1	18	1	18	15.1395	0.000	1
0	B1	19	1	18	0	B1	18	1	18	15.1406	0.001	1
0	B2	20	1	19	0	B2	19	1	19	15.9564	-0.001	1
0	B2	20	1	19	0	B2	19	1	19	15.9571	-0.001	1
0	B1	21	1	20	0	B1	20	1	20	16.7736	-0.003	1
0	B1	21	1	20	0	B1	20	1	20	16.7719	-0.005	1
0	B2	22	1	21	0	B2	21	1	21	17.5955	-0.001	1
0	B2	22	1	21	0	B2	21	1	21	17.5957	0.000	1
0	B1	23	1	22	0	B1	22	1	22	18.4141	0.001	1
0	B1	23	1	22	0	B1	22	1	22	18.4159	0.003	1
0	B1	23	1	22	0	B1	22	1	22	18.4140	0.001	1
0	B2	24	1	23	0	B2	23	1	23	19.2369	0.010	1
0	B2	24	1	23	0	B2	23	1	23	19.2369	0.010	1
0	B2	24	1	23	0	B2	23	1	23	19.2363	0.010	1
0	B2	3	3	1	0	B2	3	1	3	1.9368	0.003	1
0	B2	3	3	1	0	B2	3	1	3	1.9371	0.003	1
0	B2	3	3	1	0	B2	3	1	3	1.9377	0.003	1
0	B2	3	3	1	0	B2	2	1	1	2.8259	-0.005	1
0	B2	3	3	1	0	B2	2	1	1	2.8263	-0.004	1
0	B2	3	3	1	0	B2	2	1	1	2.8255	-0.005	1
0	B1	4	3	2	0	B1	4	1	4	2.4776	-0.003	1
0	B1	4	3	2	0	B1	4	1	4	2.4770	-0.004	1
0	B1	4	3	2	0	B1	4	1	4	2.4817	0.001	1

Upper state					Lower state					Obs. Trans. (cm^{-1})	Obs.- calc. (cm^{-1})	Ifit
m′	*Γ′*	*J′*	*Ka′*	*Kc′*	*m″*	*Γ″*	*J″*	*Ka″*	*Kc″*			
0	B1	4	3	2	0	B1	4	1	4	2.4776	-0.003	1
0	B1	4	3	2	0	B1	3	1	2	3.3516	-0.004	1
0	B1	4	3	2	0	B1	3	1	2	3.3536	-0.002	1
0	B1	4	3	2	0	B1	3	3	0	2.2642	-0.007	1
0	B2	5	3	3	0	B2	5	1	5	3.1511	-0.003	1
0	B2	5	3	3	0	B2	5	1	5	3.1505	-0.003	1
0	B2	5	3	3	0	B2	5	1	5	3.1522	-0.002	1
0	B2	5	3	3	0	B2	5	1	5	3.1529	-0.001	1
0	B2	5	3	3	0	B2	4	1	3	3.9776	-0.005	1
0	B2	5	3	3	0	B2	4	3	1	2.6115	0.000	1
0	B1	6	3	4	0	B1	6	1	6	3.8982	-0.002	1
0	B1	6	3	4	0	B1	5	1	4	4.7009	-0.010	1
0	B1	6	3	4	0	B1	5	3	2	2.7161	-0.006	1
0	B1	6	3	4	0	B1	5	3	2	2.7181	-0.004	1
0	B1	6	3	4	0	B1	5	3	2	2.7153	-0.007	1
0	B2	7	3	5	0	B2	7	1	7	4.6752	-0.003	1
0	B2	7	3	5	0	B2	7	1	7	4.6756	-0.003	1
0	B2	7	3	5	0	B2	6	1	5	5.4733	-0.012	1
0	B2	7	3	5	0	B2	6	3	3	2.6609	-0.001	1
0	B1	8	3	6	0	B1	8	1	8	5.4628	-0.003	1
0	B1	8	3	6	0	B1	8	1	8	5.4678	0.002	1
0	B1	8	3	6	0	B1	8	1	8	5.4684	0.003	1
0	B1	8	3	6	0	B1	8	1	8	5.4678	0.002	1
0	B1	8	3	6	0	B1	8	1	8	5.4683	0.003	1
0	B2	9	3	7	0	B2	9	1	9	6.2519	-0.002	1
0	B2	9	3	7	0	B2	9	1	9	6.2466	-0.008	1
0	B2	9	3	7	0	B2	9	1	9	6.2479	-0.006	1
0	B2	9	3	7	0	B2	9	1	9	6.2479	-0.006	1
0	B2	11	3	9	0	B2	11	1	11	7.8219	-0.008	1
0	B2	11	3	9	0	B2	11	1	11	7.8216	-0.009	1
0	B2	11	3	9	0	B2	10	1	9	8.6638	0.002	1
0	B2	11	3	9	0	B2	10	1	9	8.6639	0.002	1
0	B2	11	3	9	0	B2	10	1	9	8.6639	0.002	1
0	B2	11	3	9	0	B2	10	1	9	8.6638	0.002	1
0	B2	11	3	9	0	B2	10	1	9	8.6637	0.002	1
0	B2	11	3	9	0	B2	10	1	9	8.6637	0.002	1
0	B2	11	3	9	0	B2	10	1	9	8.6638	0.002	1
0	B1	12	3	10	0	B1	12	1	12	8.6159	-0.002	1
0	B1	12	3	10	0	B1	12	1	12	8.6159	-0.002	1
0	B1	12	3	10	0	B1	12	1	12	8.6171	-0.001	1
0	B1	12	3	10	0	B1	12	1	12	8.6173	0.000	1
0	B2	13	3	11	0	B2	13	1	13	9.4154	0.010	1
0	A1	14	3	12	0	A1	14	1	14	10.1999	0.006	1
0	A1	14	3	12	0	A1	14	1	14	10.1995	0.006	1
0	A1	14	3	12	0	A1	14	1	14	10.1987	0.005	1
0	A2	15	3	13	0	A2	15	1	15	10.9827	0.000	1

Upper state					Lower state					Obs. Trans.	Obs.- calc.	
m′	*Γ′*	*J′*	*Ka′*	*Kc′*	*m″*	*Γ″*	*J″*	*Ka″*	*Kc″*	(cm^{-1})	(cm^{-1})	Ifit
0	A2	15	3	13	0	A2	15	1	15	10.9836	0.001	1
0	A2	15	3	13	0	A2	15	1	15	10.9851	0.003	1
0	A1	16	3	14	0	A1	16	1	16	11.7746	0.002	1
0	A1	16	3	14	0	A1	16	1	16	11.7746	0.002	1
0	A1	16	3	14	0	A1	16	1	16	11.7747	0.003	1
0	A1	16	3	14	0	A1	16	1	16	11.7733	0.001	1
0	A1	16	3	14	0	A1	16	1	16	11.7732	0.001	1
0	A1	16	3	14	0	A1	16	1	16	11.7732	0.001	1
0	A2	17	3	15	0	A2	17	1	17	12.5564	-0.006	1
0	A2	17	3	15	0	A2	17	1	17	12.5556	-0.007	1
0	A1	18	3	16	0	A1	18	1	18	13.3487	-0.005	1
0	A1	18	3	16	0	A1	18	1	18	13.3494	-0.005	1
0	A1	18	3	16	0	A1	18	1	18	13.3500	-0.004	1
0	A1	18	3	16	0	A1	18	1	18	13.3495	-0.005	1
0	A2	19	3	17	0	A2	19	1	19	14.1406	-0.005	1
0	A2	19	3	17	0	A2	19	1	19	14.1413	-0.004	1
0	A2	19	3	17	0	A2	19	1	19	14.1396	-0.006	1
0	A1	20	3	18	0	A1	20	1	20	14.9329	-0.004	1
0	A1	20	3	18	0	A1	20	1	20	14.9340	-0.003	1
0	A1	20	3	18	0	A1	20	1	20	14.9333	-0.003	1
0	A2	21	3	19	0	A2	21	1	21	15.7482	0.022	1
0	B1	3	3	0	0	B1	3	1	2	1.0847	0.000	1
0	B1	3	3	0	0	B1	3	1	2	1.0850	0.001	1
0	B1	3	3	0	0	B1	2	1	2	3.3392	-0.004	1
0	B1	3	3	0	0	B1	2	1	2	3.3377	-0.005	1
0	B2	4	3	1	0	B2	4	1	3	1.3715	0.000	1
0	B2	4	3	1	0	B2	4	1	3	1.3742	0.003	1
0	B2	4	3	1	0	B2	3	1	3	4.4837	0.008	1
0	B2	4	3	1	0	B2	3	1	3	4.4821	0.007	1
0	B2	4	3	1	0	B2	3	3	1	2.5453	0.004	1
0	B2	4	3	1	0	B2	3	3	1	2.5314	-0.010	1
0	B2	4	3	1	0	B2	3	3	1	2.5314	-0.010	1
0	B1	5	3	2	0	B1	5	1	4	1.9778	-0.011	1
0	B1	5	3	2	0	B1	5	1	4	1.9772	-0.011	1
0	B1	5	3	2	0	B1	5	1	4	1.9776	-0.011	1
0	B1	5	3	2	0	B1	5	1	4	1.9781	-0.011	1
0	B1	5	3	2	0	B1	4	3	2	3.4190	-0.004	1
0	B1	5	3	2	0	B1	4	3	2	3.4172	-0.006	1
0	B2	6	3	3	0	B2	6	1	5	2.8170	-0.006	1
0	B2	6	3	3	0	B2	6	1	5	2.8176	-0.005	1
0	B2	6	3	3	0	B2	6	1	5	2.8173	-0.006	1
0	B2	6	3	3	0	B2	6	1	5	2.8176	-0.005	1
0	B2	6	3	3	0	B2	5	3	3	4.3883	0.007	1
0	B2	6	3	3	0	B2	5	3	3	4.3893	0.008	1
0	B2	6	3	3	0	B2	5	3	3	4.3804	-0.001	1
0	B2	6	3	3	0	B2	5	5	1	1.8044	0.011	1

Upper state					Lower state					Obs. Trans.	Obs.- calc.	
m′	*Γ′*	*J′*	*Ka′*	*Kc′*	*m″*	*Γ″*	*J″*	*Ka″*	*Kc″*	(cm^{-1})	(cm^{-1})	Ifit
0	B1	7	3	4	0	B1	7	1	6	3.7170	-0.006	1
0	B1	7	3	4	0	B1	7	1	6	3.7160	-0.007	1
0	B1	7	3	4	0	B1	6	3	4	5.3313	0.005	1
0	B1	7	3	4	0	B1	6	3	4	5.3320	0.005	1
0	B1	7	3	4	0	B1	6	3	4	5.3306	0.004	1
0	B2	8	3	5	0	B2	8	1	7	4.5827	-0.002	1
0	B2	8	3	5	0	B2	8	1	7	4.5844	0.000	1
0	B2	8	3	5	0	B2	7	1	7	10.8856	0.004	1
0	B2	8	3	5	0	B2	7	3	5	6.2099	0.007	1
0	B2	8	3	5	0	B2	7	3	5	6.2101	0.007	1
0	B1	9	3	6	0	B1	9	1	8	5.4033	-0.001	1
0	B1	9	3	6	0	B1	9	1	8	5.4034	0.000	1
0	B1	9	3	6	0	B1	9	1	8	5.4036	0.000	1
0	B1	9	3	6	0	B1	8	3	6	7.0335	0.006	1
0	B1	9	3	6	0	B1	8	3	6	7.0336	0.006	1
0	B1	9	3	6	0	B1	8	3	6	7.0334	0.005	1
0	B1	9	3	6	0	B1	8	3	6	7.0328	0.005	1
0	B1	9	3	6	0	B1	8	5	4	3.1600	0.006	1
0	B2	10	3	7	0	B2	10	1	9	6.2048	0.001	1
0	B2	10	3	7	0	B2	10	1	9	6.2054	0.001	1
0	B2	10	3	7	0	B2	10	1	9	6.2073	0.003	1
0	B2	10	3	7	0	B2	10	1	9	6.2051	0.001	1
0	B2	10	3	7	0	B2	9	3	7	7.8271	-0.007	1
0	B2	10	3	7	0	B2	9	3	7	7.8279	-0.006	1
0	B1	11	3	8	0	B1	10	3	8	8.6226	-0.013	1
0	B1	11	3	8	0	B1	10	3	8	8.6226	-0.013	1
0	B1	11	3	8	0	B1	11	1	10	7.0004	0.003	1
0	B1	11	3	8	0	B1	11	1	10	7.0014	0.004	1
0	B1	11	3	8	0	B1	11	1	10	6.9989	0.002	1
0	B1	11	3	8	0	B1	11	1	10	7.0011	0.004	1
0	B1	11	3	8	0	B1	10	3	8	8.6234	-0.012	1
0	B2	12	3	9	0	B2	12	1	11	7.7884	0.000	1
0	B2	12	3	9	0	B2	12	1	11	7.7886	0.001	1
0	B1	13	3	10	0	B1	13	1	12	8.5738	-0.004	1
0	B1	13	3	10	0	B1	13	1	12	8.5738	-0.004	1
0	B1	13	3	10	0	B1	13	1	12	8.5750	-0.002	1
0	B1	13	3	10	0	B1	12	3	10	10.2348	-0.005	1
0	B1	13	3	10	0	B1	12	3	10	10.2356	-0.004	1
0	B1	13	3	10	0	B1	12	3	10	10.2346	-0.005	1
0	B1	13	3	10	0	B1	12	3	10	10.2350	-0.005	1
0	B2	14	3	11	0	B2	14	1	13	9.3684	0.002	1
0	B2	14	3	11	0	B2	14	1	13	9.3687	0.002	1
0	B2	14	3	11	0	B2	14	1	13	9.3680	0.002	1
0	B2	14	3	11	0	B2	13	3	11	11.0372	-0.007	1
0	B2	14	3	11	0	B2	13	3	11	11.0379	-0.006	1
0	B2	14	3	11	0	B2	13	3	11	11.0371	-0.007	1

Upper state					Lower state					Obs. Trans.	Obs.- calc.	
m′	*Γ′*	*J′*	*Ka′*	*Kc′*	*m″*	*Γ″*	*J″*	*Ka″*	*Kc″*	(cm^{-1})	(cm^{-1})	Ifit
0	B1	15	3	12	0	B1	15	1	14	10.1556	0.001	1
0	B1	15	3	12	0	B1	15	1	14	10.1549	0.000	1
0	B1	15	3	12	0	B1	15	1	14	10.1552	0.000	1
0	B1	15	3	12	0	B1	15	1	14	10.1545	-0.001	1
0	B2	16	3	13	0	B2	16	1	15	10.9371	-0.007	1
0	B2	16	3	13	0	B2	16	1	15	10.9372	-0.007	1
0	B2	16	3	13	0	B2	16	1	15	10.9370	-0.007	1
0	B1	17	3	14	0	B1	17	1	16	11.7281	-0.005	1
0	B1	17	3	14	0	B1	17	1	16	11.7264	-0.006	1
0	B1	17	3	14	0	B1	17	1	16	11.7275	-0.005	1
0	B1	17	3	14	0	B1	17	1	16	11.7276	-0.005	1
0	B2	18	3	15	0	B2	18	1	17	12.5185	-0.003	1
0	B2	18	3	15	0	B2	18	1	17	12.5183	-0.003	1
0	B2	18	3	15	0	B2	18	1	17	12.5175	-0.004	1
0	B2	18	3	15	0	B2	18	1	17	12.5183	-0.003	1
0	B1	19	3	16	0	B1	19	1	18	13.3201	0.010	1
0	B1	19	3	16	0	B1	19	1	18	13.3204	0.011	1
0	B1	19	3	16	0	B1	19	1	18	13.3191	0.009	1
0	B1	19	3	16	0	B1	19	1	18	13.3204	0.011	1
0	B2	20	3	17	0	B2	20	1	19	14.0976	0.001	1
0	B2	20	3	17	0	B2	20	1	19	14.0984	0.002	1
0	B2	20	3	17	0	B2	20	1	19	14.0982	0.002	1
0	B2	20	3	17	0	B2	20	1	19	14.0975	0.001	1
0	B1	21	3	18	0	B1	21	1	20	14.8790	-0.001	1
0	B1	21	3	18	0	B1	21	1	20	14.8810	0.001	1
0	B1	21	3	18	0	B1	21	1	20	14.8793	-0.001	1
0	B2	22	3	19	0	B2	22	1	21	15.6549	-0.005	1
0	B2	22	3	19	0	B2	22	1	21	15.6596	0.000	1
0	B2	22	3	19	0	B2	22	1	21	15.6517	-0.008	1
0	B2	22	3	19	0	B2	22	1	21	15.6533	-0.006	1
0	B2	5	5	1	0	B2	4	3	1	5.1946	-0.004	1
0	B2	5	5	1	0	B2	5	3	3	2.5849	-0.002	1
0	B2	5	5	1	0	B2	5	3	3	2.5949	0.008	1
0	B2	5	5	1	0	B2	5	3	3	2.5974	0.010	1
0	B1	6	5	2	0	B1	5	3	2	5.5599	-0.002	1
0	B1	6	5	2	0	B1	6	3	4	2.8405	0.001	1
0	B1	6	5	2	0	B1	6	3	4	2.8415	0.002	1
0	B1	6	5	2	0	B1	6	3	4	2.8425	0.003	1
0	B1	6	5	2	0	B1	6	3	4	2.8416	0.002	1
0	B1	6	5	2	0	B1	6	3	4	2.8405	0.001	1
0	B2	7	5	3	0	B2	6	3	3	5.9307	-0.007	1
0	B2	7	5	3	0	B2	6	3	3	5.9307	-0.007	1
0	B2	7	5	3	0	B2	7	3	5	3.2730	-0.003	1
0	B2	7	5	3	0	B2	7	3	5	3.2733	-0.002	1
0	B2	7	5	3	0	B2	7	3	5	3.2686	-0.007	1
0	B2	7	5	3	0	B2	7	3	5	3.2686	-0.007	1

Upper state					Lower state					Obs. Trans.	Obs.- calc.	
m′	*Γ′*	*J′*	*Ka′*	*Kc′*	*m″*	*Γ″*	*J″*	*Ka″*	*Kc″*	(cm^{-1})	(cm^{-1})	Ifit
0	B1	8	5	4	0	B1	8	3	6	3.8735	-0.001	1
0	B1	8	5	4	0	B1	8	3	6	3.8728	-0.002	1
0	B1	8	5	4	0	B1	8	3	6	3.8727	-0.002	1
0	B2	9	5	5	0	B2	9	3	7	4.5875	0.002	1
0	B2	9	5	5	0	B2	9	3	7	4.5872	0.002	1
0	B2	9	5	5	0	B2	9	3	7	4.5886	0.003	1
0	B1	10	5	6	0	B1	10	3	8	5.3592	0.005	1
0	B1	10	5	6	0	B1	10	3	8	5.3591	0.005	1
0	B1	10	5	6	0	B1	10	3	8	5.3588	0.005	1
0	B2	11	5	7	0	B2	11	3	9	6.1546	0.010	1
0	B2	11	5	7	0	B2	11	3	9	6.1572	0.012	1
0	B2	11	5	7	0	B2	11	3	9	6.1569	0.012	1
0	B1	12	5	8	0	B1	12	3	10	6.9462	0.006	1
0	B1	12	5	8	0	B1	12	3	10	6.9462	0.006	1
0	B1	12	5	8	0	B1	12	3	10	6.9441	0.004	1
0	B1	12	5	8	0	B1	11	5	6	4.2460	0.001	1
0	B2	13	5	9	0	B2	13	3	11	7.7312	-0.004	1
0	B2	13	5	9	0	B2	13	3	11	7.7332	-0.002	1
0	A1	18	5	14	0	A1	18	3	16	11.6940	0.005	1
0	A1	18	5	14	0	A1	18	3	16	11.6954	0.006	1
0	A1	18	5	14	0	A1	18	3	16	11.6951	0.006	1
0	A1	18	5	14	0	A1	18	3	16	11.6944	0.005	1
0	A2	19	5	15	0	A2	19	3	17	12.4824	0.006	1
0	A2	19	5	15	0	A2	19	3	17	12.4834	0.007	1
0	A2	19	5	15	0	A2	19	3	17	12.4825	0.006	1
0	A2	19	5	15	0	A2	19	3	17	12.4828	0.006	1
0	A1	20	5	16	0	A1	20	3	18	13.2666	0.005	1
0	A1	20	5	16	0	A1	20	3	18	13.2669	0.005	1
0	A1	20	5	16	0	A1	20	3	18	13.2664	0.005	1
0	A1	20	5	16	0	A1	20	3	18	13.2659	0.004	1
0	A2	21	5	17	0	A2	21	3	19	14.0287	-0.015	1
0	A2	21	5	17	0	A2	21	3	19	14.0407	-0.003	1
0	A1	22	5	18	0	A1	22	3	20	14.8220	0.002	1
0	A1	22	5	18	0	A1	22	3	20	14.8234	0.004	1
0	A1	22	5	18	0	A1	22	3	20	14.8211	0.001	1
0	B1	5	5	0	0	B1	5	3	2	2.0171	0.010	1
0	B1	5	5	0	0	B1	5	3	2	2.0180	0.011	1
0	B1	5	5	0	0	B1	5	3	2	2.0154	0.008	1
0	B1	5	5	0	0	B1	4	3	2	5.4343	0.004	1
0	B2	6	5	1	0	B2	6	3	3	1.8217	0.002	1
0	B2	6	5	1	0	B2	6	3	3	1.8229	0.003	1
0	B2	6	5	1	0	B2	6	3	3	1.8229	0.003	1
0	B2	6	5	1	0	B2	5	3	3	6.1902	-0.010	1
0	B2	6	5	1	0	B2	5	5	1	3.6261	0.013	1
0	B2	6	5	1	0	B2	5	5	1	3.6254	0.012	1
0	B2	6	5	1	0	B2	5	5	1	3.6248	0.012	1

Upper state					Lower state					Obs. Trans.	Obs.- calc.	
m′	*Γ′*	*J′*	*Ka′*	*Kc′*	*m″*	*Γ″*	*J″*	*Ka″*	*Kc″*	(cm^{-1})	(cm^{-1})	Ifit
0	B1	7	5	2	0	B1	7	3	4	1.9148	0.000	1
0	B1	7	5	2	0	B1	7	3	4	1.9126	-0.002	1
0	B1	7	5	2	0	B1	7	3	4	1.9124	-0.002	1
0	B1	7	5	2	0	B1	7	3	4	1.9132	-0.001	1
0	B1	7	5	2	0	B1	6	3	4	7.2435	0.002	1
0	B1	7	5	2	0	B1	6	5	2	4.4033	0.002	1
0	B1	7	5	2	0	B1	6	5	2	4.4021	0.001	1
0	B1	7	5	2	0	B1	6	5	2	4.4025	0.001	1
0	B2	8	5	3	0	B2	8	3	5	2.4118	-0.008	1
0	B2	8	5	3	0	B2	8	3	5	2.4112	-0.009	1
0	B2	8	5	3	0	B2	8	3	5	2.4120	-0.008	1
0	B2	8	5	3	0	B2	7	3	5	8.6221	-0.001	1
0	B2	8	5	3	0	B2	7	5	3	5.3482	0.001	1
0	B2	8	5	3	0	B2	7	5	3	5.3486	0.001	1
0	B1	9	5	4	0	B1	9	3	6	3.2378	-0.010	1
0	B1	9	5	4	0	B1	8	5	4	6.3974	-0.004	1
0	B1	9	5	4	0	B1	8	5	4	6.3976	-0.004	1
0	B2	10	5	5	0	B2	10	3	7	4.2247	0.010	1
0	B2	10	5	5	0	B2	10	3	7	4.2244	0.010	1
0	B2	10	5	5	0	B2	10	3	7	4.2186	0.004	1
0	B2	10	5	5	0	B2	10	3	7	4.2193	0.005	1
0	B2	10	5	5	0	B2	10	3	7	4.2193	0.005	1
0	B2	10	5	5	0	B2	9	5	5	7.4656	0.002	1
0	B2	10	5	5	0	B2	9	5	5	7.4648	0.001	1
0	B2	10	5	5	0	B2	9	5	5	7.4659	0.003	1
0	B2	10	5	5	0	B2	9	5	5	7.4654	0.002	1
0	B1	11	5	6	0	B1	11	3	8	5.1673	0.008	1
0	B1	11	5	6	0	B1	11	3	8	5.1658	0.007	1
0	B1	11	5	6	0	B1	11	3	8	5.1660	0.007	1
0	B1	11	5	6	0	B1	10	5	6	8.4293	-0.011	1
0	B1	11	5	6	0	B1	10	5	6	8.4300	-0.010	1
0	B1	11	5	6	0	B1	10	5	6	8.4298	-0.011	1
0	B2	12	5	7	0	B2	12	3	9	6.0455	0.014	1
0	B2	12	5	7	0	B2	12	3	9	6.0330	0.002	1
0	B2	12	5	7	0	B2	11	5	7	9.3135	-0.010	1
0	B2	12	5	7	0	B2	11	5	7	9.3141	-0.009	1
0	B2	12	5	7	0	B2	11	5	7	9.3135	-0.010	1
0	B2	12	5	7	0	B2	11	7	5	4.7609	0.005	1
0	B2	12	5	7	0	B2	11	7	5	4.7610	0.005	1
0	B1	13	5	8	0	B1	13	3	10	6.8636	0.005	1
0	B1	13	5	8	0	B1	13	3	10	6.8639	0.005	1
0	B1	13	5	8	0	B1	13	3	10	6.8650	0.006	1
0	B1	13	5	8	0	B1	12	5	8	10.1548	-0.003	1
0	B1	13	5	8	0	B1	12	5	8	10.1547	-0.003	1
0	B1	13	5	8	0	B1	12	5	8	10.1548	-0.003	1
0	B2	14	5	9	0	B2	14	3	11	7.6721	0.005	1

Upper state					Lower state					Obs. Trans.	Obs.- calc.	
m′	*Γ′*	*J′*	*Ka′*	*Kc′*	*m″*	*Γ″*	*J″*	*Ka″*	*Kc″*	(cm^{-1})	(cm^{-1})	Ifit
0	B2	14	5	9	0	B2	14	3	11	7.6729	0.006	1
0	B2	14	5	9	0	B2	14	3	11	7.6712	0.004	1
0	B2	14	5	9	0	B2	13	5	9	10.9777	0.001	1
0	B2	14	5	9	0	B2	13	5	9	10.9775	0.001	1
0	B2	14	5	9	0	B2	13	5	9	10.9774	0.001	1
0	B2	14	5	9	0	B2	13	5	9	10.9787	0.002	1
0	B1	15	5	10	0	B1	15	3	12	8.4737	0.006	1
0	B1	15	5	10	0	B1	15	3	12	8.4755	0.007	1
0	B1	15	5	10	0	B1	15	3	12	8.4767	0.009	1
0	B1	15	5	10	0	B1	14	5	10	11.7894	-0.001	1
0	B1	15	5	10	0	B1	14	5	10	11.7918	0.001	1
0	B1	15	5	10	0	B1	14	5	10	11.7918	0.001	1
0	B1	15	5	10	0	B1	14	5	10	11.7917	0.001	1
0	B2	16	5	11	0	B2	15	5	11	12.6129	0.008	1
0	B2	16	5	11	0	B2	15	5	11	12.6116	0.007	1
0	B2	16	5	11	0	B2	15	5	11	12.6108	0.006	1
0	B1	17	5	12	0	B1	17	3	14	10.0600	0.001	1
0	B1	17	5	12	0	B1	17	3	14	10.0596	0.000	1
0	B1	17	5	12	0	B1	17	3	14	10.0590	0.000	1
0	B1	17	5	12	0	B1	17	3	14	10.0599	0.001	1
0	B1	17	5	12	0	B1	16	5	12	13.4097	-0.009	1
0	B1	17	5	12	0	B1	16	5	12	13.4107	-0.008	1
0	B1	17	5	12	0	B1	16	7	10	5.0260	0.005	1
0	B2	18	5	13	0	B2	18	3	15	10.8406	-0.011	1
0	B2	18	5	13	0	B2	18	3	15	10.8406	-0.011	1
0	B2	18	5	13	0	B2	18	3	15	10.8396	-0.012	1
0	B2	18	5	13	0	B2	18	3	15	10.8395	-0.012	1
0	B2	20	5	15	0	B2	20	3	17	12.4203	-0.008	1
0	B2	20	5	15	0	B2	20	3	17	12.4196	-0.009	1
0	B2	20	5	15	0	B2	20	3	17	12.4192	-0.009	1
0	B2	20	5	15	0	B2	20	3	17	12.4206	-0.008	1
0	B1	21	5	16	0	B1	21	3	18	13.2180	0.007	1
0	B1	21	5	16	0	B1	21	3	18	13.2170	0.006	1
0	B1	21	5	16	0	B1	21	3	18	13.2155	0.005	1
0	B1	21	5	16	0	B1	21	3	18	13.2170	0.006	1
0	B2	22	5	17	0	B2	22	3	19	13.9886	0.001	1
0	B2	22	5	17	0	B2	22	3	19	13.9887	0.001	1
0	B1	7	7	0	0	B1	7	5	2	3.3390	-0.003	1
0	B2	8	7	1	0	B2	8	5	3	2.9794	-0.002	1
0	B2	8	7	1	0	B2	8	5	3	2.9792	-0.002	1
0	B2	8	7	1	0	B2	8	5	3	2.9787	-0.002	1
0	B2	8	7	1	0	B2	8	5	3	2.9769	-0.004	1
0	B1	9	7	2	0	B1	9	5	4	2.6311	0.007	1
0	B1	9	7	2	0	B1	9	5	4	2.6295	0.005	1
0	B1	9	7	2	0	B1	9	5	4	2.6306	0.006	1
0	B1	9	7	2	0	B1	8	7	2	5.4532	0.007	1

Upper state					Lower state					Obs. Trans.	Obs.- calc.	
m′	*Γ′*	*J′*	*Ka′*	*Kc′*	*m″*	*Γ″*	*J″*	*Ka″*	*Kc″*	(cm^{-1})	(cm^{-1})	Ifit
0	B1	9	7	2	0	B1	8	7	2	5.4540	0.007	1
0	B1	9	7	2	0	B1	8	7	2	5.4537	0.007	1
0	B2	10	7	3	0	B2	10	5	5	2.5021	0.000	1
0	B2	10	7	3	0	B2	10	5	5	2.5017	0.000	1
0	B2	10	7	3	0	B2	10	5	5	2.5026	0.001	1
0	B2	10	7	3	0	B2	10	5	5	2.5035	0.002	1
0	B2	10	7	3	0	B2	9	7	3	6.2487	0.006	1
0	B2	10	7	3	0	B2	9	7	3	6.2483	0.005	1
0	B1	11	7	4	0	B1	11	5	6	2.8320	0.007	1
0	B1	11	7	4	0	B1	11	5	6	2.8312	0.006	1
0	B1	11	7	4	0	B1	11	5	6	2.8321	0.007	1
0	B1	11	7	4	0	B1	11	5	6	2.8303	0.005	1
0	B1	11	7	4	0	B1	10	7	4	7.2109	-0.004	1
0	B1	11	7	4	0	B1	10	7	4	7.2124	-0.002	1
0	B1	11	7	4	0	B1	10	7	4	7.2126	-0.002	1
0	B2	12	7	5	0	B2	12	5	7	3.5869	0.000	1
0	B2	12	7	5	0	B2	12	5	7	3.5877	0.001	1
0	B2	12	7	5	0	B2	12	5	7	3.5883	0.002	1
0	B2	12	7	5	0	B2	11	7	5	8.3473	0.005	1
0	B2	12	7	5	0	B2	11	7	5	8.3486	0.006	1
0	B2	12	7	5	0	B2	11	7	5	8.3477	0.005	1
0	B1	13	7	6	0	B1	13	5	8	4.5922	-0.003	1
0	B1	13	7	6	0	B1	13	5	8	4.5898	-0.006	1
0	B1	13	7	6	0	B1	13	5	8	4.5888	-0.007	1
0	B1	13	7	6	0	B1	12	7	6	9.5131	-0.009	1
0	B1	13	7	6	0	B1	12	7	6	9.5135	-0.008	1
0	B1	13	7	6	0	B1	12	7	6	9.5101	-0.012	1
0	B2	14	7	7	0	B2	14	5	9	5.6383	0.000	1
0	B2	14	7	7	0	B2	14	5	9	5.6384	0.000	1
0	B2	14	7	7	0	B2	14	5	9	5.6377	0.000	1
0	B2	14	7	7	0	B2	14	5	9	5.6394	0.001	1
0	B2	14	7	7	0	B2	13	7	7	10.6354	0.008	1
0	B2	14	7	7	0	B2	13	7	7	10.6365	0.009	1
0	B2	14	7	7	0	B2	13	7	7	10.6359	0.008	1
0	B1	15	7	8	0	B1	15	5	10	6.5881	-0.006	1
0	B1	15	7	8	0	B1	14	7	8	11.6056	0.004	1
0	B1	15	7	8	0	B1	14	7	8	11.6053	0.003	1
0	B1	15	7	8	0	B1	14	7	8	11.6042	0.002	1
0	B1	15	7	8	0	B1	14	7	8	11.6041	0.002	1
0	B2	16	7	9	0	B2	16	5	11	7.4569	-0.014	1
0	B2	16	7	9	0	B2	15	7	9	12.4814	-0.004	1
0	B2	16	7	9	0	B2	15	7	9	12.4810	-0.004	1
0	B2	16	7	9	0	B2	15	7	9	12.4807	-0.004	1
0	B2	16	7	9	0	B2	15	7	9	12.4812	-0.004	1
0	B1	17	7	10	0	B1	17	5	12	8.3051	-0.002	1
0	B1	17	7	10	0	B1	17	5	12	8.3050	-0.003	1

Upper state					Lower state					Obs. Trans.	Obs.- calc.	
m′	*Γ′*	*J′*	*Ka′*	*Kc′*	*m″*	*Γ″*	*J″*	*Ka″*	*Kc″*	(cm^{-1})	(cm^{-1})	Ifit
0	B1	17	7	10	0	B1	17	5	12	8.3055	-0.002	1
0	B1	17	7	10	0	B1	17	5	12	8.3072	0.000	1
0	B1	17	7	10	0	B1	16	7	10	13.3308	0.002	1
0	B1	17	7	10	0	B1	16	7	10	13.3313	0.002	1
0	B1	17	7	10	0	B1	16	7	10	13.3311	0.002	1
0	B1	17	7	10	0	B1	16	7	10	13.3320	0.003	1
0	B2	18	7	11	0	B2	18	5	13	9.1404	0.014	1
0	B2	18	7	11	0	B2	18	5	13	9.1399	0.014	1
0	B2	18	7	11	0	B2	18	5	13	9.1402	0.014	1
0	B1	19	7	12	0	B1	19	5	14	9.9493	0.014	1
0	B1	19	7	12	0	B1	19	5	14	9.9501	0.015	1
0	B1	19	7	12	0	B1	18	7	12	14.9767	-0.005	1
0	B1	19	7	12	0	B1	18	7	12	14.9753	-0.006	1
0	B1	19	7	12	0	B1	18	7	12	14.9757	-0.006	1
0	B1	19	7	12	0	B1	18	7	12	14.9747	-0.007	1
0	B2	20	7	13	0	B2	20	5	15	10.7415	0.002	1
0	B2	20	7	13	0	B2	20	5	15	10.7404	0.001	1
0	B2	20	7	13	0	B2	20	5	15	10.7425	0.003	1
0	B2	20	7	13	0	B2	19	7	13	15.8035	0.002	1
0	B2	20	7	13	0	B2	19	7	13	15.8038	0.002	1
0	B2	20	7	13	0	B2	19	7	13	15.8054	0.004	1
0	B1	21	7	14	0	B1	21	5	16	11.5286	-0.006	1
0	B1	21	7	14	0	B1	21	5	16	11.5288	-0.006	1
0	B1	21	7	14	0	B1	21	5	16	11.5270	-0.008	1
0	B2	7	7	1	0	B2	7	5	3	3.5809	0.010	1
0	B2	7	7	1	0	B2	7	5	3	3.5811	0.010	1
0	B1	8	7	2	0	B1	8	5	4	3.5740	-0.005	1
0	B1	8	7	2	0	B1	8	5	4	3.5744	-0.004	1
0	B1	8	7	2	0	B1	8	5	4	3.5746	-0.004	1
0	B1	8	7	2	0	B1	8	5	4	3.5742	-0.005	1
0	B2	9	7	3	0	B2	9	5	5	3.7200	-0.002	1
0	B2	9	7	3	0	B2	9	5	5	3.7204	-0.002	1
0	B2	9	7	3	0	B2	9	5	5	3.7196	-0.003	1
0	B2	9	7	3	0	B2	9	5	5	3.7191	-0.003	1
0	B1	10	7	4	0	B1	10	5	6	4.0498	-0.001	1
0	B1	10	7	4	0	B1	10	5	6	4.0503	0.000	1
0	B1	10	7	4	0	B1	10	5	6	4.0484	-0.002	1
0	B1	10	7	4	0	B1	10	5	6	4.0488	-0.002	1
0	B1	12	7	6	0	B1	12	5	8	5.2330	0.001	1
0	B1	12	7	6	0	B1	12	5	8	5.2319	0.000	1
0	B1	12	7	6	0	B1	12	5	8	5.2332	0.001	1
0	B1	12	7	6	0	B1	12	5	8	5.2320	0.000	1
0	B2	13	7	7	0	B2	13	5	9	5.9788	-0.008	1
0	B2	13	7	7	0	B2	13	5	9	5.9787	-0.008	1
0	B2	13	7	7	0	B2	13	5	9	5.9795	-0.007	1
0	B2	13	7	7	0	B2	13	5	9	5.9804	-0.007	1

Upper state					Lower state					Obs. Trans.	Obs.- calc.	
m′	*Γ′*	*J′*	*Ka′*	*Kc′*	*m″*	*Γ″*	*J″*	*Ka″*	*Kc″*	(cm^{-1})	(cm^{-1})	Ifit
0	B1	14	7	8	0	B1	14	5	10	6.7741	-0.009	1
0	B1	14	7	8	0	B1	14	5	10	6.7757	-0.007	1
0	B1	14	7	8	0	B1	14	5	10	6.7754	-0.007	1
0	B1	14	7	8	0	B1	14	5	10	6.7767	-0.006	1
0	B2	15	7	9	0	B2	15	5	11	7.5865	-0.004	1
0	B2	15	7	9	0	B2	15	5	11	7.5856	-0.005	1
0	B2	15	7	9	0	B2	15	5	11	7.5876	-0.003	1
0	B2	15	7	9	0	B2	15	5	11	7.5873	-0.003	1
0	B1	16	7	10	0	B1	16	5	12	8.3849	-0.013	1
0	B1	8	1	8	0	B1	7	1	6	0.7441	-0.065	0
0	B2	9	1	9	0	B2	8	1	7	0.7354	-0.079	0
0	B2	11	1	11	0	B2	10	1	9	0.7147	-0.117	0
0	B1	12	1	12	0	B1	11	1	10	0.7017	-0.142	0
0	B1	12	1	12	0	B1	11	1	10	0.7024	-0.141	0
0	B2	13	1	13	0	B2	12	1	11	0.6898	-0.167	0
0	B2	13	1	13	0	B2	12	1	11	0.6898	-0.167	0
0	B1	14	1	14	0	B1	13	1	12	0.6639	-0.208	0
0	B1	14	1	14	0	B1	13	1	12	0.6635	-0.209	0
0	B2	15	1	15	0	B2	14	1	13	0.6385	-0.250	0
0	B2	15	1	15	0	B2	14	1	13	0.6386	-0.250	0
0	B1	16	1	16	0	B1	15	1	14	0.6140	-0.294	0
0	B2	17	1	17	0	B2	16	1	15	0.5824	-0.345	0
0	B1	18	1	18	0	B1	17	1	16	0.5509	-0.398	0
0	B2	19	1	19	0	B2	18	1	17	0.5174	-0.454	0
0	B1	22	1	22	0	B1	21	1	20	0.4140	-0.636	0
0	B1	22	1	22	0	B1	21	1	20	0.4173	-0.632	0
0	B2	7	7	1	0	B2	6	5	1	7.7176	0.028	0
0	B1	8	7	2	0	B1	7	5	2	8.0226	-0.068	0
0	B1	8	7	2	0	B1	7	5	2	8.0222	-0.069	0
0	B1	8	7	2	0	B1	7	7	0	4.6831	-0.066	0
0	B2	9	7	3	0	B2	8	5	3	8.2952	-0.076	0
0	B2	9	7	3	0	B2	8	7	1	5.3157	-0.075	0
0	B2	9	7	3	0	B2	8	7	1	5.3149	-0.076	0
0	B2	13	7	7	0	B2	12	7	5	6.4087	-0.170	0
0	B1	14	7	8	0	B1	13	7	6	6.1390	-0.206	0
0	B2	15	7	9	0	B2	14	5	9	11.4938	-0.254	0
0	B1	16	7	10	0	B1	15	7	8	5.6725	-0.298	0
0	B1	16	7	10	0	B1	15	7	8	5.6697	-0.301	0
0	B2	17	7	11	0	B2	16	7	9	5.5758	-0.336	0
0	B2	17	7	11	0	B2	16	7	9	5.5766	-0.336	0
0	B1	18	7	12	0	B1	17	5	12	13.8107	-0.391	0
0	B1	18	7	12	0	B1	17	7	10	5.5052	-0.389	0
0	B2	19	7	13	0	B2	18	5	13	14.5707	-0.448	0
0	B2	19	7	13	0	B2	18	7	11	5.4311	-0.461	0
0	B1	20	7	14	0	B1	19	7	12	5.3767	-0.521	0
0	B1	20	7	14	0	B1	19	7	12	5.3776	-0.520	0